TREATMENTS TO PLASTIC WASTE FOR VALUABLE PRODUCTS

A Thesis submitted to Gujarat Technological University

for the Award of

Doctor of Philosophy

in

Chemical Engineering

by

Mishra Rohit Radheshyam

(Enrollment Number: 209999911006)

Under the supervision of

Dr. Paresh H. Rana (Supervisor)

Dr. Parimal Parikh (Co-Supervisor)

GUJARAT TECHNOLOGICAL UNIVERSITY
AHMEDABAD

July – 2026

TREATMENTS TO PLASTIC WASTE FOR VALUABLE PRODUCTS

A Thesis submitted to Gujarat Technological University

for the Award of

Doctor of Philosophy

in

Chemical Engineering

by

Mishra Rohit Radheshyam

(Enrollment Number: 209999911006)

Under the supervision of

Dr. Paresh H. Rana (Supervisor)

Dr. Parimal Parikh (Co-Supervisor)

GUJARAT TECHNOLOGICAL UNIVERSITY
AHMEDABAD

July – 2026

DECLARATION

I declare that the thesis entitled **"TREATMENTS TO PLASTIC WASTE FOR VALUABLE PRODUCTS"** submitted by me for the degree of Doctor of Philosophy is the record of research work carried out by me during the period from July 2021 to July 2026 under the supervision of **Dr. Paresh H. Rana, Professor and Dr. Parimal Parikh** and this has not formed the basis for the award of any degree, diploma, associateship, fellowship, titles in this or any other University or other institution of higher learning.

I further declare that the material obtained from other sources has been duly acknowledged in the thesis. I shall be solely responsible for any plagiarism or other irregularities, if noticed in the thesis.

Signature of the Research Scholar: ..... Date: 29/07/26

Name of Research Scholar: Mishra Rohit Radheshyam (Enrollment No.-209999911006)

Place: Ahmedabad

CERTIFICATE

I certify that the work incorporated in the thesis **"TREATMENTS TO PLASTIC WASTE FOR VALUABLE PRODUCTS"** submitted by **Mishra Rohit Radheshyam** was carri out by the candidate under my supervision/guidance. To the best of my knowledge: (i) t candidate has not submitted the same research work to any other institution for an degree/diploma, Associateship, Fellowship or other similar titles; (ii) the thesis submitted a record of original research work done by the Research Scholar during the period of stu under my supervision; and (iii) the thesis represents independent research work on the pa of the Research Scholar.

Signature of the Research Supervisor: ..... Date: 29/7/25

Name of Supervisor: Dr. Paresh H. Rana

Place: Ahmedabad

Course-work Completion Certificate

This is to certify that **Mishra Rohit Radheshyam**, enrolment no. **209999911006** is enrolled for PhD program in the faculty Chemical Engineering of Gujarat Technological University, Ahmedabad.

(Please tick the relevant option(s))

☐ He has been exempted from the coursework (successfully completed during M.Phil Course)

☐ He has been exempted from Research Methodology Course only (successfully completed during M. Phil Course)

☑ He has successfully completed the PhD course work for the partial requirement for the PhD Degree. His performance in the course work is as follows.

Grade obtained in Research Methodology [PHD2001]	Grade obtained in Research and Publication Ethics [PHD2002]	Grade obtained in Self-Study Course [PHD2003]
BC	AA	AB

Supervisor's Sign: .....

Name of Supervisor: Dr. Paresh H. Rana

Originality Report Certificate

It is certified that PhD Thesis titled **"TREATMENTS TO PLASTIC WASTE FOR VALUABLE PRODUCTS"** by **Mishra Rohit Radheshyam (Enrollment Number-209999911006)** has been examined by us. We undertake the following:

a. Thesis has significant new work / knowledge as compared to already published work or work under consideration to be published elsewhere. No sentence, equation, diagram, table, paragraph or section has been copied verbatim from previous work unless it is placed under quotation marks and duly referenced.

b. The work presented is original and the own work of the author (i.e. there is no plagiarism). No ideas, processes, results or words of others have been presented as the Author's own work.

c. There is no fabrication of data or results which have been compiled / analyzed.

d. There is no falsification by manipulating research materials, equipment or processes, or changing or omitting data or results such that the research is not accurately represented in the research record.

e. The thesis has been checked using Turnitin (copy of originality report attached) and found within limits as per GTU Plagiarism Policy and instructions issued from time to time (i.e. permitted similarity index ≤ 10%).

Signature of the Research Scholar: ..... Date: 29/07/26

Name of the Research Scholar: Mishra Rohit Radheshyam

Signature of the Research Supervisor: ..... Date: 29/7/26

Name of the Research Supervisor: Dr. Paresh H. Rana

Place: Gujarat Technological University, Ahmedabad

Dr. Paresh RANA

Thesis-Rohit Mishra

Thesis_Rohit Mishra

Jay

Gujarat Technological University

Document Details

Submission ID
trn:oid:::1:3509461354

128 Pages

Submission Date
Mar 17, 2026, 12:07 PM GMT+5:30

32,145 Words
186,982 Characters

Download Date
Mar 17, 2026, 12:11 PM GMT+5:30

File Name
Thesis.docx

File Size
13.1 MB

turnitin

4% Overall Similarity

The combined total of all matches, including overlapping sources, for each database.

Filtered from the Report

- Quoted Text

Match Groups

127 Not Cited or Quoted 4%
Matches with neither in-text citation nor quotation marks

0 Missing Quotations 0%
Matches that are still very similar to source material

0 Missing Citation 0%
Matches that have quotation marks, but no in-text citation

0 Cited and Quoted 0%
Matches with in-text citation present, but no quotation marks

Top Sources

2% Internet sources
3% Publications
1% Submitted works (Student Papers)

Integrity Flags

1 Integrity Flag for Review

Replaced Characters
111 suspect characters on 33 pages
Letters are swapped with similar characters from another alphabet.

Our system's algorithms look deeply at a document for any inconsistencies that would set it apart from a normal submission. If we notice something strange, we flag it for you to review.

A Flag is not necessarily an indicator of a problem. However, we'd recommend you focus your attention there for further review.

Ph.D. Thesis Non-Exclusive License to

GUJARAT TECHNOLOGICAL UNIVERSITY

In consideration of being a Research Scholar at Gujarat Technological University, and in the interests of the facilitation of research at the University and elsewhere, I, **Mishra Rohit Radheshyam**, having Enrollment No. **209999911006**, hereby grant a non-exclusive, royalty-free, and perpetual license to the University on the following terms:

a. The University is permitted to archive, reproduce and distribute my thesis, in whole or in part, and/or my abstract, in whole or in part (referred to collectively as the "Work") anywhere in the world, for non-commercial purposes, in all forms of media.
b. The University is permitted to authorize, sub-lease, sub-contract or procure any of the acts mentioned in paragraph (1).
c. The University is authorized to submit the Work at any National / International Library, under the authority of their "Thesis Non-Exclusive License".
d. The Universal Copyright Notice (©) shall appear on all copies made under the authority of this license.
e. I undertake to submit my thesis, through my university, to any Library and Archives. Any abstract submitted with the thesis will be considered to form part of the thesis.
f. I represent that my thesis is my original work, does not infringe any rights of others, including privacy rights, and that I have the right to make the grant conferred by this non-exclusive license.
g. If third-party copyrighted material was included in my thesis for which, under the terms of the Copyright Act, written permission from the copyright owners is required, I have obtained such permission from the copyright owners to do the acts mentioned in paragraph (1) above for the full term of copyright protection.
h. I understand that the responsibility for the matter as mentioned in paragraph (7) rests with the author / me solely. In no case shall GTU have any liability for any acts / omissions / errors / copyright infringement from the publication of the said thesis or otherwise.
i. I retain copyright ownership and moral rights in my thesis and may deal with the copyright in my thesis in any way consistent with rights granted by me to my university in this non-exclusive license.

j. GTU logo shall not be used / printed in the book (in any manner whatsoever) being published or any promotional or marketing materials or any such similar documents.

k. The following statement shall be included appropriately and displayed prominently in the book or any material being published anywhere: "The content of the published work is part of the thesis submitted in partial fulfilment for the award of the degree of Ph.D. in Chemical Engineering of the Gujarat Technological University".

l. I further promise to inform any person to whom I may hereafter assign or license my copyright in my thesis of the rights granted by me to my university in this non-exclusive license. I shall keep GTU indemnified from any and all claims from the Publisher(s) or any third parties at all times resulting or arising from the publishing or use or intended use of the book / such similar document or its contents.

m. I am aware of and agree to accept the conditions and regulations of Ph.D. including all policy matters related to authorship and plagiarism.

Date: 29/07/26

Place: Ahmedabad

P. R. Mistry

Signature of the Research Scholar:

Recommendation of the Research Supervisor: Recommended

Recommendation of the Co-Supervisor: Recommended

Signature of the Research Supervisor

Parish. P.A.

Signature of the Co- Supervisor

Thesis Approval Form

The viva-voce of the PhD Thesis submitted by **Mishra Rohit Radheshyam** (Enrollment No. **209999911006**) entitled "**TREATMENTS TO PLASTIC WASTE FOR VALUABLE PRODUCTS**" was conducted on Wednesday 29/07/2026 (day and date) at Gujarat Technological University.

(Please tick any one of the following options):

☑ The performance of the candidate was satisfactory. We recommend that he/she be awarded the PhD degree.

☐ Any further modifications in research work recommended by the panel after 3 months from the date of first viva-voce upon request of the Supervisor or request of Independent Research Scholar after which viva-voce can be re-conducted by the same panel again.

☐ The performance of the candidate was unsatisfactory. We recommend that he/she should not be awarded the PhD degree.

Name and Signature of Supervisor with Seal

1) (External Examiner 1) Name and Signature

Name and Signature of Co-Supervisor

2) (External Examiner 2) Name and Signature

ABSTRACT

Rapid accumulation of plastic trash, specifically low-density polyethylene (LDPE), creates significant environmental and resource sustainability challenges because of its chemical stability and resistance to natural degradation. Conventional recycling methods are often energy-intensive and yield low-value products, necessitating alternative routes for efficient plastic valorization. This research systematically explores microwave-assisted catalytic cracking of LDPE as an energy-efficient and sustainable pathway for producing H_2-rich gases and value-added hydrocarbons, with particular emphasis on the role of catalyst acidity, metal–support interactions, and microwave–matter coupling.

In the first phase of this work, microwave-assisted catalytic pyrolysis of LDPE was investigated using acidic zeolite catalysts (HY, HZSM-5, and Hβ) to elucidate the influence of pore structure and acidity on product distribution. These studies demonstrated that HY favors H_2 and aromatic hydrocarbon formation, HZSM-5 selectively enhances light olefins such as ethylene, and Hβ promotes propylene-rich gaseous products. H_2 yields as high as ~35 vol% were achieved under optimized conditions, highlighting the strong contribution of acid-catalyzed dehydrogenation and aromatization reactions under microwave heating.

In the second phase, the influence of catalyst acidity using a spent FCC catalyst and TiO_2 was systematically evaluated. The spent FCC catalyst, owing to its moderate acidity, produced olefin-rich gaseous streams dominated by propylene (up to ~67%), while TiO_2 favored paraffinic and olefinic gasoline-range hydrocarbons with limited aromatic formation. These results established that catalyst acidity and acid strength critically govern secondary cracking, hydrogen transfer, and aromatization reactions in microwave-assisted LDPE cracking.

Building upon these findings, the final phase of research focused on metal-supported catalysts, including Ni, Zn, and Fe based systems supported on HY, Al_2O_3, TiO_2, SiO_2, and sulphated ZrO_2. All metal-supported catalysts markedly improved hydrogen production compared with thermal pyrolysis. Zn/HY and Ni/HY showed the highest hydrogen generation, accounting for nearly 45% of the total gaseous products. In contrast, Ni/Al_2O_3, Zn/Al_2O_3, and Ni/SiO_2 produced relatively lower hydrogen yields of around 32%, 34%, and

30%, respectively. The high acidity and microporous structure of HY also promoted aromatic and gasoline-range hydrocarbons in the liquid phase. Notably, Fe/HY produced 41% H_2, 34% butene, and an exceptional 89% gasoline-range hydrocarbons, demonstrating strong cracking and olefin-forming capabilities. Ni/S-ZrO_2 and Zn/S-ZrO_2 further confirmed the role of strong Brønsted acidity in enhancing H_2 and aromatic formation.

Overall, this work provides a comprehensive understanding of microwave-assisted LDPE cracking across acidic, metal-free, and metal-supported catalytic systems. The results establish clear structure–activity relationships linking catalyst acidity, metal–support synergy, and microwave heating to H_2 yield and hydrocarbon selectivity, offering a viable route for sustainable plastic waste valorization and H_2 production.

Keywords: Microwave-assisted catalytic cracking, Low-density polyethylene (LDPE), Hydrogen production, Plastic waste valorization, Zeolite catalysts, Metal-supported catalysts, Catalyst acidity, Hydrocarbon selectivity

Acknowledgement

It gives me immense pleasure to acknowledge my indebtedness and great sense of gratitude to **Dr. Paresh H. Rana** and **Dr. Parimal Parikh**, for their able guidance and encouraging attitude throughout this research. Despite their busy schedule, they could find time to provide me with precious guidance. Thanks for all strategies applied to guide me, your encouragements, ideals, ideas, and most importantly your determination to guide and big heart you had especially when things went the other way.

I sincerely thank members of my Doctoral Progress Committee, **Dr. Asit Das and Dr. Ankush Biradar**, for their constructive feedback, critical evaluations, and scholarly insights, which greatly enhanced quality and rigor of this thesis.

I am profoundly indebted to my parents for their unconditional love, unwavering encouragement, and lifelong sacrifices. I extend my heartfelt gratitude to my wife, Nandini, for her constant support, patience, and understanding throughout this demanding journey, and to my son, Rohan, whose presence brought immense joy, motivation, and inspiration. I also gratefully acknowledge all my family members and well-wishers who, in various ways, provided support and encouragement that contributed to successful completion of this work.

Mishra Rohit Radheshyam

TABLE OF CONTENTS

TITLE PAGE		
DECLARATION		i
CERTIFICATE		ii
COURSE-WORK COMPLETION CERTIFICATE		iii
ORIGINALITY REPORT CERTIFICATE		iv
Ph.D. THESIS NON-EXCLUSIVE LICENSE TO GUJARAT TECHNOLOGICAL UNIVERSITY		vii
THESIS APPROVAL FORM		ix
ABSTRACT		x
ACKNOWLEDGEMENT		xii
TABLE OF CONTENTS		xiii
LIST OF FIGURES		xix
LIST OF TABLES		xxiii
No.	**Topic**	**Page No.**
Chapter 1.	**Introduction**	**1**
1.1	Introduction	1
1.2	Motivation of Study	2
1.3	Aims and Objectives of present work	4
1.4	Outlines of thesis	4
1.5	References	5
Chapter 2.	**Literature Review and Characterization Techniques**	**8**
2.1	Classification of Polymers	8
2.1.1	Natural Polymers	9
2.1.2	Synthetic Polymers	11
2.1.2.1	Low-density polyethylene	12
2.1.2.2	High-density polyethylene	14
2.1.2.3	Polypropylene	15
2.1.2.4	Polystyrene	16

2.1.2.5	Polyvinyl chloride	17
2.2	Methods to treat polymer waste	19
2.2.1	Recycling	19
2.2.2	Thermal Transformation	21
2.2.2.1	Gasification	21
2.2.2.2	Pyrolysis	25
2.2.2.2.1	Batch reactor	27
2.2.2.2.2	Fixed and fluidized bed reactor	27
2.2.2.2.3	Conical spouted bed reactor (CSBR)	28
2.2.2.2.4	Microwave-assisted technology	28
2.2.3	Biological Transformation	31
2.3	Effect of parameters	32
2.3.1	Temperature	33
2.3.2	Catalyst	33
2.4	Characterization Techniques	40
2.4.1	X-ray diffraction	40
2.4.2	Scanning electron microscopy	40
2.4.3	Fourier-transform infrared spectroscopy	40
2.4.4	Pyridine-adsorbed FTIR	40
2.4.5	NH_3-temperature-programmed desorption	41
2.4.6	X-ray photoelectron spectroscopy	41
2.4.7	Inductively coupled plasma mass spectrometry	41
2.4.8	Gas chromatography/mass spectrometry	42
2.5	References	42
Chapter 3.	**Microwave-assisted pyrolysis of LDPE to value-added products over HY, HZSM-5 and Hβ catalyst**	**49**
3.1	Introduction	49
3.2	Materials and methods	50
3.2.1	Materials	50
3.2.2	Desilication of Hβ	50
3.2.3	Catalyst characterization	50

3.2.4	Experimental setup	50
3.2.5	Liquid products analysis	51
3.2.6	Gaseous products analysis	51
3.2.7	Product Quantification	52
3.3	Results and discussion	52
3.3.1	Catalyst Characterization	52
3.3.1.1	Scanning Electron Microscope (SEM)	52
3.3.1.2	Fourier transform infrared spectroscopy (FTIR)	52
3.3.1.3	Powder X-ray diffraction (XRD)	54
3.3.1.4	X-ray photoelectron spectroscopy (XPS)	54
3.3.2	Catalytic performance	55
3.3.2.1	Effect of scintillator proportion	55
3.3.2.2	Effect of pyrolysis temperatures	56
3.3.2.3	Effect of catalyst proportion on gaseous product compositions	59
3.3.2.4	Influence of desilicated Hβ (D-Hβ) on product compositions	63
3.3.2.5	Reaction mechanism of catalytic pyrolysis using HZSM-5, HY, and Hβ	65
3.3.2.6	Catalyst Reusability Test	65
3.4	Conclusion	67
3.5	References	67
Chapter 4.	**Influence of acidity of spent FCC catalyst and TiO_2 on product distribution in microwave assisted LDPE cracking**	**72**
4.1	Introduction	72
4.2	Materials and methods	73
4.2.1	Materials	73
4.2.2	Catalyst characterization	73
4.3	Results and discussion	73
4.3.1	Catalyst characterization	73
4.3.1.1	Scanning electron microscope	73
4.3.1.2	Fourier transform infrared spectroscopy	74

4.3.1.3	Powder X-ray diffraction	75
4.3.1.4	NH_3 Temperature Programmed Desorption	75
4.3.1.5	X-ray photoelectron spectroscopy	77
4.3.2	Catalytic performance	77
4.3.2.1	Effect of spent FCC catalyst on product distribution	77
4.3.2.2	Influence of TiO_2 on product compositions	83
4.4	Conclusion	87
4.5	References	88
Chapter 5.	**Hydrogen-rich gas and value-added hydrocarbon production from LDPE using Ni and Zn supported catalysts**	**92**
5.1	Introduction	92
5.2	Materials and methods	93
5.2.1	Materials	93
5.2.2	Catalyst Preparation	93
5.2.3	Catalyst characterization	93
5.3	Results and discussion	94
5.3.1	Catalyst Characterization	94
5.3.1.1	Scanning Electron Microscope	94
5.3.1.2	Fourier transform infrared spectroscopy	94
5.3.1.3	Powder X-ray Diffraction	96
5.3.1.4	FTIR spectra of pyridine-adsorbed catalysts	97
5.3.1.5	Inductively Coupled Plasma Mass Spectrometry	99
5.3.2	Catalytic Performance	100
5.3.2.1	Ni/HY	100
5.3.2.2	Ni/SiO_2	102
5.3.2.3	Ni/TiO_2	104
5.3.2.4	Ni & Zn/Al_2O_3	106
5.3.2.5	Zn/HY	107
5.3.2.6	Carbon number Distribution of hydrocarbons in liquid	110
5.3.2.7	Comparative Analysis of TOF and TON for Ni	112

	and Zn Catalysts on Acidic and Non-Acidic Supports	
5.3.2.8	Cracking of LDPE dissolved in Tetralin	113
5.4	Conclusion	115
5.5	References	115
Chapter 6.	**Influence of catalyst support and metal loading on hydrogen yield**	**120**
6.1	Introduction	120
6.2	Materials and methods	120
6.2.1	Materials	120
6.2.2	Catalyst Preparation	121
6.2.3	Synthesis of sulphated ZrO_2 Catalyst	121
6.3	Results and discussion	121
6.3.1	Catalyst Characterization	121
6.3.1.1	Scanning Electron Microscope	121
6.3.1.2	Fourier transform infrared spectroscopy	122
6.3.1.3	Powder X-ray Diffraction	123
6.3.1.4	FTIR spectra of pyridine-adsorbed catalysts	124
6.3.2	Catalytic performance	126
6.3.2.1	Impact of ZrO_2, Sulphated ZrO_2 (S-ZrO_2), 15% Ni/S-ZrO_2 and 15% Zn/S-ZrO_2 catalysts	126
6.3.2.2	Effect of Fe loaded HY on product composition	129
6.3.2.4	Impact of Al_2O_3 and 15%Fe/Al_2O_3 on product composition	131
6.4	Kinetic, Thermodynamic, and Computational Studies	134
6.4.1	Kinetic Analysis of LDPE Cracking	134
6.4.2	Adsorption Energy Calculations	139
6.4.3	Thermodynamic Equilibrium Analysis	140
6.4.4	Energy Consumption Analysis	142
6.4.5	Industrial Relevance and Scale-Up Considerations	143
6.5	Conclusion	143
6.6	References	144

Chapter 7.	**Conclusion and scope for future work**	**146**
7.1	Conclusion	146
7.2	Scope for Future Work	147
List of References		149
Appendix		165
List of publications		167

LIST OF FIGURES

No.	Topic	Page No.
2.1	Classification of Polymers	8
2.2	Schematic of LDPE branching structure	14
2.3	Schematic of HDPE structure	15
2.4	Schematic of Polypropylene structure	16
2.5	Schematic of polystyrene structure	17
2.6	Polyvinyl chloride structure	18
2.7	Polymer treatment methods	19
2.8	Plastic recycling stages	21
2.9	Temperature profiles in microwave and conventional heating methods	29
3.1	(a) Schematic representation of the microwave-assisted catalytic pyrolysis setup, (b) Actual photograph of the experimental apparatus.	51
3.2	SEM images of (a) HZSM-5 (b) HY, and (c) Hβ	52
3.3	FTIR patterns of HZSM-5 HY, and Hβ catalyst	53
3.4	XRD patterns of HY, HZSM-5 and Hβ catalyst.	53
3.5	XPS spectra of (a) HY, (b) HZSM-5, and (c) Hβ.	54
3.6	Effect of G/L ratio on (a) Product distribution and (b) Liquid composition of LDPE. Temperature - 400 °C, 2g HY.	56

3.7	The effects of pyrolysis temperature on (a) gas composition at a HY to LDPE ratio of 1:10 (b) gas composition at a HZSM-5 to LDPE ratio of 1:10 (c) Product yield at a Hβ to LDPE ratio of 1:10 (d) Liquid oil composition at a Hβ to LDPE ratio of 1:10and (e) gas composition at a Hβ to LDPE ratio of 1:10.	58
3.8	Effect of catalyst proportion on (a) Gas composition at 400 °C with HY (b) Gas composition at 550 °C with HSZM-5 (c) Product yield at 450 °C (d) Liquid oil composition at 450 °C and (e) Gas composition at 450 °C	62
3.9	Effect of Hβ and D-Hβ on (a) Product yield at 450ºC, (b) Liquid composition at 450ºC and (c) Gas composition at 450ºC. Hβ to LDPE ratio was 1:10	64
3.10	Effect of catalyst reusability on gas composition (a) HY to LDPE ratio 1:10 at 450 °C. (b) HZSM-5 to LDPE ratio 1:10 at 550 °C. (c) Hβ to LDPE ratio 1:10 at 450 °C	66
4.1	SEM images of (a) spent FCC and (b) TiO_2.	74
4.2	FTIR patterns of spent FCC and TiO_2 catalyst	74
4.3	XRD patterns of spent FCC and TiO_2 catalyst.	75
4.4	NH_3-TPD Profile of spent FCC and TiO_2.	76
4.5	XPS spectra of (a) FCC, and (b) TiO_2.	77
4.6	Influence of cracking temperature on (a) Product yield at spent FCC to LDPE mass ratio of 1:10 (b) Liquid oil compositions at spent FCC to LDPE mass ratio of 1:10 (c) Gas composition at spent FCC to LDPE mass ratio of 1:10. Effect of spent FCC catalyst proportion on (d) Yield of product at 450°C (e) Liquid compositions at 450°C (f) Gaseous product composition at 450°C.	82

4.7	Impact of cracking temperatures on (a) Product yield at a TiO_2 to LDPE mass ratio of 1:10 (b) Liquid oil composition at a TiO_2 to LDPE mass ratio of 1:10 and (c) Gas composition at a TiO_2 to LDPE mass ratio of 1:10. Influence of TiO_2 proportion on (d) Product distribution at 500°C (e) Liquid oil composition at 500°C and (f) Gas composition at 500°C.	87
5.1	SEM images of synthesized catalysts: (a) 15 wt.% Ni/HY, (b) 15 wt.% Zn/HY, (c) 15 wt.% Ni/Al_2O_3, (d) 15 wt.% Zn/Al_2O_3, (e) 15 wt.% Ni/SiO_2, and (f) 15 wt.% Ni/TiO_2.	95
5.2	FTIR patterns of 15 wt.% Ni- and Zn-loaded catalysts supported HY zeolite, Al_2O_3, SiO_2, and TiO_2.	96
5.3	XRD patterns of 15 wt.% Ni and Zn loaded catalysts supported on HY zeolite, Al_2O_3, SiO_2, and TiO_2	97
5.4	Pyridine adsorbed FT-IR spectra of 15 wt.% Ni and Zn loaded catalysts supported on HY zeolite, Al_2O_3, SiO_2, and TiO_2.	98
5.5	Influence of Ni Proportion in HY on (a) Product Distribution, (b) Liquid Oil Composition, and (c) Gas Composition at 450°C and the HY to LDPE ratio was 1:10.	101
5.6	Effect of Ni/SiO_2 on (a) Product distribution, (b) Liquid composition, and (c) Gas composition at 450°C. SiO_2 to LDPE ratio was maintained at 1:10.	103
5.7	Effect of Ni/TiO_2 on (a) Product distribution, (b) Liquid composition, and (c) Gas composition at 450°C. TiO_2 to LDPE ratio was maintained at 1:10.	105
5.8	Impact of Ni and Zn in Al_2O_3 on (a) Product distribution, (b) Liquid composition, and (c) Gas composition at 450°C. Al_2O_3 to LDPE ratio was maintained at 1:10.	107
5.9	Influence of Zn Proportion in HY on (a) Product Distribution, (b) Liquid Composition, and (c) Gas Composition at 450°C and the HY to LDPE ratio was 1:10.	109

5.10	Comparison of catalytic performance during microwave-assisted LDPE pyrolysis.	110
5.11	Carbon number distribution in Liquid oil in Presence of different catalyst at 450°C and catalyst to LDPE ratio was 1:10.	111
5.12	Cracking of LDPE dissolved in Tetralin (a) Product yield at 450ºC, (b) Liquid composition at 450ºC and (c) Gas composition at 450ºC. Catalyst to LDPE ratio was 1:10.	114
6.1	SEM images of (a) 15 wt.% Ni/ZrO_2, (b) 15 wt.% Zn/ZrO_2, (c) 15 wt.% Fe/HY, (d) 15 wt.% Fe/Al_2O_3.	122
6.2	FTIR patterns of synthesized catalysts: 15 wt.% Ni/ZrO_2, 15 wt.% Zn/ZrO_2, 15 wt.% Fe/HY, 15 wt.% Fe/Al_2O_3.	123
6.3	XRD patterns of synthesized catalysts: 15 wt.% Ni/ZrO_2, 15 wt.% Zn/ZrO_2, 15 wt.% Fe/HY, 15 wt.% Fe/Al_2O_3.	124
6.4	Pyridine adsorbed FT-IR spectra of ZrO_2, S-ZrO2, 15 wt.% Ni/S-ZrO_2, and 15 wt.% Zn/S-ZrO_2.	125
6.5	Pyridine adsorbed FT-IR spectra of 15% Fe/Al_2O_3 and 15% Fe/HY.	126
6.6	Effect of ZrO_2 on (a) Product distribution, (b) Liquid composition, and (c) Gas composition at 450°C. The catalyst to LDPE ratio was maintained at 1:10.	127
6.7	Effect of Fe/HY on (a) Product distribution, (b) Liquid composition, and (c) Gas composition at 450°C. The catalyst to LDPE ratio was maintained at 1:10.	131
6.8	Effect of Al_2O_3 and 15%Fe/Al_2O_3 on (a) Product distribution, (b) Liquid composition, and (c) Gas composition at 450°C. Catalyst to LDPE ratio was maintained at 1:10.	133
6.9	First-order kinetic plots of ln(1−X) versus reaction time for microwave-assisted LDPE cracking over 15 wt.% Fe/HY catalyst at 450 °C.	135

6.10 First-order kinetic plots of ln(1−X) versus reaction time for microwave-assisted LDPE cracking over 15 wt.% Fe/HY catalyst at 550 °C. 136

6.11 Arrhenius plot (ln k vs. 1/T) for LDPE cracking in the presence of Fe/HY catalyst. 138

LIST OF TABLES

No.	Topic	Page No.
2.1	Comparative analysis of various gasifying agents.	24
2.2	Comparison of pyrolysis types based on operating conditions and main products.	26
2.3	Products of cracking of plastics.	30
2.4	Comparison of thermal and catalytic pyrolysis of LDPE: Process Parameters, Advantages, and Limitations.	34
2.5	Reaction pathway differences among catalytic and thermal Pyrolysis of LDPE.	35
2.6	Brief of key literature on polymer cracking and catalysis.	37
3.1	Summary of studies on plastic cracking for H_2 formation.	60
4.1	NH_3-TPD data of spent FCC and TiO_2	76

4.2	Variation in carbon number in liquid products at different reaction temperatures in presence of spent FCC catalyst.	78
4.3	Carbon number distribution in liquid product in presence of spent FCC at 450°C.	80
4.4	Carbon number distribution in liquid product at different temperature in presence of TiO_2. TiO_2 to LDPE ratio was 1:10.	84
4.5	Carbon number distribution in liquid product in presence of TiO_2 at 500°C.	85
5.1	Acidity of Ni and Zn loaded catalysts as determined by pyridine-IR.	99
5.2	ICP-MS data for various metal-loaded catalysts.	99
5.3	Turnover Frequency (TOF), Turnover Number (TON), and H_2 yield for 15 wt.% metal-loaded catalysts used in LDPE cracking at 450°C and catalyst to LDPE ratio was 1:10.	113
6.1	Acidity of ZrO_2, S-ZrO_2, 15 wt.% Ni/S-ZrO_2, and 15 wt.% Zn/S-ZrO_2 catalysts as determined by pyridine-IR.	125
6.2	Acidity of 15% Fe/Al_2O_3 and 15% Fe/HY as determined by pyridine-IR.	125
6.3	Carbon number distribution in Liquid in the Presence of ZrO_2 at 450°C. Catalyst to LDPE ratio was 1:10.	128
6.4	Carbon number distribution in Liquid in the Presence of Fe loaded HY at 450°C. Catalyst to LDPE ratio was 1:10.	130
6.5	Carbon number distribution in Liquid in the Presence of Al_2O_3 and 15% Fe/Al_2O_3 at 450°C. Catalyst to LDPE ratio was 1:10.	132
6.6	Adsorption energies of ethylene on Ni-supported catalysts.	139
6.7	Comparison of experimental gaseous product distribution from microwave-assisted LDPE pyrolysis (with and without Ni/S-ZrO_2 catalyst) and equilibrium composition obtained from simulation.	141

CHAPTER – 1

Introduction

This chapter presents the background of plastic waste generation and the environmental challenges associated with it. It highlights the motivation for adopting microwave-assisted catalytic pyrolysis as an efficient alternative to conventional recycling methods. The chapter further defines the aims and objectives of the present research, focusing on the development of effective catalytic strategies for low density polyethylene (LDPE) cracking and enhanced H_2 production.

1.1 Introduction

Plastics have significantly enhanced our lives by being affordable, adaptable, and hygienic materials utilized across diverse sectors such as building construction, household appliances, medical devices, and food containers [1]. Plastic is an inevitable material used by humans in their daily lives, owing to its low cost and durability. A significant increase in its usage production and usage has been observed over the last decade [2]. Their production has increased significantly over the past 70 years: in 1950, worldwide production was just two million tons, but it has since soared to more than 450 million tons in 2023 [1]. With an annual use of around 500 million tons, global plastic production will reach 34 billion tons per year by 2050 [3]. In India, around 3.5 million tons of plastic waste are generated, of which approximately 50 % (1.58 million tons) are recycled and 0.167 million tons are co-processed, respectively. The remaining 50% is disposed of without recycling in India and globally as well [3]. Also, a large chunk of plastic produced is used to make packaging items or other short-lived products which are discarded to the environment within a month of manufacture [4]. The diverse types of plastics used in the manufacturing of consumable products, including water bottles, medical devices, and food packaging often contain harmful chemicals such as bisphenol A, heavy metals, nonylphenol, phthalates, brominated flame retardants, phenanthrene, polychlorinated biphenyl ethers, and others [5]. These abandoned microplastics cause terrestrial and marine environmental pollution and affect the lives of aquatic organisms by releasing plastics into the ocean. Ultimately, they are consumed by animals and humans through the food chain [5,6]. Not only this, human health and the environment are also adversely affected by presence of various chemicals and harmful substances like bisphenol A

(BPA), brominated flame-retardants, thalates, and poly-fluorinated chemicals, etc. present in plastics if not managed properly [7]. It is projected that around 28 million metric tons of plastic will annually enter the oceans due to inadequate landfill facilities in coastal countries [8]. Toxic plastics can lead to various human health issues, including eye irritation, vision impairment, breathing and respiratory difficulties, liver dysfunction, cancer risk, skin diseases, lung problems, dizziness, headaches, birth defects, reproductive and cardiovascular issues, genotoxic effects, and gastrointestinal problems. [7]. Therefore, efforts are required to reduce the effects of waste plastic on the environment and living organisms. Researchers have explored various recycling methods namely thermal cracking [9], catalytic cracking [10] and microwave-assisted cracking [11] to transform plastic waste into valuable products such as gases, liquid hydrocarbons, and coke [12–14]. In recent years, microwave-assisted (MW) catalytic pyrolysis of waste plastic has been extensively studied to investigate product distribution and product yields with different types of plastic waste [3].

1.2 Motivation of Study

Although LDPE and HDPE possess nearly identical hydrogen contents due to their similar polyolefin composition, LDPE was selected as the feedstock because of its highly branched molecular structure, lower crystallinity, and lower thermal stability, which facilitates depolymerization during pyrolysis. In addition, LDPE is one of the most widely used plastics in packaging films, shopping bags, and agricultural applications, generating a substantial amount of post-consumer waste that is difficult to recycle mechanically. Therefore, investigating the catalytic conversion of waste LDPE into hydrogen and valuable hydrocarbons is both scientifically relevant and environmentally significant. Conventional thermal pyrolysis of plastics suffers from several limitations, including slow heat transfer, high energy consumption, temperature gradients, and limited control over product distribution. Microwave-assisted (MW) pyrolysis offers significant advantages over conventional heating methods by enabling rapid, selective, and uniform heating of materials through direct interaction with microwave radiation. When combined with suitable microwave absorbers and catalysts, MW-assisted pyrolysis can significantly intensify cracking reactions, enhance dehydrogenation, and promote secondary reactions, leading to higher gas yields and improved H_2 production.

Several studies have demonstrated the effectiveness of microwave-assisted catalytic pyrolysis of LDPE and other polymers. Ding et al. carried out the MW catalytic batch pyrolysis of LDPE at 500 °C and obtained 57 % and 43 % yields of liquid and gaseous products, respectively over

NiO and HY catalysts [2]. Vatankhah et al. investigated microwave-assisted polyethylene pyrolysis and found that Zn-promoted HZSM-5 exhibited exceptional aromatization activity [15]. The process yielded 44% liquid products with 93% consisting of aromatics compounds, including 64% selectivity toward benzene, toluene, ethylbenzene, and xylene (BTEX). Similarly, Ga/Cu/ZSM-5 produced an aromatic-rich pyrolysis oil with benzene derivatives accounting for approximately 90% of the liquid fraction during microwave-assisted catalytic pyrolysis of LDPE [16]. Gasoline-range hydrocarbons (75 – 88%) and various gases, such as ethane, H_2, and ethylene were obtained from MW-induced pyrolysis of LDPE with a ZSM-5 catalyst at 450 °C [11]. High-density polyethylene (HDPE) underwent degradation in a microwave-assisted hydrothermal process to yield several chemicals, such as glutaric, succinic, and adipic acids which were subsequently converted into a model plasticizer [17]. In a two-step, MW cracking of LDPE in the presence of molecular sieve 4A as a catalyst; and spherical activated carbon and columnar activated carbon as microwave absorbers, mainly liquid oil products were observed and distributed among C_7 to C_{26}, which are appropriate for gasoline and diesel fractions, as reported by Jing et al. [18]. Gaseous products mainly comprised of H_2, CH_4, C_2H_4, and C_3H_6. Backstrom et al. used HNO_3 as an oxidizing agent to convert LDPE into water-soluble di-carboxylic acids and reported a 71% yield of dicarboxylic acids using an MW-assisted oxidative process at 180 °C [19]. Fan et al. used MgO as a base catalyst to carry out the MW catalytic batch pyrolysis of LDPE and obtained 24-38 wt.% liquid yield under varied reaction conditions of 350-550 °C, in which the proportion of the gasoline fraction ranged from 79 % to 96% and the gas yield was around 57 wt.% at pyrolysis temperatures exceeding 500 °C. The higher production of gaseous products was due to higher catalyst-to-reactant ratios, pyrolysis temperatures, and catalytic reaction temperatures [20]. Conventional catalytic pyrolysis of HDPE was carried out using an HZSM-5 catalyst at 450 °C and products consisting of 65 wt.% gas and 35 wt.% liquid was obtained [10]. Undri et al. conducted experiment on microwave pyrolysis of HDPE and obtained products composed of short-chain hydrocarbons (C_1–C_4), long-chain waxy hydrocarbons in the solid-phase (>C_{20}), and a minor liquid fraction [21]. Chen et al. carried out the cracking reaction of n-octane at 410 °C in the presence of an Au/ZSM-5 catalyst and obtained a 42% yield of propylene. Propylene formation was attributed to a metal-acid synergistic catalysis mechanism [22]. Terapalli et al. utilized KOH in microwave cracking of polystyrene and found that KOH enhanced the generation of olefins, alkanes, and cycloalkanes [23]. Zhang et al. performed microwave-induced LDPE cracking and achieved an impressive 74-88% yield of aromatics utilizing ZSM-5 at 450°C [11]. Liu et al. converted polyethylene and CO_2 into aromatics (63 wt.% yield) and CO using an HZSM-5

+ CuZnZrOx catalyst at 380°C and under H_2 and solvent-free reaction conditions[24]. In a continuous-stirred microwave pyrolysis process, the primary gaseous products obtained were propylene and propane, along with gasoline-range hydrocarbons (C_5–C_{12}) in the presence of HZSM-5 [25].

1.3 Aims and objectives of present work

The present study aims to explore efficient catalytic strategies for microwave-assisted cracking of LDPE to enhance product distribution and H_2 production. The specific objectives are as follows:

- To investigate the effect of a low-cost microwave absorber (graphite) on product distribution using various catalysts such as HY, HZSM-5, Hβ, FCC, and TiO_2 during microwave-assisted cracking of LDPE.
- To evaluate the performance of Ni, Zn, and Fe loaded HY catalysts for H_2 production from LDPE cracking.
- To carry out the solubilization of LDPE in a solvent (e.g., tetralin) prior to pyrolysis and to modify Hβ zeolite to introduce mesoporosity, thereby assessing its impact on product distribution during catalytic conversion.
- To examine the catalytic cracking of LDPE using sulphated zirconia, with and without metal loading, for enhanced H_2 production.
- To study the influence of catalyst acidity (Lewis and Brønsted acid sites) and the catalyst to LDPE ratio on product yield and distribution.

1.4 Outlines of thesis

This thesis is organized into seven chapters, each addressing specific aspects of microwave-assisted catalytic cracking of LDPE.

Chapter 1 provides an introduction to the problem of plastic waste, the motivation for the present study, and the objectives and scope of the research.

Chapter 2 presents a comprehensive review of existing literature on plastic waste management, conventional and microwave-assisted pyrolysis, catalytic cracking of LDPE, and H_2 production using various catalyst systems.

Chapter 3 focuses on microwave-assisted cracking of LDPE using acidic zeolite catalysts, namely HY, HZSM-5, and Hβ, and discusses their effects on product yield, selectivity, and reaction pathways.

Chapter 4 examines the influence of catalyst acidity on LDPE cracking by employing a spent FCC catalyst and TiO_2, highlighting the role of acidic properties in controlling product distribution and gas formation.

Chapter 5 investigates the production of H_2-rich gas from LDPE through microwave-assisted cracking using Ni- and Zn-supported catalysts, with an emphasis on metal functionality and catalytic performance.

Chapter 6 explores the influence of catalyst support and metal loading on H_2 yield, focusing on various metal–support combinations and their impact on cracking efficiency and gas composition.

Chapter 7 summarizes the major conclusions drawn from the present work and outlines the scope for future research in the area of microwave-assisted plastic waste valorization.

1.5 References

[1] Hannah Ritchie, Veronika Samborska, Max Roser, Plastic Pollution, Our World in Data (2023).

[2] K. Ding, S. Liu, Y. Huang, S. Liu, N. Zhou, P. Peng, Y. Wang, P. Chen, R. Ruan, Catalytic microwave-assisted pyrolysis of plastic waste over NiO and HY for gasoline-range hydrocarbons production, Energy Convers. Manag. 196 (2019). https://doi.org/10.1016/j.enconman.2019.07.001.

[3] Xuan Hu, Dachao Ma, Guangyi Zhang, Mengxue Ling, Qiaoling Hu, Kangyi Liang, Jiacheng Lu, Yifan Zheng, Microwave-assisted pyrolysis of waste plastics for their resource reuse: A technical review, Carbon Resources Conversion 6 (2023) 215–228.

[4] J. Hopewell, R. Dvorak, E. Kosior, Plastics recycling: challenges and opportunities, (n.d.). https://doi.org/10.1098/rstb.2008.0311.

[5] A. Okunola A, O. Kehinde I, A. Oluwaseun, A. Olufiropo E, Public and Environmental Health Effects of Plastic Wastes Disposal: A Review, Journal of Toxicology and Risk Assessment 5 (2019). https://doi.org/10.23937/2572-4061.1510021.

[6] R. Geyer, J. R. Jambeck, K. L. Law, Production, use, and fate of all plastics ever made, Sci. Adv. (2017).

[7] R. Proshad, T. Kormoker, Md.S. Islam, M.A. Haque, Md.M. Rahman, Md.M.R. Mithu, Toxic effects of plastic on human health and environment: A consequence of health risk

assessment in Bangladesh, International Journal of Health 6 (2017) 1–5. https://doi.org/10.14419/ijh.v6i1.8655.

[8] J.R. Jambeck, R. Geyer, C. Wilcox, T.R. Siegler, M. Perryman, A. Andrady, R. Narayan, K.L. Law, Plastic waste inputs from land into the ocean, Science (1979). 347 (2015) 768–771. https://doi.org/10.1126/science.1260352.

[9] J. Aguado, D.P. Serrano, G. San Miguel, M.C. Castro, S. Madrid, Feedstock recycling of polyethylene in a two-step thermo-catalytic reaction system, J. Anal. Appl. Pyrolysis 79 (2007) 415–423. https://doi.org/10.1016/j.jaap.2006.11.008.

[10] Ting Liu, Yincui Li, Yifan Zhou, Shengnan Deng, Huawei Zhang, Efficient pyrolysis of Low-Density Polyethylene for Regulatable Oil and Gas Products by ZSM-5, HY and MCM-41 Catalyst, Catalysts (2023) 382.

[11] X. Zhang, H. Lei, G. Yadavalli, L. Zhu, Y. Wei, Y. Liu, Gasoline-range hydrocarbons produced from microwave-induced pyrolysis of low-density polyethylene over ZSM-5, Fuel 144 (2015). https://doi.org/10.1016/j.fuel.2014.12.013.

[12] L. D. Chen, H. Yin, P.H. Wang, Pyrolysis technologies for municipal solid waste: A review, Waste Manag. 34 (2014) 2466–2486.

[13] O.K.M. Ouda, S.A. Raza, A.S. Nizami, M. Rehan, R. Al-Waked, N.E. Korres, Waste to energy potential: A case study of Saudi Arabia, Renew. and Sustain. Energy (2016) 328–340.

[14] R. Miandad, M. Rehan, A.-S. Nizami, M.A. El-Fetouh Barakat, I.M. Ismail, The Energy and Value-Added Products from Pyrolysis of Waste Plastics, in: Recycl, in: Of Solid Waste for Biofuels and Biochem, 2016: pp. 333–355. https://doi.org/10.1007/978-981-10-0150-5_12.

[15] F. Vatankhah, A. Carrillo García, J. Chaouki, Role of Bifunctional Metal-Promoted Zeolitic Catalyst in Microwave-Assisted Pyrolysis of Polyethylene to Monocyclic Aromatics, Energy & Fuels 38 (2024) 20562–20576. https://doi.org/10.1021/acs.energyfuels.4c03692.

[16] K.M.O. Islam, N. Ahmad, U. Ahmed, M.N. Siddiqui, A.C. Ummer, A.G. Abdul Jameel, Producing aromatic-rich oil through microwave-assisted catalytic pyrolysis of low-density polyethylene over Ni/Co/Cu-doped Ga/ <scp>ZSM</scp> -5 catalysts, Biofuels, Bioproducts and Biorefining 19 (2025) 34–54. https://doi.org/10.1002/bbb.2690.

[17] E. Bäckström, K. Odelius, M. Hakkarainen, Designed from Recycled: Turning Polyethylene Waste to Covalently Attached Polylactide Plasticizers, ACS Sustain. Chem. Eng. 7 (2019) 11004–11013. https://doi.org/10.1021/acssuschemeng.9b02092.

[18] Xiaodong Jing, Hao Wen, Xuzhong Gong, ZhihongXu, Anna Kajetanowicz, Recycling waste plastics packaging to value-added products by two-stepmicrowave cracking with different heating strategies, Fuel Processing Technology (2020).

[19] E. Bäckström, K. Odelius, M. Hakkarainen, Trash to Treasure: Microwave-Assisted Conversion of Polyethylene to Functional Chemicals, Ind. Eng. Chem. Res. 56 (2017) 14814–14821. https://doi.org/10.1021/acs.iecr.7b04091.

[20] Liangliang Fan, Yaning Zhang, Shiyu Liu, Nan Zhou, Paul Chen, Yuhuan Liu, Yunpu Wang, PengPeng, Yanling Cheng, Min Addy, Hanwu Lei, Roger Ruan, Catalytic upgrading of vapors from microwave-assisted pyrolysis of low-density polyethylene with MgO, Energy Convers. Manag. (2017).

[21] A. Undri, L. Rosi, M. Frediani, P. Frediani, Efficient disposal of waste polyolefins through microwave assisted pyrolysis., Fuel 116 (2014) 662–671.

[22] Y. Chen, W. Wang, Y. Sun, X. Chen, Q. Lin, K. Yang, M. Zhang, L. Sun, X. Zhou, M. Zhang, Insight into metal-support synergistic effect from the perspective of increasing propylene production in catalytic cracking over Au/ZSM-5 catalysts, Microporous and Mesoporous Materials 373 (2024). https://doi.org/10.1016/j.micromeso.2024.113121.

[23] A. Terapalli, D. Kamireddi, V. Sridevi, M. Tukarambai, D.V. Suriapparao, C.S. Rao, R. Gautam, P.R. Modi, Microwave-assisted in-situ catalytic pyrolysis of polystyrene: Analysis of product formation and energy consumption using machine learning approach., Process Saf. Environ. Prot. 166 (2022) 57–67.

[24] Y. Liu, B. Ma, J. Tian, C. Zhao, Coupled conversion of polyethylene and carbon dioxide catalyzed by a zeolite–metal oxide system, Sci. Adv. 10 (2024). https://doi.org/10.1126/sciadv.adn0252.

[25] Liangliang Fan, Zheyang Su, Jiabo Wu, Zhiguo Xiao, Pei Huang, Lei Liu, Haiwei Jiang, Wenguang Zhou, Shiyu Liu, Roger Ruan, Integrating continuous-stirred microwave pyrolysis with ex-situ catalyticupgrading for linear low-density polyethylene conversion: Effects of parameter conditions, Journal of Analytical and Applied Pyrolysis (2021).

CHAPTER – 2

Literature review and characterization techniques

A polymer is a material composed of large molecules (macromolecules) formed through the repeated bonding of small molecular units called monomers. Owing to their wide range of physical and chemical characteristics, both artificial and natural polymers act vital roles in daily life. Examples include widely used synthetic materials such as polystyrene, as well as natural biopolymers like proteins and DNA, that are essential for biological structure and function. It is formed through polymerization, a process in which many small molecules, known as monomers, join together. Due to their much larger molecular weight compared to small molecules, polymers possess unique physical properties, including high elasticity, superior toughness, viscoelastic behavior, and a tendency to form amorphous or semicrystalline structures instead of well-defined crystalline arrangements.

2.1 Classification of Polymers

Polymers are broadly categorized into two major groups: synthetic polymers and natural polymers. Natural polymers are further subdivided into organic and inorganic types based on their chemical composition. Examples of natural organic polymers include Cellulose and Polypeptides, while natural inorganic polymers are represented by Ceramic and Clay.

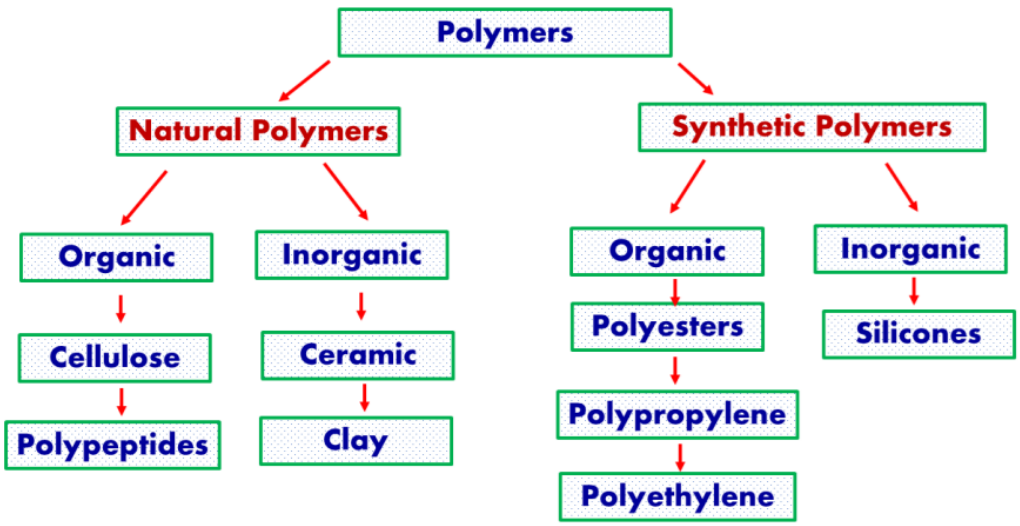

Figure 2.1 Classification of Polymers [1]

Synthetic polymers, similarly, are classified as either organic or inorganic. Synthetic organic polymers shown here are polyesters, polypropylene, and polyethylene. Synthetic inorganic polymers are specifically identified as silicones. Figure 2.1 provides a clear visual overview of the different types of polymers and their respective examples within the two primary classifications.

2.1.1 Natural Polymers

Natural polymeric substances including shellac, hemp, wool, amber, natural rubber, and silk have been utilized for times due to their versatile and sustainable properties. Other natural polymers, such as cellulose, which form the structural basis of wood and paper, also play significant roles in various applications.

Hemp

- Nature & Composition: Hemp fibers are plant-derived natural polymers composed mainly of cellulose.
- Properties: Known for high strength, durability, biodegradability, and low environmental footprint—hemp requires minimal water and no pesticides [2].
- Applications: Used in composites, building materials, textiles, and packaging. Incorporating treated hemp fibers into biopolymers like PLA improves mechanical strength, thermal stability, moisture resistance, and barrier properties for packaging [3].

Shellac

- Nature & Composition: A natural polymer (bio-adhesive), often viewed as a natural plastic. Chemically, composed of aliphatic and alicyclic hydroxy acids, notably aleuritic and shellolic acids.
- Properties: Thermoplastic with a melting point around 75 °C; UV-resistant, doesn’t darken with age. Soluble in alcohol and certain alkaline solutions; can be easily repaired by reapplication [4].
- Applications: Used as a durable, food-safe coating on apples and pills, and as a wood finish. In food industry, it is praised for biodegradability, pH-responsiveness, and biocompatibility, making it promising for edible or protective coatings [5].

Amber

- Nature & Composition: Amber is a fossilized resin formed through free-radical polymerization of diterpene precursors such as communic acid, communol, and biformene. Over time, additional reactions like crosslinking and cyclization enhance its structure.
- Properties: Typically has refractive index 1.5–1.6, hardness of 2.0–2.5 (Mohs), and specific gravity between 1.06 and 1.10. When heated (above ~200 °C), it decomposes to produce "amber varnish" [6].
- Applications: Historically valued as a gemstone and for varnish production, though more of a decorative and historical polymer rather than contemporary industrial use.

Wool

- Nature & Composition: A natural polymer composed primarily of protein keratin.
- Properties: Strong, elastic, biodegradable, and thermally insulating. When blended into bioplastic composites (e.g., with PLA), wool fibers lighten and reinforce material, increasing tensile strength and stiffness, while retaining compatibility with conventional plastic processing machinery.
- Applications: Traditional use in textiles (clothing, carpets). Recently, innovations include wool-reinforced composites used in kayaks, knives, fencing, and other molded products, thereby utilizing waste wool to reduce plastic usage.

Silk

- Nature & Composition: Silk is a protein-based polymer, primarily composed of fibroin (structural) and sericin (glue-like binder). Fibroin chains form beta-sheet structures, contributing to silk's strength and sheen.
- Properties: Smooth texture, natural luster, high tensile strength (although it loses about 20% f its strength when wet), moderate to poor elasticity, good moisture regain (~11%), and high infrared emissivity (feels cool to touch). It's weak to sunlight, perspiration, and certain chemicals (e.g., sulfuric acid, bleach) [7].
- Applications: Predominantly textiles—luxury garments, bedding, etc.—valued for comfort, aesthetic appeal, and strength.

Natural Rubber

- Nature & Composition: Composed of cis-1,4-polyisoprene (cis-polyisoprene), a high-molecular-weight elastomer (100,000–1,000,000 Da), with minor proteins, resins, and fatty acids.
- Properties: Exhibits high elasticity, tensile strength, tear and fatigue resistance, green strength, and tack. Its "strain-induced crystallization" behavior under stress enhances durability, toughness, and heat resistance, especially important in tire sidewalls [8].
- Applications: Vulcanized to improve durability, it's used extensively in tires (vehicles, aircraft), surgical gloves, footwear, anti-vibration mounts, springs, hoses, and various rubber goods.

Cellulose

- Nature & Composition: The most abundant natural polymer, composed of long, unbranched chains of D-glucose units connected through β(1→4) glycosidic linkages. It serves as a key structural material in plant cell walls.
- Properties: Strong and insoluble; decomposes under heat (melting point 500–518 °C). Major constituent of cotton (≈90%), wood (40–50%), and hemp (≈57%).
- Applications: Primarily used for paper and paperboard. Also converted into derivatives like cellophane and rayon. Cellulosic biofuels (e.g., cellulosic ethanol) are under development. Dietary fiber in humans and a key structural polysaccharide in ecology [9].

2.1.2 Synthetic Polymers

Synthetic polymers, which are produced on a massive scale, include widely used materials like polyethylene, polystyrene, polypropylene, synthetic rubber, polyvinyl chloride (PVC), neoprene, phenol-formaldehyde resin (Bakelite), polyacrylonitrile, nylon, silicone, and polyvinyl butyral (PVB), among many others. As of 2015, over 330 million tons of these polymers are produced annually to meet global demand.

Typically, the polymer backbone in plastics is primarily composed of carbon atoms. A classic example is polythene, which is formed through polymerization of ethylene monomers. While carbon is the most common backbone element, other elements like silicon and oxygen are also integral to polymer structures. For example, silicone polymers, found in products like Silly Putty and waterproof sealants, feature silicon-based backbones, while oxygen is a key

component of the backbone's structures of materials such as polysaccharides, polyethylene glycol, and DNA. Several widely used synthetic polymers, along with their properties and applications, are discussed below.

2.1.2.1 Low-density polyethylene

LDPE is a thermoplastic polymer synthesized by ethylene monomers. It represents the earliest form of polyethylene and was first developed in 1933 by M. W. Perrin and John C. Swallow at Imperial Chemical Industries through a high-pressure free-radical polymerization process [10]. LDPE is a lightweight, flexible, and soft plastic known for its excellent flexibility at low temperatures, durability, and resistance to corrosion. However, it is not ideal for applications demanding high stiffness, elevated temperature resistance, or structural strength. LDPE offers strong resistance to chemicals and impacts and is easily shaped and fabricated, making it a versatile material in various industries. LDPE has more branching compared to HDPE, which results in lower tensile strength, weaker intermolecular forces, and higher resilience. Presence of adjacent branches makes the molecules less crystalline and less tightly packed, leading to a reduced density. LDPE exhibits thermal stability from -50°C to 85°C and can withstand temperatures up to 290°C in the absence of oxygen. Beyond this threshold, LDPE starts to decompose into lower-molecular-weight products. At temperatures exceeding 350 °C, the formation of gaseous by-products increases significantly, with butene becoming the dominant component rather than ethylene. In the presence of oxygen, the thermal stability of LDPE decreases. The thermal behavior and decomposition characteristics of LDPE can be evaluated using analytical instruments such as Chip-DSC or STA PT 1000, which measure various thermal properties of the material. Due to its good thermal resistance, LDPE is widely used in routine applications, particularly in cling films production for food preservation. LDPE cling films can tolerate a broad temperature range without significant degradation, helping protect food from moisture and air and thereby extending its shelf life. These films can also be used safely in microwave applications under moderate temperatures without melting or decomposing. In addition, LDPE easily adheres to itself and other surfaces, forming an effective barrier that helps maintain food quality and flavor. LDPE typically has a density in the range of 917–930 kg/m^3 and is generally chemically inert at room temperature, although it may react with strong oxidizing agents and can swell in certain solvents. LDPE is resistant to a variety of chemicals, such as acids, alcohols, bases, and esters. It is highly flexible and can be easily molded into different shapes. Additionally, LDPE is waterproof and moisture-

resistant, serves as a good electrical insulator, and is durable against UV radiation and weathering. It is cost-effective, simple to process, and easy to manufacture. LDPE is commonly used in packaging for food, medical devices, and other consumer products. It is also utilized for manufacturing toys due to its ability to be molded into various shapes and sizes. LDPE is used in plastic wraps to protect and preserve food. Additionally, it is employed in electrical cable insulation and medical products and equipment, where it provides protection against moisture and oxygen. LDPE is also used in cleanrooms to safeguard precision equipment from contamination. LDPE exhibits a glass transition temperature (Tg) of approximately −100 °C, below which it exists in a rigid and brittle state. However, once the temperature exceeds Tg, LDPE transitions into a soft, rubber-like state. The glass Transition Temperature is a crucial factor that affects both the mechanical properties and processability of LDPE, influencing its performance in various applications. LDPE comes in various grades that differ in branching and molecular weight, resulting in products with distinct applications and physical properties.

Several common LDPE-based products along with their characteristic properties are presented below:

Carrier bags: LDPE is widely used for manufacturing shopping and retail carrier bags due to its excellent combination of strength and flexibility. These bags can safely hold a variety of items while remaining lightweight and easy to handle. The low density and low glass transition temperature of LDPE provide high flexibility, allowing the bags to be easily folded and stored. Moreover, LDPE exhibits good tensile strength and tear resistance, which enhances the durability and reliability of the carrier bags during use.

Toys: LDPE is commonly used in the production of children's toys, particularly those that require flexibility, such as bath toys or balls. The material’s chemical resistance ensures that toys are not easily damaged by exposure to water. Moreover, the softness and flexibility of LDPE provide a safer play experience by minimizing the risk of injury, making it an ideal choice for toys designed for young children.

Cable Coverings: It is commonly utilized as a protective material for wires. Its coating helps prevent short circuits and protect conductors from damage. Additionally, its flexibility allows cables to bend easily during installation without the risk of deformation, making it a durable and reliable choice for cable insulation.

LDPE Coatings: LDPE is frequently used as a coating for paper products, such as cold and hot beverage mugs and milk cartons. It provides a moisture-resistant barrier, helping to maintain the integrity of paper and prevent leaks. This makes it an ideal material for packaging liquids, ensuring durability and preventing contamination.

LDPE Bottles: LDPE is commonly utilized for manufacturing container lids, food containers, and squeezing bottles. The material's flexibility and durability make it an ideal choice for these applications, as it allows easy dispensing of contents while providing a strong, leak-resistant seal. Additionally, LDPE's chemical resistance ensures safety and preservation of food items stored within these containers.

Figure 2.2 Schematic of LDPE branching structure [11].

2.1.2.2 High-density polyethylene (HDPE)

HDPE is derived from the polymerization of ethylene and is commonly known as polythene in pipe manufacturing. It is characterized by a high strength-to-density ratio and is widely applied in corrosion-resistant pipes, plastic lumber, geomembranes, and plastic bottles. The density range for HDPE is from 930-970 kg/m^3 and it possesses a predominantly linear molecular structure with very little branching. This structural arrangement results in effective intermolecular interactions and a higher tensile strength compared to LDPE. Although the density difference between HDPE and LDPE is relatively small, the more linear structure of HDPE provides significantly greater specific strength.

It is comparatively harder, opaquer, and capable of withstanding short-term temperatures of up to 120°C. However, unlike polypropylene, it cannot withstand standard autoclaving conditions. The polymer exhibits excellent resistance to solvents, acids, bases, and environmental chemicals, but it is difficult to bond using adhesives and is typically joined by welding. Its

resistance to moisture, mold, and corrosion makes HDPE particularly suitable for underground piping and water delivery systems.

One of the primary applications of HDPE is in blow-molded hollow products such as milk bottles and jugs, which account for nearly one-third of global HDPE production, exceeding 8 million tons annually. HDPE has a relatively high melting point, allowing it to maintain rigidity during use while becoming highly moldable upon melting, enabling the manufacture of diverse products such as cutting boards, food containers, detergent bottles, geomembranes, and plastic lumber.

HDPE is also highly recyclable, contributing to waste reduction and lowering plastic production demand by up to 50%. Its durability, chemical resistance, cost-effectiveness, and environmental benefits make HDPE a preferred alternative to heavier materials in sustainable manufacturing. Common applications include plastic bottles, toys due to their UV resistance, chemical containers, and high-molecular-weight pipe systems capable of operating across a wide temperature range and in harsh chemical environments.

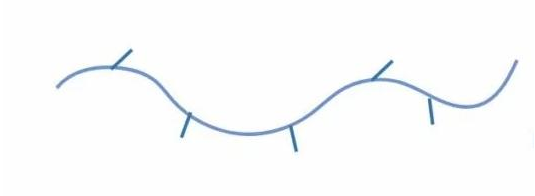

Figure 2.3 Schematic of HDPE structure [12].

2.1.2.3 Polypropylene

Polypropylene (PP) is a widely utilized thermoplastic polymer formed by chain-growth polymerization of propene monomers. It is classified as a polyolefin and is a partially crystalline, non-polar polymer. Although its properties are comparable to those of polyethylene, polypropylene generally exhibits greater stiffness and superior thermal resistance. PP exhibits high mechanical strength and excellent chemical resistance, making it suitable for diverse applications [13]. The polymerization of propylene was first demonstrated in 1951 by J. Paul Hogan and Robert Banks [14], while the discovery of stereoselective polymerization for producing isotactic polypropylene by Giulio Natta and Karl Rehn in 1954 paved the way for its large-scale commercial production starting in 1957. The properties of polypropylene are governed by molecular weight, crystallinity, isotacticity, and comonomer content. In isotactic polypropylene, methyl groups remain aligned on a single side of the

polymer, resulting in high crystallinity, increased stiffness, and superior creep resistance compared to atactic PP and polyethylene. The melting point of isotactic PP is 171 °C, whereas commercial grades typically melt between 160 and 166 °C; syndiotactic PP melts at approximately 130 °C [15]. Below 0 °C, PP becomes brittle. It is resistant to acids, fats, bases, and most organic solvents at room temperature, though it dissolves in non-polar solvents at elevated temperatures. The presence of tertiary carbon atoms in PP makes it slightly less chemically resistive than polyethylene [16].

Polypropylene is extensively used in both flexible and rigid packaging. In flexible packaging, PP films—particularly cast films and biaxially oriented polypropylene (BOPP)—are widely applied in food, tobacco, and clothing packaging due to their puncture resistance, low sealing temperature, durability, and cost-effectiveness. In rigid packaging, PP is used for reusable crates, caps and closures, blow-molded bottles, and thin-walled containers such as yogurt cups.

In the automotive sector, PP is increasingly adopted for dashboards, bumpers, and exterior trims owing to its low thermal expansion, chemical resistance, and favorable impact to stiffness balance. PP is also widely used in consumer products such as housewares, furniture, toys, appliances, battery cases, and luggage, primarily produced by injection molding. Additionally, polypropylene fibers are used in textiles, strapping, non-woven fabrics, and industrial applications including sheets, pipes, and returnable transport packaging. Owing to its versatility, low cost, and balanced mechanical and chemical properties, polypropylene remains one of the most important polymers in modern manufacturing.

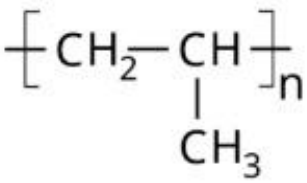

Figure 2.4 Schematic of Polypropylene structure [17].

2.1.2.4 Polystyrene

Polystyrene (PS) is an artificial thermoplastic produced from aromatic styrene and is available in foamed and solid forms. General-purpose polystyrene is brittle, rigid, and transparent, while being inexpensive and easy to process. It has poor barrier properties against air and steam and a relatively low melting point, but it can be easily colored. Common applications include protective packaging (e.g., packing peanuts, optical disc cases), disposable containers and

cutlery, trays, tumblers, and model-making materials. At room temperature, polystyrene remains in a glassy state but becomes moldable above its glass transition temperature of ~100 °C, allowing fabrication by extrusion, molding, and vacuum forming. Its thermal behavior can be further tailored through photo-crosslinking [18]. Polystyrene is chemically stable and waterproof; however, it is readily dissolved by solvents such as acetone and aromatic hydrocarbons. When exposed to high temperatures, PS combusts to produce carbon dioxide, water vapor, and thermal degradation products. Major limitations of polystyrene include brittleness, flammability, softening in boiling water, and yellowing under prolonged UV exposure. To overcome brittleness, over half of commercial polystyrene is modified with 5–10% butadiene rubber to form high-impact polystyrene (HIPS), which offers improved toughness and is widely used in toys and appliance components.

Polystyrene is used in multiple forms, including rigid solids, films, foams (expanded polystyrene, EPS), composites, and copolymers such as ABS, SAN, SBR, and HIPS. EPS is extensively applied for thermal insulation, packaging, and sound dampening, while rigid PS and films are used in food service products, electronics housings, medical items (Petri dishes and test tubes), and consumer goods. In the construction and automotive sectors, polystyrene and its copolymers are employed for insulation, protective components, and lightweight structural parts. Owing to its versatility, low cost, and wide range of physical forms, polystyrene remains an important polymer for both every day and industrial applications.

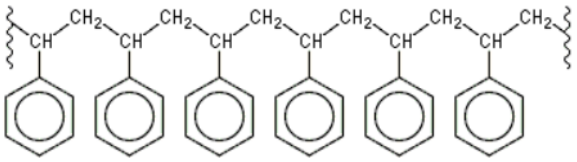

Figure 2.5 Schematic of polystyrene structure [19].

2.1.2.5 Polyvinyl chloride

The annual production of polyvinyl chloride (PVC) is about 40 million tons. PVC is available in rigid and flexible forms. It was first synthesized in the 19th century, but its commercial breakthrough occurred in 1926 when Waldo L. Semon developed plasticized PVC at B.F. Goodrich, enabling flexibility and inertness. This advancement led to widespread industrial adoption, including early applications such as wire insulation and coated fabrics. Rigid PVC is extensively used in construction materials such as pipes, windows, doors, bottles, and cards, while plasticized PVC is employed in flooring, cable insulation, signage, inflatable products,

and as a rubber substitute [20]. PVC is a thermoplastic polymer known for its excellent resistance to alkalis, salts, and polar solvents. The presence of chlorine in its structure imparts inherent flame-retardant properties; however, PVC exhibits limited thermal stability at elevated temperatures and can degrade under excessive heat. In the motorized sector, PVC is utilized for internal linings, floor coatings, and electrical insulation due to its flexibility, flame resistance, high gloss, and ease of processing, including printing and welding [21].

Approximately 50% of global PVC production is used for pipe manufacturing in municipal and industrial applications. In the U.S. residential sector, PVC accounts for nearly two-thirds of household piping, particularly in sanitary sewer systems, where gasket-sealed joints such as the Rieber system are commonly used [22]. PVC is also widely applied as electrical cable insulation because of its fire resistance, electrical insulation capability, and ease of extrusion. During combustion, PVC releases hydrogen chloride, which suppresses flame propagation, although the fumes require careful handling [23].

In the construction industry, PVC is favored for siding, window frames, gutters, and drainage systems due to its durability, weather resistance, and low maintenance requirements, often replacing traditional materials such as wood and cast iron [24].

Additionally, PVC sheets and films are extensively used in signage, graphics, and advertising applications, including vehicle wraps and vinyl decals. Plasticized PVC fabrics are utilized in clothing and protective gear for their water and weather resistance. In healthcare, PVC is indispensable for single-use medical devices such as blood bags, tubing, catheters, and dialysis equipment, accounting for nearly one-third of plastic-based medical devices in Europe. PVC is also widely used in food packaging applications, including bottles, blister packs, cling films, and seals, owing to its versatility and protective properties [25].

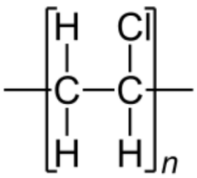

Figure 2.6 Polyvinyl chloride structure [26].

2.2 Methods to treat polymer waste

Treatment methods for polymer waste can be broadly categorized into three main processes. First is recycling, which involves reprocessing plastic waste into new products to reduce the consumption of virgin materials. The second category is thermal transformation, which includes methods such as gasification and pyrolysis. Gasification converts plastic waste into syngas through partial oxidation at high temperatures, while pyrolysis breaks down polymers in the absence of oxygen to produce fuels and valuable chemicals. The third type is biological transformation, which uses microorganisms or enzymes to degrade polymers into simpler, environmentally friendly compounds as shown in Figure 2.7.

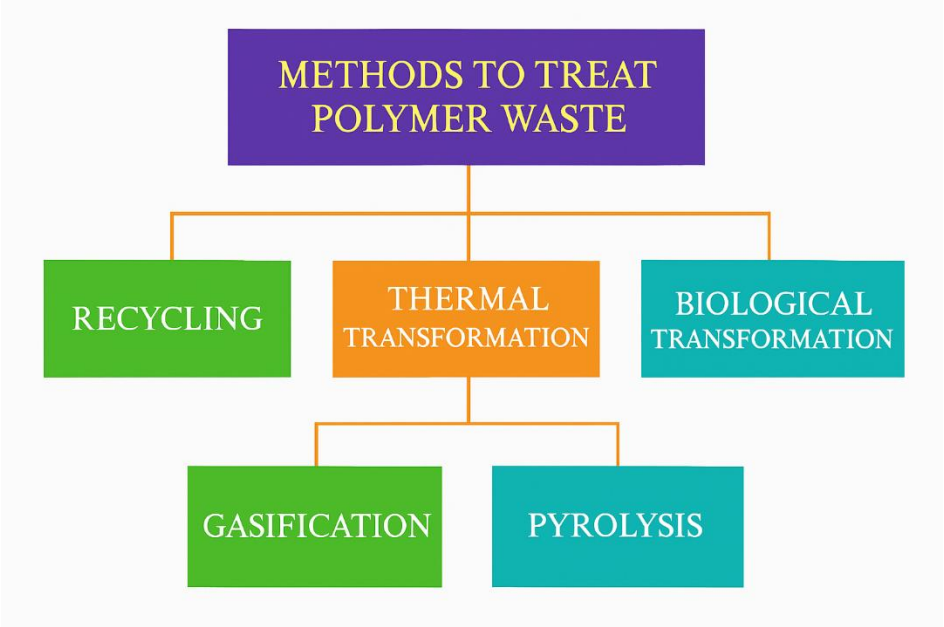

Figure 2.7 Polymer treatment methods

2.2.1 Recycling

Plastic is a widely used and highly versatile material, and its extensive use is evident in many aspects of our daily lives. By reusing and recycling plastic items as much as possible, we can significantly reduce demand for new plastic production.

This approach contributes to:

- Conserving non-renewable fossil resources, such as petroleum
- Reducing the energy demand associated with the production of virgin plastics
- Decreasing the volume of solid waste disposed of in landfills
- Mitigating the emission of greenhouse gases, particularly carbon dioxide, into the atmosphere.

Recycling and reusing plastic are critical steps toward a more sustainable future, benefiting both the environment and natural resources. LDPE is recyclable, and many facilities accept it for processing. Once recycled, LDPE is commonly transformed into products like plastic bags, trash liners, and agricultural films. However, the recycling rate for LDPE remains relatively low, with only about 8% of LDPE being recycled in the United States, compared to other types of plastic. Recycling LDPE plays a vital role in sustainable waste management. It helps reduce plastic waste that would otherwise end up in landfills and the environment, while also conserving valuable resources by providing recycled material for new product manufacturing. Recycling rates differ depending on the type of plastic. Various plastics are commonly used, each with unique chemical and physical characteristics. These differences influence sorting and reprocessing expenses, which in turn impact value and market demand for recycled materials [27]. PET and HDPE have highest recycling rates, while polystyrene and polyurethane are seldom recycled [28]. The steps involved in plastic recycling are as follows:

Collection

The collection of plastic for recycling depends largely on how individuals, businesses, and restaurants dispose of their waste. When plastic is discarded in regular trash bins, it becomes unsuitable for recycling. Therefore, proper segregation of plastic waste from general waste is essential.

Sorting

After collection, plastic waste is transported to a recycling facility where it undergoes sorting. At this stage, machines separate plastics according to their properties and the intended end product. The materials are typically classified based on type, colour, or manufacturing process. This sorting step is crucial, as different types of plastics require distinct processing techniques, and many recycling facilities are equipped to handle only specific categories of plastic.

Washing

After sorting, plastic is cleaned to eliminate impurities like adhesives and labels. This step is vital for ensuring the characteristic of the product. If other contaminants are not eliminated, they may compromise the structural integrity of final material.

Shredding

Plastic is then fed into conveyor belts that guide the material through shredders, breaking plastic into small pellets. This process increases the surface area, making material easier to reshape, process, and transport. Metal detectors are employed to eliminate any remaining metal fragments.

Melting

Shredded plastic is dried and then melted to form the desired shape or to be processed into granules. Special equipment ensures plastic is melted at the right temperature to prevent damage.

Identification

During this stage, small plastic particles are analyzed to determine their properties and classification. Initially the test checks the density of particles by submerging them in a water tank: denser particles sink, while lighter ones float. The next test involves air classification, where particles are dropped into a wind tunnel. Larger particles stay lower, while smaller ones rise higher. Samples from each batch are also tested for melting point and colour.

Extruding

In the final stage, chopped plastic is melted and extruded into small pellets, which can subsequently be used as raw material for the manufacture of new plastic products.

Figure 2.8 Plastic recycling stages [29].

2.2.2 Thermal Transformation

2.2.2.1 Gasification

Gasification is a promising thermochemical technology for converting organic compounds into fuel gases or syngas. This process typically takes place at high temperatures ranging from 800°C to 1000°C, involving partial oxidation with air, steam, or oxygen. The process can be finely adjusted to generate specific gases with targeted properties, positioning it as a valuable method for creating tailored synthetic gas mixtures [30]. Gasification of plastic waste offers

several key advantages compared to other waste disposal methods. The most notable benefit is its ability to reduce waste volume by up to 90%, leading to a significant decrease in land area required for landfills and a reduction in the resources needed for waste transportation. Furthermore, gasification can be leveraged to produce energy, adding another layer of value to this waste management approach. Gas generated during the gasification process consists of combustible gases like H_2, CO, CH_4, CO_2, N_2, and various smaller hydrocarbon compounds. This gasification process can be harnessed to produce electricity, generate transportation fuels like diesel and ethanol, or manufacture chemicals for industrial applications [31]. Advantages of Plastic Gasification are:

1. Waste Reduction: Gasification significantly reduces the volume of plastic waste, making it more manageable and easing strain on waste management systems.

2. Energy Recovery: Syngas produced during gasification can be utilized to generate energy, helping to decrease our dependence on fossil fuels.

3. Resource Recovery: Gasification can transform plastic waste into valuable by-products, such as syngas and other chemicals, which can be further used in various industrial processes.

4. Environmental Benefits: Compared to traditional waste disposal methods like landfilling or incineration, gasification offers a more environmentally friendly alternative, as it reduces pollution and minimizes waste accumulation.

Challenges of Plastic Gasification:

1. High Temperatures: The gasification process requires extremely high temperatures, which can be energy-intensive and may lead to higher operational costs.

2. Syngas Cleaning: Syngas produced by gasification can contain impurities that must be effectively cleaned before it can be used in specific applications, adding an extra step to the process.

3. Process Optimization: To make gasification more cost-effective and efficient, ongoing efforts are needed to optimize technology and ensure it operates at its optimal performance.

❖ Types of Gasifiers

Gasifiers are categorized into fluidized bed, fixed bed, and spouted bed types based on how gas and fuel interact. Regardless of gasifier type, gasification process includes steps such as drying, devolatilization, combustion, and gasification. However, sequence of these steps may vary depending on the path and place of the gasifying agent.

➢ Fixed/Moving Bed Gasifier

It is further categorized into (i) downdraft, (ii) updraft, and (iii) cross draft based on direction of gasifying agent. In a downdraft gasifier, gasifying agent, fuel, and product gas entirely proceed downward, with created gas being withdrawn from tail. Process follows sequence of drying, pyrolysis, combustion, and gasification. In an updraft gasifier, feedstock moves counter to gasifying agent, passing via pyrolysis, drying, combustion, and gasification zones in sequence. This configuration offers benefits such as simplicity, high char burnout, excellent heat exchange, efficient thermal energy use, and low exit temperature. In a cross-draft gasifier, feed is introduced from top, and combustion zone, gas injection point, syngas exit, and reduction zone all lie on equal horizontal plane [32].

➢ Fluidized Bed Gasifier

In this type of gasifier, solid fuel is gasified within a bed of minor inert elements, typically sand, using gasifying agents such as oxygen, air, CO_2, steam, or their combinations. The gasifier operates under conditions where the upward flow of the gasifying agent causes the solid bed to behave like a fluid, creating a highly dynamic reaction environment. This type of gasifier offers several advantages, including high throughput, enhanced gas–solid reactions, improved residence time, better char conversion, and better heat and mass transfer, resulting in the production of high-calorific-value gas. The excellent mixing between gas and solid particles and the uniform temperature distribution further make fluidized bed gasifiers highly suitable for plastic waste gasification. Fluidized bed gasifiers are generally classified into bubbling fluidized beds (BFB) and circulating fluidized beds (CFB), with the primary distinction between them being the fluidization velocity [32].

Table 2.1 Comparative analysis of various gasifying agents [32].

Gasifying Agent	Advantages	Constraint	Product gas
Air	Ease of use plus affordability.	Weak syngas, gas with low calorific value, and potential for NOx formation.	A considerable amount of N_2 is present in product gas.
Oxygen	It provides a higher calorific value and cleaner gas product compared to air, boosts combustion reactions in gasification, and lowers cost of preheating reactor.	Producing pure oxygen is costly and energy demanding.	It increases formation of combustible gases while decreasing N_2 content in syngas.
Steam	Improvement in gas quality and heating value, along with better reforming and water-gas shift reactions.	It requires an external heating and steam generation plant, making it potentially energy intensive. Additionally, it can result in higher formation of tar related to oxygen and air	Syngas with higher concentrations of H_2 and CO.
CO_2	Direct conversion of greenhouse gases (CO_2), while also improving variation of H_2/CO proportion for different uses.	It requires external heating and catalytic reforming of tar.	Syngas enriched with CO.

- Spouted Bed Gasifier

Key variation amongst a fluidized bed and a spouted bed lies in dynamical actions of solid elements. In a fluidized bed, gas is delivered over a multi-orifice distributor, while in a spouted bed, gasifying medium is directed up via a single, centrally placed orifice at base. Major benefits of spouted beds over fluidized beds include capacity to mix feeds that are coarse, sticky, heat sensitive, or uniform in size [32].

2.2.2.2 Pyrolysis

LDPE remains thermally stable within the range of -50°C to 85°C. In the absence of oxygen, it can withstand temperatures up to 290°C. However, when exposed to temperatures beyond this threshold, LDPE begins to decompose, breaking down into lower molecular weight thermoplastic materials. Pyrolysis is a widely used technique for transforming plastic discarded into valuable energy, producing liquid, gaseous, and solid fuels. This process involves the decomposition of plastic at temperatures ranging from 300°C to 900°C, conducted in an oxygen-free environment, resulting in the production of liquid oil [33]. The pyrolysis types are: (1) flash pyrolysis, (2) fast pyrolysis, and (3) slow pyrolysis. Table 2.2 provides a comparison of these processes based on temperature, residence time, heating rate, and the products they produce [34]. Slow pyrolysis is primarily used to alter solid materials, with a focus on minimizing oil production. In contrast, fast pyrolysis and flash pyrolysis aim to maximize the production of gases and oil. Fast pyrolysis involves fast thermal breakdown of plastic waste in the absence of oxygen, using moderate heating rates. This method is widely employed, both in practical applications and research, with bio-oil being the primary product. Flash pyrolysis is a high instant thermal degradation process that uses an extremely high heating rate. The primary products of this method are bio-oil and gases [34]. Advantages of plastic waste pyrolysis are:

1. Waste decline: Pyrolysis facilitates to decrease size of waste sent to landfills or incinerators, providing an alternative method of disposal.

2. Resource Recovery: Pyrolysis enables the recovery of valuable resources, such as fuels and chemicals, from plastic waste, turning discarded materials into usable products.

3. Energy Generation: Pyrolysis oil and gases produced can be used as alternative fuels.

4. Circular Economy: It supports the circular economy by converting plastics into valuable products, preventing them from being treated solely as waste and promoting sustainability.

Challenges and Considerations:

1. Energy Intensity: The pyrolysis process requires significant energy input to reach the high temperatures necessary for breaking down plastic waste, which can increase operational costs.

2. Environmental Concerns: The process may emit gases like SO_2, CO, and NO_x, raising concerns about air quality and potential environmental impact.

3. Product Quality: The quality and composition of pyrolysis products can vary depending on the type of plastic feedstock used and conditions during the pyrolysis process, potentially affecting marketability of outputs.

4. Contaminants: Plastic waste may contain contaminants like metals or chlorine-based compounds, which can complicate the pyrolysis process and require careful management to avoid harmful effects.

5. Economic Viability: The economic feasibility of pyrolysis plants depends on various factors, including the cost of feedstock, energy consumption, and market value of products derived from pyrolysis.

6. Regulatory Framework: Clear and supportive regulations and policies are essential to enable the growth and adoption of pyrolysis technologies for plastic waste management, ensuring they are implemented in an environmentally responsible and economically sustainable manner.

Table 2.2 compares flash, fast, and slow pyrolysis in terms of residence time, temperature range, heating rate, and major products formed.

Table 2.2: Comparison of pyrolysis types based on operating conditions and main products.

Process	Temperature (°C)	Residence Time	Rate of heating (°C/s)	Chief products
Slow pyrolysis	400-500	5-30 min	10	bio-oil (tar), gases, and char
Fast pyrolysis	400-650	0.5-2 s	100	Liquid bio-oil (less viscous), gases, and char
Flash pyrolysis	700-1000	< 0.5 s	>500	Mainly bio-oil and gases

Type of pyrolysis reactors

2.2.2.2.1 Batch reactor

A batch reactor is a closed system where reactants are placed in a reactor without any inflow or outflow of materials during the reaction process. One of the key advantages of a batch reactor is its capability to attain elevated conversion rates. There are several disadvantages to this system, including variability in product quality from one lot to next, high labor costs, and challenges in scaling up for large-scale production [35]. Onwudili et al. [36] conducted pyrolysis of polystyrene and polyethylene and found that the highest liquid yield from LDPE occurred at 425°C in a batch reactor. At this temperature, the liquid product was composed primarily of both long-chain and short-chain hydrocarbons. However, when the temperature was raised to 450°C and 500°C, the oils had higher proportions of gasoline and diesel compounds, alongside increased quantities of char and hydrocarbon gases. Even with a very low residence time, LDPE was completely decomposed, yielding a significant amount of oil at 450°C. Prolonged pyrolysis times changed the oil composition, resulting in higher concentrations of aromatic compounds and lighter fractions. In contrast, polystyrene (PS) began to degrade at approximately 350°C, primarily producing viscous oil. Char formation only showed a slight increase until 425°C and then significantly surged at 450°C and 500°C, turning up to 30 wt.%. Even at 350°C, the oil produced from PS was predominantly made up of aromatic compounds, particularly toluene, ethylbenzene, and styrene.

2.2.2.2.2 Fixed and fluidized bed reactor

In this reactor, the catalyst is generally pelletized and packed into a stationary bed through which the reactants pass. While this design is relatively simple, it has certain limitations. For example, the irregular size and shape of plastic feedstock particles can pose challenges during the feeding process. Additionally, the available catalyst surface area accessible to the reactants is restricted, which may reduce the overall efficiency of the reaction. Choi et al. [37] concluded that a fluidized-bed reactor efficiently transformed PP and ABS wastes into fuel, yielding a higher proportion of low and medium fractions (C_5–C_{22}, 89.17% for ABS) compared to a fixed-bed reactor, which yielded 84.7%. For LDPE and PP, both reactors produced similar yields of C_5–C_{22} products. However, for LDPE, a pyrolysis temperature of 520°C was insufficient to fully convert the material into fuel, leading to a predominance of heavy oil (approximately 67.4%). The results showed that oil from ABS pyrolysis mainly contained olefins, aromatic

hydrocarbons, and aromatic nitrogen-containing compounds, whereas oil from PP pyrolysis was largely composed of paraffins, olefins, and oxygenated compounds.

2.2.2.2.3 Conical spouted bed reactor (CSBR)

The CSBR offers superb mixing capabilities and is particularly effective in handling a broad range of element sizes, including larger elements and variations in element densities. This makes it a versatile option for processes that require efficient mixing and the ability to manage diverse feedstock [35]. Agglomeration issues are minimal in this reactor, thanks to excellent gas-solid contact in the spouted bed and intense particle motion facilitated by the reactor's conical geometry [38]. Arabiourrutia et al. [39] observed that during pyrolysis of polyolefins in a Conical Spouted Bed Reactor at 700°C, the wax yield was significantly reduced, while the gas proportion, primarily composed of alkenes such as propene, ethene, and butene, becomes dominant product, accounting for around 40 wt.%. This shift is attributed to cracking reactions that are favored at high temperatures. In the case of catalytic pyrolysis, the product distribution was notably altered. The wax fraction diminishes sharply due to cracking reactions induced by zeolite catalysts (Hβ, HZSM-5, and HY). When the HZSM-5 catalyst was used, olefins emerged as the primary fraction, while the non-aromatic C_5–C_{11} fraction became the predominant product when HY and Hβ zeolite catalysts were employed. Orozco et al. [40] investigated HDPE conversion into valuable products using spent FCC catalysts via fast pyrolysis in a CSBR. The CSBR facilitates continuous plastic feed without defluidization issues, making it particularly well-suited for catalytic cracking. Notably, elevated catalyst action was marked, and the waxes yield became small at temperatures beyond 550°C. The primary product composition from catalytic pyrolysis consisted of C_5–C_{11} hydrocarbons, with alkenes being predominant components. However, the olefins yield reduced as both residence time and temperature increased, because of various reactions such as hydrogen transfer, cracking, aromatization, and cyclization, which resulted in the formation of light hydrocarbons, paraffins, and aromatics.

2.2.2.2.4 Microwave-assisted technology

Microwave heating fundamentally differs from conventional heating because electromagnetic energy is absorbed directly by materials with suitable dielectric properties rather than being transferred from an external heat source [41]. Since LDPE has a low dielectric loss factor and absorbs microwaves poorly, graphite is used as a microwave susceptor to initiate rapid heating. Owing to its high dielectric loss, graphite efficiently converts microwave energy into heat,

generating localized hot spots that accelerate polymer chain scission and enhance contact between molten LDPE and the catalyst [42]. In heterogeneous catalytic systems, microwave irradiation also produces selective heating, where catalyst particles and graphite attain higher local temperatures than the surrounding polymer [43]. This promotes catalytic cracking, improves energy utilization, shortens reaction time, and enhances hydrogen and valuable hydrocarbon production compared with conventional thermal pyrolysis.

Current advancements in microwave equipment have introduced a promising approach for plastic waste recovery through pyrolysis. In this technique, microwave-absorbing substances, like carbon, are blended with plastic feedstock. The absorber captures microwave energy and converts it into thermal energy, generating the high temperatures required to efficiently initiate and sustain the pyrolysis reaction [44]. Replacing traditional heating with microwave-based heating enables more uniform volumetric heating of the plastic material as shown in Figure 2.9.

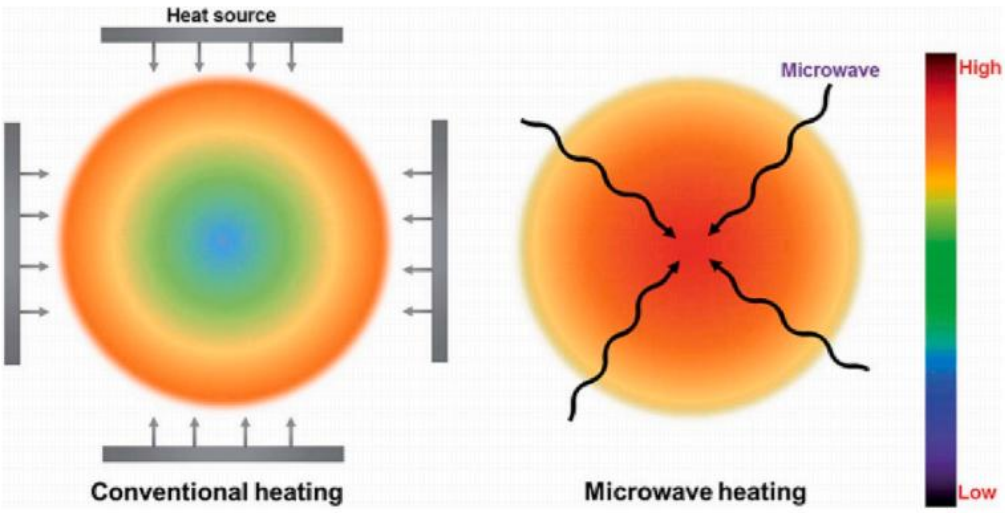

Figure 2.9 Temperature profiles in microwave and conventional heating methods [47].

This approach results in a more uniform product distribution and reduces mass transfer limitations. Consequently, reactions can proceed more rapidly, at reduced temperatures, and with enhanced selectivity [45]. Additionally, microwaves are capable of penetrating solid materials, enabling volumetric heating, unlike conventional heating methods that primarily heat the material from the surface. Jing et al. developed a two-step microwave cracking process to convert waste plastic packaging into valuable products. In the first step, the process generated wax (38–72 wt.%), gas (20–43 wt.%), and solid residues (2–24 wt.%). In the second

step, the product distribution shifted to liquid (60–79 wt.%), gas (18–38 wt.%), and solid (1–5 wt.%) phases. Commercial spherical activated carbon, columnar activated carbon, and 4A molecular sieves were used as absorbers and catalysts throughout the process. Gaseous products primarily consisted of H_2, CH_4, C_2H_4, and C_3H_6, while liquid products were predominantly composed of hydrocarbons ranging from C_7 to C_{26} [46]. Fan et al. designed a continuous stirred microwave pyrolysis (CSMP) reactor for converting LLDPE and compared its performance with batch microwave pyrolysis (BMP) under identical conditions. The continuous stirred system produced a greater volume of liquid with better selectivity for longer chains (C_{14}–C_{20}). In contrast, the batch system showed a stronger preference for gas products, particularly methane, in higher proportions [48]. Fan et al. developed a continuous process for converting LLDPE into valuable chemicals using a CSMP reactor followed by catalytic upgrading. Non-catalytic pyrolysis in the continuous reactor produced up to 84 wt.% liquids, including about 20% gasoline-range hydrocarbons. When the vapors were upgraded over HZSM-5, enhanced aromatization and cracking reactions significantly enhanced the yield of gaseous products and gasoline-range hydrocarbons. Increasing the feed rate resulted in greater formation of heavier hydrocarbons and char. The gaseous products were mainly composed of H_2 and C_1–C_4 hydrocarbons; ethylene dominated in the non-catalytic process, whereas propylene became the major component during catalytic upgrading [49].

Table 2.3: Products of cracking of plastics are as follows [50].

	Products		
	Gas	**Oil**	**Char**
Composition	Process generates combustible gases, including H_2, carbon monoxide (CO), acetylene (C_2H_2), methane (CH_4), ethylene (C_2H_4), ethane (C_2H_6), and others.	Process results in a complex mixture of various organic compounds, along with inorganic species, which can vary depending on composition of feed material.	Elemental carbon is produced during thermal decomposition of organic components and unconverted organic compounds, such as additives, within feed material.
Uses	Produced fuels can be used for direct firing in boilers, gas turbines, and engines, as well as in syngas applications.	Process can also lead to production of diesel engine fuels, as well as creation of chemicals and resins.	Process can yield solid fuels for boilers, as well as serve as feedstock for producing activated carbon, carbon nanofilaments, and high-surface-area catalysts.

2.2.3 Biological Transformation

Microorganisms, including fungi and bacteria, perform a crucial part in the degradation of both natural and synthetic plastics. Microorganisms facilitate microplastic depolymerization (MPs) by producing free radicals and extracellular enzymes that catalytically break down plastics into minute components. This microbial decomposition process involves the breakdown of polymer chains into smaller segments such as monomers, dimers, and oligomers. These small polymer fragments undergo further depolymerization into monomers, which are necessary for microbial uptake and growth. These monomers can diffuse through semi-permeable cell membranes and are subsequently mineralized within microbial cells. Once inside the cells, the monomers are mineralized into CO_2 and H_2O under aerobic conditions, while under anaerobic conditions they are converted into CO_2, H_2O, and CH_4, thereby contributing to biomass formation and energy production [51]. In general, the biodegradability of a polymer decreases as its molecular weight increases. Conversely, smaller molecules such as dimers, monomers, and oligomers derived from the polymer's repeating units are more readily degraded and mineralized by microorganisms. Polymers with high molecular weight have lower solubility, making them less accessible for microbial degradation. This is because bacteria need the substrate to be absorbed through the cellular membrane before it can be further broken down by intracellular enzymes. Biodegradation is influenced by several factors, including the characteristics of the polymer, the type of microorganism involved, and the nature of any pretreatment applied. Key polymer characteristics that affect degradation include its degree of crystallinity, mobility, molecular weight, tacticity, the presence of substituents and functional groups in its structure, as well as any plasticizers or additives incorporated into the polymer. All these elements significantly contribute to how effectively the polymer will degrade [52]. Despite its potential, bio-upcycling faces significant challenges, including high operating costs, particularly those associated with enzyme production, time-consuming processing, and low substrate loading [53].

Enzymes Involved:

Microorganisms produce several types of enzymes, such as cutinases, esterases, lipases, and laccases, to break down plastics. Among these, cutinases and laccases are particularly important in degrading polyethylene terephthalate (PET). These enzymes interact with the plastic surface through hydrophobic interactions, enabling them to cleave polymer chains, thereby facilitating the breakdown of the material.

Types of Microorganisms Involved:

Various bacteria and fungi, including species from the genera Pseudomonas, Escherichia, and Bacillus, have been identified as capable of degrading plastics. These microorganisms can be found in a range of environments, including contaminated sites such as landfills, where plastic waste is prevalent.

Factors Affecting Biodegradation:

Biodegradability of plastics is influenced by several factors, including:

- Plastic Type and Structure: The specific type of plastic, its crystallinity, molecular weight, and the presence of additives can significantly impact how easily it can be degraded.
- Environmental Conditions: Parameters such as pH, temperature, and the presence of other microorganisms influence the rate and efficiency of the biodegradation process.

Potential Applications:

Biological degradation of plastics holds great promise for plastic waste management and recycling. Some potential applications include:

- Bioplastics Production: Degradation products from plastic biodegradation can be used to create bioplastics or other valuable chemicals.
- Bio recycling: This process utilizes enzymes to break down plastics, potentially producing high-quality recycled materials, which can be reused in various applications, the reducing need for new plastic production.

2.3 Effect of parameters

Process parameters play a critical part in optimizing both the composition and the yield of products in various conversion processes. In plastic pyrolysis, important factors like pressure, temperature, residence time, catalysts, and reactor type significantly influence the formation and distribution of final products, including liquid oil and gaseous fractions.

2.3.1 Temperature

Temperature plays a crucial part in the pyrolysis of plastic waste, as it strongly influences the formation of desired products. In the pyrolysis of LDPE, Marcilla et al. [54] found that a small volume of oil began to form at temperatures ranging from 360 to 385°C. The highest oil yield was obtained at temperatures between 469 and 494°C. Thermal pyrolysis of diverse plastics reveals that at lower temperatures (460 °C), the process results in a higher proportion of viscous liquids containing long hydrocarbon chains in a semi-batch reactor. In contrast, at 600 °C, the liquid produced has a lower yield but is richer in aromatic compounds [55]. Research indicates that 500 °C is optimal for pyrolyzing plastic waste, as it offers best balance between conversion efficiency and product quality [55]. For high-density polyethylene resin, pyrolysis at temperatures of 400, 425, and 450 °C yields oil amounts of 22.5, 27, and 40.5 L, respectively, with 450 °C producing the highest quality pyrolysis oil [56]. When mixed waste plastics are pyrolyzed, complete conversion is achieved, resulting in a maximum pyrolysis oil yield of 32.80%, a gaseous product yield of 65.75%, and solid a residue of just 1.46% at 500 °C in a fixed-bed reactor [57]. Similarly, when polystyrene is pyrolyzed, the highest liquid yield occurs at 500 °C, while temperatures below this produce more wax, and those above generate significantly more gas [57].

2.3.2 Catalyst

The catalyst also plays a vital role in the pyrolysis process by lowering both the reaction temperature and the retention time, while also enhancing product selectivity. Different researchers have explored catalysts such as NiO, HY, ZSM-5, and MgO to obtain valuable products like H_2, aromatics, and fuels [58–60]. Artetxe et al. [61] demonstrated that the SiO_2/Al_2O_3 ratio in HZSM-5 zeolite significantly influences the yield of product fractions during pyrolysis of HDPE. A lesser SiO_2/Al_2O_3 proportion correlates with better acidity in zeolite. The catalyst with higher acidity ($SiO_2/Al_2O_3 = 30$) demonstrated higher activity in wax cracking, leading to enhanced formation of low-carbon olefins and a reduction in the heavier C_{12}–C_{20} fraction, compared with the less acidic catalyst ($SiO_2/Al_2O_3 = 280$). Decreasing the SiO_2/Al_2O_3 proportion from 280 to 30 increased the yield of light olefins from 35 to 58 wt.%, while the C_{12}–C_{20} fraction decreased from 28 to 5 wt.%. Aguado et al. [62] studied LDPE conversion using a double-stage reaction process, which included both fixed-bed and batch reactors. In this process, thermal cracking of the plastic occurred in the batch reactors, while the generated vapors were directed to the fixed-bed reactor containing 10 wt.% HZSM-5 catalyst. The results showed that catalytic reforming over the zeolite catalyst significantly

enhanced the gas fraction (74 wt.%) at 475 °C, while the liquid hydrocarbon yield was only 21 wt.%. Table 2.4 presents a comparative analysis of thermal and catalytic pyrolysis of LDPE in terms of process conditions, reaction mechanisms, product selectivity, advantages, and limitations. It highlights how catalytic pyrolysis offers lower operating temperatures, higher selectivity, and faster reaction rates compared to thermal pyrolysis, owing to the presence of active sites and enhanced microwave absorption.

Table 2.4: Comparison of thermal and catalytic pyrolysis of LDPE: Process Parameters, Advantages, and Limitations.

Parameter	**Thermal Pyrolysis**	**Catalytic Pyrolysis**
Operating Temperature	450–800 °C	300–550 °C
Activation Energy	High — bond breaking driven purely by heat	Lower — catalyst active sites assist bond scission
Reaction Mechanism	Free-radical random scission of C–C bonds	Carbocation mechanism (acid sites) or metal-catalyzed dehydrogenation/hydrogenation
Selectivity	Low — broad product range, heavy waxes common	High — products tuned towards aromatics, light olefins, or H_2 depending on catalyst
Product Composition	Gas, liquid (waxes, paraffins, olefins), char	Gas rich in H_2 and light hydrocarbons; liquids enriched in aromatics and light olefins; less char
Energy Demand	High due to higher temperature	Lower due to reduced temperature
Reaction Rate	Slower	Faster due to active sites and microwave absorption
Coke Formation	High — can foul reactor surfaces	Lower (metal catalysts can gasify coke), but still possible
Advantages	Simple process; no catalyst cost	Lower temperature, higher selectivity, shorter reaction time, more valuable products
Limitations	High energy consumption, low selectivity, heavy wax formation, severe coking	Catalyst deactivation (coke), cost of catalyst, potential over-cracking if too active

Table 2.5 summarizes the mechanistic differences in reaction pathways between thermal and catalytic pyrolysis of LDPE. Thermal pyrolysis of LDPE proceeds through random C–C bond scission at high temperatures, generating free radicals that undergo uncontrolled secondary reactions, resulting in a wide distribution of products with significant wax and coke formation. Product selectivity is limited because the process is governed solely by heat, leading to heavy liquids and lower-value hydrocarbons.

In contrast, catalytic pyrolysis involves adsorption of polymer chains on acidic and metal active sites, which lowers the activation energy and directs bond cleavage through controlled β-scission and carbocation mechanisms. Acid sites enhance cracking, isomerization, and aromatization, while metal sites promote dehydrogenation and hydrogen transfer, increasing the formation of hydrogen, light olefins, and aromatics. Consequently, catalytic pyrolysis yields a more tailored product distribution, reduced wax and coke formation, and improved overall process efficiency compared with thermal pyrolysis.

Table 2.5: Reaction pathway differences among catalytic and thermal Pyrolysis of LDPE.

Step	Thermal pyrolysis pathway	Catalytic pyrolysis pathway
Initiation	Heat (>450 °C) breaks random C–C bonds in LDPE → formation of long-chain macroradicals.	Polymer adsorbs on catalyst surface (acid/metal sites) → heat + active sites facilitate targeted bond cleavage.
Primary Chain Scission	Random scission produces a wide distribution of long and short radicals.	Controlled β-scission at weaker bonds → shorter, more uniform hydrocarbon fragments.
Radical Reactions	Radicals undergo hydrogen abstraction or recombination → formation of paraffins, olefins, and waxes.	Acid sites promote carbocation formation; metal sites promote dehydrogenation → favors aromatics, light olefins, and H_2.
Secondary Reactions	At high temperature, secondary cracking produces smaller molecules, but also excessive coke.	Zeolite acidity → aromatization, isomerization; metals → hydrogenation/dehydrogenation; less coke due to hydrogen transfer.
Product Formation	Broad mix of gases, liquids (often heavy), and char; high wax content.	Tuned product profile: high-value gases (H_2, C_2H_4), aromatics-rich liquids, minimal heavy wax.
Coke Formation	Random radical recombination leads to carbonaceous deposits on reactor walls.	Coke mainly forms on catalyst surface; can be minimized via regeneration or by using coke-resistant catalysts (e.g., Ni, Fe).

To provide a comparative overview, Table 2.6 summarizes selected studies on polymer pyrolysis and related catalytic systems. Extensive studies on microwave-assisted pyrolysis of plastic waste confirm that catalyst properties such as acidity, pore structure, metal functionality, and support characteristics critically govern product yield and selectivity. Ding et al. [58] demonstrated that HY zeolite significantly enhances gasoline-range hydrocarbon production, yielding up to 56.54 wt.% oil at 500 °C, while also improving the octane number due to enhanced aromatization. The large pore size and high acidity of HY facilitate cracking of long polymer chains and secondary reactions leading to high-octane gasoline components.

Incorporation of metal species further improves catalytic performance through bifunctional metal–acid synergy. The addition of NiO to HY increased the formation of high-octane substances without reducing liquid yield [58], while Zn-promoted HZSM-5 significantly increased hydrogen selectivity (32.8 vol%) and aromatic content (93.5%) by enhancing dehydrogenation at Lewis acid sites [63]. These results highlight the role of metal sites in promoting hydrogen abstraction, β-scission, and aromatization reactions during microwave-assisted pyrolysis.

Catalyst acidity strongly influences product distribution. ZSM-5, owing to its high acidity and medium pore size, favors the formation of gasoline-range hydrocarbons and mono-ring aromatics. Zhang et al. [60] reported gasoline-range hydrocarbons accounting for 74–88% of the pyrolysis oil, with optimal aromatic selectivity at 450 °C. However, excessive severity (high temperature and low catalyst-to-polymer ratio) promoted polycyclic aromatic hydrocarbons, emphasizing the need for controlled acidity. Similarly, Fan et al. [49] showed that ex-situ cracking using HZSM-5 enhanced aromatization and cracking, yielding gasoline-range liquids and propylene-rich gas.

Non-zeolitic catalysts exhibit distinct behavior due to their lower acidity and basic or amphoteric nature. MgO promoted gas formation while reducing liquid yield and facilitated hydrogenation of alkenes and conversion of diesel-range hydrocarbons into gasoline fractions (79–96%) [64]. Support morphology and porosity significantly affect mass transfer and secondary reactions. Alkaline-treated ZSM-5 developed mesoporosity, which improved diffusion of large molecules and increased aromatic liquid yields, while excessive acidity loss reduced aromatization [65].

Microwave-specific properties of catalysts and supports also play a crucial role. Graphite, activated carbon, and SiC-based materials act as effective microwave susceptors, enabling rapid and volumetric heating. Suriappara et al. [66] showed that microwave power and graphite quantity strongly influence oil and gas yields. Activated carbon derived from biomass produced significantly higher oil yields (84 wt.%) compared to commercial activated carbon (59 wt.%), due to enhanced microwave absorption and carbon-assisted polymer decomposition [67]. SiC foam-supported zeolite catalysts further improved microwave responsiveness and catalytic efficiency [65].

Process configuration additionally influences catalytic performance. Continuous-stirred microwave pyrolysis systems produce higher condensate yields with longer hydrocarbon chains, while batch systems and fixed-bed configurations favor gas production due to enhanced secondary cracking [48]. Two-step microwave cracking approaches allow the effective conversion of waxes into valuable liquid and gaseous fuels [46], highlighting the importance of integrating reactor design with catalyst functionality.

Overall, the literature clearly establishes that catalyst acidity, pore architecture, metal promotion, support morphology, and microwave absorption capability collectively determine the efficiency and selectivity of microwave-assisted plastic pyrolysis. Optimally designed bifunctional catalysts with balanced acidity and hierarchical porosity enable the selective production of hydrogen, light olefins, and high-quality gasoline-range hydrocarbons while minimizing coke formation and energy consumption, reinforcing the potential of catalytic microwave pyrolysis as a sustainable route for plastic valorization.

Table 2.6: Brief of key literature on polymer cracking and catalysis.

Catalyst	Reaction Conditions	Conversion/ Yield	Key Observations	References
HY, NiO/HY	500 °C; HY: LDPE = 1:10; microwave heating	Oil 56 wt.%; Gas 42 wt.%	HY enhanced gasoline-range hydrocarbons and octane number; NiO promoted high-ON aromatics without reducing oil yield; strong acidity and small pore size favored gasoline production	Ding et al., *Energy Convers. Manag.*, 2019. [58]

MgO	Pyrolysis 350–550 °C; catalyst ratio 0-1/10	Liquid 24-38 wt.%; Gas 56 wt.%	MgO promoted hydrogenation of alkenes, conversion of diesel-range to gasoline fraction (79-96% of oil); gases rich in C_1-C_3 hydrocarbons.	Fan et al., *Energy Convers. Manag.*, 2017. [59]
ZSM-5	450–550 °C; varying catalyst ratios	Oil 32 wt.% Gasoline fraction 74–88%	Optimal mono-aromatic formation at 450 °C; high temperature and catalyst loading favored aromatics; excess severity led to polycyclic aromatics	Zhang et al., *Fuel*, 2014. [60]
None	300–600 W microwave power	Conversion ~96 wt.%	Oil rich in C_8-C_{12} hydrocarbons at 300-450 W; higher power promoted benzene derivatives	Suriappara et al., *PSEP*, 2021. [66]
HZSM-5 (ex-situ)	Continuous-stirred microwave pyrolysis; 450–550 °C	Condensate up to 84 wt.%	HZSM-5 enhanced cracking and aromatization; gas rich in C_1–C_4 hydrocarbons with dominant propylene.	Fan et al., *J. Anal. Appl. Pyrolysis*, 2021. [49]
HZSM-5	Batch vs continuous microwave reactors	Oil 30 wt.%; Gas 70 wt.%	Continuous system favored longer hydrocarbons (C_{14}–C_{20}); batch reactor produced more gas due to secondary reactions	Fan et al., *Energy*, 2021. [48]
None (two-step microwave cracking)	Step-1 & Step-2 cracking; controlled heating	Liquid 60-79 wt.%, Gas 18–38 wt.%	Two-step strategy improved fuel-range liquids; gas rich in H_2, CH_4, C_2H_4, C_3H_6; liquids suitable for gasoline/diesel	Jing et al., *Fuel Process. Technol.*, 2020. [46]
Zn/HZSM-5	Microwave-assisted catalytic pyrolysis	Liquid 43 wt.%, Gas 55 wt.%	Zn enhanced dehydrogenation at Lewis acid sites; aromatics reached 93.5% of liquid; β-scission promoted	Vatankhah et al., *Energy Fuels*, 2024. [63]
SiC foam@ZSM-5	Microwave catalytic pyrolysis	Liquid 20 wt.%, Gas 80 wt.%	Mesoporosity improved diffusion; moderated acidity enhanced aromatics and olefins; excessive treatment suppressed aromatics	Chen et al., *Environ. Pollut.*, 2022. [65]

Activated carbon (biomass-derived)	Microwave pyrolysis of PS/PP	Oil yields up to 84 wt.%	Carbon acted as microwave absorber and cracking promoter; synthesized AC outperformed commercial AC	Rex et al., *J. Energy Inst.*, 2020. [67]
HNO_3	180 °C; 40 bars; 3 h	Dicarboxylic acids 71%	Microwave hydrothermal process converted LDPE into succinic acid (36%); non-fuel chemical recycling route	Bäckström et al., *Ind. Eng. Chem. Res.*, 2017. [68]
HNO_3	Microwave-assisted degradation	High selectivity to diacids	HDPE crystallinity influenced degradation rate; products used to synthesize bio-plasticizers	Bäckström et al., *ACS Sustain. Chem. Eng.*, 2019. [69]
Zeolite	550 °C; 90 min	Liquid 28 wt.%; solid 2.8 wt.%	Liquid rich in aromatics and hydrocarbons; effective LDPE cracking under microwave heating	Juliastuti et al., ISFAChE, 2017. [70]
None	525 °C; 1100 W	Liquid 65-75 wt.%	Liquid upgraded to low-sulfur naphtha and diesel; gas rich in propylene (40–50%)	Raj Mohan & Bhalla, *IJERT*, 2016. [71]

Despite the promise of microwave-assisted pyrolysis for converting LDPE waste into valuable fuels, significant research gaps remain. The effect of catalyst acidity on product distribution remains insufficiently investigated, and only a limited number of studies have systematically evaluated the impact of catalyst-to-polymer ratios. In addition, comparative analyses of catalyst performance at different temperatures are scarce, and research on catalysts in microwave-assisted systems is still limited, as most previous studies have primarily focused on conventional pyrolysis processes. Moreover, there is little information available on the catalytic behavior of Ni- and Zn- loaded catalysts on HY, Al_2O_3, SiO_2, and TiO_2, particularly when used in combination with low-cost microwave absorbers such as graphite. To address these research gaps, the present study systematically examines these catalyst systems to enhance the efficiency and selectivity of plastic waste conversion under microwave-assisted pyrolysis conditions.

2.4 Characterization Techniques

In this study, various physicochemical characterization techniques were employed to evaluate the catalysts and products obtained from LDPE cracking.

2.4.1 X-ray diffraction (XRD): It is employed to identify the crystalline structure and phase composition of catalysts. In this analysis, the sample is exposed to X-ray radiation, which is a type of electromagnetic energy having a wavelength of ≈ 0.1 nm. X-rays are generated by directing electrons toward a metal target within a vacuum tube, resulting in the emission of both characteristic and continuous radiation that is specific to the target material. When the X-ray beam interacts with the sample, part of the radiation is absorbed while the remainder is diffracted by the crystalline regions. The X-ray penetration depth varies with the material composition and the energy of the incident radiation. The resulting diffraction pattern provides information about the phase composition and crystalline structure of the material [72].

2.4.2 Scanning electron microscopy (SEM): It provides information on surface morphology and textural features. It is a surface imaging technique that uses a focused electron beam to scan the catalyst surface and generate high-resolution micrographs. Prior to analysis, catalyst samples are made electrically conductive, either inherently or by applying a thin conductive coating. SEM enables a detailed examination of surface morphology, particle size, agglomeration, porosity, and textural features. The large depth of field produced by SEM provides a three-dimensional-like visualization of the catalyst surface, facilitating the evaluation of structural changes before and after the reaction [73].

2.4.3 Fourier-transform infrared spectroscopy (FTIR): It is used to identify functional groups and framework vibrations. In this method, the catalyst sample is exposed to infrared radiation, and specific wavelengths are absorbed due to molecular vibrations of surface species. The transmitted radiation is measured, while the absorbed frequencies generate characteristic bands in the spectrum. These bands serve as a chemical fingerprint, providing information about the catalyst framework structure, metal–oxygen bonds, surface hydroxyl groups, and other functional groups present on the catalyst surface [74].

2.4.4 Pyridine-adsorbed FTIR (Py-FTIR): It is widely used to determine the nature and strength of acid sites present on catalyst surfaces. In this technique, pyridine is adsorbed onto the catalyst, where it interacts differently with Brønsted and Lewis acid sites. Pyridine coordinated to Brønsted acid sites (proton donors) forms pyridinium ions, giving characteristic absorption bands typically observed near ~1540 cm^{-1}. In contrast, pyridine coordinated to Lewis acid sites (electron pair acceptors) produce bands around ~1450 cm^{-1}. By analyzing the

intensity of these bands, the concentration and type of acid sites on the catalyst surface can be quantified. This method is particularly valuable for correlating catalyst acidity with cracking activity and product selectivity in hydrocarbon conversion reactions [75,76].

2.4.5 NH_3-temperature-programmed desorption (NH_3-TPD): It is conducted to assess total acidity and acid strength distribution. In this method, ammonia is first adsorbed onto the catalyst surface at low temperature, where it interacts with both Brønsted and Lewis acid sites. The physically adsorbed ammonia is removed by purging with an inert gas, and the temperature is then gradually increased. As the temperature rises, chemisorbed ammonia desorbs from acid sites at different temperatures depending on the acid strength. Weak acid sites release ammonia at lower temperatures, whereas strong acid sites require higher temperatures for desorption. The amount of desorbed ammonia is monitored, typically using a thermal conductivity detector (TCD), and is proportional to the total acidity of the catalyst. The resulting desorption profile provides quantitative information on acid site concentration and strength distribution, which are critical parameters influencing cracking activity and product selectivity in hydrocarbon conversion reactions [77].

2.4.6 X-ray photoelectron spectroscopy (XPS): It is used to examine surface carbon species and the chemical states of elements, allowing the assessment of coke deposition on spent catalysts. In XPS analysis, the sample is irradiated with a soft X-ray beam, and the kinetic energy of the emitted photoelectrons from the surface is measured. The interaction between the X-rays and the sample leads to the ejection of electrons with characteristic energies, which can be analyzed to obtain chemical information. XPS is widely applied for determining oxidation states, performing quantitative elemental analysis, and studying surface composition [78].

2.4.7 Inductively coupled plasma mass spectrometry (ICP-MS): It is used to reveal elemental composition and bulk metal loading. ICP-MS is an elemental analysis technique used to quantify individual elements rather than molecular species, which are typically analyzed by GC/MS or LC/MS. In CP-MS, the sample is introduced into a high-temperature argon plasma, where the elements present are ionized and atomized. The generated ions are subsequently transported to a mass spectrometer, to separate and quantify based on their mass-to-charge ratio. ICP-MS is similar to inductively coupled plasma optical emission spectroscopy (ICP-OES). Conversely, ICP-OES measures the characteristic light produced by excited atoms in the plasma, whereas ICP-MS detects and quantifies the generated ions. Although both techniques enable rapid multi-element analysis, ICP-MS offers significantly lower detection limits, making it particularly suitable for trace metal analysis in catalytic materials [79].

2.4.8 Gas chromatography/mass spectrometry (GC/MS): Liquid products obtained from LDPE cracking were characterized using GC–MS to determine the hydrocarbon distribution (paraffins, olefins, aromatics, and other fractions), while gaseous products were analyzed to quantify light hydrocarbons (C_1–C_4) and hydrogen content.

GC–MS integrates two complementary analytical techniques to achieve both separation and identification of complex mixtures. In the gas chromatography (GC) unit, the liquid or gaseous sample is evaporated and then transported by an inert carrier gas over a capillary column layered with a stationary phase. As the analytes pass via the column, they relate differently with the stationary phase depending on their volatility, molecular structure, and polarity. These differential interactions result in separation, with each compound eluting at a characteristic retention time [80].

The separated components are subsequently introduced into the mass spectrometer, where they are fragmented, ionized, and detected based on their mass-to-charge (m/z) ratios. While GC provides retention time and relative peak intensity, the MS supplies molecular mass and fragmentation pattern information, enabling precise compound identification and quantitative analysis. The combined technique thus allows comprehensive characterization of pyrolysis products, offering detailed insight into product selectivity and reaction pathways during LDPE cracking [80].

2.5 References

[1] M. Ravichandran, M. Balasubramanian, C. Anand Chairman, D. Pritima, V. Dhinakaran, B. Stalin, Recent developments in Polymer Matrix Composites – A review, IOP Conf. Ser. Mater. Sci. Eng. 988 (2020) 012096. https://doi.org/10.1088/1757-899X/988/1/012096.

[2] Wikipedia contributors, Hemp, Wikipedia, The Free Encyclopedia. (2025).

[3] K. Promhuad, A. Srisa, H. San, Y. Laorenza, P. Wongphan, J. Sodsai, K. Tansin, P. Phromphen, N. Chartvivatpornchai, P. Ngoenchai, N. Harnkarnsujarit, Applications of Hemp Polymers and Extracts in Food, Textile and Packaging: A Review, Polymers (Basel). 14 (2022) 4274. https://doi.org/10.3390/polym14204274.

[4] Wikipedia contributors, Shellac, Wikipedia, The Free Encyclopedia. (2025).

[5] Y. Yuan, N. He, Q. Xue, Q. Guo, L. Dong, M.H. Haruna, X. Zhang, B. Li, L. Li, Shellac: A promising natural polymer in the food industry, Trends Food Sci. Technol. 109 (2021) 139–153. https://doi.org/10.1016/j.tifs.2021.01.031.

[6] Wikipedia contributors, Amber, Wikipedia, The Free Encyclopedia. (2025).

[7] Wikipedia contributors, Silk, Wikipedia, The Free Encyclopedia. (2025).

[8] D.J. Miller, Natural Rubber: Structure and Function, Halcyon (2025).

[9] Wikipedia contributors, Cellulose, Wikipedia, The Free Encyclopedia. (2025).

[10] Dennis Malpass, Introduction to Industrial Polyethylene: Properties, Catalysts, and Processes, Wiley, 2010.

[11] GKFX, Schematic of LDPE branching structure, (2020).

[12] VEM Tooling, LDPE Versus HDPE, (2026).

[13] M. Gahleitner, C. Paulik, Polypropylene, in: Ullmann's Encyclopedia of Industrial Chemistry, Wiley-VCH Verlag GmbH & Co. KGaA, Weinheim, Germany, 2014: pp. 1–44. https://doi.org/10.1002/14356007.o21_o04.pub2.

[14] S. STINSON, Discoverers of Polypropylene Share Prize, Chemical & Engineering News Archive 65 (1987) 30. https://doi.org/10.1021/cen-v065n010.p030.

[15] C. Maier, T. Calafut, Polypropylene: the definitive user's guide and databook., in: 1998.

[16] von S. Nuyken, M. Koltzenburg, O. Maskos, Polymer: synthesis, properties and applications. , in: 1st ed., Springer., 2013.

[17] User:Cjp24, Polymerization reaction for synthesis of polypropylene, (2023).

[18] G.T. Carroll, M.E. Sojka, X. Lei, N.J. Turro, J.T. Koberstein, Photoactive Additives for Cross-Linking Polymer Films: Inhibition of Dewetting in Thin Polymer Films, Langmuir 22 (2006) 7748–7754. https://doi.org/10.1021/la0611099.

[19] H Padleckas, Chemical reaction diagram showing polystyrene formed by polymerisation of styrene., (2025).

[20] W. V. Titow, PVC technology., Springer, 1984.

[21] Strumberger N, Gospocic A, Bratulic C, Polymeric materials in automobiles., Promet Traffic- Traffico 17 (2005) 149–160.

[22] S. Rahman, Sealing Our Buried Lifelines, Opflow 33 (2007) 12–17. https://doi.org/10.1002/j.1551-8701.2007.tb02753.x.

[23] F.M. Galloway, M.M. Hirschler, G.F. Smith, Surface parameters from small-scale experiments used for measuring HCl transport and decay in fire atmospheres, Fire Mater. 15 (1991) 181–189. https://doi.org/10.1002/fam.810150405.

[24] Strong, A. Brent, Plastics: Materials and Processing., Prentice Hall, 2005.

[25] K. Marsh, B. Bugusu, Food Packaging—Roles, Materials, and Environmental Issues, J. Food Sci. 72 (2007). https://doi.org/10.1111/j.1750-3841.2007.00301.x.

[26] NEUROtiker, Repeating unit of PVC polymer chain., (2008).

[27] Wesley Stephenson, why plastic recycling is so confusing, (2018).

[28] Advancing Sustainable Materials Management: 2018 Tables and Figures, 2020.

[29] S. Khadke, P. Gupta, S. Rachakunta, C. Mahata, S. Dawn, M. Sharma, D. Verma, A. Pradhan, A.M.S. Krishna, S. Ramakrishna, S. Chakrabortty, G. Saianand, P. Sonar, S. Biring, J.K. Dash, G.K. Dalapati, Efficient Plastic Recycling and Remolding Circular Economy Using the Technology of Trust–Blockchain, Sustainability 13 (2021) 9142. https://doi.org/10.3390/su13169142.

[30] R. Hasanzadeh, P. Mojaver, T. Azdast, S. Khalilarya, A. Chitsaz, M.A. Rosen, Decision analysis for plastic waste gasification considering energy, exergy, and environmental criteria using TOPSIS and grey relational analysis, Process Safety and Environmental Protection 174 (2023) 414–423. https://doi.org/10.1016/j.psep.2023.04.028.

[31] P. Mojaver, A. Chitsaz, S.J. Hasannejad, M. Khalilian, Plastic Waste Gasification, in 2023: pp. 47–60. https://doi.org/10.1007/978-3-031-31160-4_3.

[32] S.A. Salaudeen, P. Arku, A. Dutta, Gasification of Plastic Solid Waste and Competitive Technologies, in: Plastics to Energy, Elsevier, 2019: pp. 269–293. https://doi.org/10.1016/B978-0-12-813140-4.00010-8.

[33] M. Rehan, A.S. Nizami, K. Shahzad, O.K.M. Ouda, I.M.I. Ismail, T. Almeelbi, T. Iqbal, A. Demirbas, Pyrolytic liquid fuel: A source of renewable electricity generation in Makkah, Energy Sources, Part A: Recovery, Utilization, and Environmental Effects 38 (2016) 2598–2603. https://doi.org/10.1080/15567036.2016.1153753.

[34] R. Boyt, Wood Pyrolysis, in 2003.

[35] Fogler, H. Scott, M. N. Gürmen, Elements of Chemical Reaction Engineering. 2005, Search PubMed (1999) 813–866.

[36] J.A. Onwudili, N. Insura, P.T. Williams, Composition of products from the pyrolysis of polyethylene and polystyrene in a closed batch reactor: Effects of temperature and residence time, J. Anal. Appl. Pyrolysis 86 (2009) 293–303. https://doi.org/10.1016/j.jaap.2009.07.008.

[37] Y. Choi, S. Wang, Y.M. Yoon, J.J. Jang, D. Kim, H.-J. Ryu, D. Lee, Y. Won, H. Nam, B. Hwang, Sustainable strategy for converting plastic waste into energy over pyrolysis: A comparative study of fluidized-bed and fixed-bed reactors, Energy 286 (2024) 129564. https://doi.org/10.1016/j.energy.2023.129564.

[38] R. Aguado, M. Olazar, B. Gaisán, R. Prieto, J. Bilbao, Kinetic Study of Polyolefin Pyrolysis in a Conical Spouted Bed Reactor, Ind. Eng. Chem. Res. 41 (2002) 4559–4566. https://doi.org/10.1021/ie0201260.

[39] M. Arabiourrutia, G. Elordi, M. Olazar, J. Bilbao, Pyrolysis of Polyolefins in a Conical Spouted Bed Reactor: A Way to Obtain Valuable Products, in: Pyrolysis, InTech, 2017. https://doi.org/10.5772/67706.

[40] S. Orozco, M. Artetxe, G. Lopez, M. Suarez, J. Bilbao, M. Olazar, Conversion of HDPE into Value Products by Fast Pyrolysis Using FCC Spent Catalysts in a Fountain Confined Conical Spouted Bed Reactor, ChemSusChem 14 (2021) 4291–4300. https://doi.org/10.1002/cssc.202100889.

[41] E.T. Thostenson, T.-W. Chou, Microwave processing: fundamentals and applications, Compos. Part A Appl. Sci. Manuf. 30 (1999) 1055–1071. https://doi.org/10.1016/S1359-835X(99)00020-2.

[42] K.M.O. Islam, N. Ahmad, A.C. Ummer, U. Ahmed, M.N. Siddiqui, M. Millan, A.G. Abdul Jameel, Microwave-Assisted pyrolysis of waste plastics: A comprehensive review on process parameters, catalysts, and future prospects, Results in Engineering 26 (2025) 105571. https://doi.org/10.1016/j.rineng.2025.105571.

[43] V. Palma, D. Barba, M. Cortese, M. Martino, S. Renda, E. Meloni, Microwaves and Heterogeneous Catalysis: A Review on Selected Catalytic Processes, Catalysts 10 (2020) 246. https://doi.org/10.3390/catal10020246.

[44] S.S. Lam, H.A. Chase, A Review on Waste to Energy Processes Using Microwave Pyrolysis, Energies (Basel). 5 (2012) 4209–4232. https://doi.org/10.3390/en5104209.

[45] K.N. Aishwarya, N. Sindhu, Microwave Assisted Pyrolysis of Plastic Waste, Procedia Technology 25 (2016) 990–997. https://doi.org/10.1016/j.protcy.2016.08.197.

[46] Xiaodong Jing, Hao Wen, Xuzhong Gong, ZhihongXu, Anna Kajetanowicz, Recycling waste plastics packaging to value-added products by two-stepmicrowave cracking with different heating strategies, Fuel Processing Technology (2020).

[47] X. Zhang, K. Rajagopalan, H. Lei, R. Ruan, B.K. Sharma, An overview of a novel concept in biomass pyrolysis: microwave irradiation, Sustain. Energy Fuels 1 (2017) 1664–1699. https://doi.org/10.1039/C7SE00254H.

[48] Liangliang Fan, Lei Liu, Zhiguo Xiao, Zheyang Su, Pei Huang, HongyuPeng, SenLv, Haiwei Jiang, Roger Ruan, Paul Chen, Wenguang Zhou, Comparative study of continuous-stirred and batch microwave pyrolysis of linear low-density polyethylene in the presence/absenceof HZSM-5, Energy (2021).

[49] L. Fan, Z. Su, J. Wu, Z. Xiao, P. Huang, L. Liu, H. Jiang, W. Zhou, S. Liu, R. Ruan, Integrating continuous-stirred microwave pyrolysis with ex-situ catalytic upgrading for linear low-density polyethylene conversion: Effects of parameter conditions, J. Anal. Appl. Pyrolysis 157 (2021) 105213. https://doi.org/10.1016/j.jaap.2021.105213.

[50] Y. Fernandez, A. Arenillas, J. Angel, Microwave Heating Applied to Pyrolysis, in: Advances in Induction and Microwave Heating of Mineral and Organic Materials, InTech, 2011. https://doi.org/10.5772/13548.

[51] Z. Cai, M. Li, Z. Zhu, X. Wang, Y. Huang, T. Li, H. Gong, M. Yan, Biological Degradation of Plastics and Microplastics: A Recent Perspective on Associated Mechanisms and Influencing Factors, Microorganisms 11 (2023) 1661. https://doi.org/10.3390/microorganisms11071661.

[52] T. Artham, M. Doble, Biodegradation of Aliphatic and Aromatic Polycarbonates, Macromol. Biosci. 8 (2008) 14–24. https://doi.org/10.1002/mabi.200700106.

[53] J. Mudondo, H.-S. Lee, Y. Jeong, T.H. Kim, S. Kim, B.H. Sung, S.-H. Park, K. Park, H.G. Cha, Y.J. Yeon, H.T. Kim, Recent Advances in the Chemobiological Upcycling of Polyethylene Terephthalate (PET) into Value-Added Chemicals, J. Microbiol. Biotechnol. 33 (2023) 1–14. https://doi.org/10.4014/jmb.2208.08048.

[54] A. Marcilla, M.I. Beltrán, R. Navarro, Evolution of products during the degradation of polyethylene in a batch reactor, J. Anal. Appl. Pyrolysis 86 (2009) 14–21. https://doi.org/10.1016/j.jaap.2009.03.004.

[55] A. López, I. de Marco, B.M. Caballero, M.F. Laresgoiti, A. Adrados, Influence of time and temperature on pyrolysis of plastic wastes in a semi-batch reactor, Chemical Engineering Journal 173 (2011) 62–71. https://doi.org/10.1016/j.cej.2011.07.037.

[56] R. Prurapark, K. Owjaraen, B. Saengphrom, I. Limthongtip, N. Tongam, Effect of Temperature on Pyrolysis Oil Using HDPE and PET Sources from Mobile Pyrolysis Plant, (2020). https://doi.org/10.21203/rs.3.rs-24640/v1.

[57] S. Papuga, P. Gvero, L. Vukic, Temperature and time influence on the waste plastics pyrolysis in the fixed bed reactor, Thermal Science 20 (2016) 731–741. https://doi.org/10.2298/TSCI141113154P.

[58] K. Ding, S. Liu, Y. Huang, S. Liu, N. Zhou, P. Peng, Y. Wang, P. Chen, R. Ruan, Catalytic microwave-assisted pyrolysis of plastic waste over NiO and HY for gasoline-range hydrocarbons production, Energy Convers. Manag. 196 (2019). https://doi.org/10.1016/j.enconman.2019.07.001.

[59] Liangliang Fan, Yaning Zhang, Shiyu Liu, Nan Zhou, Paul Chen, Yuhuan Liu, Yunpu Wang, PengPeng, Yanling Cheng, Min Addy, Hanwu Lei, Roger Ruan, Catalytic upgrading of vapors from microwave-assisted pyrolysis of low-density polyethylene with MgO, Energy Convers. Manag. (2017).

[60] X. Zhang, H. Lei, G. Yadavalli, L. Zhu, Y. Wei, Y. Liu, Gasoline-range hydrocarbons produced from microwave-induced pyrolysis of low-density polyethylene over ZSM-5, Fuel 144 (2015). https://doi.org/10.1016/j.fuel.2014.12.013.

[61] M. Artetxe, G. Lopez, M. Amutio, G. Elordi, J. Bilbao, M. Olazar, Cracking of High Density Polyethylene Pyrolysis Waxes on HZSM-5 Catalysts of Different Acidity, Ind. Eng. Chem. Res. 52 (2013) 10637–10645. https://doi.org/10.1021/ie4014869.

[62] J. Aguado, D.P. Serrano, G. San Miguel, M.C. Castro, S. Madrid, Feedstock recycling of polyethylene in a two-step thermo-catalytic reaction system, J. Anal. Appl. Pyrolysis 79 (2007) 415–423. https://doi.org/10.1016/j.jaap.2006.11.008.

[63] F. Vatankhah, A. Carrillo García, J. Chaouki, Role of Bifunctional Metal-Promoted Zeolitic Catalyst in Microwave-Assisted Pyrolysis of Polyethylene to Monocyclic Aromatics, Energy & Fuels 38 (2024) 20562–20576. https://doi.org/10.1021/acs.energyfuels.4c03692.

[64] Fan Liangliang, Zhang Yaning, Liu Shiyu, Zhou Nan, Chen Paul, Liu Yuhuan, Wang Yunpu, Peng Peng, Cheng Yanling, Addy Min, Lei Hanwu, Ruan Roger, Ex-situ catalytic upgrading of vapors from microwave-assisted pyrolysis of low-density polyethylene with MgO, Energy Convers. Manag. 149 (2017). https://doi.org/10.1016/j.enconman.2017.07.039.

[65] Zhaohui Chen, Mohammad Monzavi, Mohammad Latifi, Said Samih, Jamal Chaouki., Microwave-responsive SiCfoam@zeolite core-shell structured catalyst for catalytic pyrolysis of plastics, Environmental Pollution (2022).

[66] Dadi V. Suriapparao, Garlapati Nagababu, Attada Yerrayya, Veluru Sridevi, Optimization of microwave power and graphite susceptor quantityfor waste polypropylene microwave pyrolysis., Process Safety and Environmental Protection (2021) 234–243.

[67] P. Rex, I.P. Masilamani, L.R. Miranda, Microwave pyrolysis of polystyrene and polypropylene mixtures using different activated carbon from biomass, Journal of the Energy Institute 93 (2020) 1819–1832. https://doi.org/10.1016/j.joei.2020.03.013.

[68] E. Bäckström, K. Odelius, M. Hakkarainen, Trash to Treasure: Microwave-Assisted Conversion of Polyethylene to Functional Chemicals, Ind. Eng. Chem. Res. 56 (2017) 14814–14821. https://doi.org/10.1021/acs.iecr.7b04091.

[69] E. Bäckström, K. Odelius, M. Hakkarainen, Designed from Recycled: Turning Polyethylene Waste to Covalently Attached Polylactide Plasticizers, ACS Sustain. Chem. Eng. 7 (2019) 11004–11013. https://doi.org/10.1021/acssuschemeng.9b02092.

[70] S.R. Juliastuti, N. Hendrianie, P.J. Ramadhan, D.H. Satria, Microwave pyrolysis of multilayer plastic waste (LDPE) using zeolite catalyst, in: 2017: p. 110001. https://doi.org/10.1063/1.4982331.

[71] C. Dr. Raj Mohan B, Studies on microwave pyrolysis of polypropylene, International Journal of Engineering Research & Technology (2016).

[72] J. Bergström, Experimental Characterization Techniques, in: Mechanics of Solid Polymers, Elsevier, 2015: pp. 19–114. https://doi.org/10.1016/B978-0-323-31150-2.00002-9.

[73] D. Merenich, K.E. Van Manen-Brush, C. Janetopoulos, K.A. Myers, Advanced microscopy techniques for the visualization and analysis of cell behaviors, in: Cell Movement in Health and Disease, Elsevier, 2022: pp. 303–321. https://doi.org/10.1016/B978-0-323-90195-6.00010-3.

[74] K. Mattsson, S. Jocic, J.A. de Lima, L.-A. Hansson, A. Gondikas, Nanoplastics in aquatic environments—Sources, sampling techniques, and identification methods, in: Microplastic Contamination in Aquatic Environments, Elsevier, 2024: pp. 381–397. https://doi.org/10.1016/B978-0-443-15332-7.00003-X.

[75] C.A. Emeis, Determination of Integrated Molar Extinction Coefficients for Infrared Absorption Bands of Pyridine Adsorbed on Solid Acid Catalysts, J. Catal. 141 (1993) 347–354. https://doi.org/10.1006/jcat.1993.1145.

[76] G. Busca, Acid Catalysts in Industrial Hydrocarbon Chemistry, Chem. Rev. 107 (2007) 5366–5410. https://doi.org/10.1021/cr068042e.

[77] Dr. Kazuyuki Nakai, Ms. Kaori Nakamura, Ammonia Temperature Programmed Desorption (NH3- TPD) Measurement -Investigation of Desorption Energy and Heat of Adsorption, Www.Microtrac.Com © Microtrac MRB 2019 (2019).

[78] T.K. Giri, Solid lipid nanoparticles for the delivery of drug molecules, in: Materials for Biomedical Engineering, Elsevier, 2019: pp. 551–576. https://doi.org/10.1016/B978-0-12-818433-2.00016-9.

[79] Agilent Technologies, An Introduction to the Principles of Inductively Coupled Plasma – Mass Spectrometry (ICP-MS), Https://Www.Agilent.Com/En/Product/Atomic-Spectroscopy/Inductively-Coupled-Plasma-Mass-Spectrometry-Icp-Ms/What-Is-Icp-Ms-Icp-Ms-Faqs?Srsltid=AfmBOopLxJcrgQ0TocRGjBh6hWhRRwdiXYykj1TZuzXiDi0nqLG730Y4 (n.d.).

[80] Agilent Technologies, Gas Chromatography/ Mass Spectrometry Fundamentals, Https://Www.Agilent.Com/En/Product/Gas-Chromatography-Mass-Spectrometry-Gc-Ms/Gcms-Fundamentals (n.d.).

CHAPTER – 3

Microwave-assisted pyrolysis of LDPE to value-added products over HY, HZSM-5 and Hβ catalyst

3.1 Introduction

This chapter describes the materials used for the treatment of plastic waste and details the experimental procedures and treatment techniques employed. It also outlines the methodologies adopted for the characterization of catalysts and the resulting products. Furthermore, the chapter presents and discusses experimental results, analyzing the effects of process conditions and the HY, HZSM-5 and Hβ catalysts' composition on product yield and distribution, and interpreting observed trends to elucidate the underlying catalytic performance.

LDPE is one of the most widely used plastics and a major contributor to post-consumer plastic waste due to its chemical inertness. Catalytic cracking offers an effective route for converting LDPE into valuable gaseous and liquid hydrocarbons; however, product distribution is strongly influenced by catalyst acidity, pore structure, and heating mode. In this context, acidic zeolite catalysts such as HY, Hβ, and HZSM-5 have been broadly studied owing to their high surface area, well-defined pore systems, and strong Brønsted acidity, which promote C–C bond scission, β-scission, aromatization, and hydrogen transfer reactions.

The combination of microwave irradiation with acidic zeolite catalysts enhances reaction kinetics, minimizes heat transfer limitations, and intensifies secondary cracking and dehydrogenation reactions. Therefore, the present study investigates microwave-assisted cracking of LDPE over HY, HZSM-5, and Hβ catalysts to elucidate their comparative performance in terms of product yield, selectivity, and H_2-rich gas formation. Aguado et al. reported that the HZSM-5 zeolite predominantly favours the formation of C_3–C_5 olefins during the conventional pyrolysis of LDPE, resulting in a product distribution comprising 52% gaseous C_1–C_4 hydrocarbons [1]. The Y-type zeolite with a low silicon-to-aluminum ratio possesses a high density of Brønsted acid sites, which effectively facilitate C–C bond cleavage in heavy hydrocarbons, thereby significantly enhancing cracking activity [2]. Fast catalytic pyrolysis of LDPE in a Pyroprobe micro-reactor demonstrated that the type of zeolite framework significantly influences product selectivity, affecting the formation of light

paraffins and olefins (C_3–C_4), gasoline-range paraffins and olefins (C_5–C_{10}), and aromatic compounds [3].

3.2 Materials and methods

3.2.1 Materials

LDPE granules were purchased from Reliance Industries Ltd. HZSM- 5, HY, and Hβ with respective Si/Al ratios of 25, 6 and 30 were purchased from SUD CHEMIE India Pvt. Ltd. Their surface areas were 365, 750 and 622 m^2/g, respectively. Graphite powder (CAS No. 7782–42–5) with a particle size of 149 μm was procured from Fine Chemicals, Bangalore.

3.2.2 Desilication of Hβ

To disilicate Hβ, about 1 g of Hβ zeolite was suspended in 15 mL of a 0.5 M NaOH solution and stirred at 65°C for 30 minutes. Following this, the suspension was cooled and filtered. The solid was thoroughly washed with distilled water until the filtrate reached a neutral pH, followed by centrifugation and drying at 120°C for 12 hours.

3.2.3 Catalyst characterization

Scanning electron microscopy (SEM) (Thermo Fisher Scientific Apereo 2S High vac FESEM) was used to investigate the surface morphology of the catalyst.

Structures of the catalyst were ascertained by X-ray diffraction (XRD) on a PANalytical, X'Pert Pro instrument. The X-ray source was either Cu Kα radiation (λ = 1.54 Å) or Mo Kα radiation (λ = 0.71 Å). The measurement range was 5°–140°, and the operating conditions were 45 kV and 40 mA.

FTIR spectra of the samples were collected in reflection mode using KBr optics on a PerkinElmer, Spectrum Two instrument. The instrument was operated over the range of 400–4000 cm^{-1}.

3.2.4 Experimental setup

A MW reactor with a maximum power of 800 W and a frequency of 2.45 GHz was used. A 500 mL round-bottom quartz flask was used as the reactor and placed in a microwave chamber. Graphite powder (10-30 g) used as a MW absorber was mixed with 10 g of LDPE and the catalyst (0.5, 1.0, or 2.0 g) in the reactor. Graphite efficiently absorbs microwave energy and converts it into heat, generating localized high-temperature regions that promote the thermal depolymerization of LDPE. In addition, its enhanced heat transfer improves the interaction between the molten polymer and the catalyst, thereby facilitating catalytic cracking. However, graphite itself does not act as a catalyst; depolymerization reactions are primarily governed by

the acidic or metallic active sites of the catalysts. Pyrolysis temperatures were measured with a thermocouple inserted into the reaction mixture. The Vapours from the reactor were condensed using a condenser. A vacuum pump was connected to the condensate collection flask. The experimental setup used for microwave-assisted LDPE pyrolysis is shown in Figure 3.1. The schematic diagram (Figure 3.1a) illustrates the major components, while the actual laboratory setup is presented in Figure 3.1b.

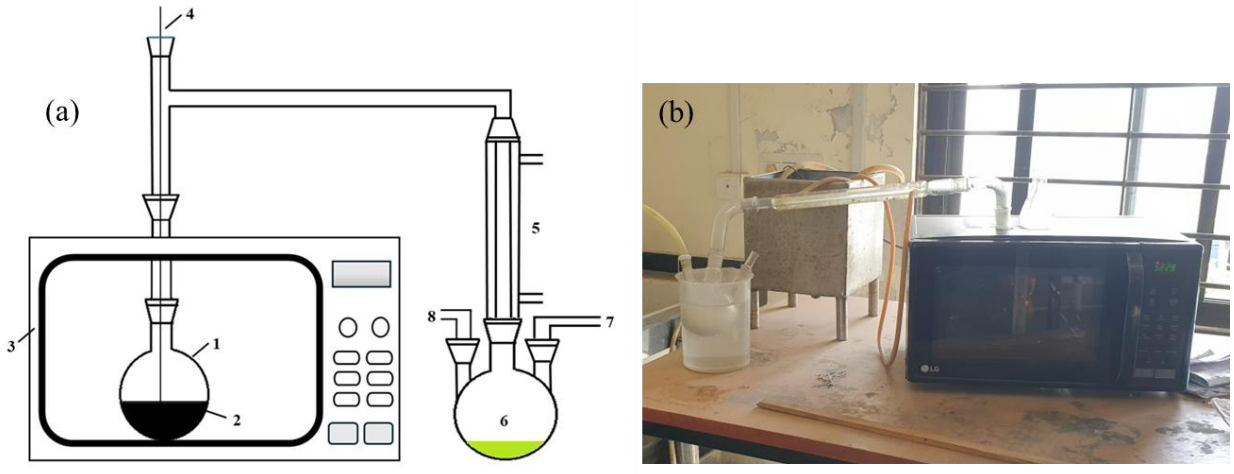

Figure 3.1. (a) Schematic representation of the microwave-assisted catalytic pyrolysis setup comprising (1) quartz reactor flask, (2) LDPE feedstock mixed with catalyst and graphite, (3) microwave heating unit, (4) thermocouple for temperature measurement, (5) water-cooled condenser, (6) liquid product collection flask, (7) vacuum line connection, and (8) gas sampling outlet; (b) Actual photograph of the experimental apparatus.

3.2.5 Liquid products analysis Composition of the liquid product was obtained using an Agilent 7890 gas chromatograph–mass spectrometer (GC/MS). The GC/MS was coupled with a hp-5 capillary column (30 m L*0.25 mm i.d) with helium as the carrier gas (flow rate: 1 mL min^{-1}). Compounds were identified according to the spectral data from the NIST library. The chromatographic area percentage (area%) of each compound was used to determine product selectivity.

3.2.6 Gaseous products analysis Gaseous product stream was collected in a Tedlar bag and analyzed by a GC Trace 1110 equipped with a Chromosorb-102 column, using nitrogen as the carrier gas. Standard gases were used for calibration.

The amount of coke formed was very low (<0.8 wt.%) which is negligible compared to the gas and liquid products.

3.2.7 Product Quantification: The yields of gas, liquid, and char were determined using a mass balance approach. The char and liquid yields were obtained by directly weighing the recovered solid residue and condensed liquid products, respectively. The gas yield was calculated by difference from the initial mass of LDPE.

3.3 Results and discussion

3.3.1 Catalyst Characterization:

3.3.1.1 Scanning Electron Microscope (SEM)

SEM images of the three different catalysts are shown in Figure 3.2. SEM analysis showed that the crystal size of HZSM-5, HY, and Hβ was in the range of 0.5 μm, 1 μm, and 0.2 – 0.5 μm, respectively. Thus, the crystal size of all the catalysts varied within a narrow range.

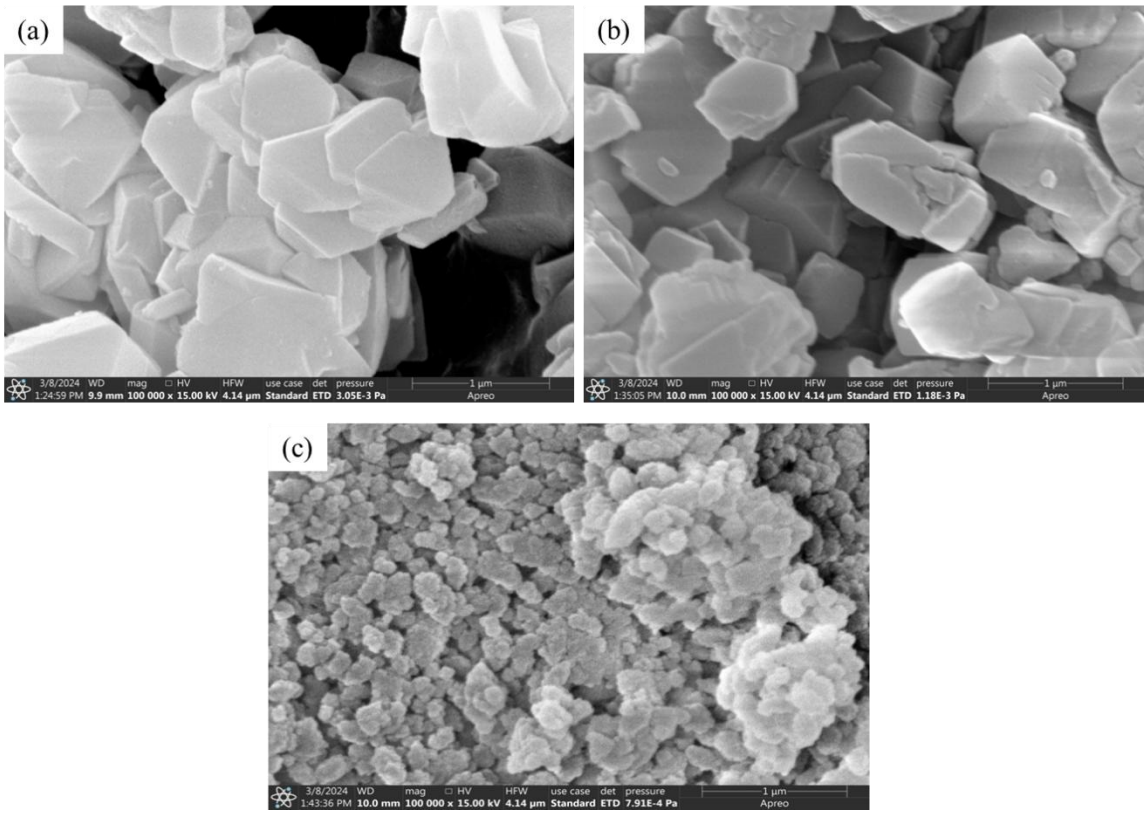

Figure 3.2: SEM images of (a) HZSM-5 (b) HY, and (c) Hβ.

3.3.1.2 Fourier transform infrared spectroscopy (FTIR)

Functional groups present on the catalysts were identified using FTIR spectroscopy as depicted in Fig. 3.3. The absorption band of the hydroxyl group (OH-) stretching vibration at the wavenumber of 3444 and 3623cm^{-1} indicated the presence of Bronsted acid sites[4,5]. A peak at the wavenumber 3595cm^{-1} confirms strong Bronsted acid sites [5]. Bands at 1637 and 807cm^{-1} were attributed to the stretching and bending vibrations of adsorbed water and the

symmetric vibration of Si/Al-O, respectively. The absorption bands at the wavenumber 1140 – 995 cm^{-1} resulted from Si–O–Si (Al) stretching bond [6,7] and the internal Si(Al)–O functional group absorption was reflected by the 420 –500 cm^{-1} band.

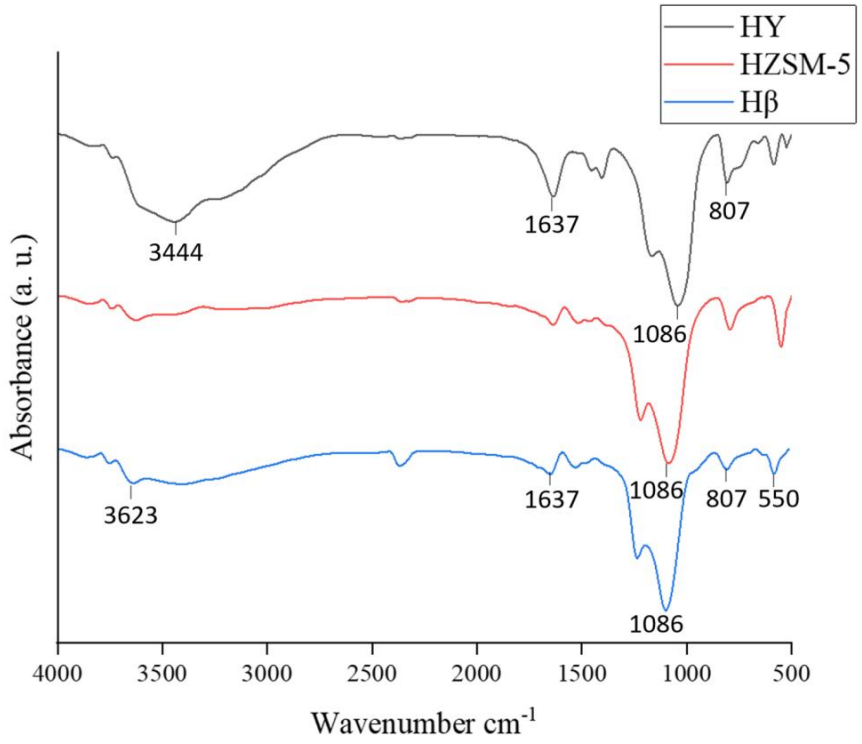

Figure 3.3: FTIR patterns of HZSM-5 HY, and Hβ catalyst

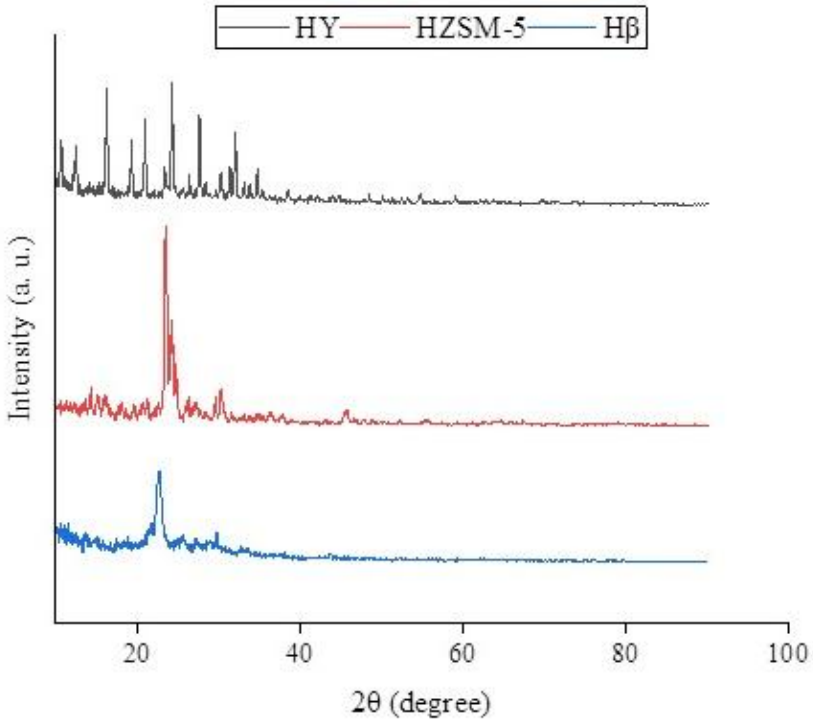

Figure 3.4: XRD patterns of HY, HZSM-5 and Hβ catalyst.

3.3.1.3 Powder X-ray Diffraction (XRD)

XRD patterns of HZSM-5, HY and Hβ are elucidated in Figure 3.4. Three peaks at 2θ =22.5°, 23.5°, and 25° denote the (010), (020), (501), (151) and (303) crystal planes of the HZSM-5 molecular sieve (MFI structure) [8]. Peaks between 2θ =20-27◦ of Hβ represent the (300), (302), (304), (306), and (308) crystal planes [9]. Peaks between 2θ = 10-33◦ signify the (220), (311), (331), (511), (440), (533), (642) and (555) crystal faces of HY [10]. The decreased peak intensity and increased line width are attributed to the small crystal size [11].

3.3.1.4 X-ray photoelectron spectroscopy (XPS)

XPS spectra of HY, HZSM-5, and Hβ are depicted in Figure 3.5. The initial peak appearing at 284.8 eV corresponds to non-oxygenated carbon rings that form C–C bonds. The second C1s peak detected at 285.3 eV indicated C-H bonds. The peak at 286.6 eV is associated with carbonyl groups that create C–O bonds [12].

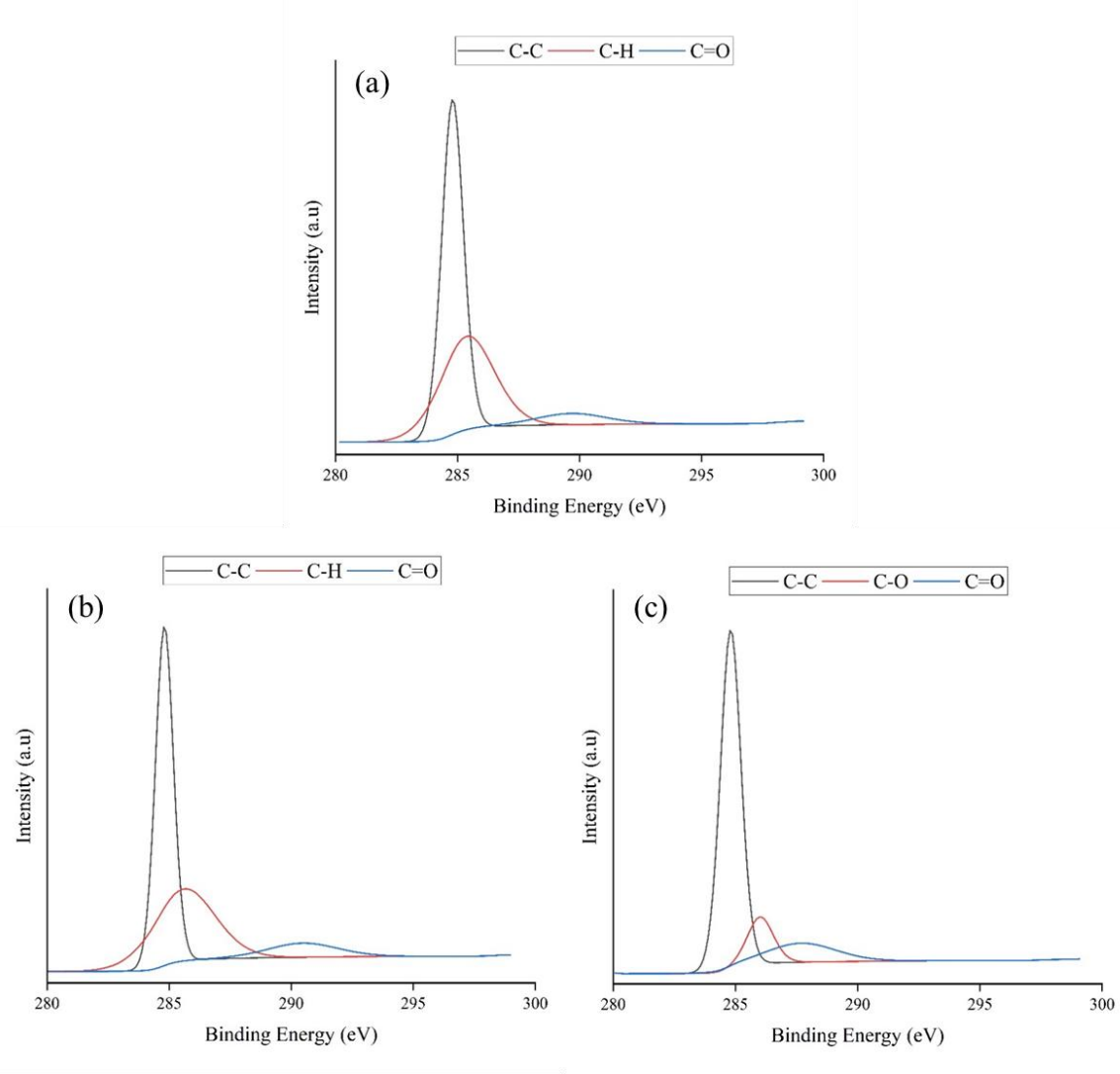

Figure 3.5: XPS spectra of (a) HY, (b) HZSM-5, and (c) Hβ.

XPS analysis of the used catalysts revealed that the quantity of coke present on the catalyst surface was so low (<0.8 wt.%) that it can be neglected compared with the gas and liquid products.

3.3.2 Catalytic performance

3.3.2.1 Effect of scintillator proportion:

Product yields under different graphite/LDPE (G/L) mass ratios are illustrated in Figure 3.6 (a). All experiments were carried out at 400 °C and the HY to LDPE ratio was kept constant at 1:5. It was observed that both the microwave power and the quantity of the absorber (graphite) played an important role as operating parameters. The addition of absorbers affords improved efficiency of the pyrolysis process in terms of conversion [13]. The amount of absorbers varied from 10 to 30g per 10g of LDPE. To discern the role played by the catalyst, the reaction was carried out in the absence of any catalyst. This rendered 40 % LDPE conversion with 30 % and 70 % yields of liquid and gaseous products, respectively at a G/L ratio of 1. The presence of HY enhanced LDPE conversion to 50 % as well as the gaseous product fraction to 72 %. A higher G/L ratio led to elevated proportion of gaseous products and LDPE conversion. MW energy prompts fast pyrolysis with higher heating rates, which subsequently lead to higher rates of cracking and higher yields of gaseous products. Ding et al. reported 50 % yields of liquid and gas products each at 600 °C in the presence of HY catalyst using MW-assisted pyrolysis[14]. Fan et al. obtained 29% liquid yield and 67% gas yield during batch MW pyrolysis of LLDPE in the presence of HZSM-5 [15]. Around 61 % of gaseous products were observed with MgO catalyst in MW-assisted pyrolysis of LDPE [16]. The addition of HY to LDPE increased yield of oil from 52% (in the absence of a catalyst) to 60 %, while the gas yield decreased from 48 % to 39 % [14]. In contrast to this, Liu et al. [17] observed higher yields of gaseous products in the presence of HY. This was ascribed to the stronger acid sites and higher acid density of HY. The increasing yields of gaseous products, as reflected in Figure 3.6 may be explained as follows: with a higher quantity of the microwave absorber (graphite), the rate of temperature rise of the reaction mass (and hence the rate of cracking) increases, leading to the formation of smaller gas molecules.

Liquid product distribution under different G/L mass ratios is shown in Figure 3.6 (b). The salient observations are as follows: In the absence of any catalyst, the liquid product did not contain aromatics. Alkene formation drastically reduced from 86 % at G/L = 1 to 6 % for G/L = 3. Alkane and aromatic yields increased with the G/L value in the presence of the HY catalyst. Aromatic formation may be ascribed to the confinement effect of HY causing cyclization of the olefins generated by LDPE cracking. Alkanes may be envisaged being formed by

hydrogenation of olefins rising from LDPE and H_2, during aromatic formation. It is worth mentioning that Bronsted acid sites are well-reported to catalyze hydrogenation-dehydrogenation reactions. Our speciation in fact, can be validated by the observation of Ding et al. [14] of increased aromatic formation at the cost of olefin formation in presence of HY. As expected, thermal pyrolysis is unlikely to give rise to aromatic formation; results of Aguado et al. [18] and Williams et al.[19] confirm this. However, Gonzalez et al. [20] did find 81% aromatics in the liquid products during thermal cracking of plastic at 600 °C.

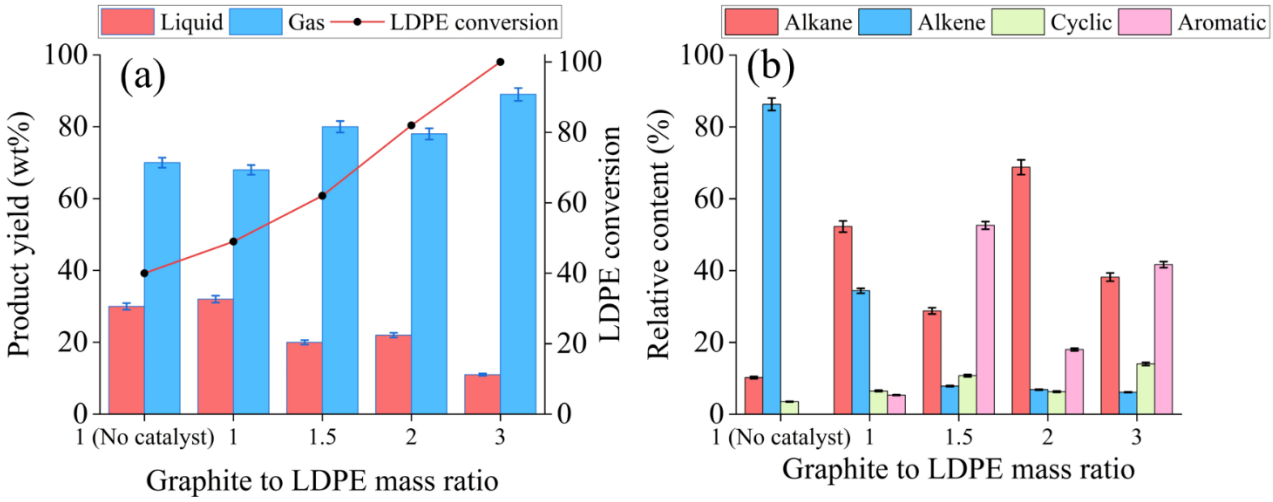

Figure 3.6: Effect of G/L ratio on (a) Product distribution and (b) Liquid composition of LDPE. Temperature - 400 °C, 2g HY.

3.3.2.2 Effect of pyrolysis temperatures

In this set of experiments the catalyst to LDPE (HY, HSZM-5 and Hβ) mass ratio of 1:10, and the G/L ratio of 3 were maintained constant while varying the pyrolysis temperatures. It is evident from Figure 3.7 (a) that up to 450°C H_2 and CH_4 are the chief gaseous products (accounting for around 63% in total). It is likely that cracking reactions dominate over dehydrogenation reactions at higher temperatures, as reflected in the increased ethylene formation. The selectivity to C_2, C_3 and C_4 gases remains almost constant over the temperature range of 400–550 °C. The higher pyrolysis temperature favors the production of C_2 and C_3 compounds. Ting et al.[17] observed a similar trend in the conventional pyrolysis of LDPE.

Compositions of gaseous products over HZSM-5 at different temperatures are presented in Figure 3.7 (b). Here, CH_4 was a key gaseous compound, constituting around 65 vol% at 400 °C. This may be due to cracking of LDPE branches at lower temperatures. A further increase in temperature resulted in reduced CH_4 selectivity, which reached 14 vol% at 550 °C. Ethylene

was another dominant product and its proportion increased with temperature from 26 % at 400 °C to 43 vol % at 550 °C. It has been reported that ZSM-5 facilitates ethylene production from dominant chains by inhibiting the formation of ethane and propane from branched chains [21]. C_2 and C_4 gases were obtained from packaging plastics, while C_3 hydrocarbons originated from polypropylene over ZSM-5[22]. Fan et al. reported higher ethylene production in gaseous products without a catalyst and propylene emerged as a major reaction product during MW-assisted catalytic pyrolysis of LLDPE using HZSM-5 catalyst [23]. Higher selectivity (58 – 65%) of C_2–C_4 olefins and aromatics was achieved with mesoporous ZSM-5 as compared to parent ZSM-5 catalyst during LDPE pyrolysis by Chenet al. [24]. In a semi-batch reactor, the catalytic degradation of HDPE was studied using USY, HZSM-5, and Hβ catalysts at 376 °C. Due to its small pore size, HZSM-5 produces lighter hydrocarbons (C_3-C_4) as compared to USY and Hβ zeolites[25]. Elordi et al. have also reported a higher yield (60%) of C_2 - C_4 olefins in the pyrolysis of HDPE at 500°C with HZSM-5 catalyst [26]. This aligns with the results obtained in this work using HZSM-5 as the catalyst, where a higher proportion of lighter hydrocarbons was observed.

Figure 3.7 (c) exhibits product yields as a function of pyrolysis temperature in the presence of Hβ. Complete (100%) conversion of LDPE was attained in both the absence and the presence of the catalyst at different pyrolysis temperatures. The yield of gaseous products improved from 70 wt.% (in the absence of the catalyst) to 92 wt.% at 550 °C with Hβ catalyst. Whereas liquid yield decreased to 8 wt.% from 30 wt.% as pyrolysis temperature increased from 400 °C to 550 °C. Higher proportion of gas may be due to higher heating rates achieved in MW and higher acidity of Hβ. It has been reported that Hβ catalyst pre-cracks polymer macromolecules on the external surface [27], and with rise in temperature, secondary cracking of macromolecules occurs which subsequently results in the generation of higher amounts of gaseous products [14].

As seen in Figure 3.7 (d), no aromatics were observed in liquid products from MW-assisted cracking of LDPE in the absence of catalyst. Around 86 % alkenes were produced without catalyst, which was reduced to 6% by the addition of Hβ. This could be due to the hydrogen transfer reaction catalyzed by Hβ, producing alkanes. Larger olefins produced by random cleavage can engage with catalytic acid sites that act as proton donors to C=C bonds, generating carbonium ions. These ions subsequently trigger reactions involving isomerization and cracking, ultimately forming branched paraffins and olefins [28,29]. External surface of Hβ

helps to pre-crack polymer macromolecules and form oligomers. Later, the polymers crack within the internal structure of the zeolite [27].

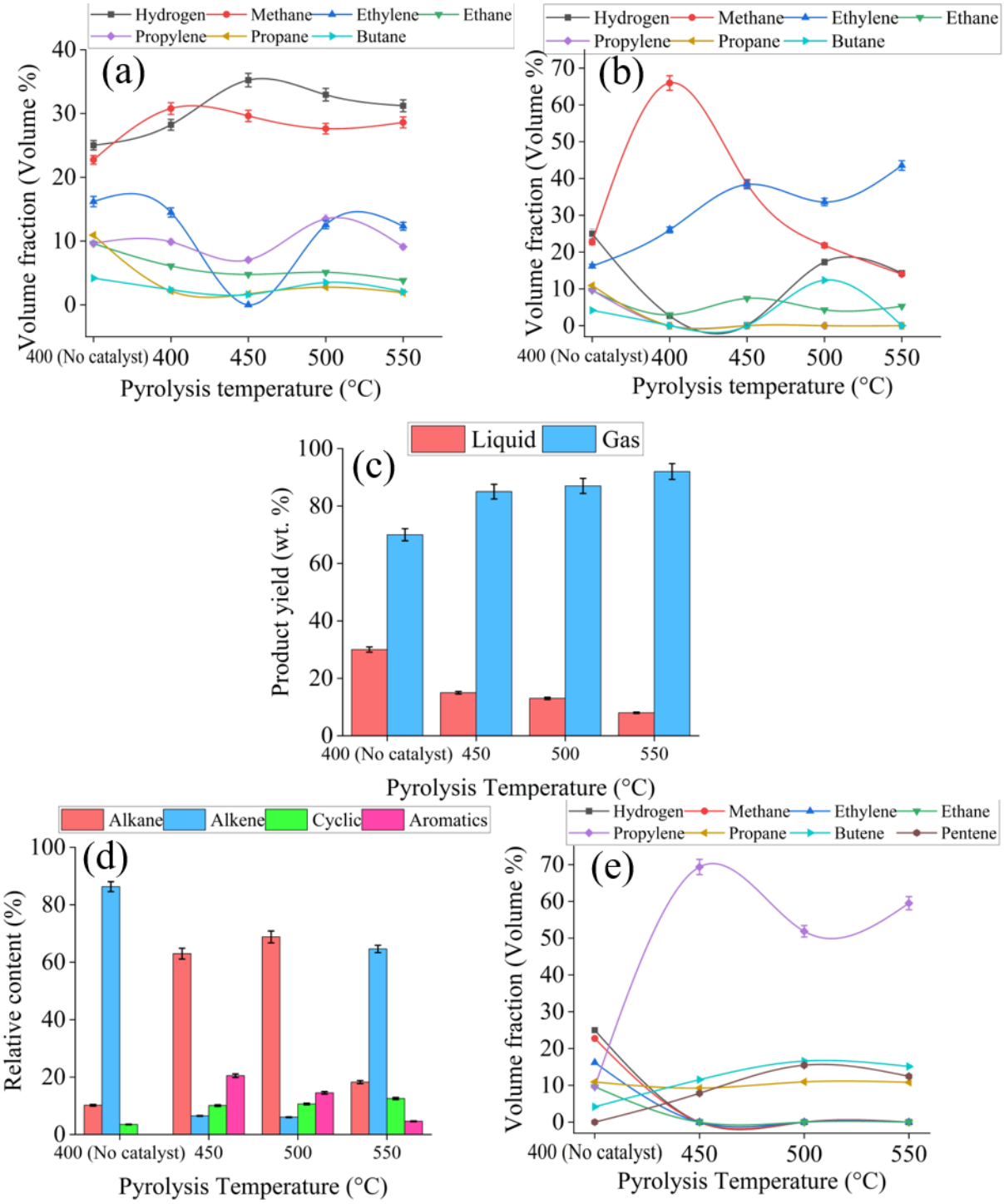

Figure 3.7: The effects of pyrolysis temperature on (a) gas composition at a HY to LDPE ratio of 1:10 (b) gas composition at a HZSM-5 to LDPE ratio of 1:10 (c) Product yield at a Hβ to LDPE ratio of 1:10 (d) Liquid oil composition at a Hβ to LDPE ratio of 1:10and (e) gas composition at a Hβ to LDPE ratio of 1:10.

Figure 3.7 (e) illustrates that the composition of the gaseous products predominantly comprises of hydrocarbon gases ranging from C_3 to C_4 which are suitable for use as fuel. Propylene production accounted for 69 vol% of the total gaseous products at 450°C. Polyethylene undergoes cracking via free radical formation and subsequently advances through the formation of carbenium ions at the secondary carbon position in the presence of the catalyst. The generated carbenium ions undergo β-scission which eventually leads to propylene formation [15,30,31]. A higher yield of propylene was attained with Hβ due to its elevated acidity as compared to the HZSM-5 and HY catalysts [32]. The reduced yield of C_3-C_5 compounds with HY and HZSM-5 catalysts confirm that catalyst acidity significantly influenced product selectivity. An elevated yield of C_4 and C_5 compounds (around 60% of the total gas generated) was attained by Marcilla et al. in the temperature range of 300 - 500°C using Hβ as the catalyst [33]. The larger pore size of Hβ contributed to a greater selectivity towards products with a higher number of carbon atoms, ranging from C_3 to C_5 [27]. Consequently, acidity and pore size of the catalysts are pivotal factors in modulating product composition.

3.3.2.3 Effect of catalyst proportion on gaseous product compositions

Since complete conversion of LDPE was achieved with a G/L ratio of 3, the same was maintained during subsequent experiments, while varying the catalyst quantity. Figure 3.8 (a) evinces the effect of HY loading on the composition of the gaseous products. H_2, methane, ethylene, ethane, propylene, propane, and butane were the constituents of the gaseous fraction. In the absence of any catalyst, H_2 (25 vol %) and CH_4 (22 vol %) were the dominant products. H_2 production increased with proportion of HY and reached a maximum of 35% at 2g (HY: LDPE of 1:5) after which it dropped to 25% at 5g (HY: LDPE of 1:2). Lower HY loading prompts dehydrogenation reaction, whereas a higher ratio of HY to LDPE (1:2) favors cracking reaction, consequently reducing H_2 production while increasing propylene formation. A maximum of 31 % CH_4 was obtained with 1g of HY. H_2 and CH_4 were the major gas products, and their combined proportions were around 50%, 47 %, 65%, and 54 %, at 0, 1, 2 and 5g of HY, respectively. As discussed earlier, the formation of aromatics is accompanied by dehydrogenation. It was observed that on HY, ethane formation dropped from 9 vol% to 5 vol% and ethylene formation decreased from 16 vol% to 9 vol.%. This may be due to higher rate of ethylene oligomerization followed by cyclization, reducing the ethylene concentration in the product stream. Stoichiometrically, LDPE typically contains 14 wt.% of H_2.

A summary of the important aspects reported for H_2 gas formation through LDPE pyrolysis/catalytic cracking is presented in Table 3.1. Ding et al. observed that the addition of NiO to HY catalyst not only enhanced the gaseous product yield but also the H_2 fraction. This was due to the exceptional dehydrogenation ability of NiO catalyst and is the reason behind the extensive usage of Ni–based catalysts in reforming of plastic [1]. In a continuous-stirred MW pyrolysis and batch MW pyrolysis of LLDPE in the presence/absence of HZSM-5, a higher amount of H_2 was reported by Fan et al. However, ethylene and propylene were the chief gaseous products both in the absence and the presence of HZSM-5 [27]. This can be attributed to different cracking mechanisms in non-catalytic (thermal) and catalytic pyrolysis. Ethylene is primarily produced through β-scission of hydrocarbon radicals; whereas propylene *via* formation of free radicals and carbenium ions at secondary carbon positions in the presence of HZSM-5. A slight increase in H_2 yield was observed with an increased amount of HZSM-5, which was attributed to enhanced aromatization, which is accompanied by H_2 liberation [31].

Table 3.1: Summary of studies on plastic cracking for H_2 formation.

Sr. No.	**Reactor (Polymer type)**	**Catalyst and Experimental conditions**	**H_2 (vol%)**	**Reference**
1	MW-assisted catalytic batch pyrolysis of LDPE	NiO to HY ratio of 1:10, 450°C	32	Ding et al.[14]
2	MW-assisted catalytic batch pyrolysis of LLDPE	HZSM-5, 550°C	12	Fan et al. [15]
3	MW assisted Continuous-stirred pyrolysis of LLDPE	HZSM-5, 500°C	13	Fan et al. [23]
4	Multi-core reactor, mixed plastic waste	Ni/Mo/MgO, 700°C	78	Bajad et al.[34]
5	MW-assisted catalytic batch pyrolysis of LDPE	HY, HY to LDPE ratio of 1:5, 400°C	35	This work

Bajad et al. [42] used mixed plastic waste and Ni/Mo/MgO as a catalyst in a multi–core reactor for the production of carbon nanotubes (CNTs) and H_2. Higher CNT synthesis and pyrolysis temperature resulted in higher production of H_2 rich gases. This is due to the higher rate of free radicals formation at elevated temperatures, which subsequently improves hydrocarbon dissociation and affords higher selectivity towards H_2.

Effect of HZSM-5 loading on the results obtained is depicted in Figure 3.8 (b). It indicates that ethylene was the major product across all catalyst-to-LDPE ratios and reaction temperatures. Notably, around 16 vol % of ethylene was observed without the catalyst. However, the presence of HZSM-5 remarkably promoted ethylene production to 33.5 vol % at a 1:20 catalyst-to-LDPE ratio. A maximum of 43 % ethylene formation was achieved with a catalyst-to-LDPE ratio of 1:10. A further increase in catalyst loading to a ratio of 1:5 resulted in reduced ethylene formation to 38 %. Conversely, due to the instability of primary carbenium ions, ethylene formation was hindered during catalytic cracking. Consequently, ethylene yield decreased with an increased amount of catalyst, as has also been reported earlier [23]. This higher ethylene formation at lower catalyst loadings can be attributed to HZSM-5's ability to promote cracking reactions by inhibiting the hydrogen transfer mechanism. H_2 production augmented with incremental addition of the catalyst, potentially attributable to the catalytic process overshadowing the cracking reaction. Methane, ethane, propane, propylene, and iso-butane were the other gaseous products, with no discernible alteration observed in their distribution. Studies indicated that the collective selectivity of benzene-toluene-xylene (BTX) and C_2-C_4 olefins surpassed 67% for LDPE and 47% for PP when subjected to MW- irradiation employing a ZSM-5 catalyst at 300 ˚C[35]. According to this report, primarily light olefins (C_3-C_5) are generated with the ZSM-5 catalyst, while aromatic production remains constrained at reaction temperatures below 500°C. The enhanced ethylene yield facilitated by HZSM-5 in the current work serves to diminish reliance on conventional fuels and paves the path toward a circular economy.

Hβ afforded a maximum propylene yield of 69% at 450°C. Consequently, the decision was made to maintain pyrolysis temperature constant at 450°C while conducting reactions with varying quantities of Hβ. Figure 3.8 (c) delineates the impact of catalyst quantity on product yield at 450°C. Gaseous products yield demonstrates a linear increase with Hβ proportion as also observed by Morais et al [36]. The yield of gases reached around 75 wt.% at 1:20 ratio of Hβ to LDPE and reached a maximum of 96 wt.% at 1:5 ratio of Hβ to LDPE. This observation confirms the catalytic enhancement provided by Hβ during the cracking of large molecular volatiles. Higher catalyst loading stimulates secondary cracking within the reaction mixture. On the other hand, the liquid yield reduced to 3.6% from 25% upon increasing the Hβ to LDPE ratio to 1:5 from 1:20. Of the three catalysts tested namely HY, HZSM-5, and Hβ, Hβ exhibited the highest gaseous product yield (96%) at 450°C. This highlights the significant influence of the acidic sites of the catalysts in reducing the pyrolysis temperature of plastics [27].

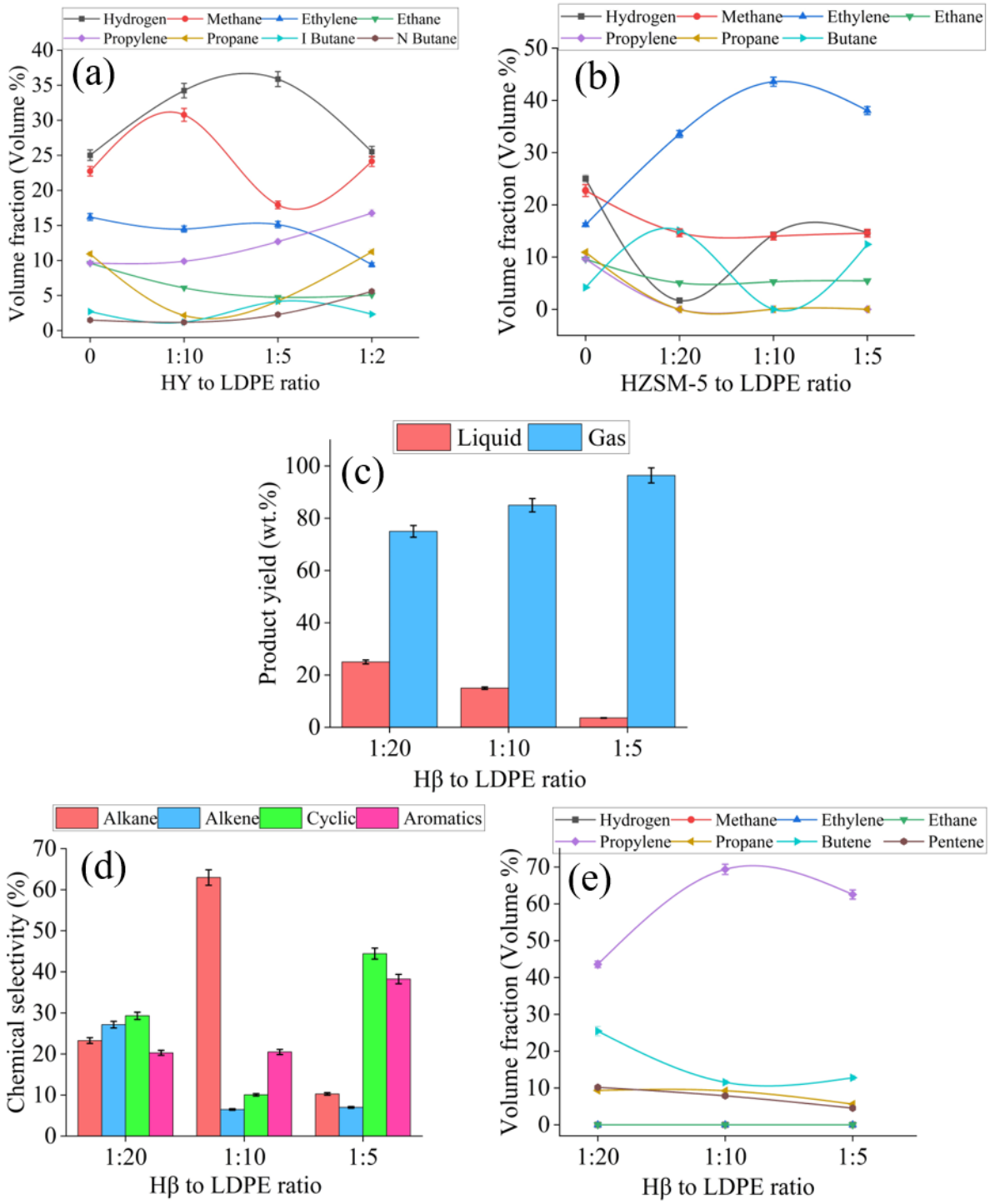

Figure 3.8: Effect of catalyst proportion on (a) Gas composition at 400 °C with HY (b) Gas composition at 550 °C with HSZM-5 (c) Product yield at 450 °C (d) Liquid oil composition at 450 °C and (e) Gas composition at 450 °C.

Figure 3.8 (d) illustrates the impact of Hβ/LDPE ratio on liquid product composition. It was observed that at the ratio of 1:20, all fractions, namely aromatics, cyclic compounds, alkanes, and alkenes, were distributed between 20% and 29%. The highest formation of aromatics and cyclic compounds reached 38% and 44%, respectively, at Hβ/LDPE ratio of 1:5. This indicates that a higher quantity of catalyst promotes a chain-end mechanism, leading to production of light olefins, which subsequently combine to form cyclic compounds. At the Hβ to LDPE ratio of 1:10, random scission occurs which generates large olefins which converted to alkanes through hydrogen transfer mechanisms. Okonsky et al. reported a 15% yield of aromatics for LDPE cracking in the presence of Hβ at 500°C [3].

Influence of the Hβ/LDPE ratio on gaseous product composition is illustrated in Figure 3.8 (e). Notably, propylene emerged as the predominant product within the gaseous mixtures. Specifically, propylene production surged to 43% at Hβ/LDPE ratio of 1:20, rising further to 69% at a ratio of 1:10, albeit experiencing a slight decline to 62% at a ratio of 1:5. Marcilla et al. also obtained gaseous compounds ranging from C_3 to C_5 using Hβ catalyst [27]. As discussed previously, lower catalyst loading favors random scission, yielding larger olefins that subsequently undergo β-scission generating propylene. On the other hand, with increased catalyst loading, propylene formation decreases because of cyclization reactions that result in the formation of aromatic and cyclic compounds, as observed in the liquid oil composition. A gradual decline in butane and pentene proportions was observed with Hβ/LDPE ratio. Their proportions were around 25% and 10%, respectively at a 1:20 ratio of the catalyst (Hβ) to LDPE, which decreased to 13% and 4%, respectively at a ratio of 1:5. These results are in agreement with those of Morais et al. [36] who identified C_3 and C_4 as significant components in the gaseous product with varying catalyst loadings from 0.2% to 0.75%.

3.3.2.4 Influence of desilicated Hβ (D-Hβ) on product compositions

In contrast to the untreated Hβ, alkali-treated Hβ produced a slightly larger volume of liquid and a reduced volume of gas as shown in Figure 3.9. Munir et al. [37] also achieved a 30% oil yield through catalytic hydrocracking of plastic waste using desilicated Hβ at 375°C in an autoclave reactor. The increase in pore size shortened the diffusion distance for the products, which in turn inhibited the hydrogen transfer reactions of olefins. Consequently, this modification effectively minimized alkane formation. Treating the zeolite with a concentrated alkaline solution substantially reduces its acidity and micropore volume. This change results in a decrease in the selectivity for aromatics while improving the selectivity for olefins.

Lee et al. [38] conducted traditional pyrolysis of HDPE and observed that heavy aliphatic hydrocarbons were absent from the chromatogram over desilicated Hβ, even at low catalyst-to-plastic ratios (1:1). Instead, the primary products were light isoparaffins and aromatic hydrocarbons. Azam et al. [39] also reported achieving around 60% paraffins and 12% aromatics during the hydrocracking of waste plastics at 325°C using 5% Ni-loaded desilicated Hβ. Munir et al. [37] obtained around 65% gasoline fraction (C_5-C_{12}) yield through catalytic hydrocracking of plastic waste with desilicated Hβ at 400°C in an autoclave reactor.

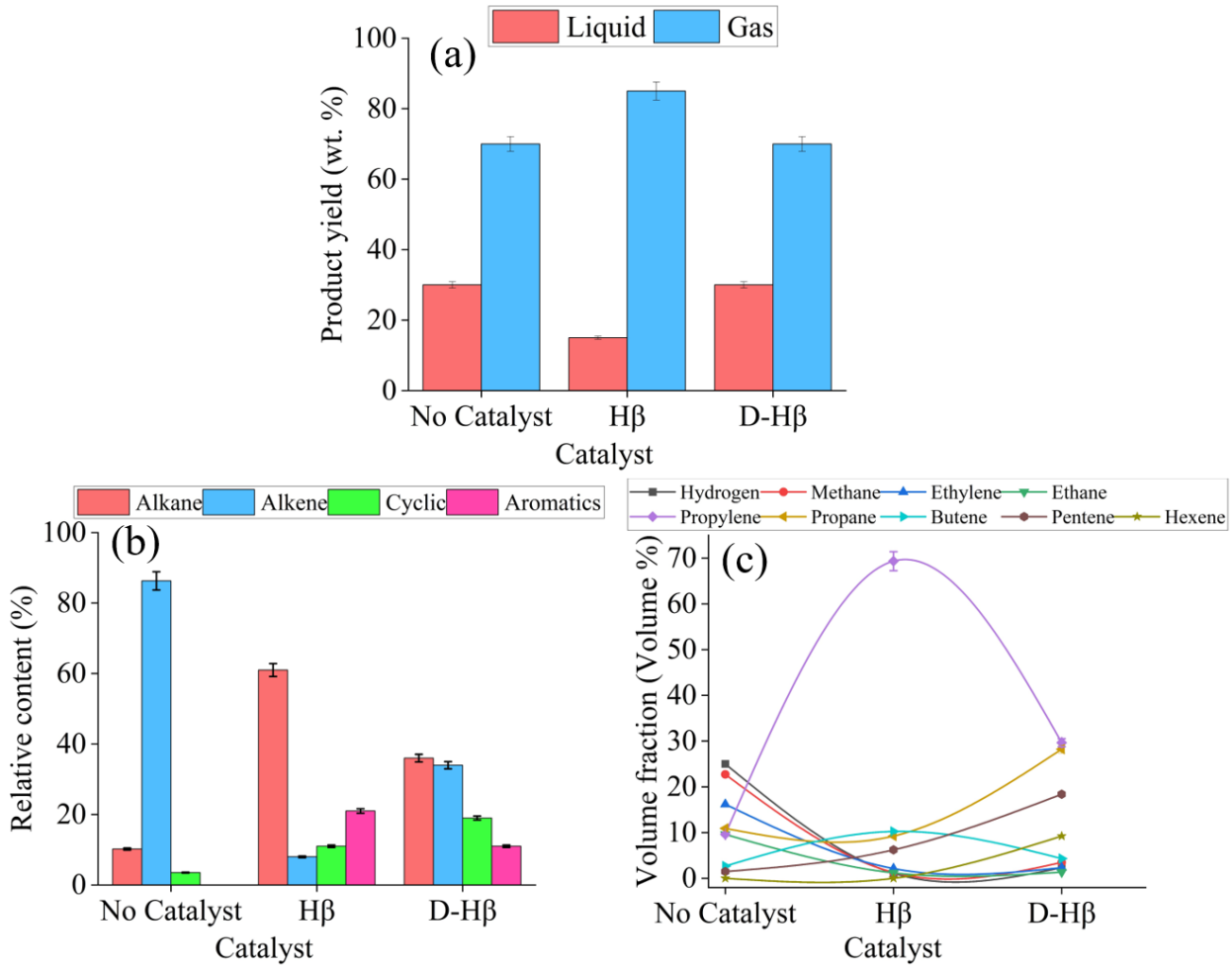

Figure 3.9: Effect of Hβ and D-Hβ on (a) Product yield at 450°C, (b) Liquid composition at 450°C and (c) Gas composition at 450°C. Hβ to LDPE ratio was 1:10.

The significant loss of micropores poses a disadvantage for the aromatization of olefins, resulting in a higher retention of olefins in gas products. As the mesoporosity of Hβ increases, the amount of propylene decreases, while the quantities of pentene and hexene increase.

3.3.2.5 Reaction mechanism of catalytic pyrolysis using HZSM-5, HY, and Hβ

In the degradation of LDPE, both random scission and chain scission can occur, resulting in the formation of either smaller or larger olefins, respectively[40,41]. The light olefins generated from end-chain cracking may undergo dehydrocyclization to produce aromatics, participate in condensation reactions to create polyaromatics and coke or undergo cyclisation to form cycloalkanes [40–42]. Conversely, the larger olefins produced from random scission can interact with catalytic acid sites which supply protons to C—C bonds and ultimately lead to the formation of carbonium ions. These carbonium ions then facilitate isomerisation and cracking reactions, resulting in creation of branched paraffins and olefins [28,29].

3.3.2.6 Catalyst Reusability Test

The catalyst's reusability is central to ensuring the cost-efficiency of the process. To assess this, experiments were conducted employing 30 g of graphite (as an absorber) and 10 g of LDPE at a constant catalyst/LDPE ratio of 1:10 for all three HY, HZSM-5, and Hβ catalysts. Following each experiment, catalysts underwent regeneration at 500°C in air in the furnace. The pyrolysis temperature for HY and Hβ catalysts was maintained at 450°C and that for HZSM-5 at 550°C, which are the temperatures at which maximum amounts of gaseous products were observed. As depicted in Figure 3.10 (a), the initial H_2 proportion of around 35% with fresh HY dropped to 33% after the first regeneration, which further fell to 32% after the second regeneration. However, CH_4 ethylene, ethane, propylene, propane, and butane concentrations remained practically unchanged. The deactivation of USY was examined by TGA and the results obtained indicated coke formation on the catalyst, which could be restored to its original state post-regeneration [43]. In this scenario, the consistent high activity of the catalyst (achieving complete conversion of LDPE) throughout all three repetitive cycles, coupled with nearly identical product compositions, indicates its robustness and stability under the reaction conditions. There was either no or minimal coke formation on its surface even after three cycles, thus posing no adverse effects on its catalytic activity. Similarly, akin to HY catalyst, product compositions remained largely unchanged across all three repetitive cycles with HZSM-5 catalyst. Ethylene emerged as the predominant product within the gaseous mixtures, constituting 43% with fresh HZSM-5 and its proportions hovered around 42% and 43% during the first and second recycling cycles, respectively. In this context, the acidic sites play an important role in dictating product distribution during catalytic cracking. USY zeolite demonstrated consistent performance even after eight regeneration cycles. From the tenth cycle onwards, a decline in its activity was observed with the emergence of wax noted by the

fourteenth cycle [44]. The HZSM-11 catalyst too maintained consistent performance over first eight reaction cycles which was followed by an uptick in production of liquid products at the expense of gaseous products [45]. At 450°C with Hβ to LDPE ratio of 1:10, propylene, the dominant product (69 %) of the gaseous mixture with fresh Hβ catalyst fell to 67 % and 66 % after first and second regeneration, respectively (Figure 3.10 (c)). Similarly, the production of other compounds (propane, butane, and pentene) remained relatively stable throughout the cycles. Renzini et al. observed a gradual decline in the yield of gaseous hydrocarbons up to seven cycles and afterwards it stabilized at a constant level. Formation of wax was reported after the fifteenth cycle using Hβ catalyst [45].

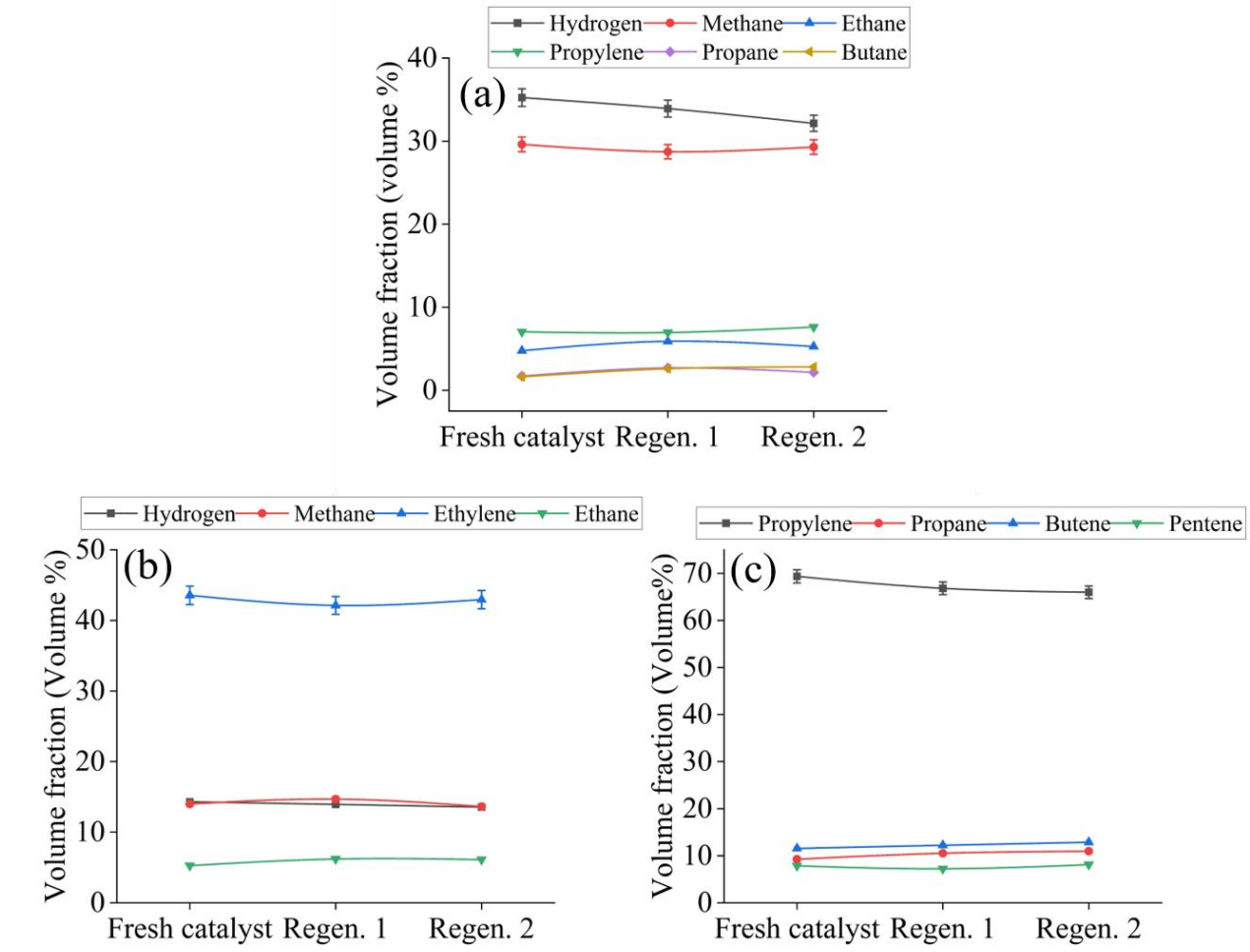

Figure 3.10: Effect of catalyst reusability on gas composition (a) HY to LDPE ratio 1:10 at 450 °C. (b) HZSM-5 to LDPE ratio 1:10 at 550 °C. (c) Hβ to LDPE ratio 1:10 at 450 °C.

3.4 Conclusion

Catalytic cracking of LDPE in MW reactor in presence of graphite as an absorber and utilizing HY, HZSM-5, and Hβ catalysts was investigated. Study explored effects of catalyst-to-reactant ratio and pyrolysis temperature. Comparatively, catalytic pyrolysis with all three catalysts yielded lower amounts of liquid when contrasted with non-catalytic pyrolysis. HY catalyst played a crucial role in formation of aromatics and alkanes, with H_2 (55%) dominating at 450◦C and methane (31%) prevailing at 400◦C as the main gases of gaseous mixture. HZSM- 5 promoted methane formation (66%) at 400◦C and ethylene (43%) at 550◦C. Increased ethylene production with HZSM-5 aims to lessen reliance on traditional fuels, representing a step towards a circular economy. Hβ contributed to generation of alkanes and aromatics, with gaseous products primarily comprising C3-C4 hydrocarbon gases, including 69% propylene at 450◦C. All three catalyst shows excellent catalytic activity and higher product selectivity indicating a way forward towards sustainability by effectively converting waste plastic to value added products.

3.5 References

[1] J. Aguado, J.L. Sotelo, D.P. Serrano, J.A. Calles, J.M. Escola, Catalytic Conversion of Polyolefins into Liquid Fuels over MCM-41: Comparison with ZSM-5 and Amorphous SiO_2 −Al_2O_3, Energy & Fuels 11 (1997) 1225–1231. https://doi.org/10.1021/ef970055v.

[2] V.G. Komvokis, S. Karakoulia, E.F. Iliopoulou, M.C. Papapetrou, I.A. Vasalos, A.A. Lappas, K.S. Triantafyllidis, Upgrading of Fischer–Tropsch synthesis bio-waxes via catalytic cracking: Effect of acidity, porosity and metal modification of zeolitic and mesoporous aluminosilicate catalysts, Catal. Today 196 (2012) 42–55. https://doi.org/10.1016/j.cattod.2012.06.029.

[3] Sean Timothy Okonsky, J.V. Jayarama Krishna, Hilal Ezgi Toraman, Catalytic co-pyrolysis of LDPE and PET with HZSM-5, H-Beta, and HY: Experiments and kinetic modelling, React. Chem. Eng. (2022).

[4] P.L. editors Weitkamp J, Catalysis and zeolites: fundamentals and applications, New York: Springer Berlin Heidelberg (1999) 546.

[5] Niwa M, Suzuki K, Katada N, Niwa M, Suzuki K, et al Isamoto K, Identification and measurements of strong brønsted acidsite in ultrastable y (USY) zeolite, J Phys Chem B (2006) 264.

[6] Handke M, Mozgawa W, Vibrational spectroscopy of theamorphous silicates, Vib Spectrosc 5 (1993) 75–84.

[7] Anggoro DD, Buchori L, Silaen GC, Utami RN, Preparation,characterization, and activation of Co-Mo/Y zeolite catalyst forcoal tar conversion to liquid fuel, Bull Chem React Eng Catal 12 (2017) 219–226.

[8] Wen Ding, Yuyang Cui, Jianjun Li, Yiquan Yang, Weiping Fang, Promoting effect of dual modification of H-ZSM-5 catalyst by alkali treating and Mg doping on catalytic performances for alkylation of benzene with ethanol to ethylbenzene, The Royal Society of Chemistry (2014) 50123–50129.

[9] M. Sahooli, M. Rahimpour, M. Khorram, Fine-Tuning Synthesis and Characterization of Mono-Sized H-Beta Zeolite-Supported Palladium-Iridium Nanoparticles and Application in the Selective Hydrogenation of Acetylene, Catalysts 7 (2017) 343. https://doi.org/10.3390/catal7110343.

[10] F. Chen, D. Zhang, L. Shi, Y. Wang, G. Xu, Optimized Pore Structures of Hierarchical HY Zeolites for Highly Selective Production of Methyl Methoxyacetate, Catalysts 9 (2019) 865. https://doi.org/10.3390/catal9100865.

[11] X.J. Cheng, X.S. Wang, H.Y. Long, Transalkylation of benzene with 1, 2, 4 trimethylbenzene over nanosized ZSM-5, Microporous and Mesoporous Materials 119 (2009) 171.

[12] R. Kumar, H. Jain, A. Chaudhary, S. Kumari, D.P. Mondal, A.K. Srivastava, Thermal conductivity and fire-retardant response in graphite foam made from coal tar pitch derived semi coke, Compos. B Eng. 172 (2019) 121–130. https://doi.org/10.1016/j.compositesb.2019.05.036.

[13] Dadi V. Suriapparao, Garlapati Nagababu, Attada Yerrayya, Veluru Sridevi, Optimization of microwave power and graphite susceptor quantityfor waste polypropylene microwave pyrolysis., Process Safety and Environmental Protection (2021) 234–243.

[14] K. Ding, S. Liu, Y. Huang, S. Liu, N. Zhou, P. Peng, Y. Wang, P. Chen, R. Ruan, Catalytic microwave-assisted pyrolysis of plastic waste over NiO and HY for gasoline-range hydrocarbons production, Energy Convers. Manag. 196 (2019). https://doi.org/10.1016/j.enconman.2019.07.001.

[15] Liangliang Fan, Lei Liu, Zhiguo Xiao, Zheyang Su, Pei Huang, HongyuPeng, SenLv, Haiwei Jiang, Roger Ruan, Paul Chen, Wenguang Zhou, Comparative study of continuous-stirred and batch microwave pyrolysis of linear low-density polyethylene in the presence/absenceof HZSM-5, Energy (2021).

[16] Liangliang Fan, Yaning Zhang, Shiyu Liu, Nan Zhou, Paul Chen, Yuhuan Liu, Yunpu Wang, PengPeng, Yanling Cheng, Min Addy, Hanwu Lei, Roger Ruan, Catalytic upgrading of vapors from microwave-assisted pyrolysis of low-density polyethylene with MgO, Energy Convers. Manag. (2017).

[17] Ting Liu, Yincui Li, Yifan Zhou, Shengnan Deng, Huawei Zhang, Efficient pyrolysis of Low-Density Polyethylene for Regulatable Oil and Gas Products by ZSM-5, HY and MCM-41 Catalyst, Catalysts (2023) 382.

[18] J. Aguado, D.P. Serrano, G. San Miguel, M.C. Castro, S. Madrid, Feedstock recycling of polyethylene in a two-step thermo-catalytic reaction system, J. Anal. Appl. Pyrolysis 79 (2007) 415–423. https://doi.org/10.1016/j.jaap.2006.11.008.

[19] P.T. Williams, E.A. Williams, Fluidised bed pyrolysis of low density polyethylene to produce petrochemical feedstock, J. Anal. Appl. Pyrolysis 51 (1999) 107–126. https://doi.org/10.1016/S0165-2370(99)00011-X.

[20] Baena-Gonzalez J, Santamaria-Echart A, Aguirre JL, Gonzalez S, Chemical recycling of plastic waste: bitumen, solvents, and polystyrene from pyrolysis oil, (2020).

[21] X. Zhang, H. Lei, G. Yadavalli, L. Zhu, Y. Wei, Y. Liu, Gasoline-range hydrocarbons produced from microwave-induced pyrolysis of low-density polyethylene over ZSM-5, Fuel 144 (2015). https://doi.org/10.1016/j.fuel.2014.12.013.

[22] N. Miskolczi, A. Angyal, L. Bartha, I. Valkai, Fuels by Pyrolysis of Waste Plastics from Agricultural and Packaging Sectors in a Pilot Scale Reactor, Fuel Process. Technol 90 (2009) 1032–1040.

[23] Liangliang Fan, Zheyang Su, Jiabo Wu, Zhiguo Xiao, Pei Huang, Lei Liu, Haiwei Jiang, Wenguang Zhou, Shiyu Liu, Roger Ruan, Integrating continuous-stirred microwave pyrolysis with ex-situ catalyticupgrading for linear low-density polyethylene conversion: Effects of parameter conditions, Journal of Analytical and Applied Pyrolysis (2021).

[24] Zhaohui Chen, Mohammad Monzavi, Mohammad Latifi, Said Samih, Jamal Chaouki., Microwave-responsive SiCfoam@zeolite core-shell structured catalyst for catalytic pyrolysis of plastics, Environmental Pollution (2022).

[25] G. Manos, A. Garfoth, J. Dwyer, Catalytic Degradation of High-Density Polyethylene over Different Zeolitic Structures, Ind. Eng. Chem. Res 39 (2000) 1198.

[26] G. Elordi, M. Olazar, G. Lopez, P. Castano, J. Bilbao, Role of pore structure in the deactivation of zeolites (HZSM-5, H and HY) by coke in the pyrolysis of polyethylene in a conical spouted bed reactor, Applied Catalysis B: Environmental (2011) 224–231.

[27] A. A. Marcilla, Gómez-Siurana, F. Valdés, Catalytic cracking of low-density polyethylene over H-Beta and HZSM-5 zeolites: Influence of the external surface. Kinetic model. Polymer Degradation and Stability, Polymer Degradation and Stability 92 (2007) 197–204.

[28] C. Wang, H. Lei, M. Qian, E. Huo, Y. Zhao, Q. Zhang, W. Mateo, X. Lin, X. Kong, R. Zou, R. Ruan, Application of highly stable biochar catalysts for efficient pyrolysis of plastics: a readily accessible potential solution to a global waste crisis, Sustain. Energy Fuels 4 (2020) 4614–4624. https://doi.org/10.1039/D0SE00652A.

[29] J.H. Harrhy, A. Wang, J.S. Jarvis, P. He, S. Meng, M. Yung, L. Liu, H. Song, Understanding zeolite deactivation by sulfur poisoning during direct olefin upgrading, Commun. Chem. 2 (2019) 37. https://doi.org/10.1038/s42004-019-0141-4.

[30] Kassargy C, Awad S, Burnens G, Kahine K, Tazerout M, Experimental study ofcatalytic pyrolysis of polyethylene and polypropylene over USY zeolite andseparation to gasoline and diesel-like fuels, J Anal Appl Pyrol (2017).

[31] Corma A, Orchilles AV, Current views on the mechanism of catalytic cracking.Microporous Mesoporous, Mater (2000).

[32] I.L. Simakova, Yu.S. Demidova, M.N. Simonov, P.S. Niphadkar, V.V. Bokade, N. Devi, P.L. Dhepe, D.Yu. Murzin, Mesoporous carbon and microporous zeolite supported Ru catalysts for selective levulinic acid hydrogenation into γ-valerolactone, Catalysis for Sustainable Energy 6 (2019) 38–50. https://doi.org/10.1515/cse-2019-0004.

[33] A. A. Marcilla, Go´mez-Siurana, F. Valde´s, Catalytic pyrolysis of LDPE over H-beta and HZSM-5 zeolites in dynamic conditions Study of the evolution of the process, J. Anal. Appl. Pyrolysis 79 (2007) 433–442.

[34] Ganesh Bajad, R.P. Vijayakumar, Prajwal Rakhunde, Amit Hete, Mahesh Bhade, Processing of mixed-plastic waste to fuel oil, carbon nanotubes and hydrogen using multi–core reactor, Chem. Eng. Process (2017) 205–214.

[35] Yuxin Wang, Tara Biddle, Changle Jiang, Thang Luong, Roujia Chen, Sean Brown, Xiangyu Jie, Jianli Hu, Microwave-driven upcycling of single-use plastics using zeolite catalyst, Chemical Engineering Journal (2023).

[36] E.K.L. Morais, S. Jiménez-Sánchez, H. Hernando, C. Ochoa-Hernández, P. Pizarro, A.S. Araujo, D.P. Serrano, Catalytic Copyrolysis of Lignocellulose and Polyethylene Blends over HBeta Zeolite, Ind. Eng. Chem. Res. 58 (2019) 6243–6254. https://doi.org/10.1021/acs.iecr.8b06158.

[37] D. Munir, H. Amer, R. Aslam, M. Bououdina, M.R. Usman, Composite zeolite beta catalysts for catalytic hydrocracking of plastic waste to liquid fuels, Mater. Renew. Sustain. Energy 9 (2020) 9. https://doi.org/10.1007/s40243-020-00169-3.

[38] H.W. Lee, Y.-K. Park, Catalytic Pyrolysis of Polyethylene and Polypropylene over Desilicated Beta and Al-MSU-F, Catalysts 8 (2018) 501. https://doi.org/10.3390/catal8110501.

[39] M.U. Azam, A. Fernandes, M.J. Ferreira, W. Afzal, I. Graça, Pore-Structure Engineering of Hierarchical β Zeolites for the Enhanced Hydrocracking of Waste Plastics to Liquid Fuels, ACS Catal. 14 (2024) 16148–16165. https://doi.org/10.1021/acscatal.4c05354.

[40] X. Zhang, H. Lei, Synthesis of high-density jet fuel from plastics via catalytically integral processes, RSC Adv. 6 (2016) 6154–6163. https://doi.org/10.1039/C5RA25327F.

[41] J. Aguado, D.P. Serrano, J.L. Sotelo, R. Van Grieken, J.M. Escola, Influence of the Operating Variables on the Catalytic Conversion of a Polyolefin Mixture over HMCM-41 and Nanosized HZSM-5, Ind. Eng. Chem. Res. 40 (2001) 5696–5704. https://doi.org/10.1021/ie010420c.

[42] S. Matsuura, T. Hashimoto, A. Ishihara, Catalytic cracking of low-density polyethylene over zeolite-containing hierarchical two-layered catalyst with different mesopore size using Curie point pyrolyzer, Fuel Processing Technology 227 (2022) 107106. https://doi.org/10.1016/j.fuproc.2021.107106.

[43] Y.-H. Lin, P.N. Sharratt, A.A. Garforth, J. Dwyer, Deactivation of US-Y zeolite by coke formation during the catalytic pyrolysis of high density polyethylene, Thermochim, Acta (1997) 45–50.

[44] Chantal Kassargya, Sary Awada, Gaëtan Burnensa, Gaurav Upretia, Khalil Kahine, Mohand Tazerout, Study of the effects of regeneration of USY zeolite on the catalytic cracking of polyethylene, Applied Catalysis B: Environmental (2019) 704–708.

[45] Maria S. Renzini, Laura C. Lerici, Ulises Sedranb, Liliana B. Pierellaa, Stability of ZSM-11 and BETA zeolites during the catalytic cracking of low-density polyethylene, Journal of Analytical and Applied Pyrolysis (2011) 450–455.

CHAPTER – 4

Influence of acidity of spent FCC catalyst and TiO_2 on product distribution in microwave assisted LDPE cracking

4.1 Introduction

In the second phase of this work, influence of catalyst acidity on microwave-assisted LDPE pyrolysis was systematically investigated using a spent FCC catalyst and TiO_2 as moderately acidic and weakly acidic catalysts, respectively. The role of acidity in governing product distribution, cracking efficiency, and gas composition was analyzed to establish correlations between catalyst properties and reaction performance.

Catalyst acidity plays a crucial role in governing the cracking behavior of polyolefins such as LDPE, influencing C–C bond scission, secondary cracking reactions, and product selectivity. The spent fluid catalytic cracking (FCC) catalyst and TiO_2 represent two contrasting catalytic materials in terms of acidity and surface properties, making them suitable model catalysts for evaluating the influence of acid strength on LDPE cracking.

TiO_2 plays a stabilizing role in heterogeneous catalysts, enhancing plastic degradation efficiency, lowering the required reaction temperature, and shifting product distribution toward increased gas formation, with liquid products exhibiting properties comparable to those of commercial gasoline [1]. Elordi et al. reported that the spent FCC catalyst features a meso- and macroporous matrix that enhances the transport of long polymer chains, whereas its microporous zeolite domains impart shape selectivity, promoting the production of gasoline-range hydrocarbons and light olefins [2].

Microwave-assisted cracking further enhances these effects by providing rapid and uniform heating, reducing heat and mass transfer limitations, and intensifying catalyst–polymer interactions. Therefore, this study investigates microwave-assisted cracking of LDPE over a spent FCC catalyst and TiO_2 to elucidate the impact of catalyst acidity on product yield and composition under identical operating conditions.

4.2 Materials and methods

4.2.1 Materials

LDPE granules were obtained from Reliance Industries Ltd. Graphite powder (CAS no. 7782-42-5) was purchased from Fine Chemicals, Bangalore, and titanium dioxide (TiO_2) (CAS no. 13463-67-7) was obtained from Loba Chemie, Mumbai. The spent FCC catalyst was sourced from a nearby refinery.

4.2.2 Catalyst characterization

Scanning electron microscopy (SEM) was used to examine the surface morphology of the catalyst using a Thermo Fisher Scientific Apereo 2S Highvac FESEM. The catalyst structures were analyzed by X-ray diffraction (XRD) using a Panalytical X'Pert Pro, with Cu Kα (1.54 Å wavelength) or Mo Kα (0.71 Å wavelength) as the X-ray source. Measurements were made within the range of 5–140◦ under operating conditions of 40 mA and 45 kV. Fourier-transform infrared (FTIR) spectra of the samples were recorded using KBr optics on a PerkinElmer Spectrum Two instrument, covering the 400-4000 cm^{-1} in reflection mode. A Belcat II instrument was employed to examine the acidity of the catalyst using the NH_3-TPD method. The heat treatment (degassing) was accomplished from room temperature to a maximum of 1000℃. XPS spectra of the catalysts were obtained using an Axis Supra (Kratos Analytical Ltd) with a monochromatic X-ray source (Al Kα, 1486.6 eV) to analyze the amount of coke on the catalyst.

Experimental setup employed in this study was the same as that described in Section 3.2.4 of Chapter 3.

4.3 Results and discussion

4.3.1 Catalyst characterization

4.3.1.1 Scanning electron microscope

SEM analysis of the structure and morphology of surface particles is presented in Figure 4.1. SEM images revealed that the crystal size of the spent FCC catalyst ranged from 0.5 to 1.0 μm, whereas that of TiO_2 ranged from 0.3 to 0.5 μm.

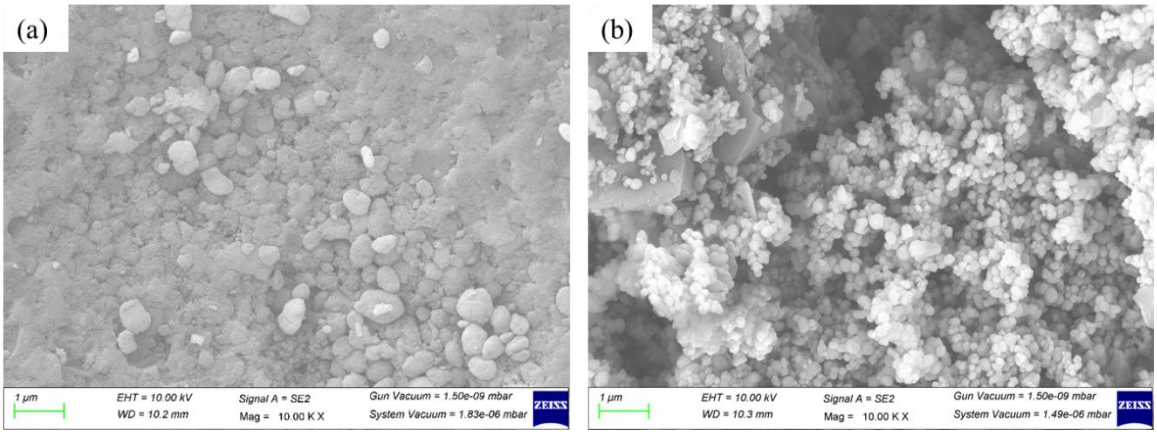

Figure 4.1: SEM images of (a) spent FCC and (b) TiO_2.

4.3.1.2 Fourier transform infrared spectroscopy (FTIR)

Functional groups on the catalysts were recognized through FTIR spectroscopy, as shown in Figure 4.2. The peaks at 3453 cm^{-1} are attributed to the absorption band associated with the stretching vibration of OH group and the peak at 1637 cm^{-1} is associated with the bending vibration of OH group [3]. The stretching and bending vibration, of Si–O–Si bonds are observed at 1092 cm^{-1} [4,5]. The strong peak at 698 cm^{-1} is ascribed to Ti–O stretching band which is a distinctive feature of TiO_2 [6].

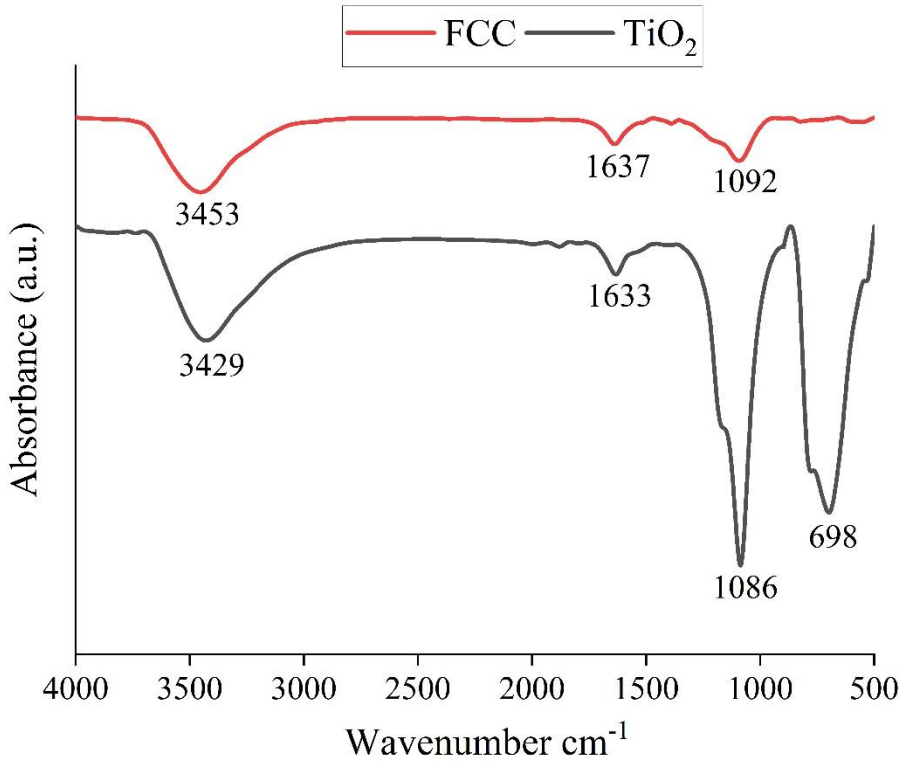

Figure 4.2: FTIR patterns of spent FCC and TiO_2 catalyst.

4.3.1.3 Powder X-ray diffraction

XRD patterns of the spent FCC and TiO_2 are elucidated in Figure 4.3. The diffraction peaks of spent FCC catalyst at 6.3˚, 10.3˚, 12.1˚and 16˚ correspond to (111), (220), (311) and (331) planes of the zeolite Y phase [7]. The XRD pattern of TiO_2 displays peaks at 2θ values of 25.35˚, 37.9˚, 48.48˚, 54.15˚, 55.1˚, and 62.9˚. These peaks closely correspond to the tetragonal planes (101), (004), (200), (105), (211), and (204), respectively [8].

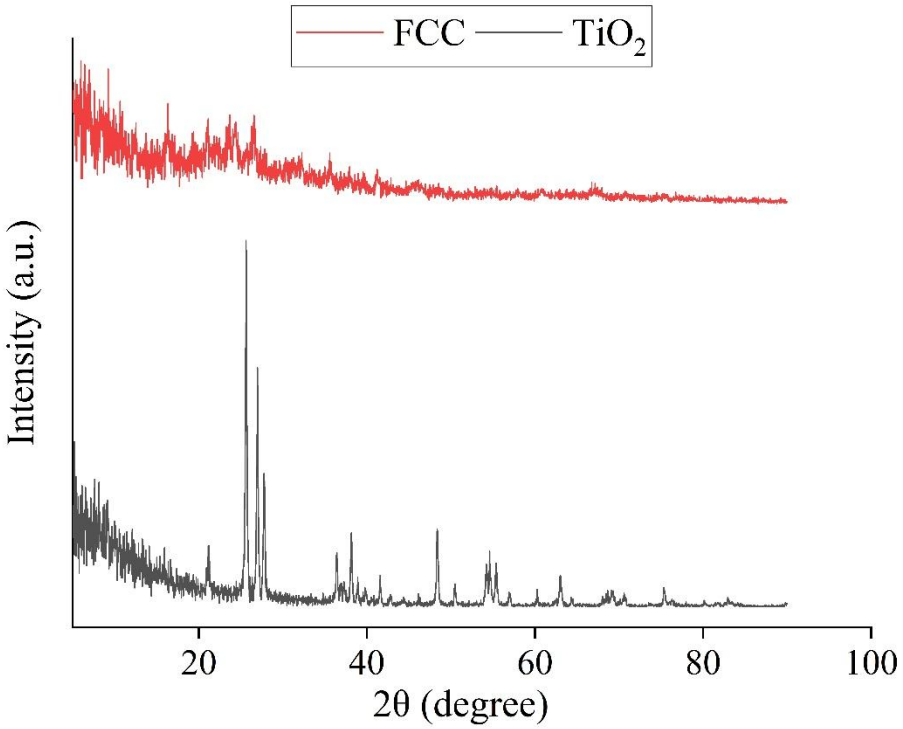

Figure 4.3: XRD patterns of spent FCC and TiO_2 catalyst.

4.3.1.4 NH_3 Temperature Programmed Desorption (NH_3-TPD)

As illustrated in Figure 4.4, the peak observed at a lower temperature is associated with ammonia (NH_3) weakly adsorbed on the weaker acid sites. In contrast, the higher temperature peak is associated with NH_3 that is strongly adsorbed on the stronger acid sites [9–11]. The NH_3-TPD data showing the acidity of the spent FCC catalyst and TiO_2 are summarized in Table 4.1. The spent FCC catalyst possesses a greater number of strong acid sites as well as higher total acidity than TiO_2. It has been established that the cracking temperature required for plastics cracking decreases with acid strength and concentration [12].

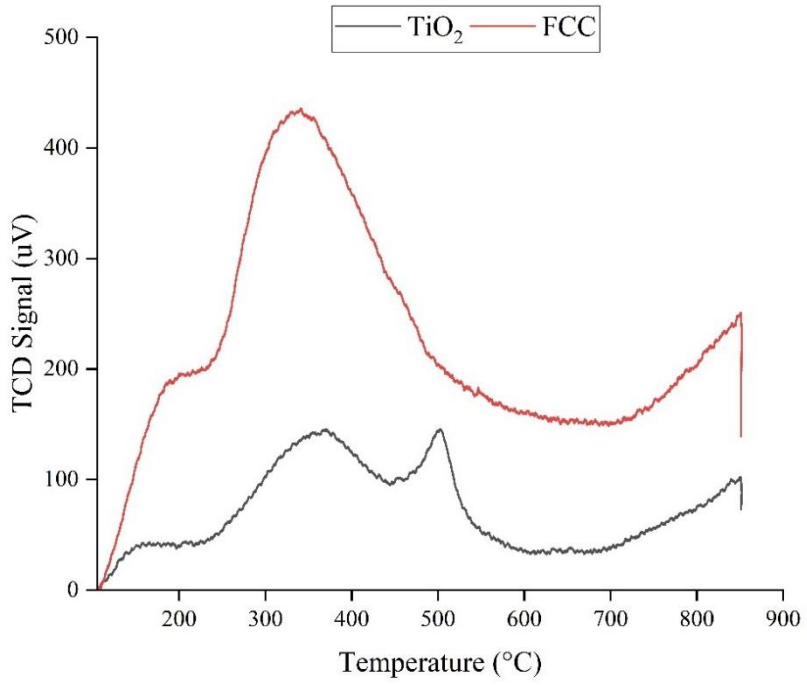

Figure 4.4: NH_3-TPD Profile of spent FCC and TiO_2.

A higher number of acid sites promotes reactions leading to the formation of aromatics and paraffins, whereas stronger acid sites are effective in cracking reactions enhancing the production of light olefins and reducing heavier fractions [13]. The two values reported for TiO_2 (0.051 and 0.033) correspond to two distinct desorption peaks observed in the NH_3-TPD profile of the TiO_2 sample under medium acidity conditions.

Table 4.1: NH_3-TPD data of spent FCC and TiO_2.

Catalyst	**Acidity, mmol NH_3/g**			
	Weak	Medium	Strong	Total
Spent FCC	0.075	0.487	0.125	0.687
TiO_2	0.008	0.051 0.033	0.024	0.116

4.3.1.5 X-ray photoelectron spectroscopy (XPS)

XPS spectra of the spent FCC catalyst, and TiO_2 are depicted in Figure 4.5. The Initial peak appearing at 284.8 eV corresponds to non-oxygenated carbon rings that form C–C bonds. The second C1s peak detected at 285.3 eV indicates C-H bonds. The Peak at 286.6 eV is associated with carbonyl groups that create C–O bonds [14]. XPS analysis of the used catalysts revealed that the quantity of coke present on the catalyst surface was so low (<1.0 wt.%) that it could be neglected in comparison with the gas and liquid products.

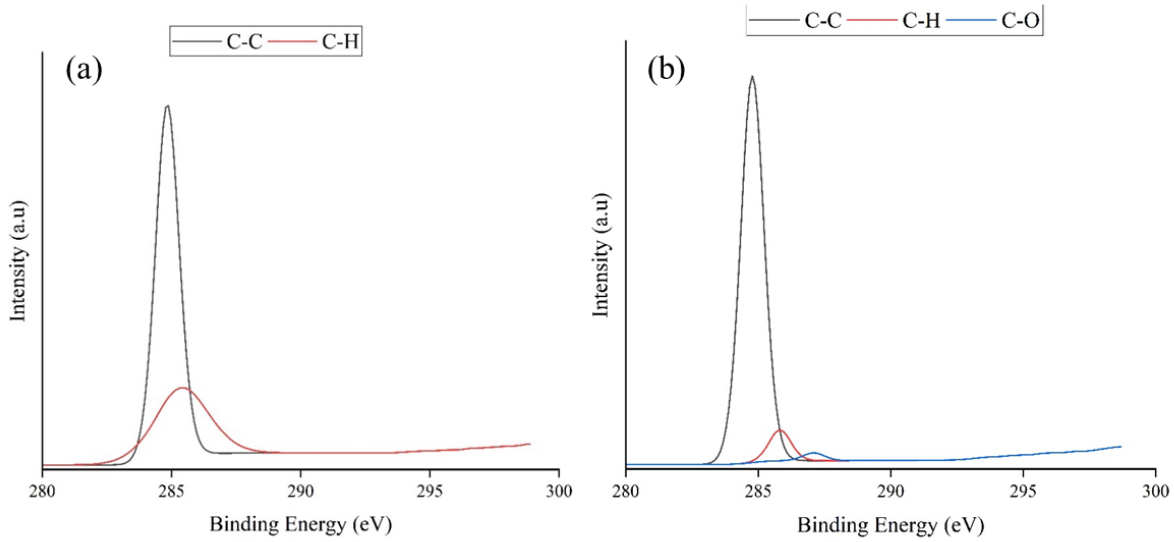

Figure 4.5: XPS spectra of (a) FCC, and (b) TiO_2.

4.3.2 Catalytic performance

4.3.2.1 Effect of spent FCC catalyst on product distribution

All experiments were conducted with FCC catalyst to LDPE mass ratio of 1:10, and a graphite to LDPE (G/L) ratio of 3, with varying temperatures. Figure 4.6 (a) shows how the product yield changes with pyrolysis temperature in the presence of the spent FCC catalyst. The gaseous product yield increased from 70 wt.% (without the catalyst) to 91 wt.% and the liquid fraction reduced to 9 wt.% as the cracking temperature rose from 400 °C to 550 °C. The increased gas percentage can be attributed to the higher rates of heating attained with MW heating and the catalyst acidity. Acidic nature of the spent FCC causes a higher amount of gas formation while reducing the formation of wax and oils. A similar observation was made by Wang et al. during the cracking of composite plastics using a spent FCC catalyst [15]. Lin et al. cracked polyethylene/polypropylene polymers employing FCC catalysts in a fluidized bed reactor and obtained 78 to 85 % gas yield with temperatures varying from 330 to 450 °C [16]. Orozco et al. also observed a similar trend where the FCC catalyst augmented the formation of

gaseous products, particularly light olefins, during oxidative fast pyrolysis of HDPE at 550°C in a conical spouted bed reactor [17]. Similar to the previously reported studies, this work also demonstrated that catalytic pyrolysis of LDPE resulted in significant gas production and relatively lower yields of liquid products using the spent FCC catalyst. In the current work, microwave energy was employed to accelerate the reaction in the presence of a low-cost graphite absorber.

Figure 4.6 (b) evinces that catalytic pyrolysis of LDPE over the spent FCC catalyst yields a liquid product comprising of alkenes (36 - 39%), alkanes (44%), and aromatic compounds (11–12%). The spent FCC catalyst possesses acidity (strength and quantity) which is well-suited for generating primary products during the cracking of polyolefins, affording olefins in a considerable proportion. This acidic nature helps minimize secondary hydrogen transfer reactions, leading to the formation of aromatics [2]. Wong et al. [18] during the catalytic cracking of plastics over FCC catalyst, obtained alkenes (38–67%), alkanes (16–25%) and minor amounts of aromatics (6–9%) which are in line with the product distribution observed in the present work. The higher acidity of zeolites, such as HY, HZSM-5 and Hβ promotes secondary reactions leading to the formation of alkanes and aromatics [19].

Table 4.2: Variation in carbon number in liquid products at different reaction temperatures in presence of spent FCC catalyst.

Sr. No.	Carbon Number	Proportion, wt.%	Temperature (°C)
1.	C_8-C_{12} (Gasoline)	34	450
		31	500
		36	550
2.	C_{12}-C_{15} (Kerosene, Jet Fuel)	21	450
		24	500
		18	550
3.	C_{15}-C_{25} (Diesel, Gas oil, Lube oil, Heating oil)	46	450
		47	500
		42	550
4.	>C_{25} (Paraffin wax, Asphalt)	8	450
		9	500
		8	550

In the same vein, other researchers have also identified attributed olefins as the predominant fraction in liquid product from plastics pyrolysis on spent FCC catalysts because of the moderate acidity of the FCC catalyst [15, 16]. The variation in carbon numbers in the liquid products at different reaction temperatures in the presence of the spent FCC catalyst is revealed in Table 4.2. Gasoline, kerosene, diesel, and paraffin wax fractions were 31%, 24%, 47%, and 9%, respectively, at 500°C. This demonstrates that the produced liquid can be used as a fuel additive. Barbarias et al. also obtained approximately 35% of C_5-C_{11} hydrocarbons at 450°C during pyrolysis of HDPE using a spent FCC catalyst [22].

Figure 4.6 (c) elucidates the effect of reaction temperature on the composition of the gaseous products. Propylene formation was observed at around 67 vol %, 62 vol % and 60 vol % at 450 °C, 500 °C, and 550 °C, respectively. This was followed by butene (13%), pentene (10%), and propane (8%) at 450°C. As was the case with the liquid products, around 90% of the gaseous products were olefins, which can be ascribed to the moderate acidity of the spent FCC catalyst. Catalytic pyrolysis primarily involves the formation of carbenium ions [23]. The 1-olefins readily convert into secondary carbenium ions on the catalyst surface which subsequently undergo β-scission resulting in enhanced formation of propylene [24]. Elordi et al. also achieved a higher fraction of propylene during polyethylene cracking using FCC catalyst [2]. The primary constituents of the gaseous products are butene and propylene, accompanied by small amounts of ethylene and other gases. Orozco et al. reported that propylene and butene were the predominant compounds during oxidative fast cracking of HDPE at 550°C using a conical spouted bed reactor [17]. Lin et al. also reported a higher proportion of olefinic materials in the C_3 - C_6 range, amounting to approximately 53 wt.% at 390 °C using FCC catalyst [16].

To understand the impact of the catalysts on the product yield, various experiments were conducted using the spent FCC by varying the catalyst amount at 450°C. As shown in Figure 4.6 (d), gas yield was 70% without a catalyst and it improved to 90% with spent FCC. An increased catalyst amount promotes secondary cracking in the reaction mixture. Wang et al. also argued that the spent FCC catalyst, due to its acidic nature, is capable of producing more gas by converting wax and oils [25].

Figure 4.6 (e) delineates the effect of FCC/LDPE mass ratio on liquid product composition. It was noticed that catalytic pyrolysis of LDPE over spent FCC produced a liquid product containing alkenes (30 -37%), alkanes (34 - 44%), and aromatic compounds (11 - 29%).

Compared with cracking without a catalyst, cracking with the spent FCC catalyst produced more alkanes due to the catalyst's ability to facilitate hydrogen transfer reactions. Aromatics formation increases with increased catalyst loading because the catalyst pores facilitate end-chain cracking and the formation of light olefins. These olefins subsequently undergo dehydrocyclisation to produce aromatics. The acid sites of the catalyst also promote aromatic formation by catalysing hydrogen transfer and Diels–Alder reactions. It has been reported that converting olefins into aromatics cannot be fully accomplished on a solo acid site. Therefore, compounds must first desorb from the initial acid site and then re-adsorb onto additional acid sites to transform into aromatics [26]. Barbarias et al. [22] observed olefins and alkanes with minimal aromatics during HDPE pyrolysis using a spent FCC catalyst. Onwudili et al. also achieved around 60% aliphatic and 36% aromatics through catalytic cracking of mixed plastics using FCC at 500 °C [27]. Wang et al. observed a higher proportion of alkanes and aromaic formation in the presence of the FCC catalyst [25]. The carbon-number distribution in the liquid products in the presence of spent FCC at 450°C is shown in Table 4.3. A higher concentration of catalysts with a significant number of micropores promotes formation of gasoline-range hydrocarbons in the liquid oil.

Table 4.3: Carbon number distribution in liquid product in presence of spent FCC at 450°C.

Sr. No.	Carbon Number	Percentage	Spent FCC to LDPE ratio
1.	C_8-C_{12} (Gasoline)	31	1:20
		34	1:10
		68	1:5
2.	C_{12}-C_{15} (Kerosene, Jet Fuel)	20	1:20
		21	1:10
		10	1:5
3.	C_{15}-C_{25} (Diesel, Gas oil, Lube oil, Heating oil)	40	1:20
		46	1:10
		21	1:5
4.	$>C_{25}$ (Paraffin wax, Asphalt)	10	1:20
		8	1:10
		4	1:5

These results were comparable to those stated by Aisien et al., [28] who obtained diesel (45%), gasoline (60%), motor oil (7.5%), and kerosene (52.5%) from liquid oil produced during LDPE cracking using FCC. Orozco et al. stated that conventional cracking of HDPE at 550°C yielded 55% of C_5-C_{11} hydrocarbons and 20% of C_{12}-C_{18} hydrocarbons [29]. Fan et al. conducted microwave-assisted pyrolysis of plastic waste and found that C_8–C_{16} hydrocarbons in aviation oil derived from low-density polyethylene accounted for 59.73 area%. In comparison, our results show that the C_8–C_{16} hydrocarbon content ranges from 50% to 78% [30].

The impact of the spent FCC/LDPE mass ratio on the gaseous products is demonstrated in Figure 4.6 (f). Propene production was 46 % at a spent FCC to LDPE ratio of 1:20, 67 % at a ratio of 1:10, and 60 % at a ratio of 1:5 at 450 °C. Pentene was the second largest product accounting for 14 %, followed by 13 % butene and 8 % propane at spent FCC to LDPE ratio of 1:10. A lower catalyst loading promotes random cracking, resulting in larger alkenes that subsequently undergo β-scission to form propene.

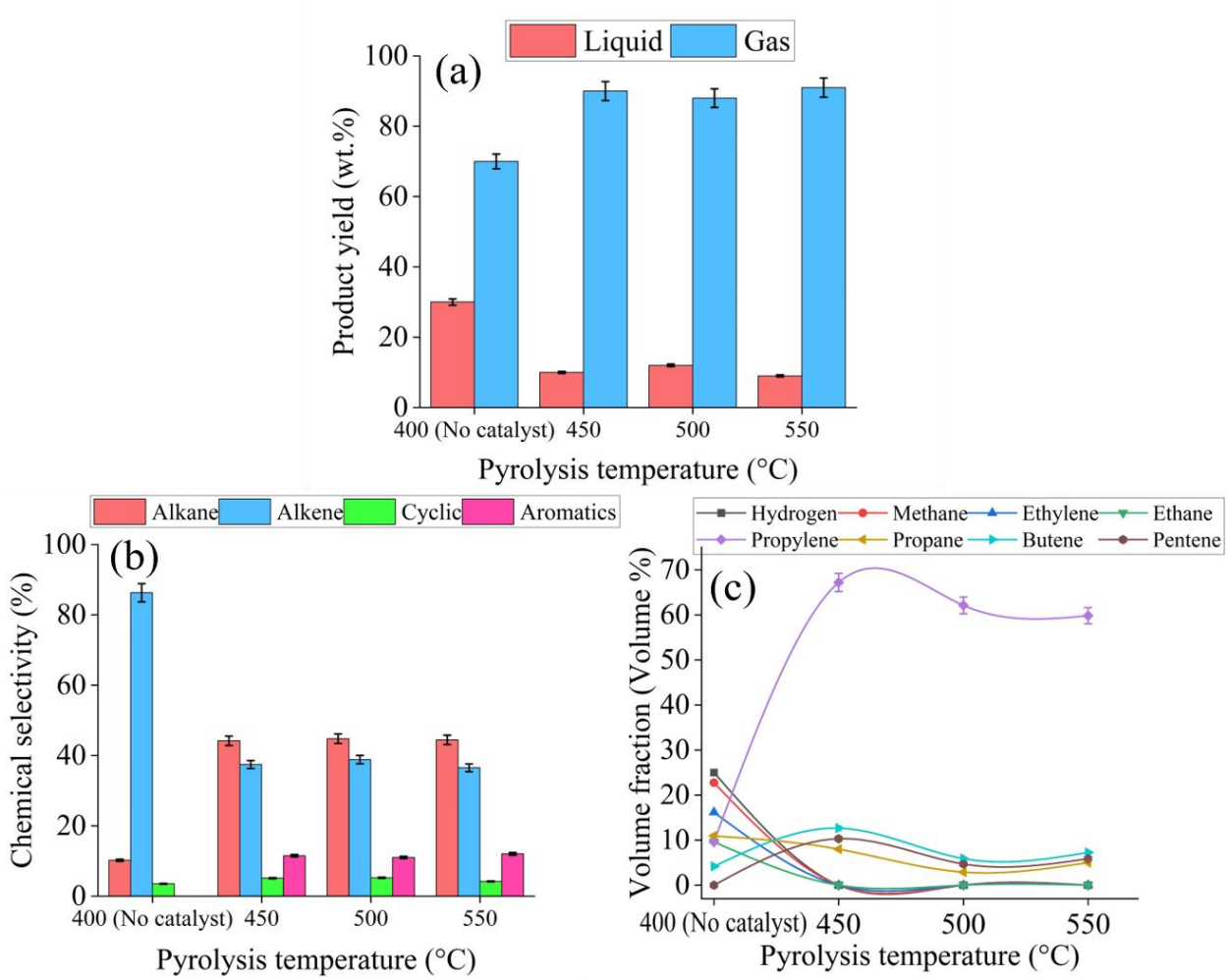

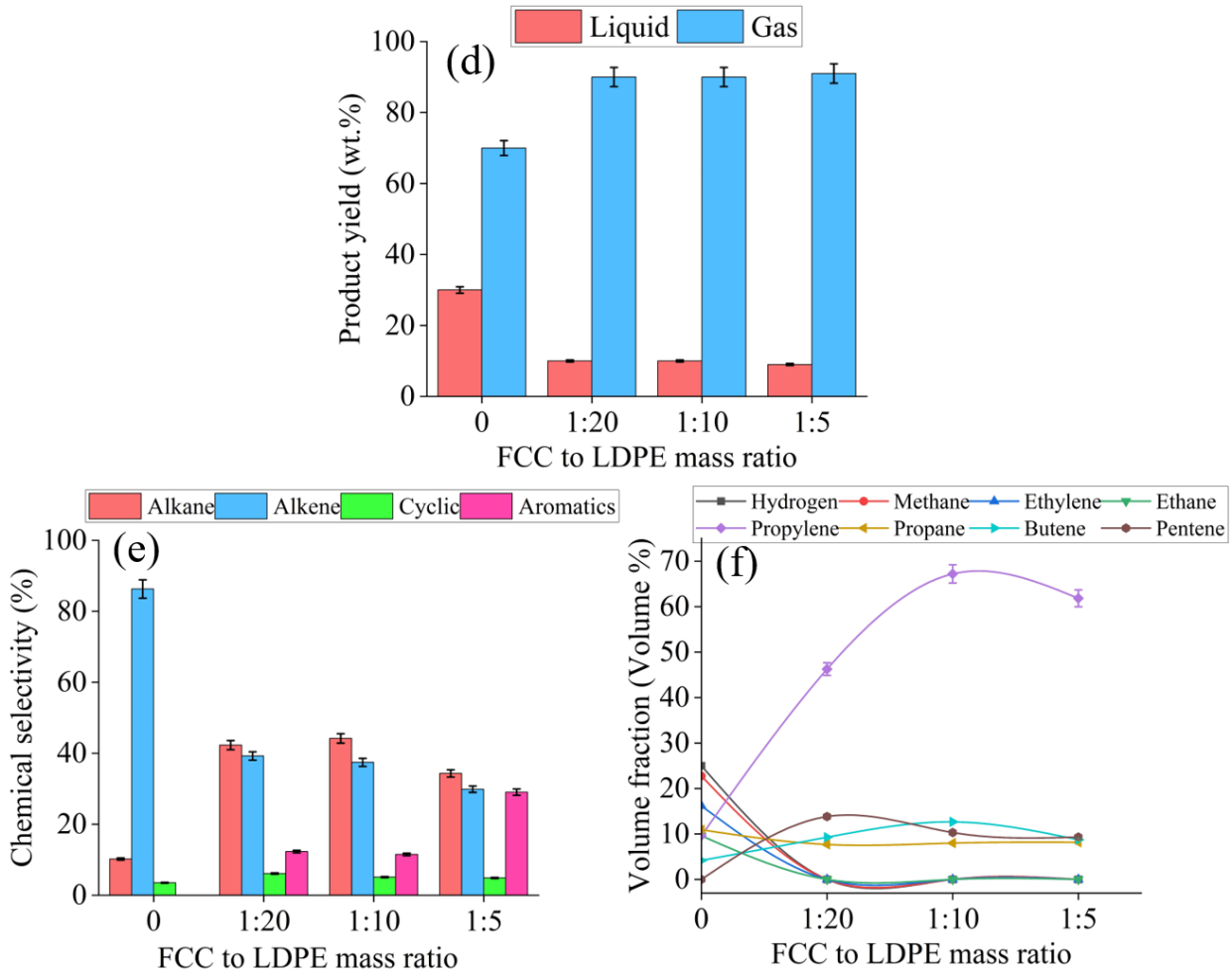

Figure 4.6: Influence of cracking temperature on (a) Product yield at spent FCC to LDPE mass ratio of 1:10 (b) Liquid oil compositions at spent FCC to LDPE mass ratio of 1:10 (c) Gas composition at spent FCC to LDPE mass ratio of 1:10. Effect of spent FCC catalyst proportion on (d) Yield of product at 450°C (e) Liquid compositions at 450°C (f) Gaseous product composition at 450°C.

Conversely, increased catalyst loading led to a slight reduction in the formation of propylene due to cyclization reactions that generate aromatic compounds. The acidic properties of zeolite also play a vital role in boosting product distribution with a high propylene concentration. It has been reported that FCC catalysts with reduced surface area and moderate acidity cannot generate small hydrocarbons like C_1 and C_2 [18]. Onwudili et al. also obtained C_3 and C_4 hydrocarbons with propene being produced in the greatest amount through the cracking of miscellaneous plastic waste at 500 °C [27]. Barbarias et al. conducted HDPE cracking using a spent FCC and obtained propylene as the predominant light olefin at 450 °C. However, with increased temperature, butane selectivity increased, making it the main light olefin at 500 °C [22]. Orozco et al. utilized a spent FCC and identified propylene and butene as the primary

gaseous products during the cracking of HDPE using a conical spouted bed reactor at 550 °C [29].

4.3.2.2 Influence of TiO_2 on product compositions

Figure 4.7 (a) depicts gas and liquid product yields as a function of cracking temperature with TiO_2 as the catalyst. The gaseous product yield was around 91% due to secondary cracking at higher temperatures and the elevated heating rates achieved through MW heating, as reported by Suriapparao et al. [31]. The liquid yield was observed to be 9% within the 450 to 550 °C temperature range. It has been reported that TiO_2 is an effective catalyst for cracking because of its porosity, selectivity, and good thermal firmness [32]. Nwankwor et al. achieved a liquid yield of 27 % in the pyrolysis of plastics with TiO_2 at 400 °C [33]. Uwagwu et al. carried out conventional catalytic cracking of LDPE using TiO_2 yielding 15% liquid hydrocarbons with a TiO_2 to LDPE mass ratio of 1:15 at 300°C [34].

The liquid product composition over TiO_2 at various temperatures is displayed in Figure 4.7 (b). Alkanes and alkenes are the major products with maximum yields of 48% and 53%, respectively. The proportions of cyclic compounds and aromatics are 14% and 9%, respectively. The hydrogen transfer reaction is regarded as a key mechanism for alkane formation. Larger olefins generated through random scission may be engaged by acid sites of the catalyst, where these sites serve as proton sources for breaking C=C by forming carbonium ions. These ions help in isomerization and pyrolysis reactions, producing branched paraffins and olefins [35,36]. Nwankwor et al. [33] investigated the production of gasoline-range hydrocarbons through the pyrolysis of plastics with TiO_2 and zeolite. They confirmed that the liquid product from LDPE cracking primarily comprised of aliphatic hydrocarbons within gasoline range which is consistent with our findings. The variation in carbon numbers of the liquid products at different temperatures in the presence of TiO_2 is shown in Table 4.4. The C_8-C_{12} hydrocarbons comprised approximately 82 % at 500 °C, whereas presence of C_{12}-C_{15}, C_{15}-C_{25}, and >C_{25} hydrocarbons were around 20 %, 46 %, and 15 % respectively at 550 °C. Chen et al. also reported a concentrated distribution of liquid products predominantly centered around C_{10} during the upcycling of polypropylene using Ru/TiO_2 [37]. A higher amount of gasoline fractions was obtained with TiO_2 compared to the spent FCC catalyst. This may be due to the properties of titanium dioxide, which, based on its particle size and surface area, provides a more controlled environment for cracking reactions that generate gasoline-range hydrocarbons. A higher number of olefins were also generated with TiO_2.

Table 4.4: Carbon number distribution in liquid product at different temperature in presence of TiO_2. TiO_2 to LDPE ratio was 1:10.

Sr. No.	Carbon Number	Percentage	Temperature (°C)
1.	C_8-C_{12} (Gasoline)	52	450
		82	500
		21	550
2.	C_{12}-C_{15}	21	450
	(Kerosene, Jet Fuel)	8	500
		20	550
3.	C_{15}-C_{25}	23	450
	(Diesel, Gas oil, Lube oil, Heating oil)	8	500
		46	550
4.	$>C_{25}$	3	450
	(Paraffin wax, Asphalt)	2	500
		15	550

The gas compositions over TiO_2 at different temperatures are illustrated in Figure 4.7 (c). The primary gaseous products are propylene (35%), butane (25%), pentane (18%), and propane (10%) at 550 °C. The propylene yield (35%, Figure 4.7 (c)) with TiO_2 is less than that obtained with the spent FCC catalyst (60%, Figure 4.6 (c)) due to the weaker acidity and fewer active sites of TiO_2 compared with the spent FCC catalyst. Chen et al. demonstrated that Ru/TiO_2 yields a substantial number of C_4-C_5 hydrocarbons while generating only minor quantity of C_2-C_3 hydrocarbons during the upcycling of polypropylene [37].

Figure 4.7 (d) exhibits the change in product distribution with the TiO_2/LDPE mass ratio at 500 °C. The gaseous product yield reached around 90% at a TiO_2 to LDPE ratio of 1:5, 88% at 1:10, and 85% at 1:20. This finding supports the catalytic enhancement that TiO_2 offers in the cracking of large molecular volatiles. The increased gas production may occur due to the rapid heating rates achieved by using a smaller quantity of the susceptor in conjunction with high microwave power. It has been reported that thermal pyrolysis produced the highest quantity of liquid oil, whereas catalytic pyrolysis decreased the liquid oil yield and increased gas production [38].

Figure 4.7 (e) delineates the effects of TiO_2/LDPE mass ratio on liquid product composition at 500 °C. It was observed that the liquid products mainly contained alkenes (48%), alkanes (20-28%), cyclic compounds (15-19%), and aromatic compounds (9-13%). Alkene formation can occur through the cracking of larger olefins produced by random scission of LDPE while minimizing secondary hydrogen transfer reactions due to the lower acidity of TiO_2. This approach also limits the formation of aromatics and alkanes. The variation in the carbon number distribution of the liquid products in the presence of TiO_2 with varying TiO_2 to LDPE ratios at 500 °C is illustrated in Table 4.5. The gasoline range hydrocarbons were present at levels between 82% and 95%, making them suitable for use as fuel. Nwankwor et al. showed that the liquid products primarily contained gasoline-range hydrocarbons in the C_5 to C_8 fraction, with smaller amounts of C_9 and C_{10} when using TiO_2 [33]. LDPE was subjected to catalytic pyrolysis under varying conditions to evaluate the distribution of hydrocarbon products. Under a nitrogen atmosphere and using activated carbon at 700 W and 480 °C with a ZSM-5 catalyst (operating between 249°C and 501°C), the process yielded predominantly gasoline-range hydrocarbons, specifically C_8-C_{12} polycyclic aromatic hydrocarbons (PAHs) in the range of 74.73–88.49% and monocyclic aromatic hydrocarbons (MAHs) at around 88.49% [39].

Table 4.5: Carbon number distribution in liquid product in presence of TiO_2 at 500°C.

Sr. No.	Carbon Number	Percentage	TiO_2 to LDPE ratio
1	C_6-C_{12} (Gasoline)	95	1:20
		82	1:10
		90	1:5
2	C_{12}-C_{15} (Kerosene, Jet Fuel)	5	1:20
		8	1:10
		5	1:5
3	C_{15}-C_{25} (Diesel, Gas oil, Lube oil, Heating oil)	3	1:20
		8	1:10
		7	1:5
4	>C_{25} (Paraffin wax, Asphalt)	0	1:20
		2	1:10
		1	1:5

In contrast, pyrolysis conducted under a nitrogen atmosphere and using activated carbon at 700 W and 350°C with a combined ZSM-5 and Raney nickel catalyst system favored the production of jet fuel range alkanes, including C_8-C_{16} cycloalkanes (84.32%) and aliphatic alkanes (8.65%), with product yields ranging from 50.77 ± 3.01% to 64.41 ± 5.20% [40]. These results demonstrate the influence of catalytic conditions and temperature on the selective conversion of LDPE into valuable hydrocarbon fuels.

The impact of the TiO_2/LDPE mass ratio on the gaseous products is demonstrated in Figure 4.7 (f). Propylene production was 29 % when the TiO_2 to LDPE mass ratio was 1:20, 33 % at a 1:10 ratio, and 30 % at a 1:5 ratio, all at 500 °C. Butene emerged as the second-largest product accounting for 26 % at 500 °C. Pentene production was around 18% across all TiO_2 to LDPE mass ratios. The total amount of olefins in the gaseous products was around 80%, which is likely due to the lower acidity of TiO_2 that restricts secondary hydrogen transfer reactions. TiO_2 improves the proportion of C_3, C_4, and C_5 gases. This suggests that it effectively facilitates the conversion of lighter gases into larger molecular compounds owing to its size selectivity.

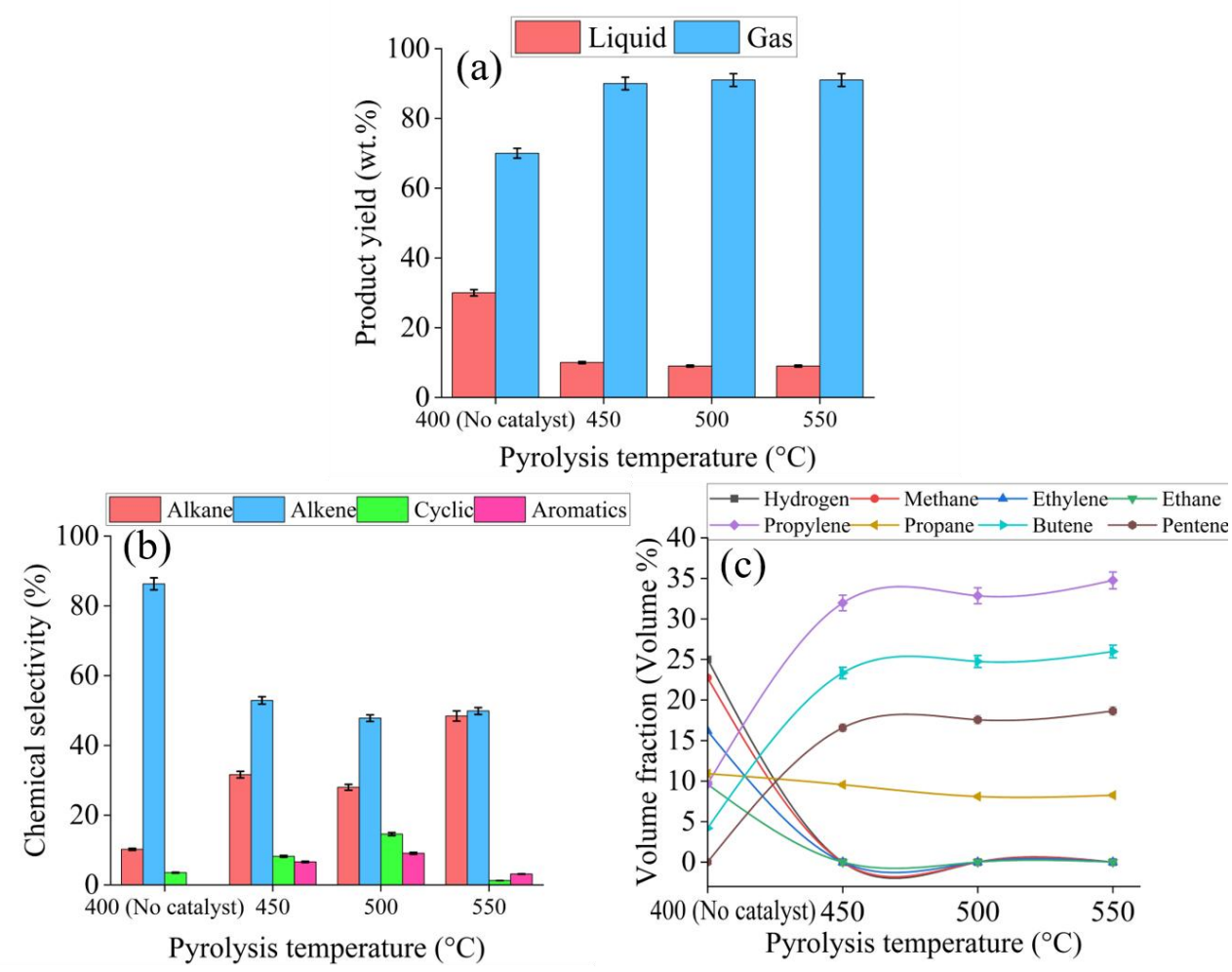

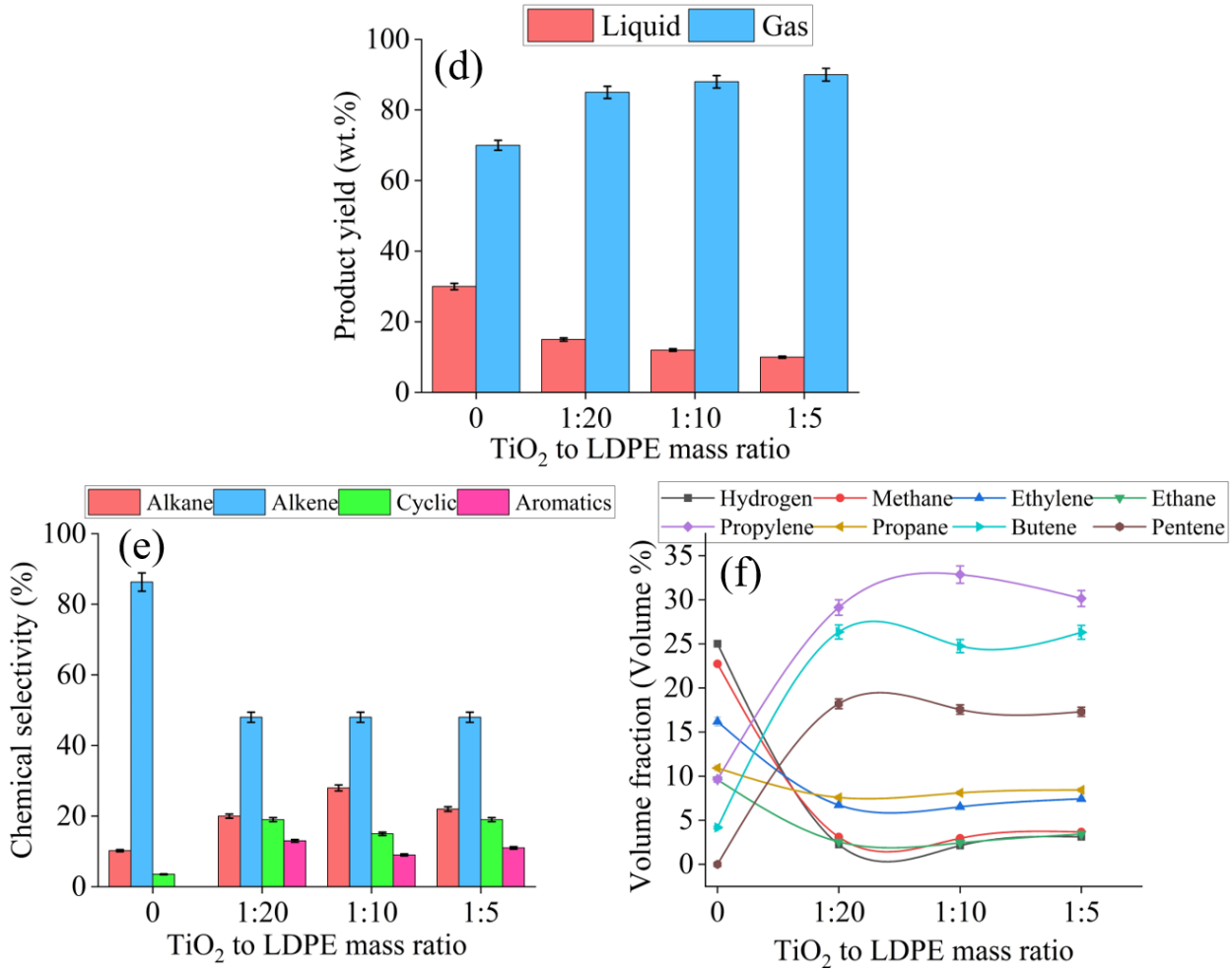

Figure 4.7: Impact of cracking temperatures on (a) Product yield at a TiO_2 to LDPE mass ratio of 1:10 (b) Liquid oil composition at a TiO_2 to LDPE mass ratio of 1:10 and (c) Gas composition at a TiO_2 to LDPE mass ratio of 1:10. Influence of TiO_2 proportion on (d) Product distribution at 500°C (e) Liquid oil composition at 500°C and (f) Gas composition at 500°C.

4.4 Conclusion

LDPE can be transformed into valuable products through catalytic microwave cracking using the spent FCC and TiO_2. This study examined the impact of the catalyst-to-reactant ratio and pyrolysis temperatures on product distribution. Compared to non-catalytic pyrolysis, which yielded 70 wt.% gaseous products, in-situ catalytic upgrading using the spent FCC and TiO_2 achieved higher gas yields ranging from 88 to 91 wt.% under various conditions. C_3 hydrocarbons were the predominant gaseous component in the presence of the spent FCC, while C_3–C_5 olefins constituted the primary components of the gaseous product, varying under different reaction conditions with TiO_2. A higher spent FCC loading enhanced the conversion of LDPE to aromatic compounds in the liquid product composition. TiO_2 predominantly

generated paraffins and olefins as its main products. The spent FCC and TiO_2 effectively enhanced the production of gasoline and diesel-range components, resulting in a higher-octane number of the liquid oil. The findings of this study indicate that catalytic microwave pyrolysis of LDPE using FCC and TiO_2 can effectively produce both high yields and high-quality products.

4.5 References

[1] M. Marhaini, D. Fernianti, M.R. Aulia, Effective pyrolysis of LDPE plastic waste to fuel using titanium dioxide catalyst, International Journal of ADVANCED AND APPLIED SCIENCES 11 (2024) 75–82. https://doi.org/10.21833/ijaas.2024.12.009.

[2] G. Elordi, M. Olazar, P. Castaño, M. Artetxe, J. Bilbao, Polyethylene Cracking on a Spent FCC Catalyst in a Conical Spouted Bed, Ind. Eng. Chem. Res. 51 (2012) 14008–14017. https://doi.org/10.1021/ie3018274.

[3] L. Yosefi, M. Haghighi, Fabrication of nanostructured flowerlike p-BiOI/p-NiO heterostructure and its efficient photocatalytic performance in water treatment under visible-light irradiation, Appl. Catal. B 220 (2018) 367–378. https://doi.org/10.1016/j.apcatb.2017.08.028.

[4] M. Król, J. Minkiewicz, W. Mozgawa, IR spectroscopy studies of zeolites in geopolymeric materials derived from kaolinite, J. Mol. Struct. 1126 (2016) 200–206. https://doi.org/10.1016/j.molstruc.2016.02.027.

[5] R. Tang, T. Chen, Y. Chen, Y. Zhang, G. Wang, Core-shell TiO2@SiO2 catalyst for transesterification of dimethyl carbonate and phenol to diphenyl carbonate, Chinese Journal of Catalysis 35 (2014) 457–461. https://doi.org/10.1016/S1872-2067(14)60059-0.

[6] M.M. Ba-Abbad, A.A.H. Kadhum, A.B. Mohamad, M.S. Takriff, K. Sopian, Synthesis and Catalytic Activity of TiO2 Nanoparticles for Photochemical Oxidation of Concentrated Chlorophenols under Direct Solar Radiation, Int. J. Electrochem. Sci. 7 (2012) 4871–4888. https://doi.org/10.1016/S1452-3981(23)19588-5.

[7] J. Xu, T. Zhang, J. Zhang, Photocatalytic degradation of methylene blue with spent FCC catalyst loaded with ferric oxide and titanium dioxide, Sci. Rep. 10 (2020) 12730. https://doi.org/10.1038/s41598-020-69643-2.

[8] R.G. Toro, M. Diab, T. de Caro, M. Al-Shemy, A. Adel, D. Caschera, Study of the Effect of Titanium Dioxide Hydrosol on the Photocatalytic and Mechanical Properties of Paper Sheets, Materials 13 (2020) 1326. https://doi.org/10.3390/ma13061326.

[9] A.S. Al-Dughaither, H. de Lasa, HZSM-5 Zeolites with Different SiO_2/Al_2O_3 Ratios. Characterization and NH_3 Desorption Kinetics, Ind. Eng. Chem. Res. 53 (2014) 15303–15316. https://doi.org/10.1021/ie4039532.

[10] F. Bin, C. Song, G. Lv, J. Song, X. Cao, H. Pang, K. Wang, Structural Characterization and Selective Catalytic Reduction of Nitrogen Oxides with Ammonia: A Comparison between Co/ZSM-5 and Co/SBA-15, The Journal of Physical Chemistry C 116 (2012) 26262–26274. https://doi.org/10.1021/jp303830x.

[11] M. Rahmani, M. Taghizadeh, Synthesis optimization of mesoporous ZSM-5 through desilication-reassembly in the methanol-to-propylene reaction, Reaction Kinetics, Mechanisms and Catalysis 122 (2017) 409–432. https://doi.org/10.1007/s11144-017-1204-0.

[12] S. Tsubota, S. Kokuryo, K. Tamura, K. Miyake, Y. Uchida, A. Mizusawa, T. Kubo, N. Nishiyama, Exploring the effect of Brønsted acidity of MFI-type zeolites on catalytic cracking temperature of low density polyethylene, Catal. Sci. Technol. 14 (2024) 1369–1374. https://doi.org/10.1039/D3CY01622F.

[13] R. Miandad, M.A. Barakat, A.S. Aburiazaiza, M. Rehan, A.S. Nizami, Catalytic pyrolysis of plastic waste: A review, Process Safety and Environmental Protection 102 (2016) 822–838. https://doi.org/10.1016/j.psep.2016.06.022.

[14] R. Kumar, H. Jain, A. Chaudhary, S. Kumari, D.P. Mondal, A.K. Srivastava, Thermal conductivity and fire-retardant response in graphite foam made from coal tar pitch derived semi coke, Compos. B Eng. 172 (2019) 121–130. https://doi.org/10.1016/j.compositesb.2019.05.036.

[15] Pengcheng Wang, Lei Qiao, Wei Wang, Jie Yu, Catalytic pyrolysis of waste composite plastics with waste FCC catalyst., Journal of the Energy Institute 110 (2023) 101338.

[16] Y.-H. Lin, M.-H. Yang, Catalytic pyrolysis of polyolefin waste into valuable hydrocarbons over reused catalyst from refinery FCC units, Appl. Catal. A Gen. 328 (2007) 132–139. https://doi.org/10.1016/j.apcata.2007.05.039.

[17] S. Orozco, G. Lopez, M.A. Suarez, M. Artetxe, J. Alvarez, J. Bilbao, M. Olazar, Oxidative Fast Pyrolysis of High-Density Polyethylene on a Spent Fluid Catalytic Cracking Catalyst in a Fountain Confined Conical Spouted Bed Reactor, ACS Sustain. Chem. Eng. 10 (2022) 15791–15801. https://doi.org/10.1021/acssuschemeng.2c04552.

[18] S.L. Wong, S. Armenise, B.B. Nyakuma, A. Bogush, S. Towers, C.H. Lee, K.Y. Wong, T.H. Lee, E. Rebrov, M. Muñoz, Plastic pyrolysis over HZSM-5 zeolite and fluid catalytic cracking catalyst under ultra-fast heating, J. Anal. Appl. Pyrolysis 169 (2023) 105793. https://doi.org/10.1016/j.jaap.2022.105793.

[19] R.R. Mishra, P.H. Rana, P.A. Parikh, Microwave-assisted pyrolysis of low-density polyethylene (LDPE)to value-added products over HY, HZSM-5 and Hβ catalyst, Mater. Today Commun. 41 (2024) 110829. https://doi.org/10.1016/j.mtcomm.2024.110829.

[20] N.S. Akpanudoh, K. Gobin, G. Manos, Catalytic degradation of plastic waste to liquid fuel over commercial cracking catalysts, J. Mol. Catal. A Chem. 235 (2005) 67–73. https://doi.org/10.1016/j.molcata.2005.03.009.

[21] K.-H. Lee, N.-S. Noh, D.-H. Shin, Y. Seo, Comparison of plastic types for catalytic degradation of waste plastics into liquid product with spent FCC catalyst, Polym. Degrad. Stab. 78 (2002) 539–544. https://doi.org/10.1016/S0141-3910(02)00227-6.

[22] Itsaso Barbarias, Maite Artetxe, Aitor Arregi, Jon Alvarez, Gartzen Lopez, Maider Amutio, Martin Olazar, Catalytic Cracking of HDPE Pyrolysis Volatiles over a Spent FCC Catalyst , CHEMICAL ENGINEERING TRANSACTIONS 43 (2015) 2029–2034.

[23] S. Kumar, A.K. Panda, R.K. Singh, A review on tertiary recycling of high-density polyethylene to fuel, Resour. Conserv. Recycl. 55 (2011) 893–910. https://doi.org/10.1016/j.resconrec.2011.05.005.

[24] L. Fan, Z. Su, J. Wu, Z. Xiao, P. Huang, L. Liu, H. Jiang, W. Zhou, S. Liu, R. Ruan, Integrating continuous-stirred microwave pyrolysis with ex-situ catalytic upgrading for linear low-density polyethylene conversion: Effects of parameter conditions, J. Anal. Appl. Pyrolysis 157 (2021) 105213. https://doi.org/10.1016/j.jaap.2021.105213.

[25] P. Wang, L. Qiao, W. Wang, J. Yu, Catalytic pyrolysis of waste composite plastics with waste FCC catalyst, Journal of the Energy Institute 110 (2023) 101338. https://doi.org/10.1016/j.joei.2023.101338.

[26] Y. Song, X. Zhu, L. Xu, Study on the process of transformation of olefin into aromatics over HZSM-5, Catal. Commun. 7 (2006) 218–223. https://doi.org/10.1016/j.catcom.2005.11.007.

[27] J.A. Onwudili, C. Muhammad, P.T. Williams, Influence of catalyst bed temperature and properties of zeolite catalysts on pyrolysis-catalysis of a simulated mixed plastics sample for the production of upgraded fuels and chemicals, Journal of the Energy Institute 92 (2019) 1337–1347. https://doi.org/10.1016/j.joei.2018.10.001.

[28] Felix Aibuedefe Aisien, Eki Tina Aisien, Liquid Fluids from Thermo-Catalytic Degradation of Waste Low-Density Polyethylene Using Spent Fcc Catalyst, Detritus 19 (2022) 75–83.

[29] S. Orozco, M. Artetxe, G. Lopez, M. Suarez, J. Bilbao, M. Olazar, Conversion of HDPE into Value Products by Fast Pyrolysis Using FCC Spent Catalysts in a Fountain Confined Conical Spouted Bed Reactor, ChemSusChem 14 (2021) 4291–4300. https://doi.org/10.1002/cssc.202100889.

[30] S. Fan, Y. Zhang, L. Cui, T. Maqsood, S. Nižetić, Cleaner production of aviation oil from microwave-assisted pyrolysis of plastic wastes, J. Clean. Prod. 390 (2023) 136102. https://doi.org/10.1016/j.jclepro.2023.136102.

[31] Dadi V. Suriapparao, Garlapati Nagababu, Attada Yerrayya, Veluru Sridevi, Optimization of microwave power and graphite susceptor quantityfor waste polypropylene microwave pyrolysis., Process Safety and Environmental Protection (2021) 234–243.

[32] T.O. Eschemann, J.H. Bitter, K.P. de Jong, Effects of loading and synthesis method of titania-supported cobalt catalysts for Fischer–Tropsch synthesis, Catal. Today 228 (2014) 89–95. https://doi.org/10.1016/j.cattod.2013.10.041.

[33] P.E. Nwankwor, I.O. Onuigbo, C.E. Chukwuneke, M.F. Yahaya, B.O. Agboola, W.J. Jahng, Synthesis of gasoline range fuels by the catalytic cracking of waste plastics using titanium dioxide and zeolite, International Journal of Energy and Environmental Engineering 12 (2021) 77–86. https://doi.org/10.1007/s40095-020-00359-9.

[34] UWAGWU CHARLES OLISEMEKE, RESEARCH ON COMPARATIVE STUDY ON THE CONVERSION OF WASTE PLASTIC MATERIALS TO LIQUID HYDROCARBONS THROUGH CATALYTIC PYROLYSIS, 2018.

[35] J.H. Harrhy, A. Wang, J.S. Jarvis, P. He, S. Meng, M. Yung, L. Liu, H. Song, Understanding zeolite deactivation by sulfur poisoning during direct olefin upgrading, Commun. Chem. 2 (2019) 37. https://doi.org/10.1038/s42004-019-0141-4.

[36] C. Wang, H. Lei, M. Qian, E. Huo, Y. Zhao, Q. Zhang, W. Mateo, X. Lin, X. Kong, R. Zou, R. Ruan, Application of highly stable biochar catalysts for efficient pyrolysis of plastics: a readily accessible potential solution to a global waste crisis, Sustain. Energy Fuels 4 (2020) 4614–4624. https://doi.org/10.1039/D0SE00652A.

[37] Linxiao Chen, Julia D. Moreira, Laura C. Meyer, Oliver Y. Gutiérrez, János Szanyi, Dual-Pathway Polyolefin Upcycling over an Unexpectedly Bifunctional Low Loading Ru/TiO2-Anatase Catalyst , ChemRxiv 1 (2022).

[38] E.T. Aisien, I.C. Otuya, F.A. Aisien, Thermal and catalytic pyrolysis of waste polypropylene plastic using spent FCC catalyst, Environ. Technol. Innov. 22 (2021) 101455. https://doi.org/10.1016/j.eti.2021.101455.

[39] X. Zhang, H. Lei, G. Yadavalli, L. Zhu, Y. Wei, Y. Liu, Gasoline-range hydrocarbons produced from microwave-induced pyrolysis of low-density polyethylene over ZSM-5, Fuel 144 (2015) 33–42. https://doi.org/10.1016/j.fuel.2014.12.013.

[40] X. Zhang, H. Lei, L. Zhu, M. Qian, G. Yadavalli, J. Wu, S. Chen, From plastics to jet fuel range alkanes via combined catalytic conversions, Fuel 188 (2017) 28–38. https://doi.org/10.1016/j.fuel.2016.10.015.

CHAPTER – 5

Hydrogen-rich gas and value-added hydrocarbon production from LDPE using Ni and Zn supported catalysts

5.1 Introduction

Initial investigations using acidic zeolite catalysts demonstrated their superior performance under microwave irradiation. Among the zeolitic systems, HY produced a significant H_2 concentration (35 vol%), HZSM-5 exhibited high selectivity toward ethylene (43 vol%), and Hβ favored propylene formation (69 vol%) at 450 °C. In comparison, non-zeolitic catalysts showed distinct behavior, with spent FCC catalyst yielding up to 67 vol% propylene, while TiO_2 predominantly promoted the formation of gasoline-range hydrocarbons.

Based on these observations, HY zeolite was identified as a suitable support for H_2-oriented catalytic systems due to its high acidity and favorable H_2 formation characteristics. Consequently, further studies were conducted to enhance H_2 production from LDPE by employing Ni- and Zn-based catalysts supported on HY, Al_2O_3, TiO_2, and SiO_2. Zhang et al. demonstrated that increasing nickel loading enhances selectivity toward benzene, toluene, and xylene (BTX), while Ni-loaded zeolites exhibit a strong synergistic effect that facilitates hydrogen radical (H·) cleavage, thereby promoting aromatization reactions during conventional pyrolysis of polyethylene [1]. Barzallo et al. reported that the Ni–Zn/ZSM-5 catalyst delivered the best performance, achieving shorter reaction times and, under optimized conditions, enabling catalytic pyrolysis to efficiently produce hydrocarbons of high industrial relevance [2]. Here Al_2O_3, TiO_2, and SiO_2 were selected as supports for Ni- and Zn-based catalysts to systematically evaluate the effect of support acidity, metal–support interaction, and metal dispersion on LDPE cracking and H_2 production under microwave irradiation. This part of the study focuses on evaluating the influence of metal type and support properties on H_2 generation, cracking efficiency, and overall product distribution under optimized microwave-assisted pyrolysis conditions.

5.2 Materials and methods

5.2.1 Materials

LDPE granules were procured from Reliance Industries Ltd. HY featuring a Si/Al ratio of 6 and a surface area of 750 m^2/g was supplied by SUD CHEMIE India Pvt. Ltd., Vadodara, India. Graphite powder (CAS No. 7782-42-5), with an average particle size of 149 µm was obtained from Bangalore Fine Chemicals, Bangalore. Silicon dioxide (SiO_2), aluminum oxide (Al_2O_3), and titanium dioxide (TiO_2) were sourced from Loba Chemie, Mumbai. Additionally, nickel nitrate hexahydrate (Ni $(NO_3)_2 \cdot 6H_2O$) was purchased from Oxford Lab Fine Chem, Palghar, and zinc nitrate hexahydrate (Zn $(NO_3)_2 \cdot 6H_2O$) was obtained from Loba Chemie, Mumbai.

5.2.2 Catalyst Preparation

A series of Ni and Zn supported catalysts were prepared with varying metal loadings (0.5 – 20 wt.%) using a facile impregnation method based on incipient wetness technique. Briefly, the required amounts of Ni $(NO_3)_2 \cdot 6H_2O$ and Zn $(NO_3)_2 \cdot 6H_2O$ were dissolved in 10 mL of deionized water. This solution was gradually added dropwise to various supports, including Al_2O_3, TiO_2, HY, and SiO_2, under continuous stirring at 80°C. The resulting wet solids were dried in air at 373 K followed by calcination at 873 K for 6 hours. Although catalysts with metal loadings ranging from 0.5 to 20 wt.% were synthesized, a 15 wt.% metal loading was selected for detailed discussion as it provided the optimal balance between active metal site density, metal dispersion, and preservation of support acidity, resulting in the highest H_2 yield. A further increase in metal loading beyond 15 wt.% did not improve the H_2 yield, indicating the onset of metal aggregation and diffusion limitations at higher loadings.

5.2.3 Catalyst characterization

Scanning Electron Microscopy (SEM; Thermo Fisher Scientific Apereo 2S Highvac FESEM) was used to examine the surface morphology of the catalysts.

FTIR spectra were recorded in reflection mode using KBr optics on a PerkinElmer Spectrum Two spectrometer, operating in the 400 - 4000 cm^{-1} range.

Structural characteristics of catalyst were determined by X-ray diffraction (XRD) using a Panalytical X'Pert Pro diffractometer with either Cu Kα (1.54 Å) or Mo Kα (0.71 Å) radiation as the X-ray source. Measurements were conducted over a 2θ range of 5°–140° with the instrument operating at 45 kV and 40 mA.

Pyridine adsorption infrared spectra (Py-IR) were analyzed on a PerkinElmer Spectrum Two spectrometer equipped with a TGS detector.

An inductively Coupled Plasma Mass Spectrometry (ICP-MS) study was performed with an Agilent 7900 system for elemental quantification, with samples introduced via a micronebulizer and measured under standard operating conditions. Calibration was performed with multi-element standards, while internal standards were used to account for matrix effects and instrumental drift.

5.3 Results and discussion

5.3.1 Catalyst Characterization:

5.3.1.1 Scanning Electron Microscope

Surface morphology of the prepared catalysts was analyzed using SEM as shown in Figure 5.1. The 15 wt. % Ni/HY (Figure 5.1a) and 15 wt.% Zn/HY (Figure 5.1b) catalysts display relatively uniform particle distributions with distinct crystal facets indicating that the HY structure remains intact after metal impregnation with crystal sizes around 0.8 µm. In contrast, the 15 wt.% Ni/Al_2O_3 (Figure 5.1c) and 15 wt.% Zn/Al_2O_3 (Figure 5.1d), catalysts exhibit more irregular and aggregated particles with sizes ranging from 0.5-0.7 µm, 0.4-0.5 µm respectively. The 15 wt.% Ni/SiO_2 catalyst (Figure 5.1e) shows a relatively smoother and less porous morphology with particle sizes between 0.2- 0.5 µm. The 15 wt.% Ni/TiO_2 sample (Figure 5.1f) reveals a highly agglomerated morphology consisting of spherical and irregularly shaped nanoparticles with sizes of 0.2-0.4 µm.

5.3.1.2 Fourier transform infrared spectroscopy

FTIR spectra of 15 wt.% Ni and Zn loaded catalysts supported on various materials (HY, Al_2O_3, SiO_2, and TiO_2) are depicted in Figure 5.2. The spectra were recorded in the wavenumber range of 4000-500 cm^{-1} to recognize the functional groups and structural characteristics of the catalysts. Broad absorption bands observed in the 3400–3600 cm^{-1} region correspond to O–H stretching vibrations, indicating the presence of surface hydroxyl groups or adsorbed water [3]. The bands near 1650 cm^{-1} are assigned to the bending vibrations of adsorbed molecular water, and the band around 800 cm^{-1} is attributed to the symmetric vibration of the Si/Al-O bond. The absorption observed in the range of 995-1140 cm^{-1} is attributed to the stretching of Si–O–Si (Al) bond [4,5]. The FTIR analysis shows weak and distinct O-H bands for Ni/SiO_2 and Ni/TiO_2, which can be attributed to the consumption of surface hydroxyl groups during the impregnation process and the formation of Ni–O–support bonds (≡Si–O–Ni and ≡Ti–O–Ni) [6]. The FTIR spectrum of nickel oxide (NiO) nanoparticles exhibits a prominent band near 600 cm^{-1} which is indicative of the stretching vibration of the

Ni-O bond [7]. FTIR peaks in the low wavenumber range of 424-549 cm^{-1} were assigned to the presence of loaded metals. Additionally, the characteristic band of ZnO in the FTIR spectrum was observed within the wavenumber range of 432-532 cm^{-1} [8].

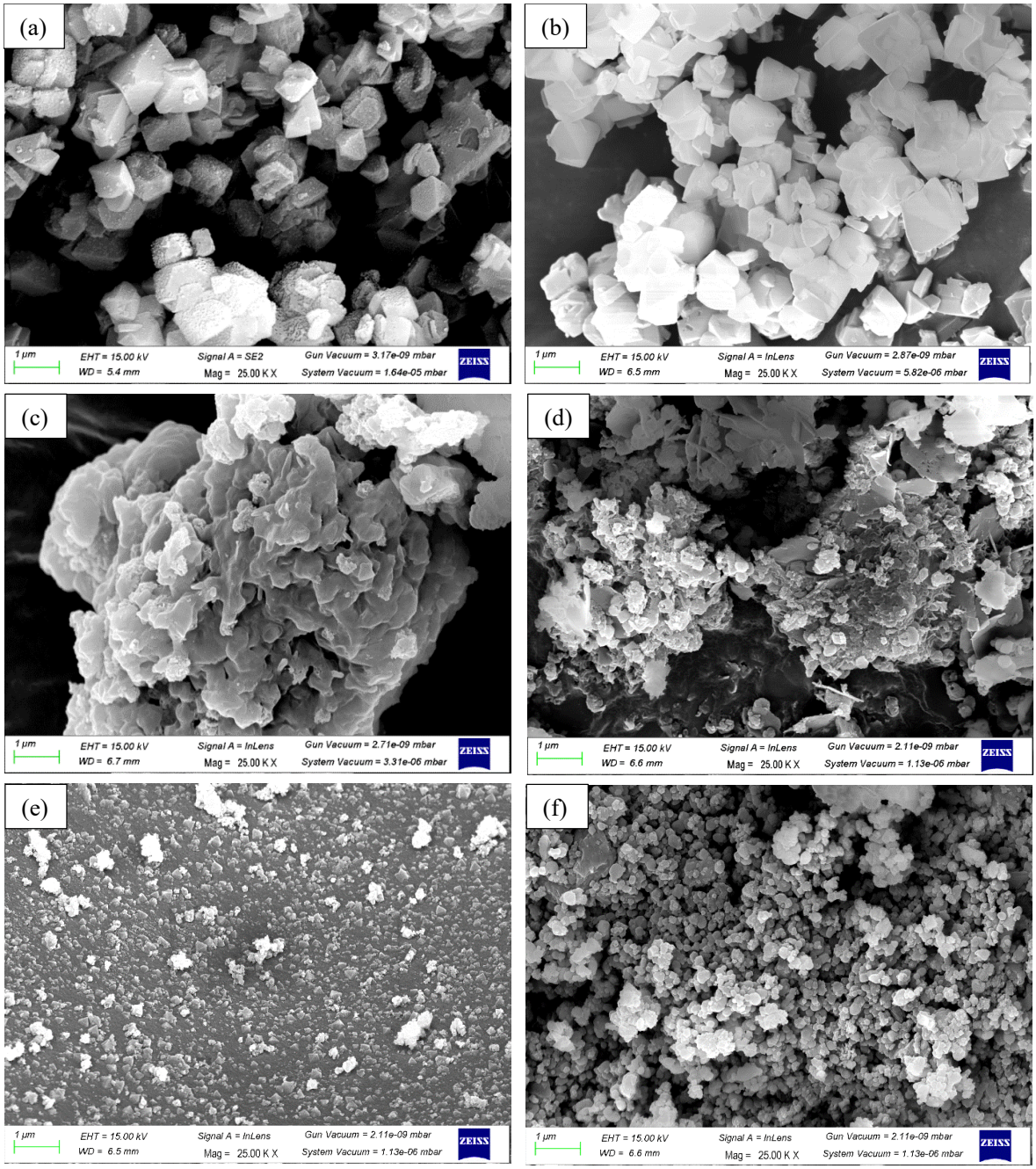

Figure 5.1: SEM images of synthesized catalysts: (a) 15 wt.% Ni/HY, (b) 15 wt.% Zn/HY, (c) 15 wt.% Ni/Al_2O_3, (d) 15 wt.% Zn/Al_2O_3, (e) 15 wt.% Ni/SiO_2, and (f) 15 wt.% Ni/TiO_2. All images were recorded at identical magnification, and scale bars correspond to 1 µm.

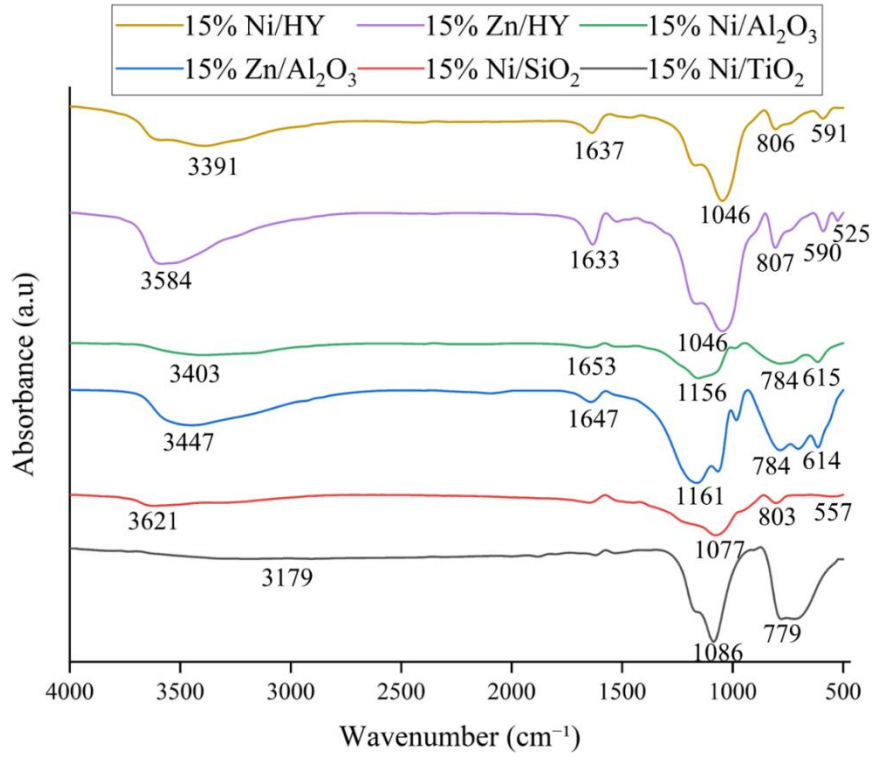

Figure 5.2: FTIR patterns of 15 wt.% Ni- and Zn-loaded catalysts supported HY zeolite, Al_2O_3, SiO_2, and TiO_2.

5.3.1.3 Powder X-ray Diffraction

XRD patterns of 15 wt.% Ni and Zn supported on HY, Al_2O_3, SiO_2, and TiO_2 are elucidated in Figure 5.3. The diffractograms confirm the crystalline phases of the support materials and the successful incorporation of Ni and Zn species. The diffraction peaks appearing in the 2θ range of 10°–33° are attributed to the (220), (331), (311), (511), (533), (440), (642), and (555) crystal planes of HY [9]. Al_2O_3 exhibits peak at 25°, 35°, 38°, and 57°, corresponding to the (012), (104), (110), and (116) crystal planes [10]. The SiO_2 sample exhibits a broad peak around 22°, which is characteristic of amorphous silica [11]. TiO_2 displays distinct diffraction peaks corresponding to the anatase and rutile phases of TiO_2 with prominent peaks around 25°, 38°, 48°, and 55°, which correspond to the (101), (004), (200), and (211) planes of anatase TiO_2, along with minor contributions from rutile phase reflections [12]. Diffraction peaks corresponding to NiO species were observed, particularly at 2θ = 43° (200) and 63° (220) planes [13]. Additionally, distinct peaks appearing at 2θ = 32.0°, 34.5°, 36.0°, 47.5°, and 56.0° can be assigned to the (100), (002), (101), (102), and (110) crystalline planes of ZnO, confirming their well-defined hexagonal wurtzite structure [14]. The absence of significant

peak broadening indicates that the metal particles are well dispersed with relatively small crystallite sizes.

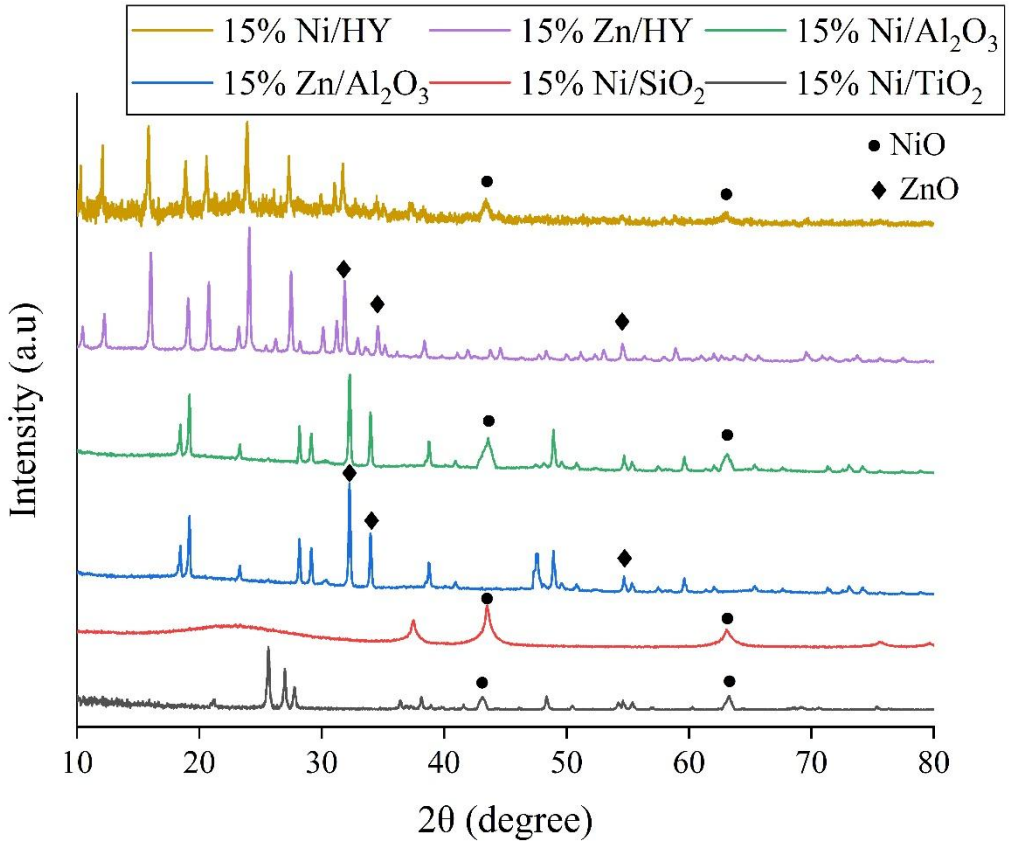

Figure 5.3: XRD patterns of 15 wt.% Ni and Zn loaded catalysts supported on HY zeolite, Al_2O_3, SiO_2, and TiO_2.

5.3.1.4 FTIR spectra of pyridine-adsorbed catalysts (Py-FTIR)

Pyridine adsorbed FT-IR spectra of the prepared catalysts are shown in Figure 5.4. The spectra correspond to the 15% Ni/HY, 15% Zn/HY, 15% Ni/Al_2O_3, 15% Zn/Al_2O_3, 15% Ni/SiO_2, and 15% Ni/TiO_2 samples in the wavenumber range of 1400-1800 cm^{-1}. The characteristic bands near 1450 cm^{-1} and 1610 cm^{-1} are assigned to pyridine coordinated to Lewis acid sites, whereas the band around 1540 cm^{-1} indicates the presence of Brønsted acid sites. The relative intensities of these bands reflect the strength and type of acid sites present on the catalyst surfaces. As seen in Table 5.1, the 15 wt.% Ni/HY exhibits more prominent Lewis acidity compared to the other prepared catalysts.

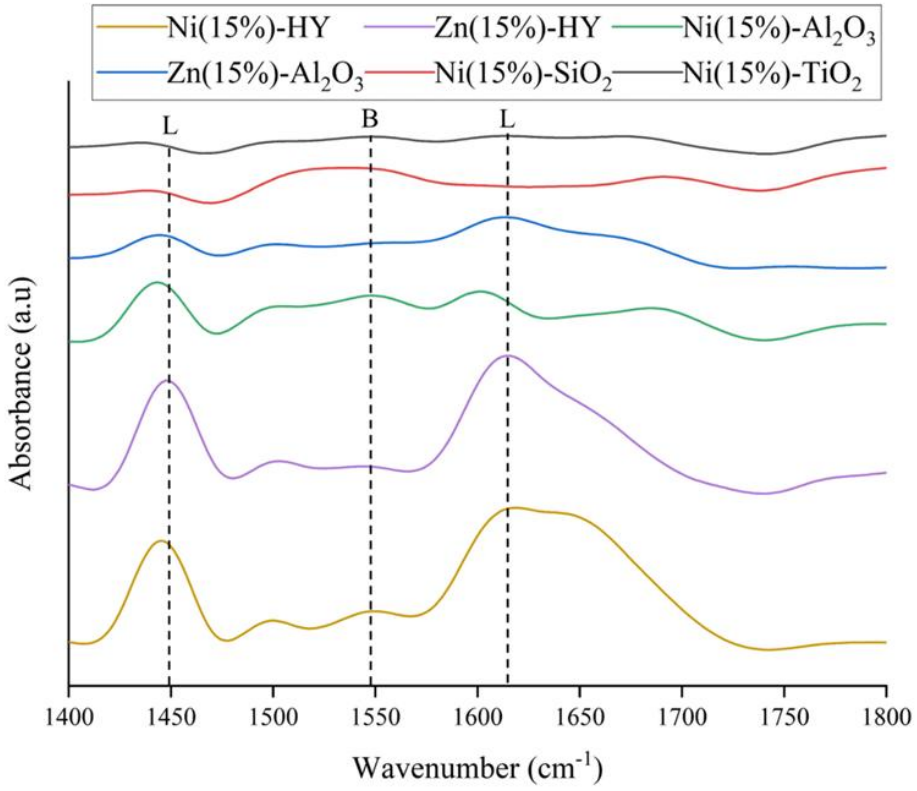

Figure 5.4: Pyridine adsorbed FT-IR spectra of 15 wt.% Ni and Zn loaded catalysts supported on HY zeolite, Al_2O_3, SiO_2, and TiO_2.

The acidity of the catalysts as measured by pyridine-IR spectroscopy, is presented in Table 5.1. Lewis acid sites play a significant role in H_2 production. The acid site concentration of the catalysts was evaluated using the equation below [15].

$$C_L = (\pi/IMEC_L) \times (r^2/w) \times A_1$$

$$C_B = (\pi/IMEC_B) \times (r^2/w) \times A_2$$

Here, C_L and C_B represent the concentrations of Lewis (L) and Brønsted (B) acid sites, respectively, expressed in μmol g^{-1}. A_1 represents the integrated areas of the absorption bands at 1450 cm^{-1} and 1610 cm^{-1}, while A_2 corresponds to the band at 1540 cm^{-1}. $IMEC_L$ and $IMEC_B$ are the molar extinction coefficients, with values of 2.22 and 1.67 cm μmol^{-1}, respectively. The variable r indicates pellet radius in centimeters, while w refers to the pellet weight in milligrams.

Table 5.1: Acidity of Ni and Zn loaded catalysts as determined by pyridine-IR.

Catalyst	**Amount of acidic sites conc. (µmol g^{-1})**	
	Lewis Acid Sites (LAS)	Bronsted Acid Sites (BAS)
15% Ni/HY	17.85	0.42
15% Zn/HY	15.26	0.127
15% Ni/Al_2O_3	2.82	0.59
15% Zn/Al_2O_3	4.16	0.042
15% Ni/SiO_2	2.59	3.69
15% Ni/TiO_2	0.51	0.27

5.3.1.5 Inductively Coupled Plasma Mass Spectrometry (ICP-MS)

ICP-MS was employed to quantify the metal loading in the prepared catalysts to determine the metal content (%). Table 5.2 presents the measured metal percentages for the various catalyst samples. ICP-MS results confirmed that the actual metal loadings in all catalyst samples closely matched the nominal value of 15 wt.%. This indicates the efficient incorporation of both Ni and Zn during catalyst preparation. Minor deviations from the theoretical value (ranging from 13.77% to 14.47%) may be attributed to experimental variations during the impregnation process.

Table 5.2: ICP-MS data for various metal-loaded catalysts.

Sr. No.	**Catalyst Name**	**Metal percentage**
1	15% Ni/HY	14.47
2	15% Ni/TiO_2	13.77
3	15% Ni/Al_2O_3	14.28
4	15% Ni/SiO_2	14.35
5	15% Zn/HY	14.23
6	15% Zn/Al_2O_3	13.97

These findings suggest that the synthesis procedures employed were effective for both Ni and Zn impregnation across different supports, ensuring consistency and reliability in metal distribution.

5.3.2 Catalytic Performance

5.3.2.1 Ni/HY

All experiments were conducted using a catalyst: LDPE: graphite mass ratio of 1:10:30 at 450 °C, and each experiment was repeated three times to ensure reproducibility. Preliminary trials were executed at 400 °C, 450 °C, 500 °C, and 550 °C to evaluate the effect of temperature on product distribution during microwave assisted LDPE pyrolysis. A catalyst to LDPE ratio of 1:10 at 450 °C was found to be optimum for maximizing H_2 yield and producing valuable hydrocarbons which is consistent with the findings from our previous study [16]. An incremental change in gas yield was observed upon addition of Ni to HY. The gas yield increased to 90 % with 15 wt.% Ni from 70 % without catalyst (Figure 5.5 (a)). This improvement is attributed to the synergistic interaction between metallic Ni sites and the acidic framework of HY. Here, Ni seems to play a vital role in promoting the initial decomposition of larger molecular fragments into smaller, more reactive radicals [17]. In addition to the catalytic effects, the microwave heating mechanism contributes to enhanced gas production. The unique heating mode of microwave-assisted pyrolysis enables rapid and volumetric heating throughout the material, resulting in greater gaseous product formation compared to conventional pyrolysis [18]. This facilitates enhanced secondary cracking reactions and faster decomposition of LDPE that ultimately provide a route to a higher yield of gaseous products. Al-Asadi et al. [19] also reported that a higher temperature and the presence of Ni on zeolite catalyst improved gas yields. They demonstrated that during polyethylene terephthalate pyrolysis at 900 °C, gas yields of around 43% and 68% were attained in the absence and presence of Ni/Y, respectively.

Beyond the total gas yield, significant changes were observed in the composition of liquid hydrocarbons. The incorporation of Ni also influenced selectivity toward different hydrocarbon families. Alkene concentrations decreased with increasing Ni proportion on HY, whereas those of alkanes increased, as shown in Figure 5.5 (b). This shift in hydrocarbon distribution also favored aromatic formation. Concurrently, aromatic selectivity increased due to the metal-acid synergy afforded by the catalyst. This phenomenon facilitates: (i) cracking larger hydrocarbons into smaller intermediates; (ii) dehydrocyclization of olefins into aromatics; and (iii) hydrogen

transfer reactions that stabilize aromatic products by removing excess H_2. The highest aromatic yield of 25% was achieved with 15% Ni/HY, while the highest paraffin yield of 50% was obtained with 10% Ni/HY. These fractions are important constituents of gasoline. In line with this, Marco et al. [20] also obtained 48% paraffins and 32% aromatics within the gasoline fraction using 5% Ni/HY during pyrolysis of mixed plastic waste collected from municipal solid waste. The maintained FAU-type crystallinity observed in XRD patterns confirms the structural stability of HY after Ni impregnation and calcination, ensuring preservation of accessible acid sites required for aromatization pathways. Zhang et al. [21] observed iso-paraffins to be predominant in liquid products generated during waste polyolefins hydrocracking using Ni/Hβ. Vance et al. [22] described the effectiveness of Ni/SiO_2 in breaking down LDPE into n-alkanes (C_6-C_{35}) at 300 °C and 30 bar H_2.

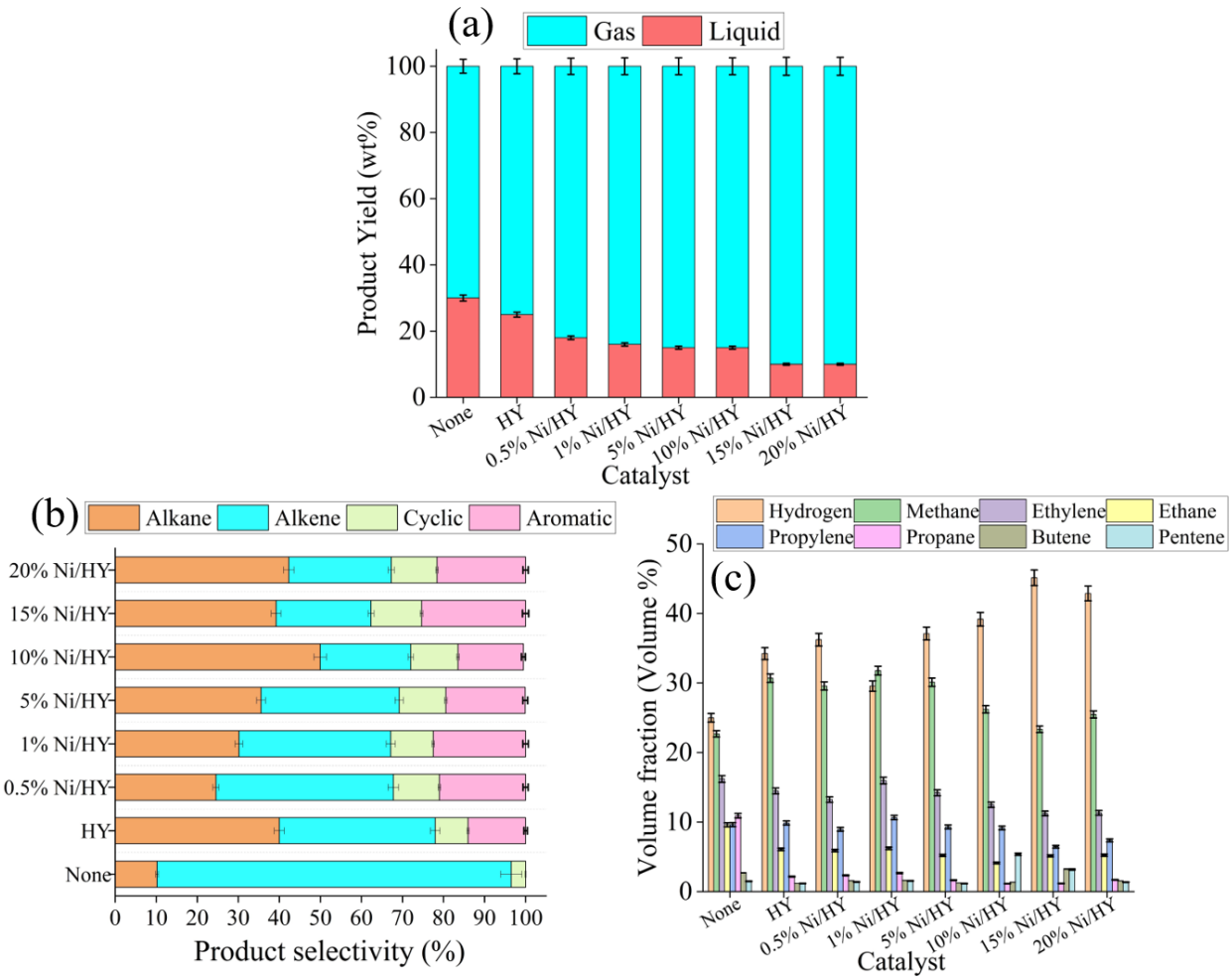

Figure 5.5: Influence of Ni Proportion in HY on (a) Product Distribution, (b) Liquid Oil Composition, and (c) Gas Composition at 450°C and the HY to LDPE ratio was 1:10.

The most significant impact of Ni incorporation was observed in hydrogen production. H_2 concentration increased significantly from 25% (without catalyst) to 45% with 15 wt.% Ni/HY (Figure 5.5 c). The enhanced hydrogen formation can be correlated with catalyst physicochemical properties: (i) High Lewis acidity (Py-FTIR), (ii) Effective Ni dispersion (supported by XRD phase identification), and (iii) Confirmed metal loading via ICP-MS (Table 5.2). The increased H_2 fraction reflects the superior dehydrogenation capability of Ni, consistent with observations by Ding et al. [23]. In addition to H_2, methane and ethylene emerged as the second-most abundant compounds produced followed by other components such as propylene and ethane. However, higher Ni loadings may alter the physical properties of the catalyst, causing mass transfer limitations. If reactants cannot efficiently access the active sites, H_2 production may be hindered. This may be the reason for the decline in H_2 production (42%) with 20 wt.% Ni/HY as compared to 45 % with 15 wt.% Ni/HY. Al-Asadi et al. [19] similarly concluded that zeolites loaded with Ni enhance the production of H_2 and branched hydrocarbons from polyethylene terephthalate pyrolysis.

5.3.2.2 Ni/SiO_2

Liquid and gas yields were approximately 25% and 75% over SiO_2, and 18% and 82% over 15% Ni/SiO_2 at 450 °C, respectively, as shown in Figure 5.6 (a). Elevated gas production could be attributed to the rapid heating rates resulting from the use of a lesser amount of susceptor combined with high microwave power. Klaimy et al. [24] similarly reported liquid and gas yields of 18% and 50%, respectively, during the flash pyrolysis of polyethylene over SiO_2 at 450 °C.

To further understand the selectivity of these catalysts, the composition of the liquid fraction was analyzed. As illustrated in Figure 5.6 (b), paraffins and olefins were major products with maximum yields of 47% and 39%, respectively, for 15% Ni/SiO_2 and 38% and 37% respectively, for SiO_2. The proportions of cyclic compounds were 5% with 15% Ni/SiO_2 and 4% with SiO_2, while aromatics accounted for 7% with 15% Ni/SiO_2 and 19% with SiO_2, respectively. Enhanced paraffin and olefin formation over Ni/SiO_2 can be ascribed to the bifunctional role of Ni, which facilitates C-C bond cleavage through β-scission and promotes hydrogenation of reactive intermediates, converting olefins and radicals into stable paraffins. Moreover, Ni suppresses the formation of aromatics by hydrogenating olefinic precursors and reducing the residence time of intermediates required for cyclization and aromatization. On the other hand, the higher aromatic yield observed with SiO_2 is due to its lack of hydrogenation

activity which allows thermally generated olefins to undergo secondary reactions such as cyclization and aromatization under microwave conditions. Klaimy et al. [24] also reported 37% paraffins and 35% olefins during flash catalytic pyrolysis of polyethylene over SiO_2 at 450 °C.

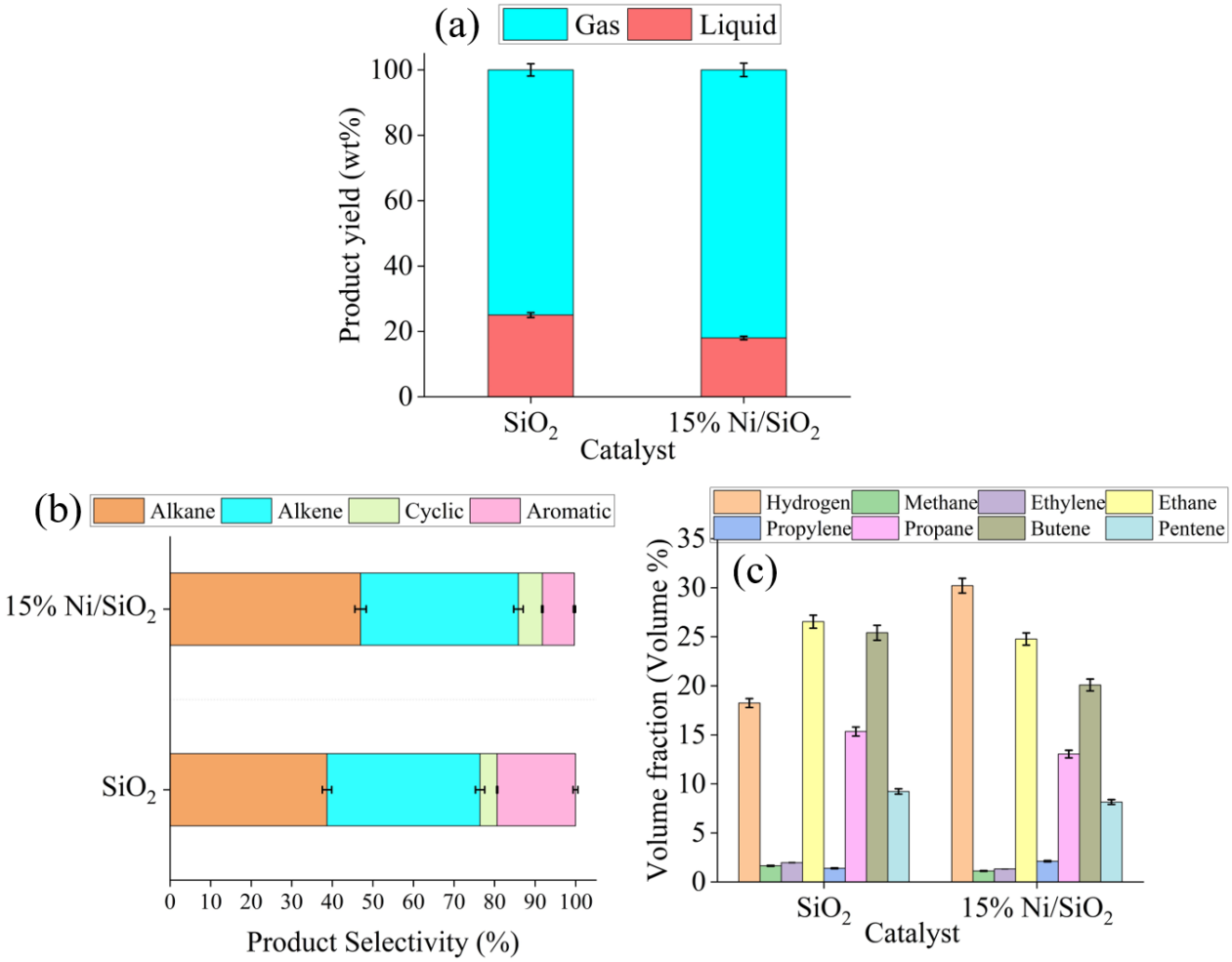

Figure 5.6: Effect of Ni/SiO_2 on (a) Product distribution, (b) Liquid composition, and (c) Gas composition at 450°C. SiO_2 to LDPE ratio was maintained at 1:10.

In addition to liquid selectivity, significant differences were observed in the gaseous products. In the case of LDPE pyrolysis with SiO_2 and 15 wt.% Ni/SiO_2, the primary gaseous products were H_2, ethane, and butene. H_2 content increased from 18% with SiO_2 to 30% with 15 wt.% Ni/SiO_2 confirming the superior dehydrogenation capability of Ni, as shown in Figure 5.6 (c). However, hydrogen formation is not governed solely by metal function but also by catalyst acidity. H_2 concentration was lower than that observed for 15 wt.% Ni/HY, possibly due to the lower LAS of 15wt% Ni/SiO_2 (2.59 µmol g^{-1}) compared to that of Ni/HY (Table-5.1). It has

been reported that catalyst acidity plays a significant role in H_2 formation during plastic pyrolysis, with H_2 production generally increasing with the acidity of the catalyst [25]. This increase in hydrogen concentration was accompanied by changes in other gaseous hydrocarbons. Ethane constituted around 26%, while butene accounted for around 25% of gas products in the presence of SiO_2. With Ni doping on SiO_2, a slight reduction in ethane and butene formation was observed. This was due to the dominance of the dehydrogenation reaction over the cracking reaction. These findings are consistent with previous reports. Klaimy et al. [24] similarly reported that 40% of the gaseous product consisted of C_3–C_5 compounds during flash catalytic pyrolysis of polyethylene over SiO_2 at 450 °C, whereas in the present study the fraction of C_3–C_5 compounds were 50% with SiO_2 and 43% with 15 wt.% Ni/SiO_2.

5.3.2.3 Ni/TiO_2

At high temperatures and higher heating rates, the additional thermal energy supplied to polymers weakens their chain structure and leads to the breakage of more polymer chains. This accelerates oligomer cracking, resulting in smaller hydrocarbons in the form of gases. While this mechanism is general to both catalytic and non-catalytic pyrolysis, the presence of catalysts such as Ni/TiO_2 enhances the rate and selectivity of these transformations, as elucidated in Figure 5.7 (a). Here the catalysts predominantly produced gaseous products, with a slight increase in gas yield upon incorporating Ni into TiO_2. Similar observations of lower liquid product yields, around 15% and 27%, were also reported by Uwagwu et al. [26] and Nwankwor et al. [27] during pyrolysis of LDPE over TiO_2 at 300 °C and 400 °C, respectively.

To further elucidate catalytic selectivity, the composition of the liquid phase was analyzed. As Figure 5.7 (b) evinces, liquid products consisted of alkanes, alkenes, and cyclic compounds at 32%, 53%, and 8%; and 30%, 48%, and 10%, respectively in the absence and presence of Ni on TiO_2. The predominance of olefins can be correlated with the moderate acidity of the support. This moderate acid strength helps to minimize secondary hydrogen transfer reactions, thereby limiting the formation of aromatics. Nwankwor et al. [27] confirmed that the liquid product obtained from catalytic cracking of LDPE over TiO_2 at 400 °C primarily consisted of aliphatic hydrocarbons in the gasoline range which aligns with the results of present study.

In addition to the liquid composition, significant changes were observed in the gaseous products. As seen in Figure 5.7 (c), H_2 content increased from 2% to 16% in the presence of Ni/TiO_2. Apart from H_2, propylene (32%) and butene (23%) were the two other major gaseous

products. The lowest H_2 yield (16%) was recorded with 15% Ni/TiO_2, which also exhibited the lowest LAS (0.51 μmol g^{-1}) confirming that low acid site density is unfavourable for H_2 production. The reduced acidity of TiO_2, in combination with metal functionality and support properties, resulted in the extended retention of olefins in the gaseous products and the reduction in aromatics in the liquid products (Figure 5.7 (b)). A mechanistic interpretation of this behavior has been proposed in previous studies. Chen et al. [28] demonstrated that Ni/TiO_2 to causes rapid isomerization and exhibits strong polymer–surface interactions. The latter limits the access of other molecules to the active sites, thereby suppressing secondary reactions. As a result, the reaction pathway favors sequential β-scissions, selectively enhancing the formation of C_4–C_{12} hydrocarbons with particular emphasis on the C_4–C_5 fractions.

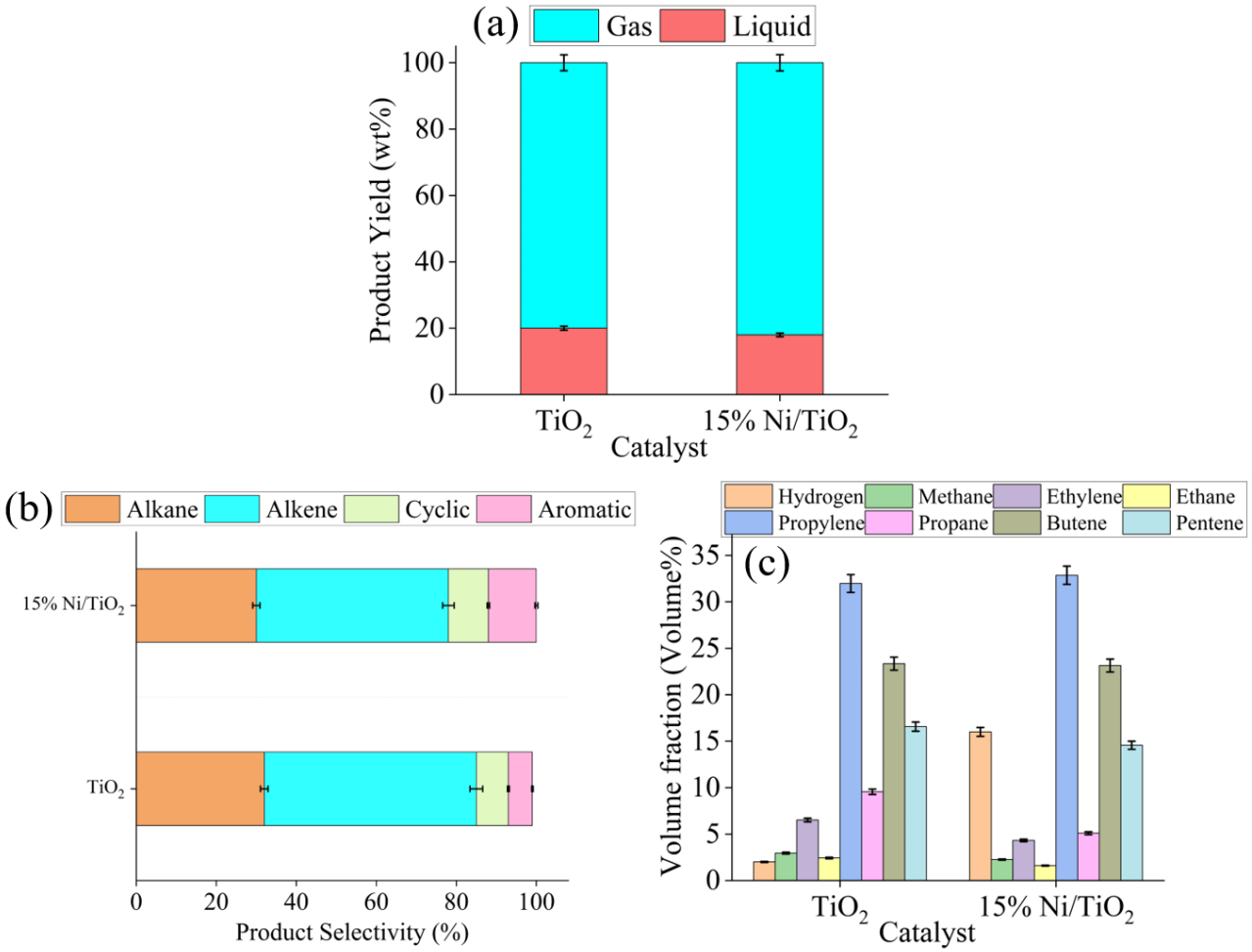

Figure 5.7: Effect of Ni/TiO_2 on (a) Product distribution, (b) Liquid composition, and (c) Gas composition at 450°C. TiO_2 to LDPE ratio was maintained at 1:10.

5.3.2.4 Ni & Zn/Al_2O_3

Significant H_2 formation was observed during LDPE cracking over Al_2O_3-supported catalysts containing 15 wt.% Ni and Zn. As revealed in Figure 5.8 (a), the total gas yield reached around 80% over Al_2O_3, 82% with 15% Ni/Al_2O_3, and 80% with 15% Zn/Al_2O_3 at 450°C. These results indicate enhanced cracking activity under catalytic conditions compared to the non-metal-loaded support. Such trends are consistent with previous reports that catalytic pyrolysis favors gaseous product formation over liquid oil fractions [29]. These results are in concurrence with those reported by Rachmadena et al. [30]. They observed 19% liquid and 67% gaseous product yields from polypropylene using Al_2O_3 at 350 °C. Similarly, Terry et al. [31] reported a maximum pyrolysis oil yield of 17 wt.%, and a gas yield of approximately 50% at 500°C in the catalytic co-pyrolysis of polypropylene and oil palm trunk using Ni/Al_2O_3. This supports our observation of the low oil yield with 15% Ni/Al_2O_3.

Liquid products consisted of alkanes (30-52%), alkenes (30-39%), cyclic compounds (8-17%), and aromatic compounds (9-17%) as shown in Figure 5.8 (b). The Al_2O_3 support mainly yielded alkanes and alkenes, while the introduction of Ni or Zn to Al_2O_3 led to increased formation of cyclic and aromatic compounds. Alkane formation can result from cracking larger olefins formed by random scission of LDPE. The 15 wt.% Ni/Al_2O_3 led to the highest aromatic content, indicating the role of Ni in promoting dehydrogenation and secondary aromatization reactions. Zn/ Al_2O_3 also favored aromatic and cyclic formation. The addition of Ni and Zn facilitates hydrogen abstraction from hydrocarbon fragments, thereby boosting the formation of alkenes. Sivakumar et al. [32] also reported that the liquid product obtained from catalytic pyrolysis of waste LDPE film at 380 °C with a NiMo/Al_2O_3 catalyst consisted predominantly of aliphatic compounds (85%) with a small fraction of aromatic compounds. Similarly, Li et al. [33] observed that during pyrolysis-catalytic decomposition of plastics using Fe_2O_3/Al_2O_3 catalyst at 800 °C resulted in hydrocarbon products being predominantly composed of alkanes and alkenes ranging from C_2 to C_9.

Gas analysis (Figure 5.8 (c)) shows that H_2 concentration increased from 23% over Al_2O_3 to 32% with Ni/Al_2O_3 and 34% with Zn/Al_2O_3. The enhancement in hydrogen formation suggests that both Ni and Zn promote hydrogen abstraction and dehydrogenation reactions during microwave-assisted pyrolysis. During polyethylene pyrolysis, random scission of C–C bonds generate free radicals, which then undergo intramolecular or intermolecular H_2 transfer, leading to the creation of low molecular weight hydrocarbons such as ethane. Yang et al. reported a

34% H_2 yield through waste plastic gasification at 600 °C in the presence of Ni/Al_2O_3 [34]. The comparatively higher H_2 concentration over Al_2O_3-supported catalysts relative to SiO_2- and TiO_2-based systems appears to be associated with stronger Lewis acidity and metal–support interactions. Overall, the results indicate that the incorporation of Ni and Zn into Al_2O_3 enhances gas yield, hydrogen concentration, and secondary aromatization reactions, although the observed performance reflects the combined influence of metal functionality and support properties.

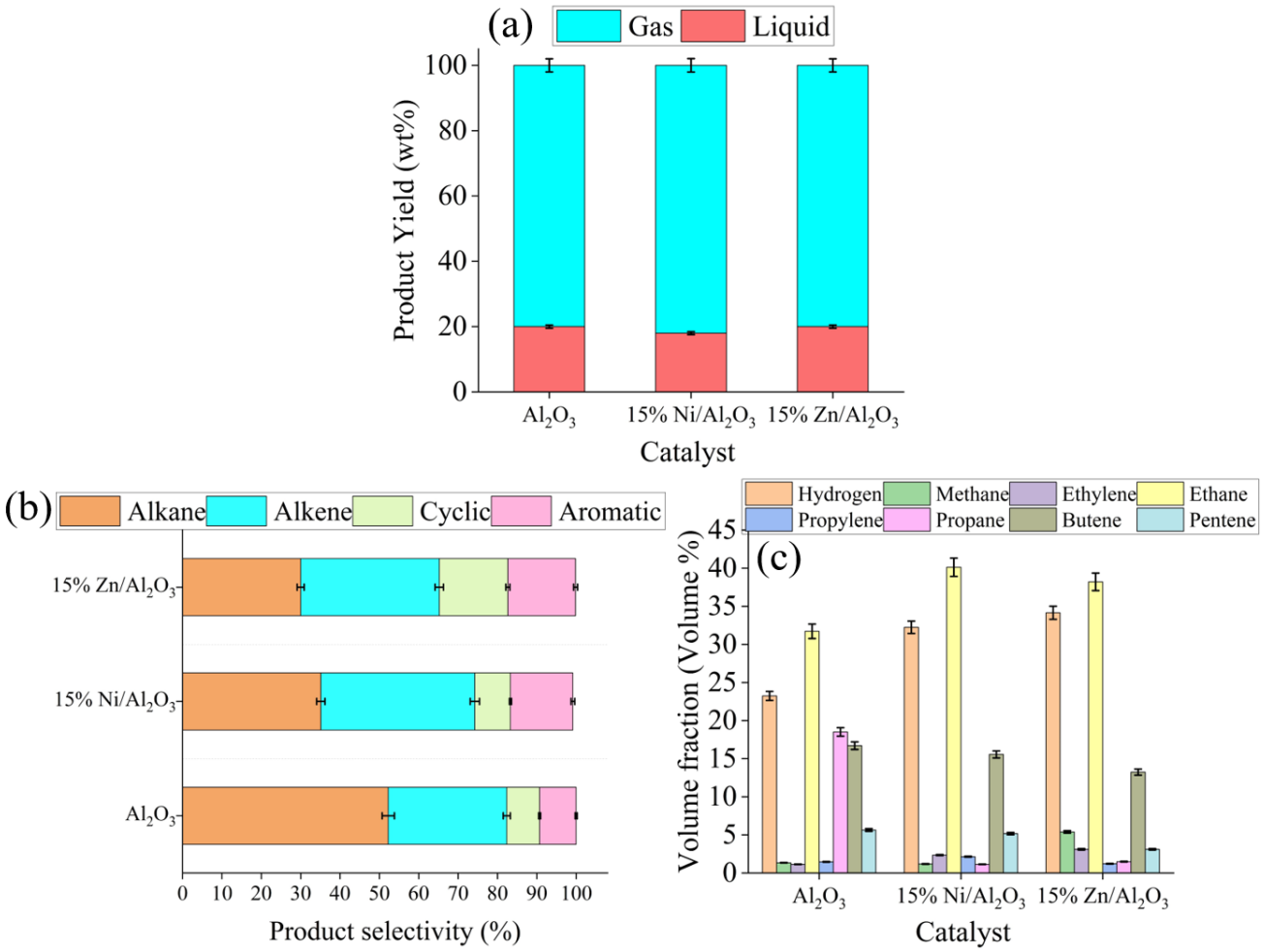

Figure 5.8: Impact of Ni and Zn in Al_2O_3 on (a) Product distribution, (b) Liquid composition, and (c) Gas composition at 450°C. Al_2O_3 to LDPE ratio was maintained at 1:10.

5.3.2.5 Zn/HY

In these experiments, HY contained 10, 15, and 20 wt.% Zn. As illustrated in Figure 5.9 (a), an increase in gas yield from 70 wt.% to 80 wt.% was achieved with Zn supported on HY, which facilitates the initial breakdown of larger hydrocarbon fragments into smaller radicals.

The increased gas yield may also be influenced by secondary vapor-phase cracking reactions under microwave heating. Vatankhah et al. [35] reported a 60% gas yield from microwave-assisted pyrolysis of polyethylene employing Zn (2%)/ZSM-5 at 360 °C.

The product distribution in the liquid phase (Figure 5.9(b)) shows a clear compositional shift with increasing Zn content. The alkene fraction decreased significantly from 38% to 14%, while paraffin selectivity increased in most cases. The aromatics yield slightly increased from 25% to 28% with the increase in Zn loading on HY. The observed increase in aromatics with Zn loading suggests enhanced dehydrogenation and hydrogen-transfer reactions, which are commonly associated with Zn-modified zeolites. Dong et al. [36] observed that introducing Zn into HZSM-5 significantly enhanced aromatics production during the conversion of HDPE at 500°C. In the present work, the maximum aromatic yield of 30% was achieved with 15 wt.% Zn/HY, while 46% paraffins were obtained with 10 wt.% Zn/HY. Barzallo et al. [37] demonstrated that impregnating ZSM-5 with 1% Zn notably improved selectivity toward aromatics during catalytic pyrolysis of polypropylene (PP) at 450 °C. Here, the presence of HY may further promote Diels-Alder and other aromatization reactions involving alkenes thereby enhancing aromatic compound formation while simultaneously reducing alkene yields. In another study, approximately a 30% yield of aromatics was obtained from polyethylene conversion over Zn/ZSM-5 at 400 °C [38]. Similarly, Zn species have been shown to significantly promote the aromatization mechanism, contributing to improved formation of aromatic hydrocarbons during microwave-assisted pyrolysis over Zn/HZSM-5 at 360 °C [39].

Gas analysis (Figure 5.9(c)) further indicates that Zn presence increases H_2 concentration and total gas production. Besides H_2, ethane (26%) and propylene (25%) were the major gaseous components, reflecting extensive cracking and olefin transformation pathways. The latter is reflected in the increased formation of aromatics and alkenes in the liquid products. Notably, although 15 wt.% Zn/HY exhibits comparable Lewis acidity (15.26 μmol g^{-1}) to 15 wt.% Ni/HY, it produces a slightly lower hydrogen concentration (43%), suggesting that hydrogen evolution is governed not solely by acid site density but also by intrinsic metal functionality and metal-acid synergy. However, increased Zn loading can affect the physical properties of the catalyst, potentially leading to mass transfer limitations. If reactants cannot effectively access the active sites, H_2 production may be restricted. Vatankhah et al. [35] reported a 32% H_2 yield from microwave-assisted pyrolysis of polyethylene using Zn (2%)/ZSM-5 at 360 °C. Similarly, Duan et al. [38] achieved a 40% yield of C_2–C_4 compounds from the conversion of

polyethylene over Zn/ZSM-5 at 400 °C, which aligns with the findings of the present work. Zn species facilitate the formation of a hydrocarbon pool consisting of C_1–C_3 intermediates during microwave-assisted pyrolysis, which promotes aromatization [39].

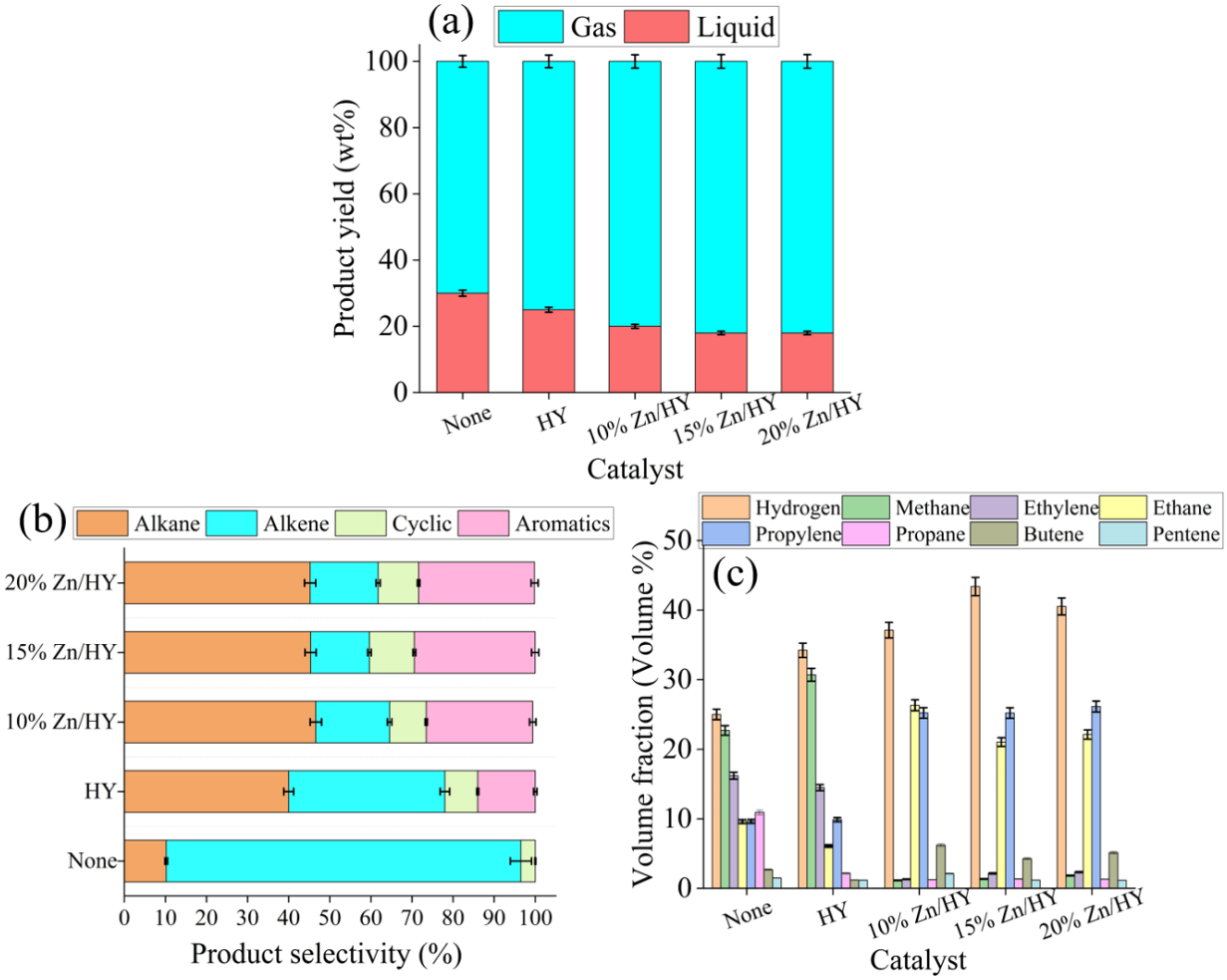

Figure 5.9: Influence of Zn Proportion in HY on (a) Product Distribution, (b) Liquid Composition, and (c) Gas Composition at 450°C and the HY to LDPE ratio was 1:10.

Figure 5.10 presents the overall product yield (gas and liquid, wt.%) together with detailed gas composition (H_2, C_1-C_3, and C_{4+} vol%) for all catalysts investigated under identical reaction conditions. The comparison highlights the influence of metal identity and support properties on hydrogen concentration, light hydrocarbon formation, and product distribution trends across the catalytic systems.

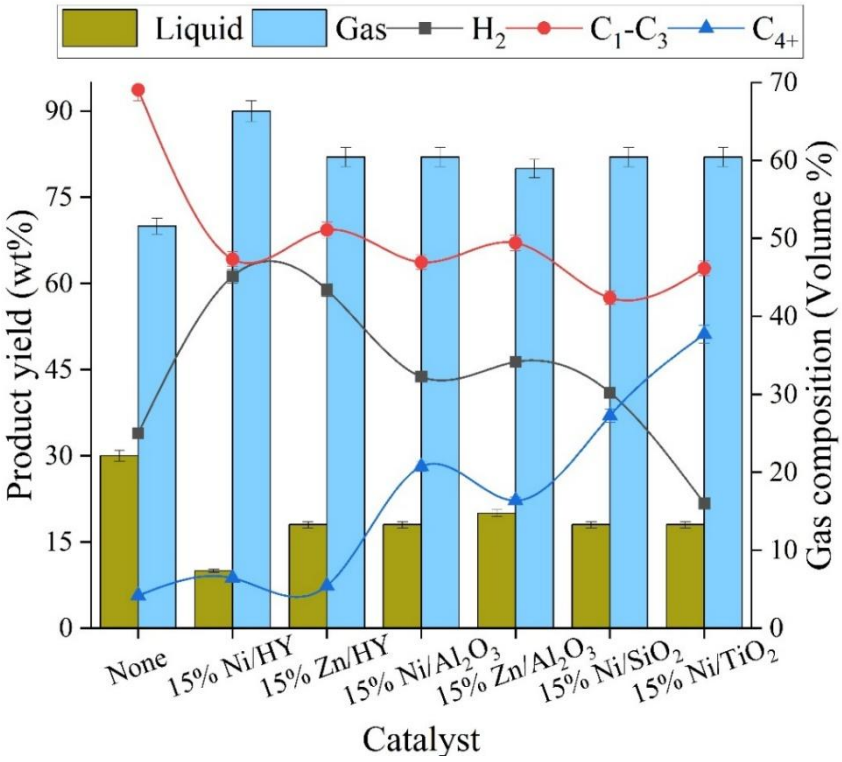

Figure 5.10: Comparison of catalytic performance during microwave-assisted LDPE pyrolysis.

5.3.2.6 Carbon number Distribution of hydrocarbons in liquid:

Liquid products distribution based on carbon number ranges (C_6–C_{12}: gasoline, C_{12}–C_{15}: kerosene, C_{15}–C_{25}: diesel, >C_{25}: wax) for different 15 wt.% metal-loaded catalysts used in LDPE cracking is presented in Figure 5.11. Among these, 15% Ni/HY and 15% Zn/HY exhibited the highest selectivity toward gasoline-range hydrocarbons (C_6–C_{12}), accounting for more than 80% of the liquid products. Thus, Ni/HY and Zn/HY can be considered as the most effective catalysts for producing gasoline with a high-octane number. In this context, Ni and Zn serve as hydrogenation catalysts that facilitate the breakdown of polymer chains into smaller hydrocarbons, while HY acts as an acidic catalyst that further cracks these fragments into lighter and more valuable products, such as gasoline-range hydrocarbons and aromatics. This bifunctional effect enhances both the yield and the quality of the liquid products obtained during pyrolysis. Marco et al. [20] reported a 45% yield of gasoline-range hydrocarbons using 5 wt.% Ni/HY for the pyrolysis of plastic waste. In contrast, the current study achieved an 85% gas yield, likely due to the higher heating rates enabled by microwave irradiation. Similarly, Sun et al. [40] developed a catalytic system combining Ni–WO_3/Al_2O_3 with Hβ, which showed outstanding hydrocracking performance for polyethylene, yielding 78% liquid hydrocarbons

in the gasoline–jet fuel range (primarily C_5–C_{16}, with minor C_{16+} components) after 4 hours at 280 °C.

In the present study, Ni- and Zn-loaded Al_2O_3 catalysts (15 wt.%) yielded around 63% and 65% gasoline-range hydrocarbons, respectively, at 450 °C. Al_2O_3 possesses moderate LAS, which is sufficient to promote the cracking of polymer chains (such as LDPE) into smaller fragments. This moderate acidity helps maintain a higher yield in the gasoline range rather than shifting toward heavier waxes (>C_{25}). Rachmadena et al. [30] also observed that catalytic conversion of polypropylene waste using Al_2O_3 predominantly produced gasoline-range hydrocarbons, with a smaller fraction in the diesel range and only trace amounts of other products.

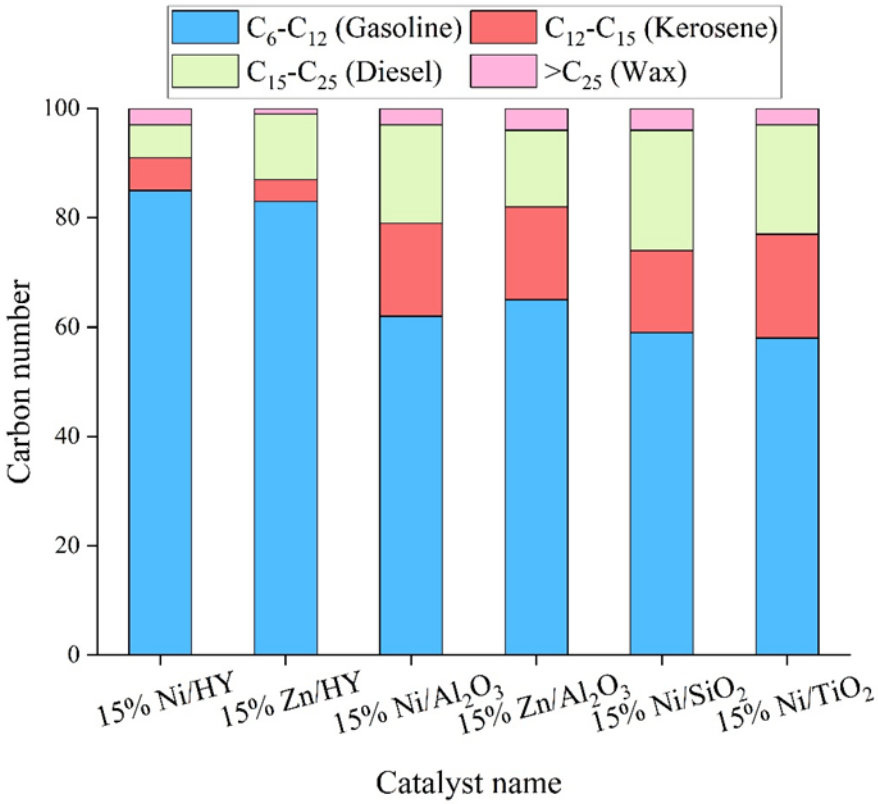

Figure 5.11: Carbon number distribution in Liquid oil in Presence of different catalyst at 450°C and catalyst to LDPE ratio was 1:10.

Additionally, 59% of gasoline-range hydrocarbons were obtained using 15% Ni/SiO_2 with diesel-range hydrocarbons being the second major fraction (22%). Ni contributes to dehydrogenation functionality, which helps in breaking C–C bonds and forming olefins and aromatics, contributing to the gasoline-range fraction. However, without sufficient acidity from

the support (as in HY), the extent of cracking remains moderate. A similar trend was reported by Dzol et al. during the catalytic pyrolysis of high-density polyethylene over Ni/HZSM-5 [41].

For 15 wt.% Ni/TiO_2, around 58% gasoline-range and 20% diesel-range hydrocarbons were produced. The lower gasoline-range product yield compared to Ni/HY may be attributed to the lower acidity of the TiO_2 support. Marhaini et al. [42] also reported a 49% gasoline-range fraction from conventional pyrolysis of LDPE waste over TiO_2 at 350 °C, aligning with the current findings.

5.3.2.7 Comparative Analysis of TOF and TON for Ni and Zn Catalysts on Acidic and Non-Acidic Supports:

TOF and TON were calculated using the following expressions:

$$\text{TOF}=\frac{\text{moles of H2 formed}}{\text{total moles of metal}*t}$$

where: t= reaction time (s)

$$\text{TON}=\frac{\text{moles of H2 formed}}{\text{total moles of metal}}$$

TOF and TON values (Table 5.3) reveal a clear influence of both the metal type and the support on catalytic performance in LDPE cracking for H_2 production. HY-supported catalysts showed excellent activity, with 15% Zn/HY demonstrating the highest TOF (0.098 s^{-1}) and TON (59), closely followed by 15% Ni/HY (TOF: 0.092 s^{-1}; TON: 55). These catalysts also delivered the highest H_2 yields (43–45%) which can be attributed to their higher LAS that promotes effective cracking and H_2 release. Al_2O_3-supported catalysts demonstrated moderate activity, with 15% Zn/Al_2O_3 (TOF: 0.066 s^{-1}; TON: 43) slightly outperforming 15% Ni/Al_2O_3 (TOF: 0.056 s^{-1}; TON: 36), likely due to improved metal dispersion or favorable metal-support interactions. In contrast, catalysts supported on SiO_2 and TiO_2, which lack sufficient acidity, exhibited the lowest TOFs and TONs values. The 15% Ni/SiO_2 (TOF: 0.052 s^{-1}; TON: 31) and 15% Ni/TiO_2 (TOF: 0.026 s^{-1}; TON: 15) resulted in low H_2 yields.

Overall, catalysts with higher LAS, particularly HY demonstrated superior performance in terms of both TOF and TON highlighting the importance of support acidity in enhancing H_2 production during LDPE cracking. Al-Asadi et al. [19] conducted the pyrolysis of polyethylene terephthalate using 10% Ni/Y and 10% Ni/ZSM-5 and reported TOF values of 0.027 s^{-1} and 0.034 s^{-1}, and TON values of 31.9 and 40.8, respectively. The gas yield was 65 wt.%, with a

H_2 yield of 32.6 vol %. Similarly, Akubo et al. [43] performed the pyrolysis of polyethylene with Ni/Y in a fixed-bed system and achieved a TOF of 0.0028 s^{-1} and a TON of 4.97, along with a 36 wt.% gas yield and 66 vol.% H_2. In this study, significantly higher TOF and TON values were achieved which can be attributed to the reduced reaction time under microwave irradiation and enhanced H_2 production. This may be due to the higher LAS and strong metal-support synergy, resulting in improved H_2 production and valuable gasoline range hydrocarbons (C_6–C_{12}).

Table 5.3: Turnover Frequency (TOF), Turnover Number (TON), and H_2 yield for 15 wt.% metal-loaded catalysts used in LDPE cracking at 450°C, where the catalyst to LDPE ratio was 1:10.

Sr. No.	**Catalyst**	**Gaseous product (wt.%)**	**H_2 (vol%)**	**H_2 production ($mmol/g_{plastic}$)**	**TOF (s^{-1})**	**TON**
1	15% Ni/HY	90	45	14.05	0.092	55
2	15% Zn/HY	82	43	13.43	0.098	59
3	15% Ni/Al_2O_3	82	32	9.27	0.056	36
4	15% Zn/Al_2O_3	80	34	9.86	0.066	43
5	15% Ni/SiO_2	82	30	8.03	0.052	31
6	15% Ni/TiO_2	82	16	3.93	0.026	15

5.3.2.8 Cracking of LDPE dissolved in Tetralin:

Figure 5.12 illustrates the influence of the 15 wt.% Ni/HY catalyst on the microwave-assisted cracking of LDPE at 450 °C. Prior to cracking, LDPE was dissolved in tetralin at a concentration of 0.16 g mL^{-1} by heating it to 100 °C to ensure complete dissolution. The resulting LDPE solution was mixed with the graphite microwave absorber and subjected to microwave irradiation in the absence (non-catalytic) and presence of the Ni/HY catalyst.

Figure 5.12(a) compares the overall product distribution obtained from non-catalytic and catalytic microwave cracking of LDPE. In the absence of the catalyst, the process yielded approximately 70 wt.% gaseous products and 30 wt.% liquid products. Upon introduction of the 15 wt.% Ni/HY, the gas yield increased to about 75 wt.%, accompanied by a corresponding decrease in the liquid yield. This enhancement in gas production indicates that the Ni/HY

catalyst effectively promotes secondary cracking and dehydrogenation reactions under microwave heating, favoring the formation of lighter gaseous hydrocarbons and H_2.

Figure 5.12 (b) presents the chemical selectivity of the liquid fraction in terms of alkanes, alkenes, cycloalkanes, and aromatics. For non-catalytic cracking, the liquid products consisted predominantly of aromatic compounds (60%), followed by alkanes (30%), with minor contributions from cycloalkanes and alkenes. The presence of Ni/HY significantly increased aromatic selectivity to nearly 70%, while the alkane fraction decreased. This shift suggests enhanced aromatization and hydrogen transfer reactions facilitated by the acidic sites of the HY zeolite in combination with the metallic Ni sites, which are known to promote dehydrogenation and ring-forming reactions.

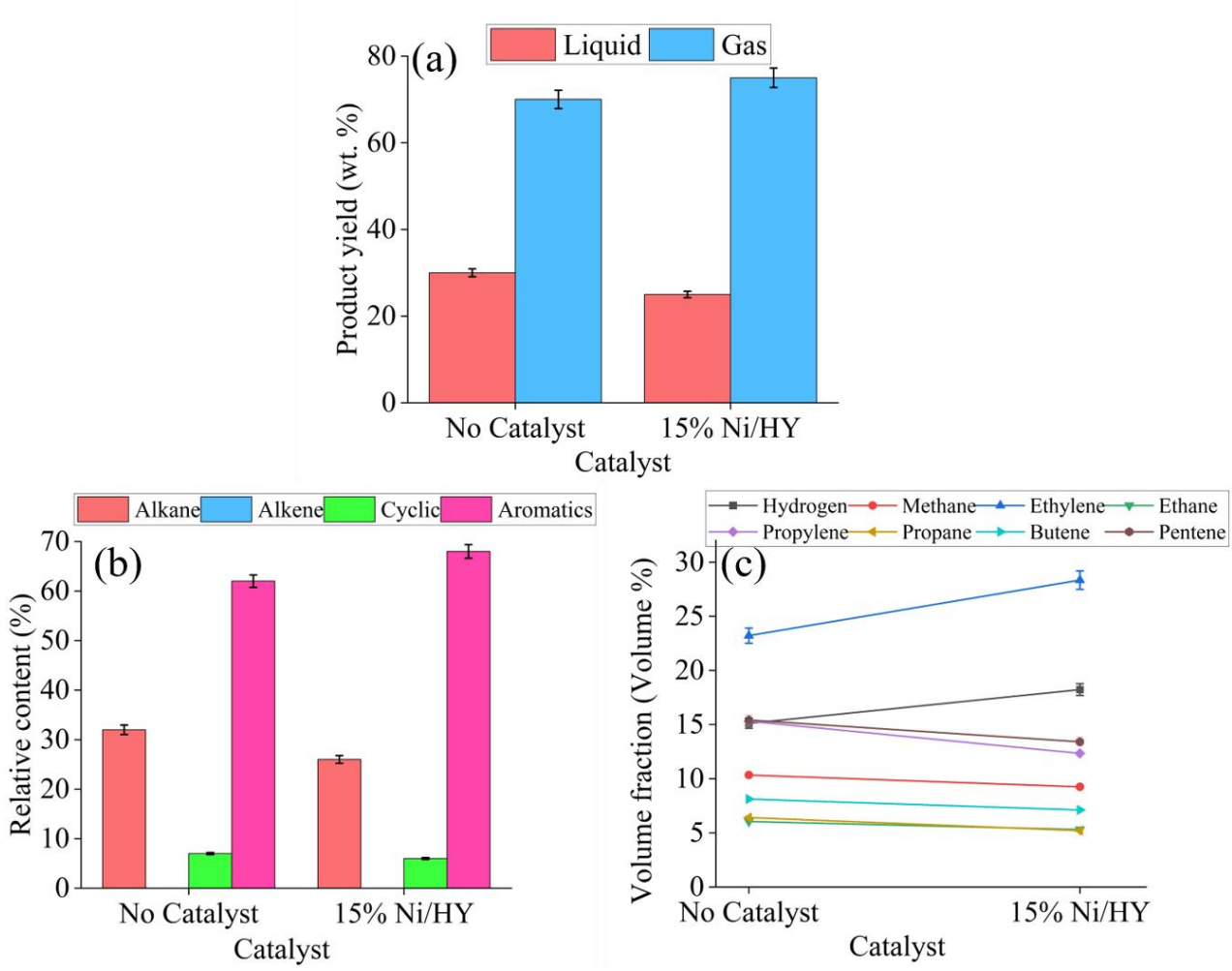

Figure 5.12: Cracking of LDPE dissolved in Tetralin (a) Product yield at 450°C, (b) Liquid composition at 450°C and (c) Gas composition at 450°C. Catalyst to LDPE ratio was 1:10.

Figure 5.12 (c) shows the volume fraction distribution of the major gaseous components produced during LDPE cracking. The catalytic system exhibited a notable increase in H_2 concentration compared to the non-catalytic case, confirming the strong dehydrogenation activity of Ni/HY under microwave irradiation. Additionally, an increase in ethylene content was observed, while methane, propane, butane, and higher hydrocarbons showed a slight decline. This trend indicates that the catalyst favors β-scission and secondary cracking of long-chain hydrocarbons, leading to the formation of light olefins and H_2. Overall, these results demonstrate that microwave-assisted LDPE cracking in the presence of the 15 wt.% Ni/HY significantly enhances gas yield, H_2 production, and aromatic selectivity compared to non-catalytic operation. The synergistic interaction between microwave heating, the graphite absorber, and the bifunctional Ni/HY catalyst plays a crucial role in intensifying cracking, dehydrogenation, and aromatization reactions.

5.4 Conclusion

This study demonstrated that catalytic microwave-assisted cracking of LDPE using Ni and Zn supported on HY, Al_2O_3, TiO_2, and SiO_2 is an effective approach for producing H_2 and valuable hydrocarbons. All tested catalysts significantly enhanced H_2 generation compared to thermal pyrolysis. Among them, Ni/HY and Zn/HY exhibited the highest H_2 yields, contributing up to 45% of the total gaseous products. While Ni/Al_2O_3 and Zn/Al_2O_3 and Ni/SiO_2 achieved approximately 32%, 34% and 30% H_2, respectively. The results confirm that metal – support synergy boosts the formation of H_2 rich gases and aromatic hydrocarbons. Notably, Ni/HY and Zn/HY catalysts promoted higher aromatic content in the liquid fractions, particularly the gasoline-range hydrocarbons. This can be attributed to the greater acidity and microporous structure of HY which favor dehydrogenation and aromatization reactions. Overall, the findings underscore the importance of catalyst selection and support characteristics in optimizing product distribution during microwave-assisted pyrolysis of plastic waste.

5.5 References

[1] Y. Zhang, A. Li, Y.S. Zhang, W. Xie, C. Liu, Y. Peng, H. Zhang, Y. Kang, B. Qu, G. Ji, In-situ catalytic pyrolysis of polyethylene to co-produce BTX aromatics and H2 by Ni/ZSM-5 in the rotary reactor with solid heat carriers, Fuel 371 (2024) 131950. https://doi.org/10.1016/j.fuel.2024.131950.

[2] D. Barzallo, R. Lazo, C. Medina, C. Guashpa, C. Tacuri, P. Palmay, Synthesis and Application of ZSM-5 Catalyst Supported with Zinc and/or Nickel in the Conversion of Pyrolytic Gases from Recycled Polypropylene and Polystyrene Mixtures under Hydrogen Atmosphere, Polymers (Basel). 15 (2023) 3329. https://doi.org/10.3390/polym15163329.

[3] P.L. editors Weitkamp J, Catalysis and zeolites: fundamentals and applications, New York: Springer Berlin Heidelberg (1999) 546.

[4] Anggoro DD, Buchori L, Silaen GC, Utami RN, Preparation,characterization, and activation of Co-Mo/Y zeolite catalyst forcoal tar conversion to liquid fuel, Bull Chem React Eng Catal 12 (2017) 219–226.

[5] Handke M, Mozgawa W, Vibrational spectroscopy of theamorphous silicates, Vib Spectrosc 5 (1993) 75–84.

[6] T.Y. Yun, B.D. Chandler, Surface Hydroxyl Chemistry of Titania- and Alumina-Based Supports: Quantitative Titration and Temperature Dependence of Surface Brønsted Acid–Base Parameters, ACS Appl. Mater. Interfaces 15 (2023) 6868–6876. https://doi.org/10.1021/acsami.2c20370.

[7] J. Li, R. Yan, B. Xiao, D.T. Liang, D.H. Lee, Preparation of Nano-NiO Particles and Evaluation of Their Catalytic Activity in Pyrolyzing Biomass Components, Energy & Fuels 22 (2008) 16–23. https://doi.org/10.1021/ef700283j.

[8] A.Q. Saeed, B.Y. Al-Zaidi, A.S. Hamadi, H.Sh. Majdi, A.A. AbdulRazak, Upgrade of heavy crude oil via aquathermolysis over several types of catalysts, Materials Express 12 (2022) 278–287. https://doi.org/10.1166/mex.2022.2139.

[9] F. Chen, D. Zhang, L. Shi, Y. Wang, G. Xu, Optimized Pore Structures of Hierarchical HY Zeolites for Highly Selective Production of Methyl Methoxyacetate, Catalysts 9 (2019) 865. https://doi.org/10.3390/catal9100865.

[10] A.A. Mohammed, Z.T. Khodair, A.A. Khadom, Preparation and investigation of the structural properties of α-Al2O3 nanoparticles using the sol-gel method, Chemical Data Collections 29 (2020) 100531. https://doi.org/10.1016/j.cdc.2020.100531.

[11] N.N.A. Mohamed Abdul Ghani, M.A. Saeed, I.H. Hashim, Thermoluminescence (TL) response of silica nanoparticles subjected to 50 Gy gamma irradiation., Malaysian Journal of Fundamental and Applied Sciences 13 (2017). https://doi.org/10.11113/mjfas.v13n3.593.

[12] A.K. John, S. Palaty, S.S. Sharma, Greener approach towards the synthesis of titanium dioxide nanostructures with exposed {001} facets for enhanced visible light photodegradation of organic pollutants, Journal of Materials Science: Materials in Electronics 31 (2020) 20868–20882. https://doi.org/10.1007/s10854-020-04602-1.

[13] A. Martínez, M.A. Arribas, P. Concepción, S. Moussa, New bifunctional Ni–H-Beta catalysts for the heterogeneous oligomerization of ethylene, Appl. Catal. A Gen. 467 (2013) 509–518. https://doi.org/10.1016/j.apcata.2013.08.021.

[14] Z. Ahmad, F. UllahKha, S. Mahmood, T. Mahmood, A. Shamim, Different Approaches for the Synthesis of Zinc Oxide Nanoparticles, Open Journal of Chemistry 1 (2018) 19–25. https://doi.org/10.30538/psrp-ojc2018.0003.

[15] Y. Jia, J. Wang, K. Zhang, W. Feng, S. Liu, C. Ding, P. Liu, Nanocrystallite self-assembled hierarchical ZSM-5 zeolite microsphere for methanol to aromatics, Microporous and Mesoporous Materials 247 (2017) 103–115. https://doi.org/10.1016/j.micromeso.2017.03.035.

[16] R.R. Mishra, P.H. Rana, P.A. Parikh, Influence of catalyst acidity of spent FCC catalyst and TiO2 on product distribution in microwave assisted LDPE cracking, Journal of the Indian Chemical Society 102 (2025) 101873. https://doi.org/10.1016/j.jics.2025.101873.

[17] A. Palčić, V. Valtchev, Analysis and control of acid sites in zeolites, Appl. Catal. A Gen. 606 (2020) 117795. https://doi.org/10.1016/j.apcata.2020.117795.

[18] C. Mohabeer, N. Guilhaume, D. Laurenti, Y. Schuurman, Microwave-Assisted Pyrolysis of Biomass with and without Use of Catalyst in a Fluidised Bed Reactor: A Review, Energies (Basel). 15 (2022) 3258. https://doi.org/10.3390/en15093258.

[19] M. Al-asadi, N. Miskolczi, Pyrolysis of polyethylene terephthalate containing real waste plastics using Ni loaded zeolite catalysts, IOP Conf. Ser. Earth Environ. Sci. 154 (2018) 012021. https://doi.org/10.1088/1755-1315/154/1/012021.

[20] M.F. Paucar-Sánchez, M. Calero, G. Blázquez, R.R. Solís, M.J. Muñoz-Batista, M.Á. Martín-Lara, Impact of Metal Impregnation of Commercial Zeolites in the Catalytic Pyrolysis of Real Mixture of Post-Consumer Plastic Waste, Catalysts 14 (2024) 168. https://doi.org/10.3390/catal14030168.

[21] G. Zhang, Q. Mao, Y. Yue, R. Gao, Y. Duan, H. Du, Ni-based catalysts supported on Hbeta zeolite for the hydrocracking of waste polyolefins, RSC Adv. 14 (2024) 15856–15861. https://doi.org/10.1039/D4RA02809K.

[22] B.C. Vance, P.A. Kots, C. Wang, J.E. Granite, D.G. Vlachos, Ni/SiO2 catalysts for polyolefin deconstruction via the divergent hydrogenolysis mechanism, Appl. Catal. B 322 (2023) 122138. https://doi.org/10.1016/j.apcatb.2022.122138.

[23] K. Ding, S. Liu, Y. Huang, S. Liu, N. Zhou, P. Peng, Y. Wang, P. Chen, R. Ruan, Catalytic microwave-assisted pyrolysis of plastic waste over NiO and HY for gasoline-range hydrocarbons production, Energy Convers. Manag. 196 (2019). https://doi.org/10.1016/j.enconman.2019.07.001.

[24] S. Klaimy, C. Ciotonea, J. Dhainaut, S. Royer, M. Casetta, S. Duquesne, G. Tricot, J. Lamonier, Flash Catalytic Pyrolysis of Polyethylene over (Alumino)silicate Materials, ChemCatChem 12 (2020) 1109–1116. https://doi.org/10.1002/cctc.201901819.

[25] M.Á. Martín-Lara, R. Moreno, G. Blázquez, M. Calero, Hydrogen Production Came from Catalytic Reforming of Volatiles Generated by Waste-Plastic Pyrolysis Over Sepiolite-Based Catalysts, Top. Catal. 68 (2025) 33–48. https://doi.org/10.1007/s11244-024-01981-1.

[26] Uwagwu Charles Olisemeke, Research on Comparative Study on the Conversion of Waste Plastic Materials to Liquid Hydrocarbons Through Catalytic Pyrolysis, 2018.

[27] P.E. Nwankwor, I.O. Onuigbo, C.E. Chukwuneke, M.F. Yahaya, B.O. Agboola, W.J. Jahng, Synthesis of gasoline range fuels by the catalytic cracking of waste plastics using titanium dioxide and zeolite, International Journal of Energy and Environmental Engineering 12 (2021) 77–86. https://doi.org/10.1007/s40095-020-00359-9.

[28] L. Chen, J.B. Moreira, L.C. Meyer, J. Szanyi, Efficient and selective dual-pathway polyolefin hydro-conversion over unexpectedly bifunctional M/TiO2-anatase catalysts, Appl. Catal. B 335 (2023) 122897. https://doi.org/10.1016/j.apcatb.2023.122897.

[29] E.T. Aisien, I.C. Otuya, F.A. Aisien, Thermal and catalytic pyrolysis of waste polypropylene plastic using spent FCC catalyst, Environ. Technol. Innov. 22 (2021) 101455. https://doi.org/10.1016/j.eti.2021.101455.

[30] D. Rachmadena, M. Faizal, M. Said, Conversion of Polypropylene Plastic Waste Into Liquid Fuel with Catalytic Cracking Process Using Al2O3 as Catalyst, Int. J. Adv. Sci. Eng. Inf. Technol. 8 (2018) 694. https://doi.org/10.18517/ijaseit.8.3.2586.

[31] L.M. Terry, M.X.J. Wee, J.J. Chew, D.S. Khaerudini, N. Darsono, A. Aqsha, A. Saptoro, J. Sunarso, Catalytic co-pyrolysis of oil palm trunk and polypropylene with Ni–Mo/TiO2 and Ni/Al2O3: Oil composition and mechanism, Environ. Res. 224 (2023) 115550. https://doi.org/10.1016/j.envres.2023.115550.

[32] K. ANBARASU, P. SIVAKUMAR, CATALYTIC PYROLYSIS OF DAIRY INDUSTRIAL WASTE LDPE FILM INTO FUEL, International Journal of Chemistry Research 3 (2012) 52–55. https://ijcr.info/index.php/journal/article/view/78.

[33] S. Li, Y. Xue, Y. Lin, B. Wang, X. Gao, Synergistic Activity of the Fe_2O_3/Al_2O_3 Catalyst for Hydrogen Production through Pyrolysis-Catalytic Decomposition of Plastics, ACS Sustain. Chem. Eng. 11 (2023) 10108–10118. https://doi.org/10.1021/acssuschemeng.3c02178.

[34] R.-X. Yang, K.-H. Chuang, M.-Y. Wey, Effects of Nickel Species on Ni/Al_2O_3 Catalysts in Carbon Nanotube and Hydrogen Production by Waste Plastic Gasification: Bench- and Pilot-Scale Tests, Energy & Fuels 29 (2015) 8178–8187. https://doi.org/10.1021/acs.energyfuels.5b01866.

[35] F. Vatankhah, A. Carrillo García, J. Chaouki, Role of Bifunctional Metal-Promoted Zeolitic Catalyst in Microwave-Assisted Pyrolysis of Polyethylene to Monocyclic Aromatics, Energy & Fuels 38 (2024) 20562–20576. https://doi.org/10.1021/acs.energyfuels.4c03692.

[36] Son Dong, Taekyung Ryu, Collin Oi, Jiayang Wu, Natalie R. Altvater, Ryan Hagmann, Zahra Alikhani, Edgard A. Lebrón-Rodríguez, Jacob H. Jansen, Victor S. Cecon, Greg W. Curtzwiler, Keith L. Vorst, George W. Huber, Ive Hermans, Catalytic conversion of post-consumer recycled high-density polyethylene 2 oil over Zn-impregnated ZSM-5 catalysts, (n.d.).

[37] D. Barzallo, M.A. Reinoso, G. Miranda, T. Romero, M. Franco, P. Palmay, Bifunctional Catalytic Performance of Zn/ZSM-5 in the Aromatization of LPG and the Conversion of Pyrolytic Gases from Recycled Polypropylene, ChemEngineering 8 (2024) 108. https://doi.org/10.3390/chemengineering8060108.

[38] J. Duan, H. Wang, H. Li, L. Liu, K. Fan, X. Meng, Z. Zhang, L. Wang, F.-S. Xiao, Selective conversion of polyethylene wastes to methylated aromatics through cascade catalysis, EES Catalysis 1 (2023) 529–538. https://doi.org/10.1039/D3EY00011G.

[39] F. Vatankhah, A. Carrillo García, J. Chaouki, Role of Bifunctional Metal-Promoted Zeolitic Catalyst in Microwave-Assisted Pyrolysis of Polyethylene to Monocyclic Aromatics, Energy & Fuels 38 (2024) 20562–20576. https://doi.org/10.1021/acs.energyfuels.4c03692.

[40] J. Sun, C. Wu, Y. Zhou, J. Zhang, Z. Qu, F. Zeng, Z. Tang, W. Xing, R. Chen, Noble metal-free tandem catalysis enables efficient upcycling plastic waste into liquid fuel components, Chemical Engineering Journal 500 (2024) 156988. https://doi.org/10.1016/j.cej.2024.156988.

[41] M.A.A. Mohamad Dzol, V. Balasundram, K. Shameli, N. Ibrahim, Z.A. Manan, R. Isha, Catalytic pyrolysis of high-density polyethylene over nickel-waste chicken eggshell/HZSM-5, J. Environ. Manage. 324 (2022) 116392. https://doi.org/10.1016/j.jenvman.2022.116392.

[42] M. Marhaini, D. Fernianti, M.R. Aulia, Effective pyrolysis of LDPE plastic waste to fuel using titanium dioxide catalyst, International Journal of ADVANCED AND APPLIED SCIENCES 11 (2024) 75–82. https://doi.org/10.21833/ijaas.2024.12.009.

[43] K. Akubo, M.A. Nahil, P.T. Williams, Aromatic fuel oils produced from the pyrolysis-catalysis of polyethylene plastic with metal-impregnated zeolite catalysts, Journal of the Energy Institute 92 (2019) 195–202. https://doi.org/10.1016/j.joei.2017.10.009.

CHAPTER – 6

Influence of catalyst support and metal loading on hydrogen yield

6.1 Introduction

The incorporation of transition metals such as Ni and Zn was found to significantly enhance H_2 production during microwave-assisted LDPE cracking. Among the catalysts evaluated in Chapter 5, Ni/HY exhibited the highest H_2 yield (45 vol% H_2), followed closely by Zn/HY (43 vol% H_2). In comparison, metal oxide-supported systems showed moderate performance, with Zn/Al_2O_3, Ni/Al_2O_3, and Ni/SiO_2 producing 34, 32, and 30 vol% H_2, respectively. These results highlight the critical influence of both metal functionality and support properties on H_2 evolution.

Based on these findings, the present chapter focuses on advanced metal-supported catalytic systems, namely Ni/ZrO_2, Zn/ZrO_2, Fe/HY, and Fe/Al_2O_3, with the primary objective of maximizing H_2 generation from LDPE. Some researchers have reported that incorporation of Fe species significantly enhances alkene formation, light oil selectivity, and the yield of aromatic compounds in the liquid oil fraction [1,2]. The interaction between microwave irradiation and Fe species promotes C–H bond dissociation, thereby significantly enhancing H_2 production [3]. Chen et al. demonstrated that Ni/ZrO_2 can be effectively employed for producing H_2-rich gas from biomass [4]. This study aims to elucidate the combined effects of metal loading and support acidity on dehydrogenation reactions, secondary cracking pathways, and the suppression of heavy hydrocarbon formation in microwave-assisted pyrolysis conditions.

6.2 Materials and methods

6.2.1 Materials

LDPE granules were purchased from Reliance Industries Ltd. HY zeolite (Si/Al = 6), was obtained from SUD CHEMIE India Pvt. Ltd., and had a surface area of 750 m^2/g. Aluminum oxide (Al_2O_3) was sourced from Loba Chemie, Mumbai. Zirconium oxide was procured from Sisco Research Laboratories, Taloja. Nickel nitrate hexahydrate was obtained from Oxford Lab

Fine Chem LLP, Palghar, while zinc nitrate hexahydrate and ferric nitrate nonahydrate were purchased from Loba Chemie, Mumbai. Graphite powder (CAS No. 7782-42-5) with a particle size of 149 µm was procured from Fine Chemicals, Bangalore.

6.2.2 Catalyst Preparation

Ni, Zn, and Fe supported catalysts were prepared with varying metal loadings using a facile impregnation method based on incipient wetness technique. Briefly, required amounts of Ni $(NO_3)_2 \cdot 6H_2O$, Zn $(NO_3)_2 \cdot 6H_2O$, and Fe $(NO_3)_2 \cdot 9H_2O$ were dissolved in 10 mL of deionized water. This solution was then gradually added dropwise to various supports, under continuous stirring at 80°C. The resulting wet solids were dried in air at 373 K followed by calcination at 873 K for 6 hours.

6.2.3 Synthesis of sulphated ZrO_2 Catalyst

For the synthesis of the sulphated zirconia catalyst, ZrO_2 powder with 99% purity was used as the starting material. The ZrO_2 powder was added to a 0.5 M H_2SO_4 solution at a ratio of 50 mL of solution per 5g of solid and stirred for 3h to facilitate the sulfation process. After sulfation, the solid catalyst was separated by centrifugation at 2500 rpm for 20 min at room temperature. The supernatant liquid was then decanted, and the recovered solid was dried at 100°C for 12 h. Finally, the dried catalyst was calcined in air at 400°C for 3h to obtain the sulphated zirconia catalyst.

6.3 Results and discussion

6.3.1 Catalyst Characterization:

6.3.1.1 Scanning Electron Microscope

As represented in Figure 6.1, the Ni/ZrO_2 catalyst exhibits well-defined, closely packed crystallites with an average size of 80–100 nm, indicating uniform Ni dispersion. Zn/ZrO_2 shows irregular, agglomerated particles with a particle size of 100–130 nm, suggesting partial ZnO aggregation. The Fe/HY catalyst presents a porous morphology with fine particles (90–120 nm) uniformly distributed over the HY framework. In contrast, Fe/Al_2O_3 displays dense, spherical agglomerates with crystallite sizes of 110–150 nm, reflecting strong metal–support interaction and slight sintering upon calcination.

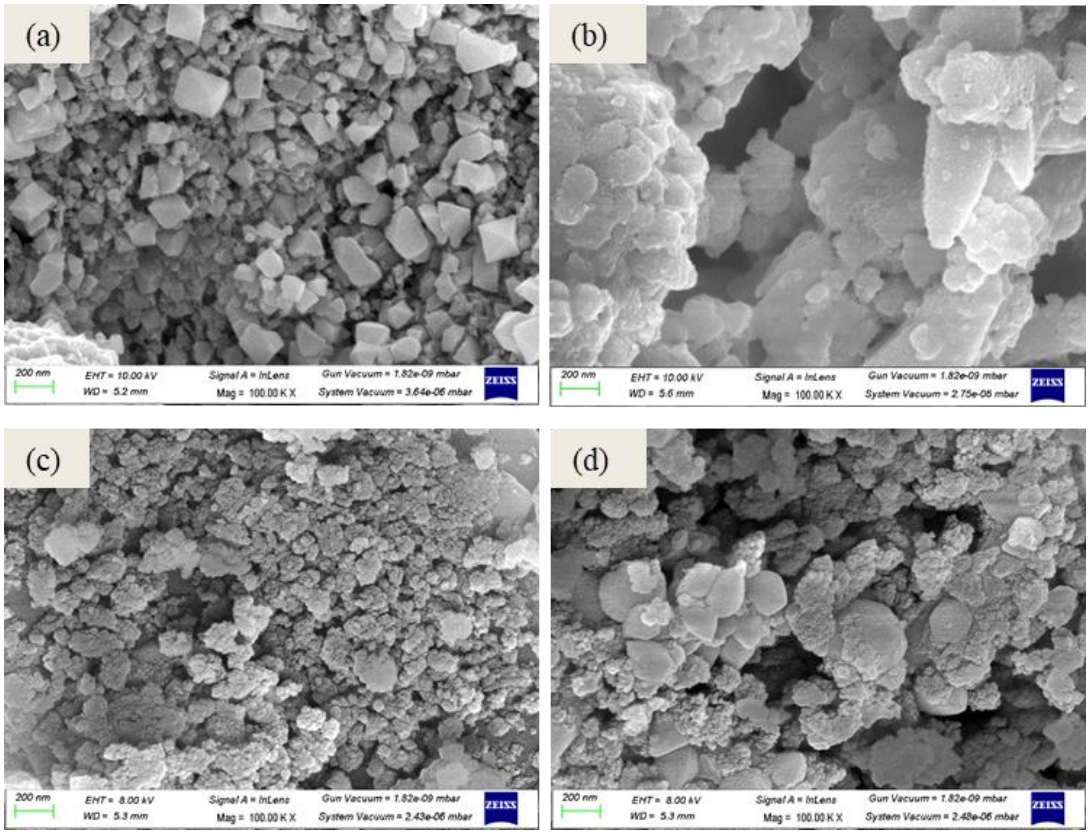

Figure 6.1: SEM images of (a) 15 wt.% Ni/ZrO_2, (b) 15 wt.% Zn/ZrO_2, (c) 15 wt.% Fe/HY, (d) 15 wt.% Fe/Al_2O_3.

6.3.1.2 Fourier transform infrared spectroscopy

Function groups present on the catalysts were identified using FTIR spectroscopy as depicted in Figure 6.2. Broad absorption bands observed in the 3400–3600 cm^{-1} region correspond to O–H stretching vibrations, indicating the presence of surface hydroxyl groups or adsorbed water [5]. Bands around 1600 cm^{-1} and 800 cm^{-1} were attributed to the bending vibration of adsorbed water and the symmetric stretching vibration of the Si/Al-O bond, respectively. The absorption bands at 1140–995 cm^{-1} resulted from the stretching vibration of the Si–O–Si (Al) bond [6,7]. The FTIR spectrum of nickel oxide (NiO) nanoparticles exhibited a prominent band near 600 cm^{-1}, which is indicative of the stretching vibration of the Ni-O bond [8]. FTIR peaks in the low wavenumber range of 424-549 cm^{-1} were assigned to the presence of loaded metals.

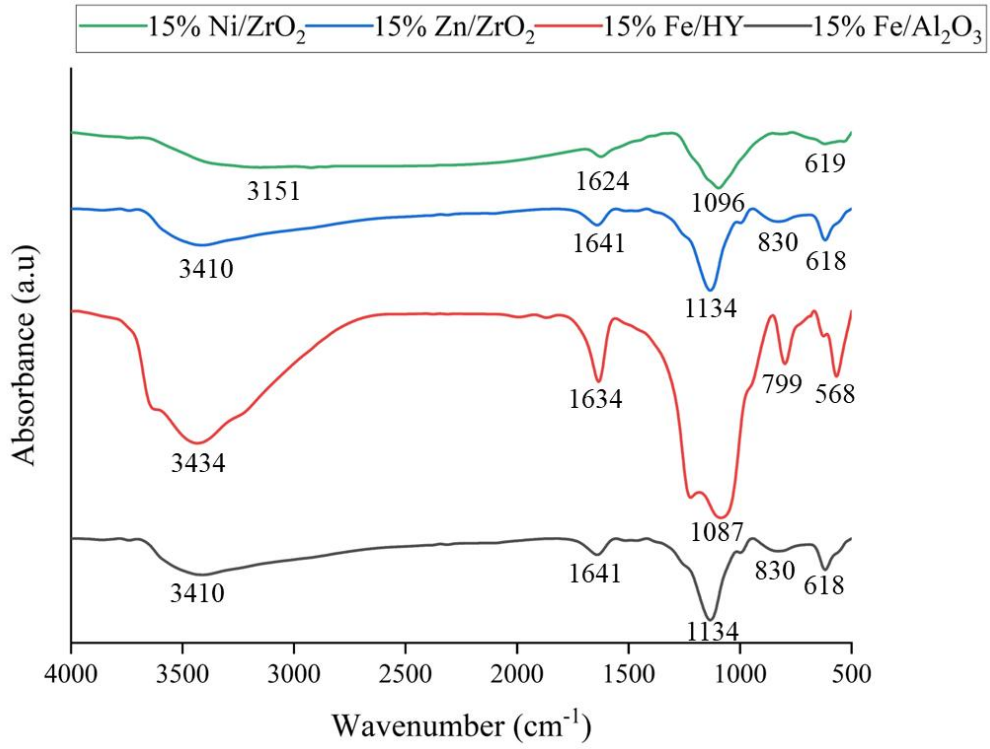

Figure 6.2: FTIR patterns of synthesized catalysts: 15 wt.% Ni/ZrO_2, 15 wt.% Zn/ZrO_2, 15 wt.% Fe/HY, 15 wt.% Fe/Al_2O_3.

6.3.1.3 Powder X-ray Diffraction

XRD patterns confirm the crystalline phases of the support and the successful incorporation of Ni, Zn, and Fe species as presented in Figure 6.3. ZrO_2 shows monoclinic peaks at 2θ = 28°, 31.5°, 50°, and 60°, corresponding to the (−111), (111), (022), and (131) crystal planes. Peaks between 2θ = 10° and 33° represent the (220), (311), (331), (511), (440), (533), (642) and (555) crystal planes of the HY catalyst [9]. Al_2O_3 exhibits peaks at 25°, 35°, 38°, and 57°, corresponding to the (012), (104), (110), and (116) crystal planes [10]. Diffraction peaks corresponding to NiO species were observed, particularly at 2θ = 43° (200) and 63° (220), while FeO exhibited characteristic peaks at 33° (104) and 36° (111) [11]. Additionally, distinct peaks appearing at 2θ = 32.0°, 34.5°, 36.0°, 47.5°, and 56.0° can be assigned to (100), (002), (101), (102), and (110) crystalline planes of ZnO, confirming their well-defined hexagonal wurtzite structure [12]. The sharp peaks indicate good crystallinity and well-dispersed metal particles with small crystallite sizes.

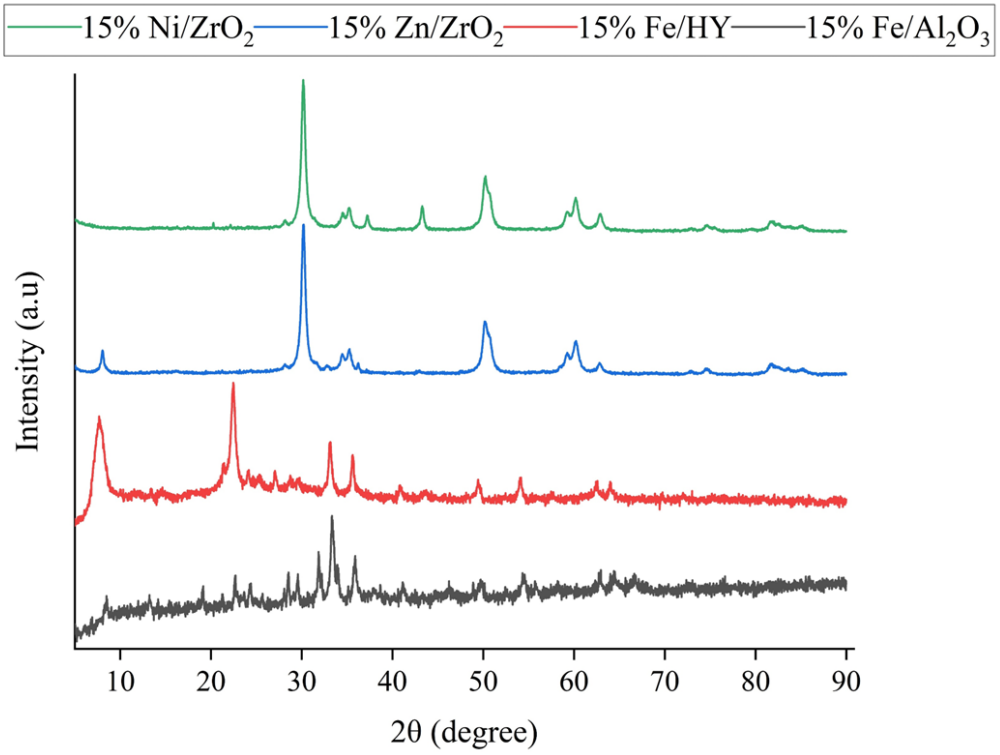

Figure 6.3: XRD patterns of synthesized catalysts: 15 wt.% Ni/ZrO_2, 15 wt.% Zn/ZrO_2, 15 wt.% Fe/HY, 15 wt.% Fe/Al_2O_3.

6.3.1.4 FTIR spectra of pyridine-adsorbed catalysts (Py-FTIR)

Pyridine-adsorbed FTIR spectra of the prepared catalysts are shown in Figure 6.4. The spectra correspond to ZrO_2, S-ZrO2, 15 wt.% $Ni/S\text{-}ZrO_2$, and 15 wt.% $Zn/S\text{-}ZrO_2$ samples in the wavenumber range of 1400-1800 cm^{-1}. The characteristic bands near 1450 cm^{-1} and 1610 cm^{-1} are assigned to pyridine coordinated to Lewis acid sites, whereas the band around 1540 cm^{-1} indicates the presence of Brønsted acid sites. The relative intensities of these bands reflect the strength and type of acid sites present on the catalyst surfaces. The acidity of the catalysts, as measured by pyridine-IR spectroscopy, is presented in Table 6.1.

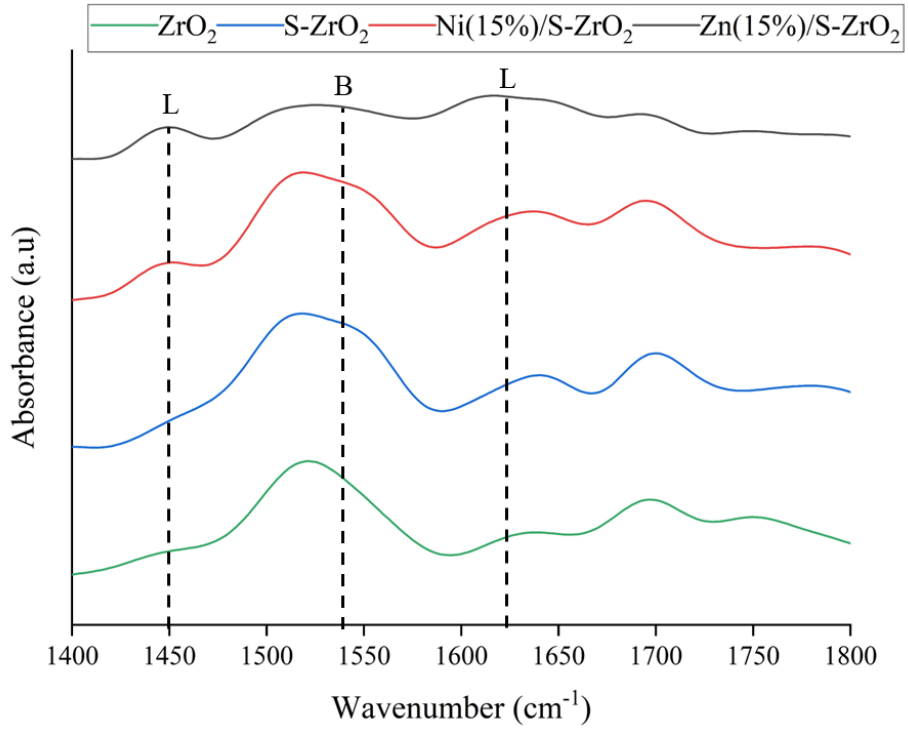

Figure 6.4: Pyridine adsorbed FT-IR spectra of ZrO_2, S-ZrO2, 15 wt.% Ni/S-ZrO_2, and 15 wt.% Zn/S-ZrO_2.

Table 6.1: Acidity of ZrO_2, S-ZrO_2, 15 wt.% Ni/S-ZrO_2, and 15 wt.% Zn/S-ZrO_2 catalysts as determined by pyridine-IR.

Catalyst	**Amount of acidic sites conc. (µmol g^{-1})**	
	Lewis Acid Sites (LAS)	Bronsted Acid Sites (BAS)
ZrO_2	0.382	7.39
S-ZrO_2	0.941	8.17
15% Ni/S-ZrO_2	1.20	7.01
15% Zn/S-ZrO_2	1.65	4.74

Table 6.2: Acidity of 15% Fe/Al_2O_3 and 15% Fe/HY as determined by pyridine-IR.

Catalyst	**Amount of acidic sites conc. (µmol g^{-1})**	
	Lewis Acid Sites (LAS)	Bronsted Acid Sites (BAS)
15% Fe/HY	17.21	0.40
15% Fe/Al_2O_3	4.37	0.93

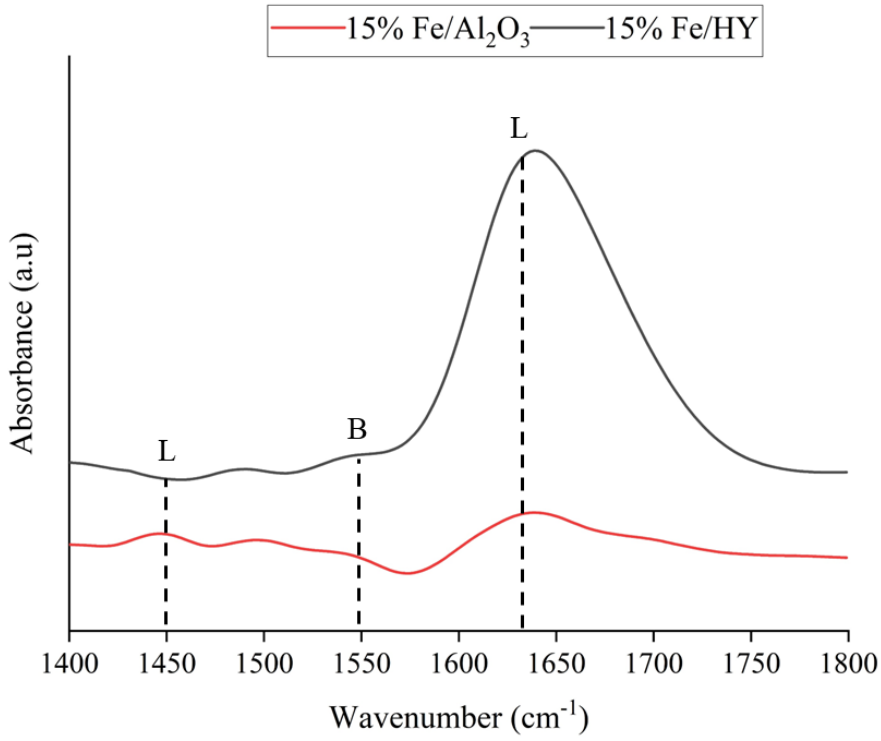

Figure 6.5: Pyridine adsorbed FT-IR spectra of 15% Fe/Al_2O_3 and 15% Fe/HY.

6.3.2 Catalytic performance

6.3.2.1 Impact of ZrO_2, Sulphated ZrO_2 (S-ZrO_2), 15% Ni/S-ZrO_2 and 15% Zn/S-ZrO_2 catalysts:

Figure 6.6 (a) illustrates the overall product yield distribution (wt.%) obtained from microwave-assisted pyrolysis of LDPE at 450°C over ZrO_2, Sulphated ZrO_2 (S-ZrO_2), 15% Ni/S-ZrO_2 and 15% Zn/S-ZrO_2 catalysts. For ZrO_2, the yields were 70% gas and 30% liquid products. Upon Ni and Zn incorporation, gas yield increased to 78% and 79% respectively. Amin et al obtained 60%, 59.8% and 59% gaseous products over ZrO_2, S-ZrO_2, and 0.5% Ni/S-ZrO_2, respectively, during conventional hydrocracking of LDPE [13]. In another study 82% gaseous products and 16% liquid products were obtained from conventional hydrocracking reaction of LDPE plastic waste over 1.19% Pt/S-ZrO_2 at 350 °C [14].

In the presence of ZrO_2, the liquid products were mainly alkanes (39.88%) and alkenes (40.77%), with minor amounts of cyclic compounds (6.47%) and aromatics (12.88%). The use of sulphated ZrO_2 altered the product distribution by reducing alkane formation (27.6%) and enhancing the formation of cyclic hydrocarbons (22.2%), while the alkene fraction (37.1%) remained relatively high. The incorporation of transition metals further influenced selectivity.

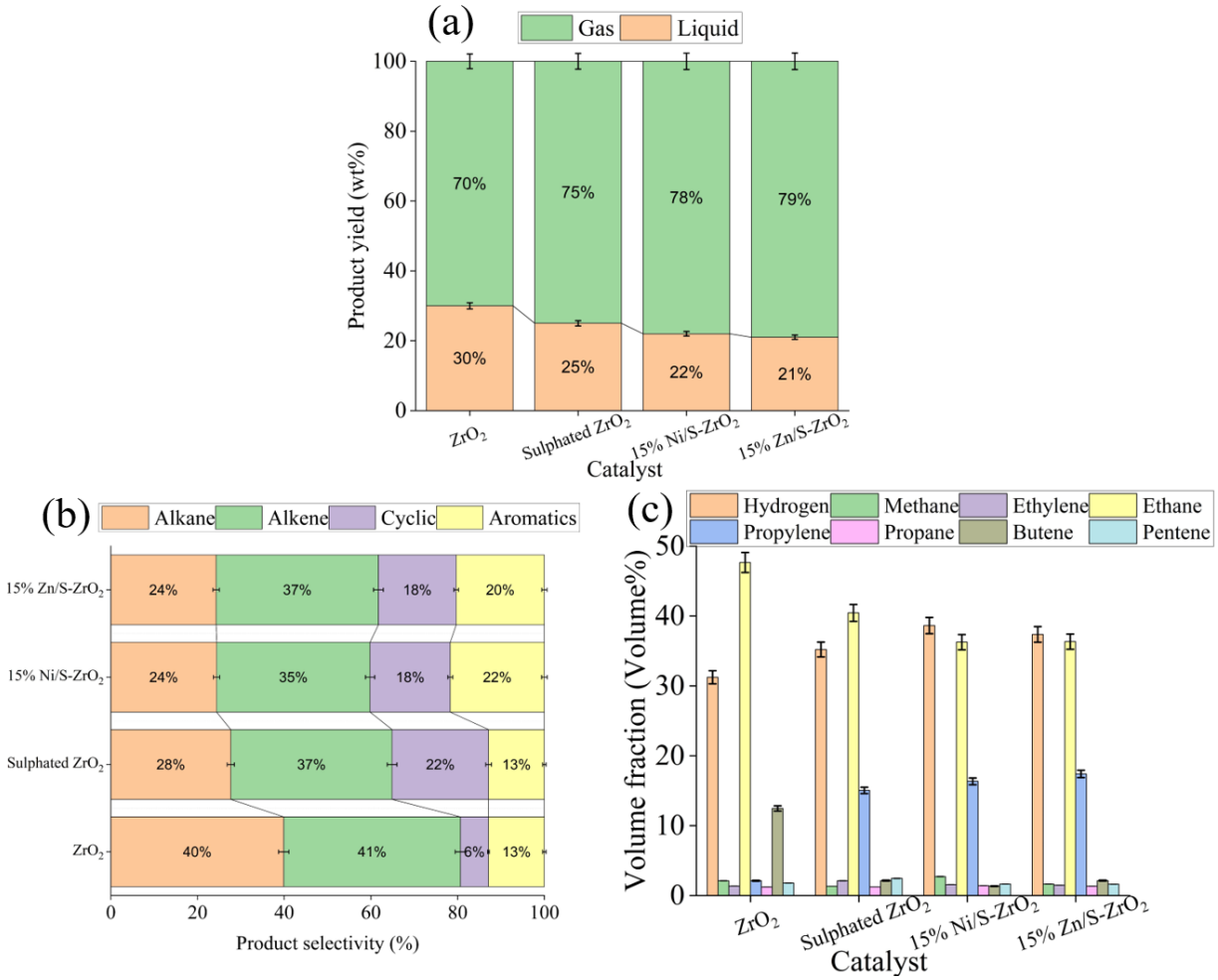

Figure 6.6: Effect of ZrO_2 on (a) Product distribution, (b) Liquid composition, and (c) Gas composition at 450°C. Catalyst to LDPE ratio was maintained at 1:10.

The 15% Ni/S-ZrO_2 catalyst favored the formation of aromatics (21.68%) and cyclic compounds (18.47%) while suppressing alkane formation (24.36%). This indicates that Ni promoted dehydrogenation and cyclization reactions, thereby enhancing aromatic yields. Similarly, the 15% Zn/S-ZrO_2 catalyst increased the fraction of alkenes (36.54%) and aromatics (19.84%), while reducing alkanes (23.72%). Thus, Zn exhibited a tendency to promote olefin and aromatic selectivity. Overall, while bare ZrO_2 mainly produced alkanes and alkenes, sulphation enhanced the formation of cyclic compounds, and Ni/Zn modification shifted selectivity toward aromatics, suggesting improved catalytic cracking and dehydrogenation activity. Amin et al obtained 22% paraffins, 17% naphthenes, 55% olefins, and 1% aromatics in the presence of 1.5% Ni/S-ZrO_2 during conventional hydrocracking of LDPE[13]. In another study Utami et al. carried out conventional hydrocracking reaction of LDPE plastic waste over 1.19% Pt/S-ZrO_2 at 250 °C and obtained 34% paraffins, 6.8%

naphthenes, 56% Olefins, and 0.7% aromatics [14]. Table 6.3 presents the carbon number distribution of liquid products obtained from LDPE cracking at 450°C using ZrO_2-based catalysts at a catalyst-to-LDPE ratio of 1:10. The gasoline-range fraction (C_6–C_{12}) was the dominant product for all catalysts and increased progressively from ZrO_2 (50.61%) to S-ZrO_2 (55.41%), 15% Ni/S-ZrO_2 (59.32%), and 15% Zn/S-ZrO_2 (63.24%). Simultaneously, the heavier fractions (C_{15}–C_{25} and >C_{25}) decreased, indicating enhanced cracking activity. These results show that sulfation and metal loading significantly improve the conversion of long-chain hydrocarbons into lighter, fuel-range liquids, with 15% Zn/S-ZrO_2 showing highest selectivity toward gasoline-range products.

Table 6.3: Carbon number distribution in Liquid in Presence of ZrO_2 at 450°C. Catalyst to LDPE ratio was 1:10.

Sr. No.	Carbon Number	Percentage	Catalyst
1	C_6-C_{12} (Gasoline)	50.61	ZrO_2
		55.41	S-ZrO_2
		59.32	15% Ni/S-ZrO_2
		63.24	15% Zn/S-ZrO_2
2	C_{12}-C_{15} (Kerosene, Jet Fuel)	22.64	ZrO_2
		22.86	S-ZrO_2
		20.34	15% Ni/S-ZrO_2
		18.54	15% Zn/S-ZrO_2
3	C_{15}-C_{25} (Gas oil, Heating oil, Diesel, Lube oil)	25.12	ZrO_2
		27.43	S-ZrO_2
		21.34	15% Ni/S-ZrO_2
		22.75	15% Zn/S-ZrO_2
4	>C_{25} (Paraffin wax, Asphalt)	7.2	ZrO_2
		4.14	S-ZrO_2
		3.21	15% Ni/S-ZrO_2
		2.64	15% Zn/S-ZrO_2

For ZrO_2, gases were dominated by ethane among saturated hydrocarbons. Moderate amounts of H_2 and butene were also present, reflecting the cracking of LDPE chains into light paraffins and olefins. Sulphated ZrO_2 reduced proportion of ethane while enhancing propylene and H_2 production, consistent with its higher acidity, which favors β-scission and secondary cracking. In case of 15% Ni/S-ZrO_2, there was a marked increase in H_2 production, accompanied by higher propylene yields, while ethane remained lower compared to bare ZrO_2. This demonstrates the dehydrogenation and aromatization roles of Ni. With 15% Zn/S-ZrO_2, the gas phase contained significant amounts of propylene, along with moderate H_2 evolution. Ethane was further reduced, while ethylene remained low, showing Zn's ability to stabilize olefinic intermediates and promote partial aromatization.

6.3.2.2 Effect of Fe loaded HY on product composition:

Gas yield increases progressively from 72% for 1% Fe/HY to 77% for 15% Fe/HY, while the liquid yield decreases correspondingly from 28% to 23% as shown in Figure 6.7 (a). This trend indicates that higher Fe loading on HY zeolite enhances catalytic cracking activity, promoting greater gas formation at the expense of liquid products.

As Fe loading increased, selectivity toward alkanes decreases from 43% (1% Fe/HY) to 32% (15% Fe/HY), while selectivity for aromatic compounds increases from 8% to 14%, respectively also reported by Tang et al.[15]. The proportion of cyclic hydrocarbons also rose from 10% to 19%. This trend indicates that higher Fe loading promotes secondary dehydrogenation and aromatization reactions, enhancing formation of unsaturated and aromatic products while reducing share of saturated hydrocarbons. During pyrolysis of LDPE in an atmospheric fixed-bed reactor at 550 ℃ Tang et al. [15] obtained 72% alkanes, 5% alkenes, and 25% aromatics in the presence of 10% Fe/HY while 61% alkane, 9% alkene, and 29% aromatics with 15% Fe/HY. Table 6.4 shows the carbon number distribution of liquid products obtained from LDPE cracking at 450 °C using Fe-loaded HY catalysts at a catalyst-to-LDPE ratio of 1:10. The gasoline-range fraction (C_6–C_{12}) increased markedly with Fe loading, rising from 62.32% for 1% Fe/HY to 89.36% for 15% Fe/HY. In contrast, kerosene-range fraction (C_{12}–C_{15}) decreased significantly, while heavier fractions (C_{15}–C_{25} and >C_{25}) were minimized, with complete suppression of >C_{25} products at 15% Fe/HY. These results indicate that higher Fe loading on HY strongly enhances cracking efficiency and promotes formation of lighter, gasoline-range hydrocarbons.

Table 6.4: Carbon number distribution in Liquid in Presence of Fe loaded HY at 450°C. Catalyst to LDPE ratio was 1:10.

Sr. No.	Carbon Number	Percentage	Catalyst
1	C_6-C_{12} (Gasoline)	62.32	1% Fe/HY
		71.32	5% Fe/HY
		85.21	10% Fe/HY
		89.36	15% Fe/HY
2	C_{12}-C_{15} (Kerosene, Jet Fuel)	30.11	1% Fe/HY
		22.42	5% Fe/HY
		10.42	10% Fe/HY
		7.44	15% Fe/HY
3	C_{15}-C_{25} (Gas oil, Heating oil, Diesel, Lube oil)	8.22	1% Fe/HY
		8.17	5% Fe/HY
		8.34	10% Fe/HY
		7.72	15% Fe/HY
4	$>C_{25}$ (Paraffin wax, Asphalt)	6.23	1% Fe/HY
		5.41	5% Fe/HY
		3.26	10% Fe/HY
		0	15% Fe/HY

H_2 and butene are predominant gaseous components across all catalysts, with the H_2 yield increasing from 32% for 1% Fe/HY to 41% for 15% Fe/HY, indicating enhanced alkane dehydrogenation activity at higher Fe loadings. This observation is supported by the decrease in alkane formation and the corresponding increase in aromatic content in the liquid products.Butene remains relatively high (30–33%), while ethane and propylene appear as secondary products in range of 10–15% and 10–12%, respectively. Minor quantities of methane, propane, ethylene, and pentene are also detected. These results suggest that increasing Fe content on HY promotes H_2 evolution and formation of unsaturated hydrocarbons through intensified cracking and dehydrogenation reactions. Tang et al. obtained 22%, 28%, and 30% H_2 with 6%, 10% and 15% Fe loading on HY at 550 ℃ during pyrolysis of LDPE in an atmospheric fixed-bed reactor [15].

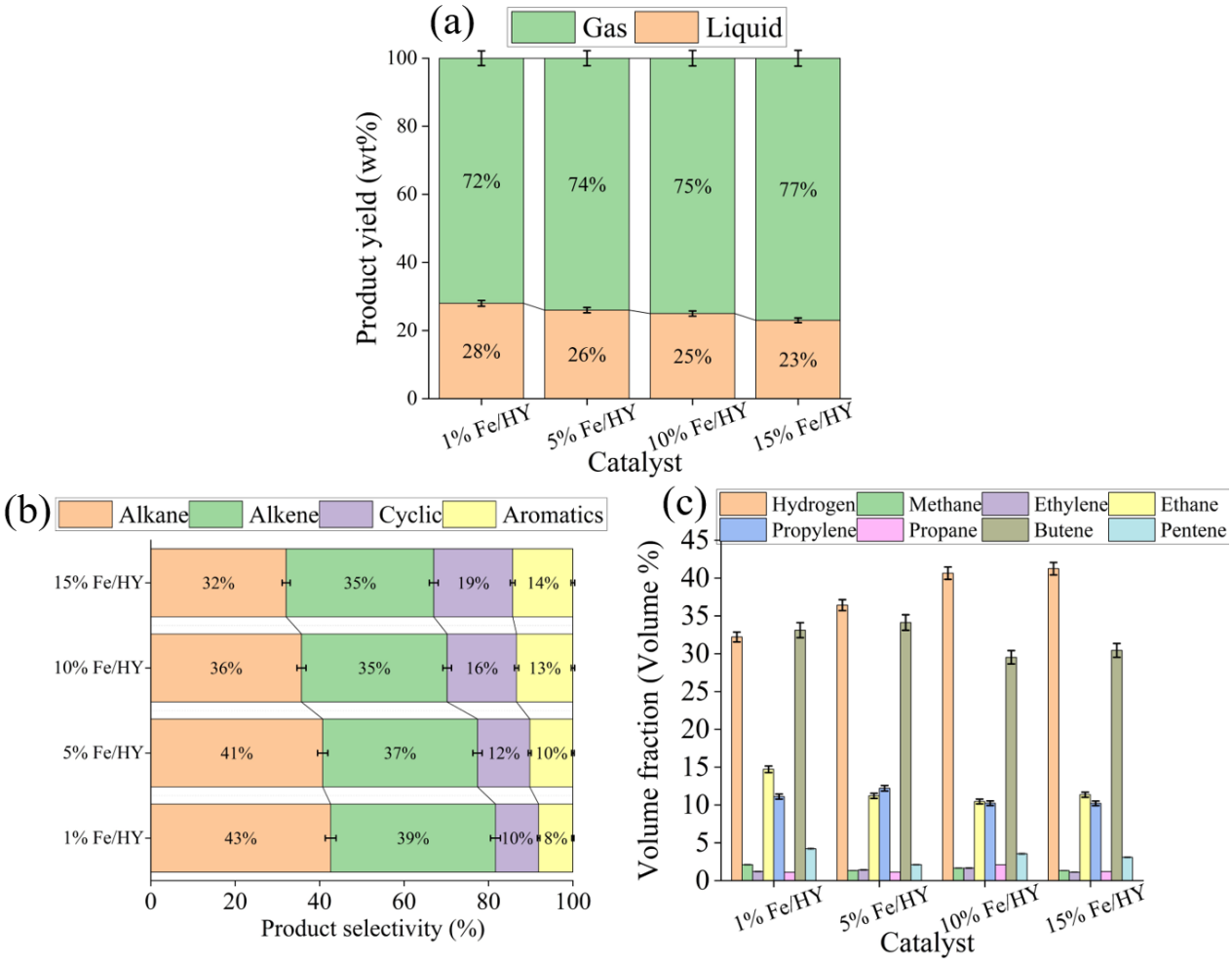

Figure 6.7: Effect of Fe/HY on (a) Product distribution, (b) Liquid composition, and (c) Gas composition at 450°C. Catalyst to LDPE ratio was maintained at 1:10.

6.3.2.4 Impact of Al_2O_3 and 15%Fe/Al_2O_3 on product composition:

Figure 6.8 (a) illustrates the overall product yield distribution (wt.%) obtained from microwave-assisted pyrolysis of LDPE at 450 °C using Al_2O_3 and 15 wt.% Fe/Al_2O_3 catalysts. For Al_2O_3, yields were 80% gas and 20% liquid products. Upon Fe incorporation, gas yield increased to 84%, while liquid fraction decreased to 16%. These results indicate that Fe addition enhances the gasification of LDPE, favoring gaseous hydrocarbon and H_2 formation at the expense of liquid products, thereby improving catalytic efficiency toward gas-phase products.

Figure 6.8 (b) presents the chemical selectivity distribution of products obtained from microwave-assisted pyrolysis of LDPE at 450 °C using Al_2O_3 and 15 wt.% Fe/Al_2O_3 catalysts. With Al_2O_3, the dominant products were alkanes (52%), followed by alkenes (30%), cyclic compounds (8%), and aromatics (9%). Upon incorporation of Fe into Al_2O_3, a significant shift

in product selectivity was observed. The alkane fraction decreased to 40%, while the alkene fraction increased to 39%. Additionally, yields of cyclic compounds (12%) and aromatics (9%) were slightly higher than those obtained with Al_2O_3 alone. These results indicate that Fe addition enhances formation of unsaturated hydrocarbons and cyclic compounds, while suppressing excessive alkane production, thereby improving catalytic performance toward more valuable hydrocarbon fractions. During conventional pyrolysis of LDPE at 425 °C over 0.5wt% Pt/Al_2O_3, 50% alkanes, 15% alkenes, and 13% aromatics were obtained, whereas 05% Rh/Al_2O_3 produced 50% alkanes, 14% alkenes and 13% aromatics [16]. Table 6.5 presents the carbon number distribution of liquid products obtained from LDPE cracking at 450 °C using Al_2O_3 and 15% Fe/Al_2O_3 catalysts at a catalyst-to-LDPE ratio of 1:10. Bare Al_2O_3 produced a higher proportion of heavier hydrocarbons (C_{15}–C_{25} and >C_{25}), whereas Fe incorporation significantly enhanced cracking, increasing gasoline-range fraction (C_6–C_{12}) from 45.25% to 71.02%. Simultaneously, heavier fractions were substantially reduced, indicating that Fe loading improves catalytic activity and promotes formation of lighter, fuel-range hydrocarbons.

Table 6.5: Carbon number distribution in Liquid in Presence of Al_2O_3 and 15% Fe/Al_2O_3 at 450°C. Catalyst to LDPE ratio was 1:10.

Sr. No.	Carbon Number	Percentage	Catalyst
1	C_6-C_{12}	45.25	Al_2O_3
	(Gasoline)	71.02	15% Fe/Al_2O_3
2	C_{12}-C_{15}	15.32	Al_2O_3
	(Kerosene, Jet Fuel)	12.04	15% Fe/Al_2O_3
3	C_{15}-C_{25}	36.34	Al_2O_3
	(Gas oil, Heating oil, Diesel, Lube oil)	17.81	15% Fe/Al_2O_3
4	>C_{25}	8.11	Al_2O_3
	(Paraffin wax, Asphalt)	5.75	15% Fe/Al_2O_3

Figure 6.8 (c) shows the gaseous product distribution (vol.%) obtained from microwave-assisted LDPE pyrolysis at 450 °C over Al_2O_3 and 15 wt.% Fe/Al_2O_3 catalysts. Using Al_2O_3, major products were ethane (32%) and H_2 (23%), followed by propane (19%), butene (17%), and smaller amounts of propylene, methane, ethylene, and pentene. When Fe was incorporated into Al_2O_3, a marked increase in H_2 production (33%) was observed, while ethane (30%) remained a dominant product.

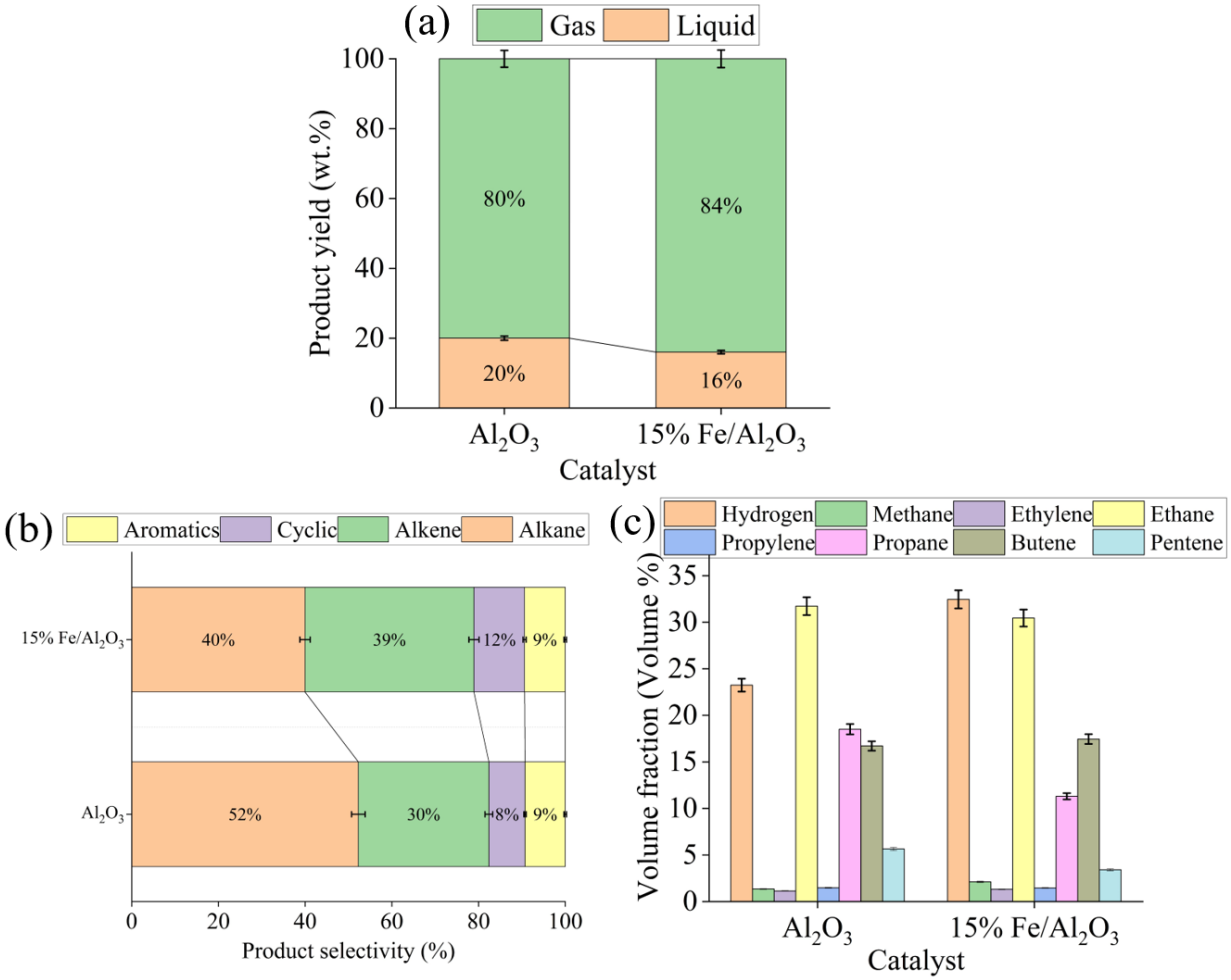

Figure 6.8: Impact of Al_2O_3 and 15%Fe/Al_2O_3 on (a) Product distribution, (b) Liquid composition, and (c) Gas composition at 450°C. Catalyst to LDPE ratio was maintained at 1:10.

Yields of propane (11%) decreased, whereas butene (17%) and methane (2%) were slightly increased. Minor olefins (ethylene, propylene, pentene) showed only slight variations. Overall, Fe addition favored H_2 generation and a more balanced hydrocarbon distribution, highlighting its role in promoting dehydrogenation and unsaturated hydrocarbon formation during LDPE pyrolysis. Insura et al. [16] obtained 1% H_2, 23% ethane, 28% propane, and 14% butane over 0.5wt% Pt/Al_2O_3 while 1% H_2, 21% ethane, 22% propane, and 13% butane were obtained over 0.5% Rh/Al_2O_3 during pyrolysis of LDPE at 425 °C. In the present study, a significantly higher H2 concentration was achieved, which may be attributed to the higher Fe loading that promotes dehydrogenation reactions under microwave-assisted catalytic conditions.

6.4 Kinetic, Thermodynamic, and Computational Studies

6.4.1 Kinetic Analysis of LDPE Cracking

Kinetics of LDPE cracking under microwave-assisted catalytic conditions was investigated to establish the reaction order and evaluate the rate parameters. The degradation behaviour of LDPE in the presence of a 15 wt.% Fe/HY catalyst was analyzed at two reaction temperatures, namely 450 °C and 550 °C. The experimental data were fitted to a first-order kinetic model, which is commonly applied for polymer degradation reactions.

The first-order kinetic expression used is:

$$\ln(1 - X) = -kt$$

where X is the conversion of LDPE, k is the rate constant (s^{-1}), and t is reaction time (s).

- LDPE cracking in presence of 15wt.% Fe/HY at 450 ℃.

Run	Time (Sec)	Temperature (℃)	LDPE initial mass (M_0)	LDPE mass at time t (M_t)
1	0	25	10	10
2	100	250	10	10
3	300	450	10	7.8
4	420	450	10	4.3
5	540	450	10	1.9
6	660	450	10	0.09

Time (Sec)	Conversion, X	ln (1-X)
300	0.22	-0.248
420	0.57	-0.844
540	0.82	-1.715

Conversion, X = $\frac{Mo-Mt}{Mo-Mr}$

Where:
M_0= initial mass (10 g)
M_t= mass at time t
M_r= final mass (residue ~0.09 g at 660 s)

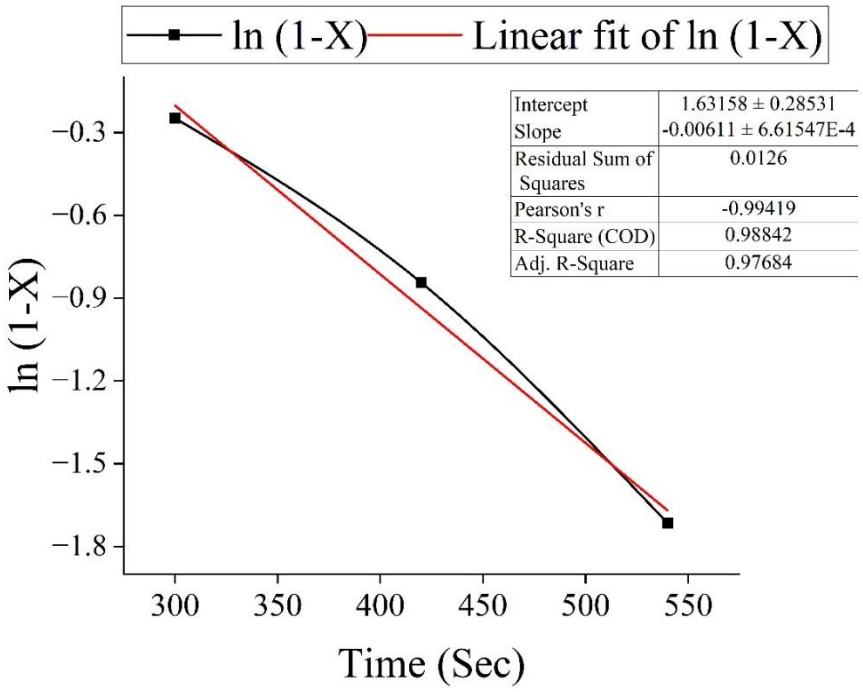

Figure 6.9: First-order kinetic plots of ln(1−X) versus reaction time for microwave-assisted LDPE cracking over 15 wt.% Fe/HY catalyst at 450 °C.

At 450 °C, the linear fit of ln(1−X) versus time yielded a slope of −0.0061, corresponding to a rate constant of 6.1 × 10^{-3} s^{-1} as depicted in Figure 6.9. The half-life of the reaction, calculated using the relation $t_{1/2} = \ln 2/k$, was 113.63 s.

- LDPE cracking in presence of 15wt.% Fe/HY at 550 °C.

Run	Time (Sec)	Temperature (°C)	LDPE initial mass (M_0)	LDPE mass at time t (M_t)
1	0	25	10	10
2	100	280	10	10
3	300	550	10	7.5
4	420	550	10	3.9
5	540	550	10	1.5
6	600	550	10	0.08

Time (Sec)	Conversion, X	ln (1-X)
300	0.25	-0.287
420	0.61	-0.941
540	0.85	-1.897

Conversion, $X = \frac{Mo-Mt}{Mo-Mr}$

Where:

M_0= initial mass (10 g)

M_t= mass at time *t*

M_r= final mass (residue ~0.08 g at 600 s)

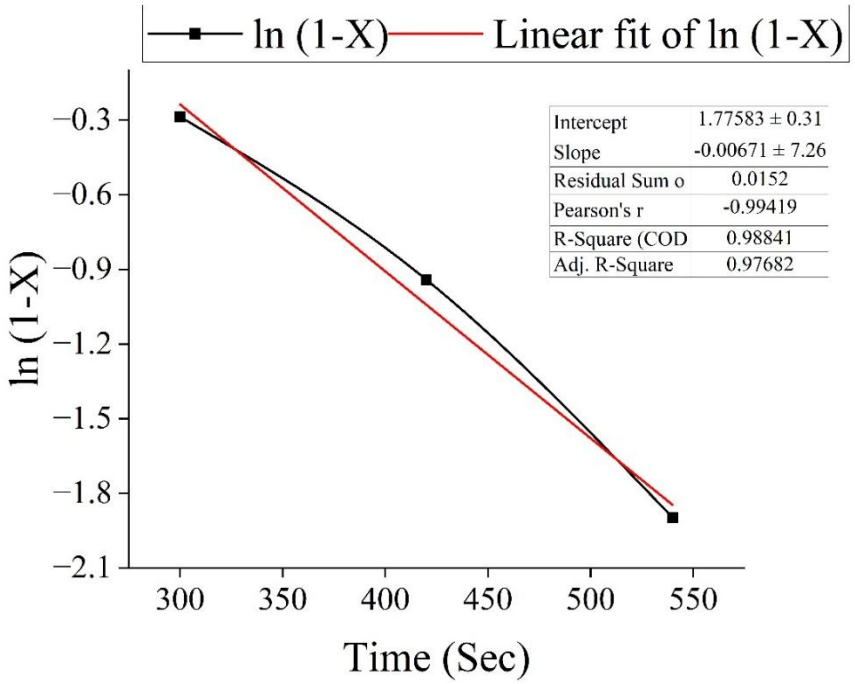

Figure 6.10: First-order kinetic plots of ln(1−X) versus reaction time for microwave-assisted LDPE cracking over 15 wt.% Fe/HY catalyst at 550 °C.

As shown in Figure 6.10 at 550 °C, the slope increased to −0.0067, resulting in a higher rate constant of 6.7×10^{-3} s^{-1} and a reduced half-life of 103.45 s, indicating accelerated LDPE cracking at the elevated temperature.

These results confirm that LDPE degradation in the presence of Fe/HY catalyst follows first-order kinetics and the increase in the rate constant with temperature reflects enhanced chain scission and catalytic activity under microwave irradiation. The first-order kinetic model employed in the present study provides a simplified representation of the overall LDPE depolymerization process and facilitates the comparison of catalyst performance under identical reaction conditions. However, the thermal degradation of LDPE is widely recognized as a multistep process involving random chain scission, β-scission, hydrogen transfer, oligomer cracking, cyclization, aromatization, and coke formation. Consequently, advanced kinetic approaches such as the distributed activation energy models (DAEM), parallel reaction models, or mechanistic kinetic models have been proposed to describe these complex reaction pathways more accurately. While these models provide deeper mechanistic insight, they require

extensive time-resolved experimental or thermogravimetric data that were beyond the scope of the present study. Therefore, the first-order model was considered appropriate for comparing the relative catalytic performance of the investigated catalysts under identical microwave-assisted reaction conditions.

Activation Energy and Arrhenius Parameters

Temperature dependence of reaction rate constants was evaluated using Arrhenius equation:

$$k = Ae^{-Ea/RT}$$

where A is pre-exponential factor, E_a is activation energy, R is universal gas constant, and T is absolute temperature.

From two rate constants k_1 and k_2 , activation energy can be determined as:

$$E_a = \frac{R \ln\left(\frac{k_2}{k_1}\right)}{\left(\frac{1}{T_1} - \frac{1}{T_2}\right)}$$

Here
$k_1 = 0.0061\ Sec^{-1}$
$T_1 = 450\ ℃ = 450+273 = 723\ K$
$k_2 = 0.0067\ Sec^{-1}$
$T_2 = 550\ ℃ = 550+273 = 823\ K$
$R = 8.314\ J\ mol^{-1}K^{-1}$

$$E_a = \frac{8.314 \ln\left(\frac{0.0067}{0.0061}\right)}{\left(\frac{1}{723} - \frac{1}{823}\right)}$$

$$E_a = \frac{8.314\ x\ 0.0940}{0.000168}$$

$$E_a = 4652\ J/mol$$

$$E_a = 4.65\ KJ/mol$$

Relatively low activation energy obtained indicates that Fe/HY catalyst effectively lowers energy barrier for polymer chain scission, facilitating rapid degradation under microwave heating. This behavior is attributed to the combined effect of acidic sites of HY zeolite and redox-active Fe species, which promote β-scission, dehydrogenation, and olefin formation.

Arrhenius pre-exponential factor (A)

Arrhenius equation:

$$k = Ae^{-Ea/RT}$$

Taking natural log:

$$\ln k = \ln A - \frac{E_a}{RT}$$

So,

$$\ln A = \ln K + \frac{E_a}{RT}$$

We already found:

$E_a = 4652\, J/mol$

$R = 8.314\, J/mol \cdot K$

Use $k_1 = 0.0061\, s^{-1}$ at $T_1 = 723\, K$.

$$\ln A = \ln(0.0061) + \frac{4652}{8.314\ x\ 723}$$

$$\ln A = -5.103 + 0.774 = -4.329$$

$$A = e^{-4.329} = 0.0132\ Sec^{-1}$$

As depicted in Figure 6.11 Arrhenius plot (ln k vs. 1/T) was used to determine activation energy and pre-exponential factor for LDPE cracking in presence of Fe/HY catalyst.

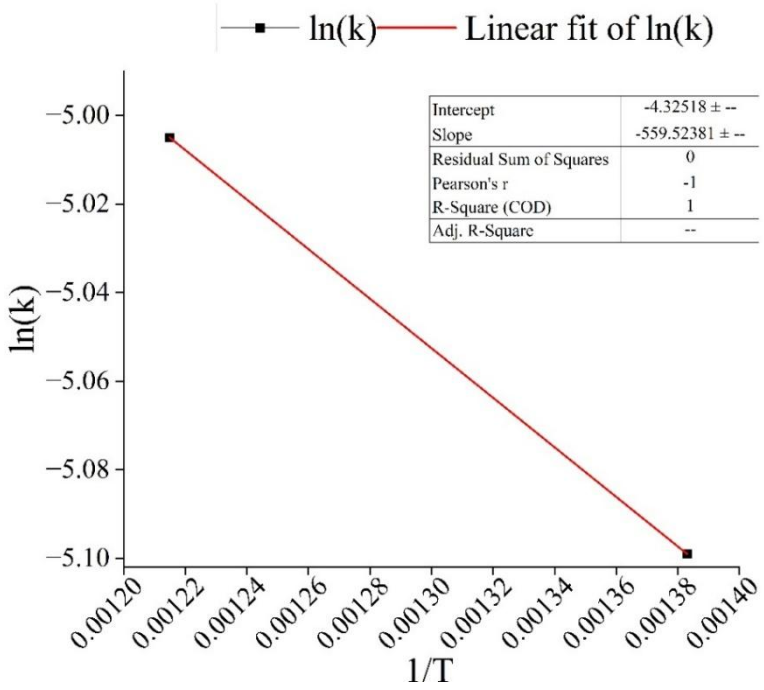

Figure 6.11: Arrhenius plot (ln k vs. 1/T) for LDPE cracking in presence of Fe/HY catalyst.

Here, Slope = - $\frac{E_a}{R}$

E_a = slope x R = 559.523 x 8.341 = 4652 J/mol

Intercept = ln A

A= $e^{-4.325}$ = 0.0132 Sec^{-1}

6.4.2 Adsorption Energy Calculations

To gain molecular-level insight into catalyst–reactant interactions, adsorption energy calculations were performed. Ethylene was selected as a representative pyrolysis intermediate to evaluate the adsorption strength on different Ni-supported catalysts. Calculated adsorption energies for ethylene on different Ni-supported catalysts are summarized in Table 6.6.

Table 6.6: Adsorption energies of ethylene on Ni-supported catalysts.

Catalyst	E (catalyst + C_2H_4)	E (catalyst)	E (C_2H_4)	Eads (Hartree)	Eads (kJ/mol)	Eads (eV)
15% Ni/HY	−5689.11990 1203901	−5610.6944 28338458	−78.36775 7479084	−0.0577	−151.49	−1.57
15% Ni/TiO_2	−5659.15437 3991486	−5582.4585 53244366	−78.36775 7479084	−0.0180	−47.26	−0.49
15% Ni/Al_2O_3	−3384.26065 6027010	−3305.8637 33091086	−78.36775 7479084	−0.0291	−76.40	−0.79
15% Ni/SiO_2	−2984.44206 8269590	−2906.0496 41157926	−78.36775 7479084	−0.0246	−64.59	−0.67

Among investigated systems, Ni/HY exhibited most negative adsorption energy (−151.5 kJ mol^{-1} or −1.57 eV), indicating strongest interaction between ethylene and catalytic surface. Adsorption strength followed the order:

$$Ni/HY > Ni/Al_2O_3 > Ni/SiO_2 > Ni/TiO_2$$

Superior adsorption behavior of Ni/HY is attributed to high acidity and microporous framework of HY zeolite, which enhances metal dispersion and strengthens metal–adsorbate interactions. Strong ethylene adsorption facilitates secondary reactions such as dehydrogenation, oligomerization, and aromatization, explaining the experimentally observed high H_2 yield and aromatic selectivity.

6.4.3 Thermodynamic Equilibrium Analysis

Thermodynamic feasibility of LDPE cracking was evaluated through Gibbs free energy minimization using the Peng–Robinson property package. Equilibrium analysis yielded an initial Gibbs free energy of 0.0283173 kW and a final Gibbs free energy of 0.0282158 kW, resulting in a negative Gibbs energy change:

$$\Delta G^{\cdot} = -0.0001015 \text{ kJ } S^{-1}$$

The negative value of $\Delta \dot{G}$ confirms that the reaction pathway leading to the computed product distribution is thermodynamically favorable under the investigated temperature, pressure, and feed conditions. This supports the experimental observation of spontaneous LDPE cracking and H_2 formation under microwave-assisted catalytic conditions. Table 6.7 presents a comparison between the experimentally obtained gaseous product distribution from LDPE pyrolysis carried out without a catalyst and in the presence of Ni/S-ZrO_2 catalyst, and the corresponding equilibrium product composition predicted by simulation. Table 6.7 highlights deviations between the experimental and equilibrium results, demonstrating the strong influence of microwave heating and catalyst acidity on promoting non-equilibrium dehydrogenation pathways, particularly enhanced H_2 formation and suppressed methane production.

Combined kinetic, computational, and thermodynamic analyses provide strong mechanistic validation for the experimental findings of this thesis. First-order kinetic behavior, reduced activation energy, strong ethylene adsorption on Ni/HY, and the negative Gibbs free energy collectively demonstrate that microwave-assisted catalytic LDPE cracking is both kinetically accelerated and thermodynamically feasible, with catalyst acidity and metal–support interactions playing a dominant role.

Table 6.7: Comparison of experimental gaseous product distribution from microwave-assisted LDPE pyrolysis (with and without Ni/S-ZrO_2 catalyst) and equilibrium composition obtained from simulation.

Sr. No.	Compound Name	Experimental Result without catalyst (Vol%)	Experimental Result with Ni/S-ZrO_2 (Vol%)	Simulation Equilibrium Result (Vol%)	Interpretation
1.	Hydrogen	25	38.64	27.37	Catalysts + microwaves promote strong dehydrogenation → far above equilibrium
2.	Methane	22.73	2.71	12.75	DWSIM predicts moderate CH_4 because methane is thermodynamically stable in pyrolysis conditions.
3.	Ethylene	16.13	1.56	14.16	Catalyst promotes hydrogenation/cracking, reducing ethylene experimentally.
4.	Ethane	9.6	36.2	7.36	Catalyst strongly increases C_2H_6 (due to hydrogenation of ethylene). Equilibrium predicts low ethane because C_2H_6 tends to convert to ethylene + H_2 at high T.
5.	Propylene	9.63	16.34	8.01	Propylene is stable both kinetically (experiment) and thermodynamically (equilibrium).
6.	Propane	10.92	1.42	4.56	Propane cracks/dehydrogenates easily → not stable under pyrolysis.

7.	Butene	2.69	1.35	4.93	DWSIM predicts more because equilibrium does not consider catalytic secondary cracking.
8.	Pentene	1.48	1.64	3.05	Pentene is unstable and quickly cracks into smaller olefins.

6.4.4 Energy Consumption Analysis

The electrical energy consumption of the microwave-assisted LDPE depolymerization process was estimated using the nominal microwave power and reaction time. For a reaction time of 15 min, the estimated electrical energy input ranged from 0.432 MJ (480 W) to 0.720 MJ (800 W). Although these values represent the maximum theoretical electrical energy supplied to the reactor, the actual energy absorbed by the reaction mixture may be lower due to power cycling and system losses. Luo et al. [17] reported that conventional catalytic pyrolysis requires 80–200 $MJkg^{-1}$ of energy, whereas non-catalytic pyrolysis consumes more than 220 $MJkg^{-1}$. Zhou et al. [18] demonstrated that microwave-assisted pyrolysis over ZSM-5 achieved 73.5% C_5–C_{12} hydrocarbons with an overall energy efficiency of 89.6%, offering superior product selectivity and significantly higher efficiency than conventional pyrolysis. Compared with conventional thermal pyrolysis, microwave heating provides direct volumetric heating of microwave-absorbing materials, resulting in rapid temperature rise, shorter reaction times, and reduced thermal losses associated with heating the reactor walls. Consequently, microwave-assisted pyrolysis has been widely recognized as an energy-efficient alternative for plastic waste valorization, particularly for catalytic hydrogen production.

Microwave Power (W)	**Reaction Time (min)**	**Energy Consumption (kWh)**	**Energy Consumption (MJ)**
480	15	0.120	0.432
640	15	0.160	0.576
800	15	0.200	0.720

6.4.5 Industrial Relevance and Scale-Up Considerations

The results of this study demonstrate that microwave-assisted catalytic depolymerization is a promising technology for the sustainable conversion of LDPE waste into hydrogen-rich gas and value-added hydrocarbons. While the present work was conducted at the laboratory scale, successful industrial implementation will require advances in reactor design, continuous operation, microwave energy management, and efficient product recovery systems.

Continuous microwave reactors could overcome the throughput limitations associated with batch processing and improve process efficiency for large-scale plastic waste valorisation. However, challenges related to microwave field distribution, penetration depth, reactor design, and continuous feeding of plastic waste require further investigation.

Catalyst stability is another critical factor influencing industrial feasibility. The regeneration studies performed for the HY, HZSM-5, and Hβ catalysts demonstrated satisfactory catalytic stability over repeated cycles, indicating their potential for reuse. Future work should extend regeneration studies to metal-supported catalysts and investigate catalyst deactivation mechanisms using advanced characterization techniques.

In addition, a comprehensive techno-economic analysis considering capital investment, operating costs, catalyst lifetime, energy consumption, hydrogen production cost, and process economics should be carried out to evaluate the commercial viability of microwave-assisted catalytic LDPE depolymerization.

6.5 Conclusion

Microwave-assisted pyrolysis (MAP) of LDPE was successfully investigated using various oxide- and metal-supported catalysts to evaluate their effects on product yield, selectivity, and H_2 production. In all cases, MAP resulted in high gas yields compared to liquid products, demonstrating effectiveness of microwave heating in promoting rapid polymer cracking and secondary reactions. ZrO_2-based catalysts showed improved performance upon sulphation and metal incorporation. Sulphated ZrO_2 enhanced cracking due to increased acidity, while Ni- and Zn-loaded systems further increased gas yield and H_2 formation, with 15% Zn/S-ZrO_2 exhibiting superior performance. These catalysts also promoted a shift in liquid product selectivity from alkanes toward alkenes, cyclic compounds, and aromatics, indicating enhanced dehydrogenation and aromatization reactions. Fe-loaded HY catalysts exhibited a strong dependence on Fe loading, with increasing metal content leading to higher gas yields and H_2

concentrations. At higher Fe loadings, a significant reduction in heavy liquid fractions was observed, confirming the synergistic effect of Fe sites and zeolitic acidity in enhancing β-scission and hydrogen transfer reactions. Similarly, Fe/Al_2O_3 outperformed bare Al_2O_3 by increasing gas and H_2 yields while suppressing heavy hydrocarbon formation.

6.6 References

[1] Z. Chen, B.J. Erwin, L. Che, Recycling waste polyethylene into fuels over Fe/USY catalyst: Evaluation on the catalytic activities of varied iron states, Fuel 363 (2024) 131007. https://doi.org/10.1016/j.fuel.2024.131007.

[2] Z. Chen, L. Xu, X. Zhang, Upgrading of polyethylene to hydrocarbon fuels over the Fe-modified Pt/Al2O3 catalysts at a mild condition without external H2, Chemical Engineering Journal 446 (2022) 136213. https://doi.org/10.1016/j.cej.2022.136213.

[3] L. Yao, X. Liu, Z. Song, Z. Wang, Y. Pang, S. Li, C. Huang, Microwave-assisted Fe-based catalytic conversion of plastic waste to hydrogen: ReaxFF-MD and DFT insights, Chemical Engineering Journal 520 (2025) 166127. https://doi.org/10.1016/j.cej.2025.166127.

[4] G. Chen, J. Yao, J. Liu, B. Yan, R. Shan, Biomass to hydrogen-rich syngas via catalytic steam reforming of bio-oil, Renew. Energy 91 (2016) 315–322. https://doi.org/10.1016/j.renene.2016.01.073.

[5] P.L. editors Weitkamp J, Catalysis and zeolites: fundamentals and applications, New York: Springer Berlin Heidelberg (1999) 546.

[6] Handke M, Mozgawa W, Vibrational spectroscopy of theamorphous silicates, Vib Spectrosc 5 (1993) 75–84.

[7] Anggoro DD, Buchori L, Silaen GC, Utami RN, Preparation,characterization, and activation of Co-Mo/Y zeolite catalyst forcoal tar conversion to liquid fuel, Bull Chem React Eng Catal 12 (2017) 219–226.

[8] J. Li, R. Yan, B. Xiao, D.T. Liang, D.H. Lee, Preparation of Nano-NiO Particles and Evaluation of Their Catalytic Activity in Pyrolyzing Biomass Components, Energy & Fuels 22 (2008) 16–23. https://doi.org/10.1021/ef700283j.

[9] F. Chen, D. Zhang, L. Shi, Y. Wang, G. Xu, Optimized Pore Structures of Hierarchical HY Zeolites for Highly Selective Production of Methyl Methoxyacetate, Catalysts 9 (2019) 865. https://doi.org/10.3390/catal9100865.

[10] A.A. Mohammed, Z.T. Khodair, A.A. Khadom, Preparation and investigation of the structural properties of α-Al2O3 nanoparticles using the sol-gel method, Chemical Data Collections 29 (2020) 100531. https://doi.org/10.1016/j.cdc.2020.100531.

[11] A. Martínez, M.A. Arribas, P. Concepción, S. Moussa, New bifunctional Ni–H-Beta catalysts for the heterogeneous oligomerization of ethylene, Appl. Catal. A Gen. 467 (2013) 509–518. https://doi.org/10.1016/j.apcata.2013.08.021.

[12] Z. Ahmad, F. UllahKha, S. Mahmood, T. Mahmood, A. Shamim, Different Approaches for the Synthesis of Zinc Oxide Nanoparticles, Open Journal of Chemistry 1 (2018) 19–25. https://doi.org/10.30538/psrp-ojc2018.0003.

[13] A. Kurnia Amin, K. Wijaya, W. Trisunaryanti, The Catalytic Performance of ZrO2-SO4 and Ni/ZrO2-SO4 Prepared from Commercial ZrO2 in Hydrocracking of LDPE Plastic Waste into Liquid Fuels, Oriental Journal of Chemistry 34 (2018) 3070–3078. https://doi.org/10.13005/ojc/340650.

[14] M. Utami, K. Wijaya, W. Trisunaryanti, Pt-promoted sulfated zirconia as catalyst for hydrocracking of LDPE plastic waste into liquid fuels, Mater. Chem. Phys. 213 (2018) 548–555. https://doi.org/10.1016/j.matchemphys.2018.03.055.

[15] H. Tang, D. Chen, M.H. Tahir, K. Qian, Y. Hu, L. Yin, Y. Feng, Catalytic pyrolysis of low-density polyethylene to produce sustainable aviation fuel fractions: Improving isomerized alkane selectivity via magnetic metal-modified HY zeolites, Energy 330 (2025) 136908. https://doi.org/10.1016/j.energy.2025.136908.

[16] N. Insura, J.A. Onwudili, P.T. Williams, Catalytic Pyrolysis of Low-Density Polyethylene over Alumina-Supported Noble Metal Catalysts, Energy & Fuels 24 (2010) 4231–4240. https://doi.org/10.1021/ef100227f.

[17] J. Luo, G. Gong, R. Ma, S. Sun, C. Cui, H. Cui, J. Sun, N. Ma, Study on high-value products of waste plastics from microwave catalytic pyrolysis: Construction and performance evaluation of advanced microwave absorption-catalytic bifunctional catalysts, Fuel 346 (2023) 128296. https://doi.org/10.1016/j.fuel.2023.128296.

[18] N. Zhou, L. Dai, Y. Lv, H. Li, W. Deng, F. Guo, P. Chen, H. Lei, R. Ruan, Catalytic pyrolysis of plastic wastes in a continuous microwave assisted pyrolysis system for fuel production, Chemical Engineering Journal 418 (2021) 129412. https://doi.org/10.1016/j.cej.2021.129412.

CHAPTER – 7
Conclusion and scope for future work

7.1 Conclusion

This research conclusively demonstrates that microwave-assisted catalytic cracking of LDPE is an effective and energy-efficient strategy for converting plastic waste into H_2-rich gases and high-value hydrocarbon products. Through a systematic progression from zeolites to spent industrial catalysts and finally to metal-supported systems, this work establishes a comprehensive framework for understanding and optimizing catalyst performance under microwave irradiation.

Initial investigations using zeolites (HY, HZSM-5, and Hβ) revealed that catalyst acidity and pore architecture play a decisive role in product selectivity. HY favored H_2 and aromatic formation through enhanced dehydrogenation and cyclization reactions, HZSM-5 selectively promoted ethylene production, and Hβ yielded propylene-rich gaseous streams due to its strong acidity and larger pore size. These results confirmed that microwave-assisted pyrolysis enables rapid cracking and efficient utilization of catalyst active sites at relatively lower temperatures.

Subsequent studies employing spent FCC catalyst and TiO_2 further highlighted the importance of acid strength and density. Spent FCC catalyst, with moderate acidity, predominantly generated olefin-rich gases, particularly propylene, while suppressing excessive aromatization. In contrast, TiO_2, with weaker acidity, favored formation of paraffinic and olefinic gasoline-range hydrocarbons with minimal aromatic content. Reuse of spent FCC catalyst also demonstrated feasibility of integrating industrial waste catalysts into sustainable plastic recycling processes.

Incorporation of transition metals (Ni, Zn, and Fe) onto acidic and non-acidic supports led to a substantial enhancement in H_2 production, confirming critical role of metal-catalyzed dehydrogenation under microwave heating. Among all catalysts evaluated, Ni/HY and Zn/HY exhibited highest H_2 yields, reaching up to 45% of gaseous products, while also producing aromatics and gasoline-range hydrocarbons in liquid fraction. Fe/HY showed exceptional performance, yielding 41% H_2 and nearly complete conversion to gasoline-range hydrocarbons, underscoring its strong cracking and olefin-forming capability. Moderate H_2 yields obtained with Al_2O_3, SiO_2, and TiO_2 supported catalysts further reinforced importance

of support acidity and metal–support interactions. Additionally, sulphated zirconia-supported catalysts demonstrated that strong Brønsted acidity can effectively promote both H_2 generation and aromatic hydrocarbon formation.

In summary, this thesis establishes that synergistic combination of microwave heating, catalyst acidity, and metal functionality is key to maximizing H_2 yield and tailoring hydrocarbon selectivity during LDPE cracking. Insights derived from this work significantly advance fundamental understanding of microwave-driven catalytic plastic pyrolysis and provide a strong scientific basis for developing scalable, energy-efficient technologies for H_2 production and circular plastic waste management.

7.2 Scope for Future Work

Although present research has successfully demonstrated effectiveness of microwave-assisted catalytic cracking of LDPE for H_2 and value-added hydrocarbon production, several avenues remain open for further investigation to enhance process efficiency, mechanistic understanding, and industrial applicability.

1. Continuous microwave reactors: Future research should focus on the design and optimization of continuous microwave-assisted reactors capable of processing larger quantities of plastic waste while ensuring uniform microwave distribution, efficient heat transfer, and continuous product recovery.

2. Co-pyrolysis with biomass: Co-processing LDPE with lignocellulosic biomass or other renewable feedstocks may improve hydrogen production and hydrocarbon selectivity through synergistic interactions between hydrogen-rich plastics and oxygenated biomass-derived intermediates.

3. AI-assisted process optimization: Artificial intelligence and machine learning techniques can be employed to optimize operating parameters such as microwave power, catalyst loading, reaction temperature, and residence time. Data-driven models may also facilitate catalyst design and predictive optimization of product yields.

4. Life cycle assessment (LCA): A comprehensive life cycle assessment should be performed to evaluate the environmental impacts of microwave-assisted catalytic depolymerization, including greenhouse gas emissions, energy consumption, and resource utilization, and to compare the process with conventional recycling and thermal pyrolysis technologies.

5. Treatment of mixed plastic waste: Since municipal plastic waste consists of mixtures of polyethylene, polypropylene, polystyrene, PET, and multilayer plastics, future studies should investigate the applicability of microwave-assisted catalytic depolymerization to mixed plastic waste streams under realistic operating conditions.

List of References

1. Hannah Ritchie, Veronika Samborska, Max Roser, Plastic Pollution, Our World in Data (2023).
2. K. Ding, S. Liu, Y. Huang, S. Liu, N. Zhou, P. Peng, Y. Wang, P. Chen, R. Ruan, Catalytic microwave-assisted pyrolysis of plastic waste over NiO and HY for gasoline-range hydrocarbons production, Energy Convers. Manag. 196 (2019). https://doi.org/10.1016/j.enconman.2019.07.001.
3. Xuan Hu, Dachao Ma, Guangyi Zhang, Mengxue Ling, Qiaoling Hu, Kangyi Liang, Jiacheng Lu, Yifan Zheng, Microwave-assisted pyrolysis of waste plastics for their resource reuse: A technical review, Carbon Resources Conversion 6 (2023) 215–228.
4. J. Hopewell, R. Dvorak, E. Kosior, Plastics recycling: challenges and opportunities, (n.d.). https://doi.org/10.1098/rstb.2008.0311.
5. Okunola A, O. Kehinde I, A. Oluwaseun, A. Olufiropo E, Public and Environmental Health Effects of Plastic Wastes Disposal: A Review, Journal of Toxicology and Risk Assessment 5 (2019). https://doi.org/10.23937/2572-4061.1510021.
6. R. Geyer, J. R. Jambeck, K. L. Law, Production, use, and fate of all plastics ever made, Sci. Adv. (2017).
7. R. Proshad, T. Kormoker, Md.S. Islam, M.A. Haque, Md.M. Rahman, Md.M.R. Mithu, Toxic effects of plastic on human health and environment: A consequence of health risk assessment in Bangladesh, International Journal of Health 6 (2017) 1–5. https://doi.org/10.14419/ijh.v6i1.8655.
8. J.R. Jambeck, R. Geyer, C. Wilcox, T.R. Siegler, M. Perryman, A. Andrady, R. Narayan, K.L. Law, Plastic waste inputs from land into the ocean, Science (1979). 347 (2015) 768–771. https://doi.org/10.1126/science.1260352.
9. J. Aguado, D.P. Serrano, G. San Miguel, M.C. Castro, S. Madrid, Feedstock recycling of polyethylene in a two-step thermo-catalytic reaction system, J. Anal. Appl. Pyrolysis 79 (2007) 415–423. https://doi.org/10.1016/j.jaap.2006.11.008.
10. Ting Liu, Yincui Li, Yifan Zhou, Shengnan Deng, Huawei Zhang, Efficient pyrolysis of Low-Density Polyethylene for Regulatable Oil and Gas Products by ZSM-5, HY and MCM-41 Catalyst, Catalysts (2023) 382.
11. X. Zhang, H. Lei, G. Yadavalli, L. Zhu, Y. Wei, Y. Liu, Gasoline-range hydrocarbons produced from microwave-induced pyrolysis of low-density polyethylene over ZSM-5, Fuel 144 (2015). https://doi.org/10.1016/j.fuel.2014.12.013.
12. L. D. Chen, H. Yin, P.H. Wang, Pyrolysis technologies for municipal solid waste: A review, Waste Manag. 34 (2014) 2466–2486.
13. O.K.M. Ouda, S.A. Raza, A.S. Nizami, M. Rehan, R. Al-Waked, N.E. Korres, Waste to energy potential: A case study of Saudi Arabia, Renew. and Sustain. Energy (2016) 328–340.
14. R. Miandad, M. Rehan, A.-S. Nizami, M.A. El-Fetouh Barakat, I.M. Ismail, The Energy and Value-Added Products from Pyrolysis of Waste Plastics, in: Recycl, in: Of Solid Waste for Biofuels and Biochem, 2016: pp. 333–355. https://doi.org/10.1007/978-981-10-0150-5_12.
15. F. Vatankhah, A. Carrillo García, J. Chaouki, Role of Bifunctional Metal-Promoted Zeolitic Catalyst in Microwave-Assisted Pyrolysis of Polyethylene to Monocyclic Aromatics, Energy & Fuels 38 (2024) 20562–20576. https://doi.org/10.1021/acs.energyfuels.4c03692.
16. K.M.O. Islam, N. Ahmad, U. Ahmed, M.N. Siddiqui, A.C. Ummer, A.G. Abdul Jameel, Producing aromatic-rich oil through microwave-assisted catalytic pyrolysis of low-

density polyethylene over Ni/Co/Cu-doped Ga/ <scp>ZSM</scp> -5 catalysts, Biofuels, Bioproducts and Biorefining 19 (2025) 34–54. https://doi.org/10.1002/bbb.2690.
17. E. Bäckström, K. Odelius, M. Hakkarainen, Designed from Recycled: Turning Polyethylene Waste to Covalently Attached Polylactide Plasticizers, ACS Sustain. Chem. Eng. 7 (2019) 11004–11013. https://doi.org/10.1021/acssuschemeng.9b02092.
18. Xiaodong Jing, Hao Wen, Xuzhong Gong, ZhihongXu, Anna Kajetanowicz, Recycling waste plastics packaging to value-added products by two-stepmicrowave cracking with different heating strategies, Fuel Processing Technology (2020).
19. E. Bäckström, K. Odelius, M. Hakkarainen, Trash to Treasure: Microwave-Assisted Conversion of Polyethylene to Functional Chemicals, Ind. Eng. Chem. Res. 56 (2017) 14814–14821. https://doi.org/10.1021/acs.iecr.7b04091.
20. Liangliang Fan, Yaning Zhang, Shiyu Liu, Nan Zhou, Paul Chen, Yuhuan Liu, Yunpu Wang, PengPeng, Yanling Cheng, Min Addy, Hanwu Lei, Roger Ruan, Catalytic upgrading of vapors from microwave-assisted pyrolysis of low-density polyethylene with MgO, Energy Convers. Manag. (2017).
21. A. Undri, L. Rosi, M. Frediani, P. Frediani, Efficient disposal of waste polyolefins through microwave assisted pyrolysis., Fuel 116 (2014) 662–671.
22. Y. Chen, W. Wang, Y. Sun, X. Chen, Q. Lin, K. Yang, M. Zhang, L. Sun, X. Zhou, M. Zhang, Insight into metal-support synergistic effect from the perspective of increasing propylene production in catalytic cracking over Au/ZSM-5 catalysts, Microporous and Mesoporous Materials 373 (2024). https://doi.org/10.1016/j.micromeso.2024.113121.
23. A. Terapalli, D. Kamireddi, V. Sridevi, M. Tukarambai, D.V. Suriapparao, C.S. Rao, R. Gautam, P.R. Modi, Microwave-assisted in-situ catalytic pyrolysis of polystyrene: Analysis of product formation and energy consumption using machine learning approach., Process Saf. Environ. Prot. 166 (2022) 57–67.
24. Y. Liu, B. Ma, J. Tian, C. Zhao, Coupled conversion of polyethylene and carbon dioxide catalyzed by a zeolite–metal oxide system, Sci. Adv. 10 (2024). https://doi.org/10.1126/sciadv.adn0252.
25. Liangliang Fan, Zheyang Su, Jiabo Wu, Zhiguo Xiao, Pei Huang, Lei Liu, Haiwei Jiang, Wenguang Zhou, Shiyu Liu, Roger Ruan, Integrating continuous-stirred microwave pyrolysis with ex-situ catalyticupgrading for linear low-density polyethylene conversion: Effects of parameter conditions, Journal of Analytical and Applied Pyrolysis (2021).
26. M. Ravichandran, M. Balasubramanian, C. Anand Chairman, D. Pritima, V. Dhinakaran, B. Stalin, Recent developments in Polymer Matrix Composites – A review, IOP Conf. Ser. Mater. Sci. Eng. 988 (2020) 012096. https://doi.org/10.1088/1757-899X/988/1/012096.
27. Wikipedia contributors, Hemp, Wikipedia, The Free Encyclopedia. (2025).
28. K. Promhuad, A. Srisa, H. San, Y. Laorenza, P. Wongphan, J. Sodsai, K. Tansin, P. Phromphen, N. Chartvivatpornchai, P. Ngoenchai, N. Harnkarnsujarit, Applications of Hemp Polymers and Extracts in Food, Textile and Packaging: A Review, Polymers (Basel). 14 (2022) 4274. https://doi.org/10.3390/polym14204274.
29. Wikipedia contributors, Shellac, Wikipedia, The Free Encyclopedia. (2025).
30. Y. Yuan, N. He, Q. Xue, Q. Guo, L. Dong, M.H. Haruna, X. Zhang, B. Li, L. Li, Shellac: A promising natural polymer in the food industry, Trends Food Sci. Technol. 109 (2021) 139–153. https://doi.org/10.1016/j.tifs.2021.01.031.
31. Wikipedia contributors, Amber, Wikipedia, The Free Encyclopedia. (2025).
32. Wikipedia contributors, Silk, Wikipedia, The Free Encyclopedia. (2025).
33. D.J. Miller, Natural Rubber: Structure and Function, Halcyon (2025).

34. Wikipedia contributors, Cellulose, Wikipedia, The Free Encyclopedia. (2025).
35. Dennis Malpass, Introduction to Industrial Polyethylene: Properties, Catalysts, and Processes, Wiley, 2010.
36. GKFX, Schematic of LDPE branching structure, (2020).
37. VEM Tooling, LDPE Versus HDPE, (2026).
38. M. Gahleitner, C. Paulik, Polypropylene, in: Ullmann's Encyclopedia of Industrial Chemistry, Wiley-VCH Verlag GmbH & Co. KGaA, Weinheim, Germany, 2014: pp. 1–44. https://doi.org/10.1002/14356007.o21_o04.pub2.
39. S. STINSON, Discoverers of Polypropylene Share Prize, Chemical & Engineering News Archive 65 (1987) 30. https://doi.org/10.1021/cen-v065n010.p030.
40. C. Maier, T. Calafut, Polypropylene: the definitive user's guide and databook., in: 1998.
41. Von S. Nuyken, M. Koltzenburg, O. Maskos, Polymer: synthesis, properties and applications.in: 1st ed., Springer., 2013.
42. User:Cjp24, Polymerization reaction for synthesis of polypropylene, (2023).
43. G.T. Carroll, M.E. Sojka, X. Lei, N.J. Turro, J.T. Koberstein, Photoactive Additives for Cross-Linking Polymer Films: Inhibition of Dewetting in Thin Polymer Films, Langmuir 22 (2006) 7748–7754. https://doi.org/10.1021/la0611099.
44. H Padleckas, Chemical reaction diagram showing polystyrene formed by polymerisation of styrene., (2025).
45. W. V. Titow, PVC technology., Springer, 1984.
46. Strumberger N, Gospocic A, Bratulic C, Polymeric materials in automobiles., Promet Traffic- Traffico 17 (2005) 149–160.
47. S. Rahman, Sealing Our Buried Lifelines, Opflow 33 (2007) 12–17. https://doi.org/10.1002/j.1551-8701.2007.tb02753.x.
48. F.M. Galloway, M.M. Hirschler, G.F. Smith, Surface parameters from small-scale experiments used for measuring HCl transport and decay in fire atmospheres, Fire Mater. 15 (1991) 181–189. https://doi.org/10.1002/fam.810150405.
49. Strong, A. Brent, Plastics: Materials and Processing., Prentice Hall, 2005.
50. K. Marsh, B. Bugusu, Food Packaging—Roles, Materials, and Environmental Issues, J. Food Sci. 72 (2007). https://doi.org/10.1111/j.1750-3841.2007.00301.x.
51. NEUROtiker, Repeating unit of PVC polymer chain., (2008).
52. Wesley Stephenson, Why plastic recycling is so confusing, (2018).
53. Advancing Sustainable Materials Management: 2018 Tables and Figures , 2020.
54. S. Khadke, P. Gupta, S. Rachakunta, C. Mahata, S. Dawn, M. Sharma, D. Verma, A. Pradhan, A.M.S. Krishna, S. Ramakrishna, S. Chakrabortty, G. Saianand, P. Sonar, S. Biring, J.K. Dash, G.K. Dalapati, Efficient Plastic Recycling and Remolding Circular Economy Using the Technology of Trust–Blockchain, Sustainability 13 (2021) 9142. https://doi.org/10.3390/su13169142.
55. R. Hasanzadeh, P. Mojaver, T. Azdast, S. Khalilarya, A. Chitsaz, M.A. Rosen, Decision analysis for plastic waste gasification considering energy, exergy, and environmental criteria using TOPSIS and grey relational analysis, Process Safety and Environmental Protection 174 (2023) 414–423. https://doi.org/10.1016/j.psep.2023.04.028.
56. P. Mojaver, A. Chitsaz, S.J. Hasannejad, M. Khalilian, Plastic Waste Gasification, in: 2023: pp. 47–60. https://doi.org/10.1007/978-3-031-31160-4_3.
57. S.A. Salaudeen, P. Arku, A. Dutta, Gasification of Plastic Solid Waste and Competitive Technologies, in: Plastics to Energy, Elsevier, 2019: pp. 269–293. https://doi.org/10.1016/B978-0-12-813140-4.00010-8.
58. M. Rehan, A.S. Nizami, K. Shahzad, O.K.M. Ouda, I.M.I. Ismail, T. Almeelbi, T. Iqbal, A. Demirbas, Pyrolytic liquid fuel: A source of renewable electricity generation in

Makkah, Energy Sources, Part A: Recovery, Utilization, and Environmental Effects 38 (2016) 2598–2603. https://doi.org/10.1080/15567036.2016.1153753.
59. R. Boyt, Wood Pyrolysis, in: 2003.
60. Fogler, H. Scott, M. N. Gürmen, Elements of Chemical Reaction Engineering. 2005, Search PubMed (1999) 813–866.
61. J.A. Onwudili, N. Insura, P.T. Williams, Composition of products from the pyrolysis of polyethylene and polystyrene in a closed batch reactor: Effects of temperature and residence time, J. Anal. Appl. Pyrolysis 86 (2009) 293–303. https://doi.org/10.1016/j.jaap.2009.07.008.
62. Y. Choi, S. Wang, Y.M. Yoon, J.J. Jang, D. Kim, H.-J. Ryu, D. Lee, Y. Won, H. Nam, B. Hwang, Sustainable strategy for converting plastic waste into energy over pyrolysis: A comparative study of fluidized-bed and fixed-bed reactors, Energy 286 (2024) 129564. https://doi.org/10.1016/j.energy.2023.129564.
63. R. Aguado, M. Olazar, B. Gaisán, R. Prieto, J. Bilbao, Kinetic Study of Polyolefin Pyrolysis in a Conical Spouted Bed Reactor, Ind. Eng. Chem. Res. 41 (2002) 4559–4566. https://doi.org/10.1021/ie0201260.
64. M. Arabiourrutia, G. Elordi, M. Olazar, J. Bilbao, Pyrolysis of Polyolefins in a Conical Spouted Bed Reactor: A Way to Obtain Valuable Products, in: Pyrolysis, InTech, 2017. https://doi.org/10.5772/67706.
65. S. Orozco, M. Artetxe, G. Lopez, M. Suarez, J. Bilbao, M. Olazar, Conversion of HDPE into Value Products by Fast Pyrolysis Using FCC Spent Catalysts in a Fountain Confined Conical Spouted Bed Reactor, ChemSusChem 14 (2021) 4291–4300. https://doi.org/10.1002/cssc.202100889.
66. E.T. Thostenson, T.-W. Chou, Microwave processing: fundamentals and applications, Compos. Part A Appl. Sci. Manuf. 30 (1999) 1055–1071. https://doi.org/10.1016/S1359-835X(99)00020-2.
67. K.M.O. Islam, N. Ahmad, A.C. Ummer, U. Ahmed, M.N. Siddiqui, M. Millan, A.G. Abdul Jameel, Microwave-Assisted pyrolysis of waste plastics: A comprehensive review on process parameters, catalysts, and future prospects, Results in Engineering 26 (2025) 105571. https://doi.org/10.1016/j.rineng.2025.105571.
68. V. Palma, D. Barba, M. Cortese, M. Martino, S. Renda, E. Meloni, Microwaves and Heterogeneous Catalysis: A Review on Selected Catalytic Processes, Catalysts 10 (2020) 246. https://doi.org/10.3390/catal10020246.
69. S.S. Lam, H.A. Chase, A Review on Waste to Energy Processes Using Microwave Pyrolysis, Energies (Basel). 5 (2012) 4209–4232. https://doi.org/10.3390/en5104209.
70. K.N. Aishwarya, N. Sindhu, Microwave Assisted Pyrolysis of Plastic Waste, Procedia Technology 25 (2016) 990–997. https://doi.org/10.1016/j.protcy.2016.08.197.
71. Xiaodong Jing, Hao Wen, Xuzhong Gong, ZhihongXu, Anna Kajetanowicz, Recycling waste plastics packaging to value-added products by two-stepmicrowave cracking with different heating strategies, Fuel Processing Technology (2020).
72. X. Zhang, K. Rajagopalan, H. Lei, R. Ruan, B.K. Sharma, An overview of a novel concept in biomass pyrolysis: microwave irradiation, Sustain. Energy Fuels 1 (2017) 1664–1699. https://doi.org/10.1039/C7SE00254H.
73. Liangliang Fan, Lei Liu, Zhiguo Xiao, Zheyang Su, Pei Huang, HongyuPeng, SenLv, Haiwei Jiang, Roger Ruan, Paul Chen, Wenguang Zhou, Comparative study of continuous-stirred and batch microwave pyrolysis of linear low-density polyethylene in the presence/absenceof HZSM-5, Energy (2021).
74. L. Fan, Z. Su, J. Wu, Z. Xiao, P. Huang, L. Liu, H. Jiang, W. Zhou, S. Liu, R. Ruan, Integrating continuous-stirred microwave pyrolysis with ex-situ catalytic upgrading for

linear low-density polyethylene conversion: Effects of parameter conditions, J. Anal. Appl. Pyrolysis 157 (2021) 105213. https://doi.org/10.1016/j.jaap.2021.105213.
75. Y. Fernandez, A. Arenillas, J. Angel, Microwave Heating Applied to Pyrolysis, in: Advances in Induction and Microwave Heating of Mineral and Organic Materials, InTech, 2011. https://doi.org/10.5772/13548.
76. Z. Cai, M. Li, Z. Zhu, X. Wang, Y. Huang, T. Li, H. Gong, M. Yan, Biological Degradation of Plastics and Microplastics: A Recent Perspective on Associated Mechanisms and Influencing Factors, Microorganisms 11 (2023) 1661. https://doi.org/10.3390/microorganisms11071661.
77. T. Artham, M. Doble, Biodegradation of Aliphatic and Aromatic Polycarbonates, Macromol. Biosci. 8 (2008) 14–24. https://doi.org/10.1002/mabi.200700106.
78. J. Mudondo, H.-S. Lee, Y. Jeong, T.H. Kim, S. Kim, B.H. Sung, S.-H. Park, K. Park, H.G. Cha, Y.J. Yeon, H.T. Kim, Recent Advances in the Chemobiological Upcycling of Polyethylene Terephthalate (PET) into Value-Added Chemicals, J. Microbiol. Biotechnol. 33 (2023) 1–14. https://doi.org/10.4014/jmb.2208.08048.
79. A. Marcilla, M.I. Beltrán, R. Navarro, Evolution of products during the degradation of polyethylene in a batch reactor, J. Anal. Appl. Pyrolysis 86 (2009) 14–21. https://doi.org/10.1016/j.jaap.2009.03.004.
80. López, I. de Marco, B.M. Caballero, M.F. Laresgoiti, A. Adrados, Influence of time and temperature on pyrolysis of plastic wastes in a semi-batch reactor, Chemical Engineering Journal 173 (2011) 62–71. https://doi.org/10.1016/j.cej.2011.07.037.
81. R. Prurapark, K. Owjaraen, B. Saengphrom, I. Limthongtip, N. Tongam, Effect of Temperature on Pyrolysis Oil Using HDPE and PET Sources from Mobile Pyrolysis Plant, (2020). https://doi.org/10.21203/rs.3.rs-24640/v1.
82. S. Papuga, P. Gvero, L. Vukic, Temperature and time influence on the waste plastics pyrolysis in the fixed bed reactor, Thermal Science 20 (2016) 731–741. https://doi.org/10.2298/TSCI141113154P.
83. K. Ding, S. Liu, Y. Huang, S. Liu, N. Zhou, P. Peng, Y. Wang, P. Chen, R. Ruan, Catalytic microwave-assisted pyrolysis of plastic waste over NiO and HY for gasoline-range hydrocarbons production, Energy Convers. Manag. 196 (2019). https://doi.org/10.1016/j.enconman.2019.07.001.
84. Liangliang Fan, Yaning Zhang, Shiyu Liu, Nan Zhou, Paul Chen, Yuhuan Liu, Yunpu Wang, PengPeng, Yanling Cheng, Min Addy, Hanwu Lei, Roger Ruan, Catalytic upgrading of vapors from microwave-assisted pyrolysis of low-density polyethylene with MgO, Energy Convers. Manag. (2017).
85. X. Zhang, H. Lei, G. Yadavalli, L. Zhu, Y. Wei, Y. Liu, Gasoline-range hydrocarbons produced from microwave-induced pyrolysis of low-density polyethylene over ZSM-5, Fuel 144 (2015). https://doi.org/10.1016/j.fuel.2014.12.013.
86. M. Artetxe, G. Lopez, M. Amutio, G. Elordi, J. Bilbao, M. Olazar, Cracking of High Density Polyethylene Pyrolysis Waxes on HZSM-5 Catalysts of Different Acidity, Ind. Eng. Chem. Res. 52 (2013) 10637–10645. https://doi.org/10.1021/ie4014869.
87. J. Aguado, D.P. Serrano, G. San Miguel, M.C. Castro, S. Madrid, Feedstock recycling of polyethylene in a two-step thermo-catalytic reaction system, J. Anal. Appl. Pyrolysis 79 (2007) 415–423. https://doi.org/10.1016/j.jaap.2006.11.008.
88. F. Vatankhah, A. Carrillo García, J. Chaouki, Role of Bifunctional Metal-Promoted Zeolitic Catalyst in Microwave-Assisted Pyrolysis of Polyethylene to Monocyclic Aromatics, Energy & Fuels 38 (2024) 20562–20576. https://doi.org/10.1021/acs.energyfuels.4c03692.
89. Fan Liangliang, Zhang Yaning, Liu Shiyu, Zhou Nan, Chen Paul, Liu Yuhuan, Wang Yunpu, Peng Peng, Cheng Yanling, Addy Min, Lei Hanwu, Ruan Roger, Ex-situ

catalytic upgrading of vapors from microwave-assisted pyrolysis of low-density polyethylene with MgO, Energy Convers. Manag. 149 (2017). https://doi.org/10.1016/j.enconman.2017.07.039.
90. Zhaohui Chen, Mohammad Monzavi, Mohammad Latifi, Said Samih, Jamal Chaouki., Microwave-responsive SiCfoam@zeolite core-shell structured catalyst for catalytic pyrolysis of plastics, Environmental Pollution (2022).
91. Dadi V. Suriapparao, Garlapati Nagababu, Attada Yerrayya, Veluru Sridevi, Optimization of microwave power and graphite susceptor quantityfor waste polypropylene microwave pyrolysis., Process Safety and Environmental Protection (2021) 234–243.
92. P. Rex, I.P. Masilamani, L.R. Miranda, Microwave pyrolysis of polystyrene and polypropylene mixtures using different activated carbon from biomass, Journal of the Energy Institute 93 (2020) 1819–1832. https://doi.org/10.1016/j.joei.2020.03.013.
93. E. Bäckström, K. Odelius, M. Hakkarainen, Trash to Treasure: Microwave-Assisted Conversion of Polyethylene to Functional Chemicals, Ind. Eng. Chem. Res. 56 (2017) 14814–14821. https://doi.org/10.1021/acs.iecr.7b04091.
94. E. Bäckström, K. Odelius, M. Hakkarainen, Designed from Recycled: Turning Polyethylene Waste to Covalently Attached Polylactide Plasticizers, ACS Sustain. Chem. Eng. 7 (2019) 11004–11013. https://doi.org/10.1021/acssuschemeng.9b02092.
95. S.R. Juliastuti, N. Hendrianie, P.J. Ramadhan, D.H. Satria, Microwave pyrolysis of multilayer plastic waste (LDPE) using zeolite catalyst, in: 2017: p. 110001. https://doi.org/10.1063/1.4982331.
96. A. Dr. Raj Mohan B, Studies on microwave pyrolysis of polypropylene, International Journal of Engineering Research & Technology (2016).
97. J. Bergström, Experimental Characterization Techniques, in: Mechanics of Solid Polymers, Elsevier, 2015: pp. 19–114. https://doi.org/10.1016/B978-0-323-31150-2.00002-9.
98. Merenich, K.E. Van Manen-Brush, C. Janetopoulos, K.A. Myers, Advanced microscopy techniques for the visualization and analysis of cell behaviors, in: Cell Movement in Health and Disease, Elsevier, 2022: pp. 303–321. https://doi.org/10.1016/B978-0-323-90195-6.00010-3.
99. K. Mattsson, S. Jocic, J.A. de Lima, L.-A. Hansson, A. Gondikas, Nanoplastics in aquatic environments—Sources, sampling techniques, and identification methods, in: Microplastic Contamination in Aquatic Environments, Elsevier, 2024: pp. 381–397. https://doi.org/10.1016/B978-0-443-15332-7.00003-X.
100. C.A. Emeis, Determination of Integrated Molar Extinction Coefficients for Infrared Absorption Bands of Pyridine Adsorbed on Solid Acid Catalysts, J. Catal. 141 (1993) 347–354. https://doi.org/10.1006/jcat.1993.1145.
101. G. Busca, Acid Catalysts in Industrial Hydrocarbon Chemistry, Chem. Rev. 107 (2007) 5366–5410. https://doi.org/10.1021/cr068042e.
102. Dr. Kazuyuki Nakai, Ms. Kaori Nakamura, Ammonia Temperature Programmed Desorption (NH3- TPD) Measurement -Investigation of Desorption Energy and Heat of Adsorption, Www.Microtrac.Com © Microtrac MRB 2019 (2019).
103. T.K. Giri, Solid lipid nanoparticles for the delivery of drug molecules, in: Materials for Biomedical Engineering, Elsevier, 2019: pp. 551–576. https://doi.org/10.1016/B978-0-12-818433-2.00016-9.
104. Agilent Technologies, An Introduction to the Principles of Inductively Coupled Plasma – Mass Spectrometry (ICP-MS), Https://Www.Agilent.Com/En/Product/Atomic-Spectroscopy/Inductively-Coupled-Plasma-Mass-Spectrometry-Icp-Ms/What-Is-Icp-Ms-Icp-

105. Agilent Technologies, Gas Chromatography/ Mass Spectrometry Fundamentals, Https://Www.Agilent.Com/En/Product/Gas-Chromatography-Mass-Spectrometry-Gc-Ms/Gcms-Fundamentals (n.d.).
106. J. Aguado, J.L. Sotelo, D.P. Serrano, J.A. Calles, J.M. Escola, Catalytic Conversion of Polyolefins into Liquid Fuels over MCM-41: Comparison with ZSM-5 and Amorphous SiO_2 $-Al_2O_3$, Energy & Fuels 11 (1997) 1225–1231. https://doi.org/10.1021/ef970055v.
107. V.G. Komvokis, S. Karakoulia, E.F. Iliopoulou, M.C. Papapetrou, I.A. Vasalos, A.A. Lappas, K.S. Triantafyllidis, Upgrading of Fischer–Tropsch synthesis bio-waxes via catalytic cracking: Effect of acidity, porosity and metal modification of zeolitic and mesoporous aluminosilicate catalysts, Catal. Today 196 (2012) 42–55. https://doi.org/10.1016/j.cattod.2012.06.029.
108. Sean Timothy Okonsky, J.V. Jayarama Krishna, Hilal Ezgi Toraman, Catalytic co-pyrolysis of LDPE and PET with HZSM-5, H-Beta, and HY: Experiments and kinetic modelling, React. Chem. Eng. (2022).
109. P.L. editors Weitkamp J, Catalysis and zeolites: fundamentals and applications, New York: Springer Berlin Heidelberg (1999) 546.
110. Niwa M, Suzuki K, Katada N, Niwa M, Suzuki K, et al Isamoto K, Identification and measurements of strong brønsted acidsite in ultrastable y (USY) zeolite, J Phys Chem B (2006) 264.
111. Handke M, Mozgawa W, Vibrational spectroscopy of theamorphous silicates, Vib Spectrosc 5 (1993) 75–84.
112. Anggoro DD, Buchori L, Silaen GC, Utami RN, Preparation,characterization, and activation of Co-Mo/Y zeolite catalyst forcoal tar conversion to liquid fuel, Bull Chem React Eng Catal 12 (2017) 219–226.
113. Wen Ding, Yuyang Cui, Jianjun Li, Yiquan Yang, Weiping Fang, Promoting effect of dual modification of H-ZSM-5 catalyst by alkali treating and Mg doping on catalytic performances for alkylation of benzene with ethanol to ethylbenzene, The Royal Society of Chemistry (2014) 50123–50129.
114. M. Sahooli, M. Rahimpour, M. Khorram, Fine-Tuning Synthesis and Characterization of Mono-Sized H-Beta Zeolite-Supported Palladium-Iridium Nanoparticles and Application in the Selective Hydrogenation of Acetylene, Catalysts 7 (2017) 343. https://doi.org/10.3390/catal7110343.
115. F. Chen, D. Zhang, L. Shi, Y. Wang, G. Xu, Optimized Pore Structures of Hierarchical HY Zeolites for Highly Selective Production of Methyl Methoxyacetate, Catalysts 9 (2019) 865. https://doi.org/10.3390/catal9100865.
116. X.J. Cheng, X.S. Wang, H.Y. Long, Transalkylation of benzene with 1, 2, 4 trimethylbenzene over nanosized ZSM-5, Microporous and Mesoporous Materials 119 (2009) 171.
117. R. Kumar, H. Jain, A. Chaudhary, S. Kumari, D.P. Mondal, A.K. Srivastava, Thermal conductivity and fire-retardant response in graphite foam made from coal tar pitch derived semi coke, Compos. B Eng. 172 (2019) 121–130. https://doi.org/10.1016/j.compositesb.2019.05.036.
118. Dadi V. Suriapparao, Garlapati Nagababu, Attada Yerrayya, Veluru Sridevi, Optimization of microwave power and graphite susceptor quantityfor waste polypropylene microwave pyrolysis., Process Safety and Environmental Protection (2021) 234–243.
119. K. Ding, S. Liu, Y. Huang, S. Liu, N. Zhou, P. Peng, Y. Wang, P. Chen, R. Ruan, Catalytic microwave-assisted pyrolysis of plastic waste over NiO and HY for gasoline-

range hydrocarbons production, Energy Convers. Manag. 196 (2019). https://doi.org/10.1016/j.enconman.2019.07.001.
120. Liangliang Fan, Lei Liu, Zhiguo Xiao, Zheyang Su, Pei Huang, HongyuPeng, SenLv, Haiwei Jiang, Roger Ruan, Paul Chen, Wenguang Zhou, Comparative study of continuous-stirred and batch microwave pyrolysis of linear low-density polyethylene in the presence/absenceof HZSM-5, Energy (2021).
121. Liangliang Fan, Yaning Zhang, Shiyu Liu, Nan Zhou, Paul Chen, Yuhuan Liu, Yunpu Wang, PengPeng, Yanling Cheng, Min Addy, Hanwu Lei, Roger Ruan, Catalytic upgrading of vapors from microwave-assisted pyrolysis of low-density polyethylene with MgO, Energy Convers. Manag. (2017).
122. Ting Liu, Yincui Li, Yifan Zhou, Shengnan Deng, Huawei Zhang, Efficient pyrolysis of Low-Density Polyethylene for Regulatable Oil and Gas Products by ZSM-5, HY and MCM-41 Catalyst, Catalysts (2023) 382.
123. J. Aguado, D.P. Serrano, G. San Miguel, M.C. Castro, S. Madrid, Feedstock recycling of polyethylene in a two-step thermo-catalytic reaction system, J. Anal. Appl. Pyrolysis 79 (2007) 415–423. https://doi.org/10.1016/j.jaap.2006.11.008.
124. P.T. Williams, E.A. Williams, Fluidised bed pyrolysis of low density polyethylene to produce petrochemical feedstock, J. Anal. Appl. Pyrolysis 51 (1999) 107–126. https://doi.org/10.1016/S0165-2370(99)00011-X.
125. Baena-Gonzalez J, Santamaria-Echart A, Aguirre JL, Gonzalez S, Chemical recycling of plastic waste: bitumen, solvents, and polystyrene from pyrolysis oil, (2020).
126. X. Zhang, H. Lei, G. Yadavalli, L. Zhu, Y. Wei, Y. Liu, Gasoline-range hydrocarbons produced from microwave-induced pyrolysis of low-density polyethylene over ZSM-5, Fuel 144 (2015). https://doi.org/10.1016/j.fuel.2014.12.013.
127. N. Miskolczi, A. Angyal, L. Bartha, I. Valkai, Fuels by Pyrolysis of Waste Plastics from Agricultural and Packaging Sectors in a Pilot Scale Reactor, Fuel Process. Technol 90 (2009) 1032–1040.
128. Liangliang Fan, Zheyang Su, Jiabo Wu, Zhiguo Xiao, Pei Huang, Lei Liu, Haiwei Jiang, Wenguang Zhou, Shiyu Liu, Roger Ruan, Integrating continuous-stirred microwave pyrolysis with ex-situ catalyticupgrading for linear low-density polyethylene conversion: Effects of parameter conditions, Journal of Analytical and Applied Pyrolysis (2021).
129. Zhaohui Chen, Mohammad Monzavi, Mohammad Latifi, Said Samih, Jamal Chaouki., Microwave-responsive SiCfoam@zeolite core-shell structured catalyst for catalytic pyrolysis of plastics, Environmental Pollution (2022).
130. G. Manos, A. Garfoth, J. Dwyer, Catalytic Degradation of High-Density Polyethylene over Different Zeolitic Structures, Ind. Eng. Chem. Res 39 (2000) 1198.
131. G. Elordi, M. Olazar, G. Lopez, P. Castano, J. Bilbao, Role of pore structure in the deactivation of zeolites (HZSM-5, H and HY) by coke in the pyrolysis of polyethylene in a conical spouted bed reactor, Applied Catalysis B: Environmental (2011) 224–231.
132. A. Marcilla, Gómez-Siurana, F. Valdés, Catalytic cracking of low-density polyethylene over H-Beta and HZSM-5 zeolites: Influence of the external surface. Kinetic model. Polymer Degradation and Stability, Polymer Degradation and Stability 92 (2007) 197–204.
133. A. Wang, H. Lei, M. Qian, E. Huo, Y. Zhao, Q. Zhang, W. Mateo, X. Lin, X. Kong, R. Zou, R. Ruan, Application of highly stable biochar catalysts for efficient pyrolysis of plastics: a readily accessible potential solution to a global waste crisis, Sustain. Energy Fuels 4 (2020) 4614–4624. https://doi.org/10.1039/D0SE00652A.

134. J.H. Harrhy, A. Wang, J.S. Jarvis, P. He, S. Meng, M. Yung, L. Liu, H. Song, Understanding zeolite deactivation by sulfur poisoning during direct olefin upgrading, Commun. Chem. 2 (2019) 37. https://doi.org/10.1038/s42004-019-0141-4.
135. Kassargy C, Awad S, Burnens G, Kahine K, Tazerout M, Experimental study ofcatalytic pyrolysis of polyethylene and polypropylene over USY zeolite andseparation to gasoline and diesel-like fuels, J Anal Appl Pyrol (2017).
136. Corma A, Orchilles AV, Current views on the mechanism of catalytic cracking.Microporous Mesoporous, Mater (2000).
137. I.L. Simakova, Yu.S. Demidova, M.N. Simonov, P.S. Niphadkar, V.V. Bokade, N. Devi, P.L. Dhepe, D.Yu. Murzin, Mesoporous carbon and microporous zeolite supported Ru catalysts for selective levulinic acid hydrogenation into γ-valerolactone, Catalysis for Sustainable Energy 6 (2019) 38–50. https://doi.org/10.1515/cse-2019-0004.
138. A. A. Marcilla, Go´mez-Siurana, F. Valde´s, Catalytic pyrolysis of LDPE over H-beta and HZSM-5 zeolites in dynamic conditions Study of the evolution of the process, J. Anal. Appl. Pyrolysis 79 (2007) 433–442.
139. Ganesh Bajad, R.P. Vijayakumar, Prajwal Rakhunde, Amit Hete, Mahesh Bhade, Processing of mixed-plastic waste to fuel oil, carbon nanotubes and hydrogen using multi–core reactor, Chem. Eng. Process (2017) 205–214.
140. Yuxin Wang, Tara Biddle, Changle Jiang, Thang Luong, Roujia Chen, Sean Brown, Xiangyu Jie, Jianli Hu, Microwave-driven upcycling of single-use plastics using zeolite catalyst, Chemical Engineering Journal (2023).
141. E.K.L. Morais, S. Jiménez-Sánchez, H. Hernando, C. Ochoa-Hernández, P. Pizarro, A.S. Araujo, D.P. Serrano, Catalytic Copyrolysis of Lignocellulose and Polyethylene Blends over HBeta Zeolite, Ind. Eng. Chem. Res. 58 (2019) 6243–6254. https://doi.org/10.1021/acs.iecr.8b06158.
142. A. Munir, H. Amer, R. Aslam, M. Bououdina, M.R. Usman, Composite zeolite beta catalysts for catalytic hydrocracking of plastic waste to liquid fuels, Mater. Renew. Sustain. Energy 9 (2020) 9. https://doi.org/10.1007/s40243-020-00169-3.
143. H.W. Lee, Y.-K. Park, Catalytic Pyrolysis of Polyethylene and Polypropylene over Desilicated Beta and Al-MSU-F, Catalysts 8 (2018) 501. https://doi.org/10.3390/catal8110501.
144. M.U. Azam, A. Fernandes, M.J. Ferreira, W. Afzal, I. Graça, Pore-Structure Engineering of Hierarchical β Zeolites for the Enhanced Hydrocracking of Waste Plastics to Liquid Fuels, ACS Catal. 14 (2024) 16148–16165. https://doi.org/10.1021/acscatal.4c05354.
145. X. Zhang, H. Lei, Synthesis of high-density jet fuel from plastics via catalytically integral processes, RSC Adv. 6 (2016) 6154–6163. https://doi.org/10.1039/C5RA25327F.
146. J. Aguado, D.P. Serrano, J.L. Sotelo, R. Van Grieken, J.M. Escola, Influence of the Operating Variables on the Catalytic Conversion of a Polyolefin Mixture over HMCM-41 and Nanosized HZSM-5, Ind. Eng. Chem. Res. 40 (2001) 5696–5704. https://doi.org/10.1021/ie010420c.
147. S. Matsuura, T. Hashimoto, A. Ishihara, Catalytic cracking of low-density polyethylene over zeolite-containing hierarchical two-layered catalyst with different mesopore size using Curie point pyrolyzer, Fuel Processing Technology 227 (2022) 107106. https://doi.org/10.1016/j.fuproc.2021.107106.
148. Y.-H. Lin, P.N. Sharratt, A.A. Garforth, J. Dwyer, Deactivation of US-Y zeolite by coke formation during the catalytic pyrolysis of high density polyethylene, Thermochim, Acta (1997) 45–50.

149. Chantal Kassargya, Sary Awada, Gaëtan Burnensa, Gaurav Upretia, Khalil Kahine, Mohand Tazerout, Study of the effects of regeneration of USY zeolite on the catalytic cracking of polyethylene, Applied Catalysis B: Environmental (2019) 704–708.
150. Maria S. Renzini, Laura C. Lerici, Ulises Sedranb, Liliana B. Pierellaa, Stability of ZSM-11 and BETA zeolites during the catalytic cracking of low-density polyethylene, Journal of Analytical and Applied Pyrolysis (2011) 450–455.
151. M. Marhaini, D. Fernianti, M.R. Aulia, Effective pyrolysis of LDPE plastic waste to fuel using titanium dioxide catalyst, International Journal of ADVANCED AND APPLIED SCIENCES 11 (2024) 75–82. https://doi.org/10.21833/ijaas.2024.12.009.
152. G. Elordi, M. Olazar, P. Castaño, M. Artetxe, J. Bilbao, Polyethylene Cracking on a Spent FCC Catalyst in a Conical Spouted Bed, Ind. Eng. Chem. Res. 51 (2012) 14008–14017. https://doi.org/10.1021/ie3018274.
153. L. Yosefi, M. Haghighi, Fabrication of nanostructured flowerlike p-BiOI/p-NiO heterostructure and its efficient photocatalytic performance in water treatment under visible-light irradiation, Appl. Catal. B 220 (2018) 367–378. https://doi.org/10.1016/j.apcatb.2017.08.028.
154. M. Król, J. Minkiewicz, W. Mozgawa, IR spectroscopy studies of zeolites in geopolymeric materials derived from kaolinite, J. Mol. Struct. 1126 (2016) 200–206. https://doi.org/10.1016/j.molstruc.2016.02.027.
155. R. Tang, T. Chen, Y. Chen, Y. Zhang, G. Wang, Core-shell TiO2@SiO2 catalyst for transesterification of dimethyl carbonate and phenol to diphenyl carbonate, Chinese Journal of Catalysis 35 (2014) 457–461. https://doi.org/10.1016/S1872-2067(14)60059-0.
156. M.M. Ba-Abbad, A.A.H. Kadhum, A.B. Mohamad, M.S. Takriff, K. Sopian, Synthesis and Catalytic Activity of TiO2 Nanoparticles for Photochemical Oxidation of Concentrated Chlorophenols under Direct Solar Radiation, Int. J. Electrochem. Sci. 7 (2012) 4871–4888. https://doi.org/10.1016/S1452-3981(23)19588-5.
157. J. Xu, T. Zhang, J. Zhang, Photocatalytic degradation of methylene blue with spent FCC catalyst loaded with ferric oxide and titanium dioxide, Sci. Rep. 10 (2020) 12730. https://doi.org/10.1038/s41598-020-69643-2.
158. R.G. Toro, M. Diab, T. de Caro, M. Al-Shemy, A. Adel, D. Caschera, Study of the Effect of Titanium Dioxide Hydrosol on the Photocatalytic and Mechanical Properties of Paper Sheets, Materials 13 (2020) 1326. https://doi.org/10.3390/ma13061326.
159. A.S. Al-Dughaither, H. de Lasa, HZSM-5 Zeolites with Different SiO_2/Al_2O_3 Ratios. Characterization and NH_3 Desorption Kinetics, Ind. Eng. Chem. Res. 53 (2014) 15303–15316. https://doi.org/10.1021/ie4039532.
160. Bin, C. Song, G. Lv, J. Song, X. Cao, H. Pang, K. Wang, Structural Characterization and Selective Catalytic Reduction of Nitrogen Oxides with Ammonia: A Comparison between Co/ZSM-5 and Co/SBA-15, The Journal of Physical Chemistry C 116 (2012) 26262–26274. https://doi.org/10.1021/jp303830x.
161. M. Rahmani, M. Taghizadeh, Synthesis optimization of mesoporous ZSM-5 through desilication-reassembly in the methanol-to-propylene reaction, Reaction Kinetics, Mechanisms and Catalysis 122 (2017) 409–432. https://doi.org/10.1007/s11144-017-1204-0.
162. S. Tsubota, S. Kokuryo, K. Tamura, K. Miyake, Y. Uchida, A. Mizusawa, T. Kubo, N. Nishiyama, Exploring the effect of Brønsted acidity of MFI-type zeolites on catalytic cracking temperature of low density polyethylene, Catal. Sci. Technol. 14 (2024) 1369–1374. https://doi.org/10.1039/D3CY01622F.

163. R. Miandad, M.A. Barakat, A.S. Aburiazaiza, M. Rehan, A.S. Nizami, Catalytic pyrolysis of plastic waste: A review, Process Safety and Environmental Protection 102 (2016) 822–838. https://doi.org/10.1016/j.psep.2016.06.022.
164. R. Kumar, H. Jain, A. Chaudhary, S. Kumari, D.P. Mondal, A.K. Srivastava, Thermal conductivity and fire-retardant response in graphite foam made from coal tar pitch derived semi coke, Compos. B Eng. 172 (2019) 121–130. https://doi.org/10.1016/j.compositesb.2019.05.036.
165. Pengcheng Wang, Lei Qiao, Wei Wang, Jie Yu, Catalytic pyrolysis of waste composite plastics with waste FCC catalyst., Journal of the Energy Institute 110 (2023) 101338.
166. Y.-H. Lin, M.-H. Yang, Catalytic pyrolysis of polyolefin waste into valuable hydrocarbons over reused catalyst from refinery FCC units, Appl. Catal. A Gen. 328 (2007) 132–139. https://doi.org/10.1016/j.apcata.2007.05.039.
167. S. Orozco, G. Lopez, M.A. Suarez, M. Artetxe, J. Alvarez, J. Bilbao, M. Olazar, Oxidative Fast Pyrolysis of High-Density Polyethylene on a Spent Fluid Catalytic Cracking Catalyst in a Fountain Confined Conical Spouted Bed Reactor, ACS Sustain. Chem. Eng. 10 (2022) 15791–15801. https://doi.org/10.1021/acssuschemeng.2c04552.
168. S.L. Wong, S. Armenise, B.B. Nyakuma, A. Bogush, S. Towers, C.H. Lee, K.Y. Wong, T.H. Lee, E. Rebrov, M. Muñoz, Plastic pyrolysis over HZSM-5 zeolite and fluid catalytic cracking catalyst under ultra-fast heating, J. Anal. Appl. Pyrolysis 169 (2023) 105793. https://doi.org/10.1016/j.jaap.2022.105793.
169. R.R. Mishra, P.H. Rana, P.A. Parikh, Microwave-assisted pyrolysis of low-density polyethylene (LDPE)to value-added products over HY, HZSM-5 and Hβ catalyst, Mater. Today Commun. 41 (2024) 110829. https://doi.org/10.1016/j.mtcomm.2024.110829.
170. N.S. Akpanudoh, K. Gobin, G. Manos, Catalytic degradation of plastic waste to liquid fuel over commercial cracking catalysts, J. Mol. Catal. A Chem. 235 (2005) 67–73. https://doi.org/10.1016/j.molcata.2005.03.009.
171. K.-H. Lee, N.-S. Noh, D.-H. Shin, Y. Seo, Comparison of plastic types for catalytic degradation of waste plastics into liquid product with spent FCC catalyst, Polym. Degrad. Stab. 78 (2002) 539–544. https://doi.org/10.1016/S0141-3910(02)00227-6.
172. Itsaso Barbarias, Maite Artetxe, Aitor Arregi, Jon Alvarez, Gartzen Lopez, Maider Amutio, Martin Olazar, Catalytic Cracking of HDPE Pyrolysis Volatiles over a Spent FCC Catalyst , CHEMICAL ENGINEERING TRANSACTIONS 43 (2015) 2029–2034.
173. S. Kumar, A.K. Panda, R.K. Singh, A review on tertiary recycling of high-density polyethylene to fuel, Resour. Conserv. Recycl. 55 (2011) 893–910. https://doi.org/10.1016/j.resconrec.2011.05.005.
174. L. Fan, Z. Su, J. Wu, Z. Xiao, P. Huang, L. Liu, H. Jiang, W. Zhou, S. Liu, R. Ruan, Integrating continuous-stirred microwave pyrolysis with ex-situ catalytic upgrading for linear low-density polyethylene conversion: Effects of parameter conditions, J. Anal. Appl. Pyrolysis 157 (2021) 105213. https://doi.org/10.1016/j.jaap.2021.105213.
175. P. Wang, L. Qiao, W. Wang, J. Yu, Catalytic pyrolysis of waste composite plastics with waste FCC catalyst, Journal of the Energy Institute 110 (2023) 101338. https://doi.org/10.1016/j.joei.2023.101338.
176. Y. Song, X. Zhu, L. Xu, Study on the process of transformation of olefin into aromatics over HZSM-5, Catal. Commun. 7 (2006) 218–223. https://doi.org/10.1016/j.catcom.2005.11.007.
177. J.A. Onwudili, C. Muhammad, P.T. Williams, Influence of catalyst bed temperature and properties of zeolite catalysts on pyrolysis-catalysis of a simulated mixed plastics

sample for the production of upgraded fuels and chemicals, Journal of the Energy Institute 92 (2019) 1337–1347. https://doi.org/10.1016/j.joei.2018.10.001.
178. Felix Aibuedefe Aisien, Eki Tina Aisien, Liquid Fluids from Thermo-Catalytic Degradation of Waste Low-Density Polyethylene Using Spent Fcc Catalyst, Detritus 19 (2022) 75–83.
179. S. Orozco, M. Artetxe, G. Lopez, M. Suarez, J. Bilbao, M. Olazar, Conversion of HDPE into Value Products by Fast Pyrolysis Using FCC Spent Catalysts in a Fountain Confined Conical Spouted Bed Reactor, ChemSusChem 14 (2021) 4291–4300. https://doi.org/10.1002/cssc.202100889.
180. S. Fan, Y. Zhang, L. Cui, T. Maqsood, S. Nižetić, Cleaner production of aviation oil from microwave-assisted pyrolysis of plastic wastes, J. Clean. Prod. 390 (2023) 136102. https://doi.org/10.1016/j.jclepro.2023.136102.
181. Dadi V. Suriapparao, Garlapati Nagababu, Attada Yerrayya, Veluru Sridevi, Optimization of microwave power and graphite susceptor quantityfor waste polypropylene microwave pyrolysis., Process Safety and Environmental Protection (2021) 234–243.
182. T.O. Eschemann, J.H. Bitter, K.P. de Jong, Effects of loading and synthesis method of titania-supported cobalt catalysts for Fischer–Tropsch synthesis, Catal. Today 228 (2014) 89–95. https://doi.org/10.1016/j.cattod.2013.10.041.
183. P.E. Nwankwor, I.O. Onuigbo, C.E. Chukwuneke, M.F. Yahaya, B.O. Agboola, W.J. Jahng, Synthesis of gasoline range fuels by the catalytic cracking of waste plastics using titanium dioxide and zeolite, International Journal of Energy and Environmental Engineering 12 (2021) 77–86. https://doi.org/10.1007/s40095-020-00359-9.
184. Uwagwu charles olisemeke, research on comparative study on the conversion of waste plastic materials to liquid hydrocarbons through catalytic pyrolysis, 2018.
185. J.H. Harrhy, A. Wang, J.S. Jarvis, P. He, S. Meng, M. Yung, L. Liu, H. Song, Understanding zeolite deactivation by sulfur poisoning during direct olefin upgrading, Commun. Chem. 2 (2019) 37. https://doi.org/10.1038/s42004-019-0141-4.
186. C. Wang, H. Lei, M. Qian, E. Huo, Y. Zhao, Q. Zhang, W. Mateo, X. Lin, X. Kong, R. Zou, R. Ruan, Application of highly stable biochar catalysts for efficient pyrolysis of plastics: a readily accessible potential solution to a global waste crisis, Sustain. Energy Fuels 4 (2020) 4614–4624. https://doi.org/10.1039/D0SE00652A.
187. Linxiao Chen, Julia D. Moreira, Laura C. Meyer, Oliver Y. Gutiérrez, János Szanyi, Dual-Pathway Polyolefin Upcycling over an Unexpectedly Bifunctional Low Loading Ru/TiO2-Anatase Catalyst , ChemRxiv 1 (2022).
188. E.T. Aisien, I.C. Otuya, F.A. Aisien, Thermal and catalytic pyrolysis of waste polypropylene plastic using spent FCC catalyst, Environ. Technol. Innov. 22 (2021) 101455. https://doi.org/10.1016/j.eti.2021.101455.
189. X. Zhang, H. Lei, G. Yadavalli, L. Zhu, Y. Wei, Y. Liu, Gasoline-range hydrocarbons produced from microwave-induced pyrolysis of low-density polyethylene over ZSM-5, Fuel 144 (2015) 33–42. https://doi.org/10.1016/j.fuel.2014.12.013.
190. X. Zhang, H. Lei, L. Zhu, M. Qian, G. Yadavalli, J. Wu, S. Chen, From plastics to jet fuel range alkanes via combined catalytic conversions, Fuel 188 (2017) 28–38. https://doi.org/10.1016/j.fuel.2016.10.015.
191. Y. Zhang, A. Li, Y.S. Zhang, W. Xie, C. Liu, Y. Peng, H. Zhang, Y. Kang, B. Qu, G. Ji, In-situ catalytic pyrolysis of polyethylene to co-produce BTX aromatics and H2 by Ni/ZSM-5 in the rotary reactor with solid heat carriers, Fuel 371 (2024) 131950. https://doi.org/10.1016/j.fuel.2024.131950.
192. D. Barzallo, R. Lazo, C. Medina, C. Guashpa, C. Tacuri, P. Palmay, Synthesis and Application of ZSM-5 Catalyst Supported with Zinc and/or Nickel in the Conversion

of Pyrolytic Gases from Recycled Polypropylene and Polystyrene Mixtures under Hydrogen Atmosphere, Polymers (Basel). 15 (2023) 3329. https://doi.org/10.3390/polym15163329.
193. P.L. editors Weitkamp J, Catalysis and zeolites: fundamentals and applications, New York: Springer Berlin Heidelberg (1999) 546.
194. Anggoro DD, Buchori L, Silaen GC, Utami RN, Preparation,characterization, and activation of Co-Mo/Y zeolite catalyst forcoal tar conversion to liquid fuel, Bull Chem React Eng Catal 12 (2017) 219–226.
195. Handke M, Mozgawa W, Vibrational spectroscopy of theamorphous silicates, Vib Spectrosc 5 (1993) 75–84.
196. T.Y. Yun, B.D. Chandler, Surface Hydroxyl Chemistry of Titania- and Alumina-Based Supports: Quantitative Titration and Temperature Dependence of Surface Brønsted Acid–Base Parameters, ACS Appl. Mater. Interfaces 15 (2023) 6868–6876. https://doi.org/10.1021/acsami.2c20370.
197. J. Li, R. Yan, B. Xiao, D.T. Liang, D.H. Lee, Preparation of Nano-NiO Particles and Evaluation of Their Catalytic Activity in Pyrolyzing Biomass Components, Energy & Fuels 22 (2008) 16–23. https://doi.org/10.1021/ef700283j.
198. A.Q. Saeed, B.Y. Al-Zaidi, A.S. Hamadi, H.Sh. Majdi, A.A. AbdulRazak, Upgrade of heavy crude oil via aquathermolysis over several types of catalysts, Materials Express 12 (2022) 278–287. https://doi.org/10.1166/mex.2022.2139.
199. Chen, D. Zhang, L. Shi, Y. Wang, G. Xu, Optimized Pore Structures of Hierarchical HY Zeolites for Highly Selective Production of Methyl Methoxyacetate, Catalysts 9 (2019) 865. https://doi.org/10.3390/catal9100865.
200. A.A. Mohammed, Z.T. Khodair, A.A. Khadom, Preparation and investigation of the structural properties of α-Al2O3 nanoparticles using the sol-gel method, Chemical Data Collections 29 (2020) 100531. https://doi.org/10.1016/j.cdc.2020.100531.
201. N.N.A. Mohamed Abdul Ghani, M.A. Saeed, I.H. Hashim, Thermoluminescence (TL) response of silica nanoparticles subjected to 50 Gy gamma irradiation., Malaysian Journal of Fundamental and Applied Sciences 13 (2017). https://doi.org/10.11113/mjfas.v13n3.593.
202. A.K. John, S. Palaty, S.S. Sharma, Greener approach towards the synthesis of titanium dioxide nanostructures with exposed {001} facets for enhanced visible light photodegradation of organic pollutants, Journal of Materials Science: Materials in Electronics 31 (2020) 20868–20882. https://doi.org/10.1007/s10854-020-04602-1.
203. Martínez, M.A. Arribas, P. Concepción, S. Moussa, New bifunctional Ni–H-Beta catalysts for the heterogeneous oligomerization of ethylene, Appl. Catal. A Gen. 467 (2013) 509–518. https://doi.org/10.1016/j.apcata.2013.08.021.
204. Z. Ahmad, F. UllahKha, S. Mahmood, T. Mahmood, A. Shamim, Different Approaches for the Synthesis of Zinc Oxide Nanoparticles, Open Journal of Chemistry 1 (2018) 19–25. https://doi.org/10.30538/psrp-ojc2018.0003.
205. Y. Jia, J. Wang, K. Zhang, W. Feng, S. Liu, C. Ding, P. Liu, Nanocrystallite self-assembled hierarchical ZSM-5 zeolite microsphere for methanol to aromatics, Microporous and Mesoporous Materials 247 (2017) 103–115. https://doi.org/10.1016/j.micromeso.2017.03.035.
206. R.R. Mishra, P.H. Rana, P.A. Parikh, Influence of catalyst acidity of spent FCC catalyst and TiO2 on product distribution in microwave assisted LDPE cracking, Journal of the Indian Chemical Society 102 (2025) 101873. https://doi.org/10.1016/j.jics.2025.101873.
207. Palčić, V. Valtchev, Analysis and control of acid sites in zeolites, Appl. Catal. A Gen. 606 (2020) 117795. https://doi.org/10.1016/j.apcata.2020.117795.

208. Mohabeer, N. Guilhaume, D. Laurenti, Y. Schuurman, Microwave-Assisted Pyrolysis of Biomass with and without Use of Catalyst in a Fluidised Bed Reactor: A Review, Energies (Basel). 15 (2022) 3258. https://doi.org/10.3390/en15093258.
209. M. Al-asadi, N. Miskolczi, Pyrolysis of polyethylene terephthalate containing real waste plastics using Ni loaded zeolite catalysts, IOP Conf. Ser. Earth Environ. Sci. 154 (2018) 012021. https://doi.org/10.1088/1755-1315/154/1/012021.
210. M.F. Paucar-Sánchez, M. Calero, G. Blázquez, R.R. Solís, M.J. Muñoz-Batista, M.Á. Martín-Lara, Impact of Metal Impregnation of Commercial Zeolites in the Catalytic Pyrolysis of Real Mixture of Post-Consumer Plastic Waste, Catalysts 14 (2024) 168. https://doi.org/10.3390/catal14030168.
211. Zhang, Q. Mao, Y. Yue, R. Gao, Y. Duan, H. Du, Ni-based catalysts supported on Hbeta zeolite for the hydrocracking of waste polyolefins, RSC Adv. 14 (2024) 15856–15861. https://doi.org/10.1039/D4RA02809K.
212. B.C. Vance, P.A. Kots, C. Wang, J.E. Granite, D.G. Vlachos, Ni/SiO2 catalysts for polyolefin deconstruction via the divergent hydrogenolysis mechanism, Appl. Catal. B 322 (2023) 122138. https://doi.org/10.1016/j.apcatb.2022.122138.
213. K. Ding, S. Liu, Y. Huang, S. Liu, N. Zhou, P. Peng, Y. Wang, P. Chen, R. Ruan, Catalytic microwave-assisted pyrolysis of plastic waste over NiO and HY for gasoline-range hydrocarbons production, Energy Convers. Manag. 196 (2019). https://doi.org/10.1016/j.enconman.2019.07.001.
214. S. Klaimy, C. Ciotonea, J. Dhainaut, S. Royer, M. Casetta, S. Duquesne, G. Tricot, J. Lamonier, Flash Catalytic Pyrolysis of Polyethylene over (Alumino)silicate Materials, ChemCatChem 12 (2020) 1109–1116. https://doi.org/10.1002/cctc.201901819.
215. M.Á. Martín-Lara, R. Moreno, G. Blázquez, M. Calero, Hydrogen Production Came from Catalytic Reforming of Volatiles Generated by Waste-Plastic Pyrolysis Over Sepiolite-Based Catalysts, Top. Catal. 68 (2025) 33–48. https://doi.org/10.1007/s11244-024-01981-1.
216. Uwagwu Charles Olisemeke, Research on Comparative Study on the Conversion of Waste Plastic Materials to Liquid Hydrocarbons Through Catalytic Pyrolysis, 2018.
217. P.E. Nwankwor, I.O. Onuigbo, C.E. Chukwuneke, M.F. Yahaya, B.O. Agboola, W.J. Jahng, Synthesis of gasoline range fuels by the catalytic cracking of waste plastics using titanium dioxide and zeolite, International Journal of Energy and Environmental Engineering 12 (2021) 77–86. https://doi.org/10.1007/s40095-020-00359-9.
218. L. Chen, J.B. Moreira, L.C. Meyer, J. Szanyi, Efficient and selective dual-pathway polyolefin hydro-conversion over unexpectedly bifunctional M/TiO2-anatase catalysts, Appl. Catal. B 335 (2023) 122897. https://doi.org/10.1016/j.apcatb.2023.122897.
219. E.T. Aisien, I.C. Otuya, F.A. Aisien, Thermal and catalytic pyrolysis of waste polypropylene plastic using spent FCC catalyst, Environ. Technol. Innov. 22 (2021) 101455. https://doi.org/10.1016/j.eti.2021.101455.
220. D. Rachmadena, M. Faizal, M. Said, Conversion of Polypropylene Plastic Waste Into Liquid Fuel with Catalytic Cracking Process Using Al2O3 as Catalyst, Int. J. Adv. Sci. Eng. Inf. Technol. 8 (2018) 694. https://doi.org/10.18517/ijaseit.8.3.2586.
221. L.M. Terry, M.X.J. Wee, J.J. Chew, D.S. Khaerudini, N. Darsono, A. Aqsha, A. Saptoro, J. Sunarso, Catalytic co-pyrolysis of oil palm trunk and polypropylene with Ni–Mo/TiO2 and Ni/Al2O3: Oil composition and mechanism, Environ. Res. 224 (2023) 115550. https://doi.org/10.1016/j.envres.2023.115550.
222. K. Anbarasu, p. Sivakumar, catalytic pyrolysis of dairy industrial waste ldpe film into fuel, international journal of chemistry research 3 (2012) 52–55. Https://ijcr.info/index.php/journal/article/view/78.

223. S. Li, Y. Xue, Y. Lin, B. Wang, X. Gao, Synergistic Activity of the Fe_2O_3/Al_2O_3 Catalyst for Hydrogen Production through Pyrolysis-Catalytic Decomposition of Plastics, ACS Sustain. Chem. Eng. 11 (2023) 10108–10118. https://doi.org/10.1021/acssuschemeng.3c02178.
224. R.-X. Yang, K.-H. Chuang, M.-Y. Wey, Effects of Nickel Species on Ni/Al_2O_3 Catalysts in Carbon Nanotube and Hydrogen Production by Waste Plastic Gasification: Bench- and Pilot-Scale Tests, Energy & Fuels 29 (2015) 8178–8187. https://doi.org/10.1021/acs.energyfuels.5b01866.
225. F. Vatankhah, A. Carrillo García, J. Chaouki, Role of Bifunctional Metal-Promoted Zeolitic Catalyst in Microwave-Assisted Pyrolysis of Polyethylene to Monocyclic Aromatics, Energy & Fuels 38 (2024) 20562–20576. https://doi.org/10.1021/acs.energyfuels.4c03692.
226. Son Dong, Taekyung Ryu, Collin Oi, Jiayang Wu, Natalie R. Altvater, Ryan Hagmann, Zahra Alikhani, Edgard A. Lebrón-Rodríguez, Jacob H. Jansen, Victor S. Cecon, Greg W. Curtzwiler, Keith L. Vorst, George W. Huber, Ive Hermans, Catalytic conversion of post-consumer recycled high-density polyethylene 2 oil over Zn-impregnated ZSM-5 catalysts, (n.d.).
227. D. Barzallo, M.A. Reinoso, G. Miranda, T. Romero, M. Franco, P. Palmay, Bifunctional Catalytic Performance of Zn/ZSM-5 in the Aromatization of LPG and the Conversion of Pyrolytic Gases from Recycled Polypropylene, ChemEngineering 8 (2024) 108. https://doi.org/10.3390/chemengineering8060108.
228. J. Duan, H. Wang, H. Li, L. Liu, K. Fan, X. Meng, Z. Zhang, L. Wang, F.-S. Xiao, Selective conversion of polyethylene wastes to methylated aromatics through cascade catalysis, EES Catalysis 1 (2023) 529–538. https://doi.org/10.1039/D3EY00011G.
229. F. Vatankhah, A. Carrillo García, J. Chaouki, Role of Bifunctional Metal-Promoted Zeolitic Catalyst in Microwave-Assisted Pyrolysis of Polyethylene to Monocyclic Aromatics, Energy & Fuels 38 (2024) 20562–20576. https://doi.org/10.1021/acs.energyfuels.4c03692.
230. J. Sun, C. Wu, Y. Zhou, J. Zhang, Z. Qu, F. Zeng, Z. Tang, W. Xing, R. Chen, Noble metal-free tandem catalysis enables efficient upcycling plastic waste into liquid fuel components, Chemical Engineering Journal 500 (2024) 156988. https://doi.org/10.1016/j.cej.2024.156988.
231. M.A.A. Mohamad Dzol, V. Balasundram, K. Shameli, N. Ibrahim, Z.A. Manan, R. Isha, Catalytic pyrolysis of high-density polyethylene over nickel-waste chicken eggshell/HZSM-5, J. Environ. Manage. 324 (2022) 116392. https://doi.org/10.1016/j.jenvman.2022.116392.
232. M. Marhaini, D. Fernianti, M.R. Aulia, Effective pyrolysis of LDPE plastic waste to fuel using titanium dioxide catalyst, International Journal of ADVANCED AND APPLIED SCIENCES 11 (2024) 75–82. https://doi.org/10.21833/ijaas.2024.12.009.
233. K. Akubo, M.A. Nahil, P.T. Williams, Aromatic fuel oils produced from the pyrolysis-catalysis of polyethylene plastic with metal-impregnated zeolite catalysts, Journal of the Energy Institute 92 (2019) 195–202. https://doi.org/10.1016/j.joei.2017.10.009.
234. Z. Chen, B.J. Erwin, L. Che, Recycling waste polyethylene into fuels over Fe/USY catalyst: Evaluation on the catalytic activities of varied iron states, Fuel 363 (2024) 131007. https://doi.org/10.1016/j.fuel.2024.131007.
235. Z. Chen, L. Xu, X. Zhang, Upgrading of polyethylene to hydrocarbon fuels over the Fe-modified Pt/Al2O3 catalysts at a mild condition without external H2, Chemical Engineering Journal 446 (2022) 136213. https://doi.org/10.1016/j.cej.2022.136213.
236. L. Yao, X. Liu, Z. Song, Z. Wang, Y. Pang, S. Li, C. Huang, Microwave-assisted Fe-based catalytic conversion of plastic waste to hydrogen: ReaxFF-MD and DFT

insights, Chemical Engineering Journal 520 (2025) 166127. https://doi.org/10.1016/j.cej.2025.166127.
237. Chen, J. Yao, J. Liu, B. Yan, R. Shan, Biomass to hydrogen-rich syngas via catalytic steam reforming of bio-oil, Renew. Energy 91 (2016) 315–322. https://doi.org/10.1016/j.renene.2016.01.073.
238. P.L. editors Weitkamp J, Catalysis and zeolites: fundamentals and applications, New York: Springer Berlin Heidelberg (1999) 546.
239. Handke M, Mozgawa W, Vibrational spectroscopy of theamorphous silicates, Vib Spectrosc 5 (1993) 75–84.
240. Anggoro DD, Buchori L, Silaen GC, Utami RN, Preparation,characterization, and activation of Co-Mo/Y zeolite catalyst forcoal tar conversion to liquid fuel, Bull Chem React Eng Catal 12 (2017) 219–226.
241. Li, R. Yan, B. Xiao, D.T. Liang, D.H. Lee, Preparation of Nano-NiO Particles and Evaluation of Their Catalytic Activity in Pyrolyzing Biomass Components, Energy & Fuels 22 (2008) 16–23. https://doi.org/10.1021/ef700283j.
242. F. Chen, D. Zhang, L. Shi, Y. Wang, G. Xu, Optimized Pore Structures of Hierarchical HY Zeolites for Highly Selective Production of Methyl Methoxyacetate, Catalysts 9 (2019) 865. https://doi.org/10.3390/catal9100865.
243. A.A. Mohammed, Z.T. Khodair, A.A. Khadom, Preparation and investigation of the structural properties of α-Al2O3 nanoparticles using the sol-gel method, Chemical Data Collections 29 (2020) 100531. https://doi.org/10.1016/j.cdc.2020.100531.
244. Martínez, M.A. Arribas, P. Concepción, S. Moussa, New bifunctional Ni–H-Beta catalysts for the heterogeneous oligomerization of ethylene, Appl. Catal. A Gen. 467 (2013) 509–518. https://doi.org/10.1016/j.apcata.2013.08.021.
245. Z. Ahmad, F. UllahKha, S. Mahmood, T. Mahmood, A. Shamim, Different Approaches for the Synthesis of Zinc Oxide Nanoparticles, Open Journal of Chemistry 1 (2018) 19–25. https://doi.org/10.30538/psrp-ojc2018.0003.
246. Kurnia Amin, K. Wijaya, W. Trisunaryanti, The Catalytic Performance of ZrO2-SO4 and Ni/ZrO2-SO4 Prepared from Commercial ZrO2 in Hydrocracking of LDPE Plastic Waste into Liquid Fuels, Oriental Journal of Chemistry 34 (2018) 3070–3078. https://doi.org/10.13005/ojc/340650.
247. M. Utami, K. Wijaya, W. Trisunaryanti, Pt-promoted sulfated zirconia as catalyst for hydrocracking of LDPE plastic waste into liquid fuels, Mater. Chem. Phys. 213 (2018) 548–555. https://doi.org/10.1016/j.matchemphys.2018.03.055.
248. H. Tang, D. Chen, M.H. Tahir, K. Qian, Y. Hu, L. Yin, Y. Feng, Catalytic pyrolysis of low-density polyethylene to produce sustainable aviation fuel fractions: Improving isomerized alkane selectivity via magnetic metal-modified HY zeolites, Energy 330 (2025) 136908. https://doi.org/10.1016/j.energy.2025.136908.
249. N. Insura, J.A. Onwudili, P.T. Williams, Catalytic Pyrolysis of Low-Density Polyethylene over Alumina-Supported Noble Metal Catalysts, Energy & Fuels 24 (2010) 4231–4240. https://doi.org/10.1021/ef100227f.
250. Luo, G. Gong, R. Ma, S. Sun, C. Cui, H. Cui, J. Sun, N. Ma, Study on high-value products of waste plastics from microwave catalytic pyrolysis: Construction and performance evaluation of advanced microwave absorption-catalytic bifunctional catalysts, Fuel 346 (2023) 128296. https://doi.org/10.1016/j.fuel.2023.128296.
251. N. Zhou, L. Dai, Y. Lv, H. Li, W. Deng, F. Guo, P. Chen, H. Lei, R. Ruan, Catalytic pyrolysis of plastic wastes in a continuous microwave assisted pyrolysis system for fuel production, Chemical Engineering Journal 418 (2021) 129412. https://doi.org/10.1016/j.cej.2021.129412.

APPENDIX

Detailed Mass and Carbon Balance

Table A presents the detailed mass and carbon balance for all catalytic pyrolysis experiments performed in this study. The table includes the mass of individual gaseous products, total gas yield, and the corresponding carbon mass for each catalyst. The satisfactory mass and carbon closure confirms the reliability of the experimental measurements and product quantification.

Table A. Detailed Mass and Carbon Balance for Gaseous Products Obtained during Microwave-Assisted Catalytic Pyrolysis of LDPE.

Sr. No.	Catalyst	Gas Yield (g)	Total Gas Yield (g)	Carbon mass (g)
1	HY	H_2-0.94, Methane-4.05, Ethane-1.23, Propylene-2.42, Propane-0.61, C_4-0.72	10	8.45
2	Hβ	Propylene-5.52, Propane-0.76, C_4-1.19, C_5-1.02	8.5	7.3
3	HZSM-5	H_2-0.18, Methane-1.44, Ethylene-7.35, Ethane-1.02	10	8.5
4	FCC	Propylene-5.55, Propane-0.68, C_4-1.35, C_5-1.39	9	7.68
5	TiO_2	Propylene-2.25, Propane-0.59, C_4-2.44, C_5-2.21	9.1	7.77
6	Ni/HY	H_2-0.5, Methane-2.1, Ethylene- 1.65, Ethane-0.87, Propylene-1.45, Propane-0.27, C_4-0.95, C_5-1.18	9	7.6
7	Ni/SiO_2	H_2-0.16, Methane-0.04, Ethylene-0.09, Ethane-1.99, Propylene-0.22, Propane-1.45, C_4-2.79, C_5-1.43	8.2	6.81
8	Ni/TiO_2	H_2-0.06, Methane-0.07, Ethylene-2.36, Ethane-0.10, Propylene-2.75, Propane-0.44, C_4-2.52, C_5-2	8.2	6.94
9	Ni/Al_2O_3	H_2-0.2, Methane-0.05, Ethylene-0.19, Ethane-3.76, Propylene-0.26, Propane-0.14, C_4-2.52, C_5-1.05	8.2	6.93
10	Zn/Al_2O_3	H_2-0.22, Methane-0.28, Ethylene-0.27, Ethane-3.85, Propylene-0.16, Propane-0.20, C_4-2.3, C_5-0.68	8	6.7
11	Zn/HY	H_2-0.32, Methane-0.08, Ethylene-0.21, Ethane-2.4, Propylene-3.83, Propane-0.21, C_4-0.83, C_5-0.29	8.2	6.92
12	Ni/S-ZrO_2	H_2-0.28, Methane-0.15, Ethylene- 0.14, Ethane-3.9, Propylene-2.38, Propane-0.21, C_4-0.25, C_5-0.39	7.80	6.5
13	Zn/S-ZrO_2	H_2-0.26, Methane-0.09, Ethylene- 0.13, Ethane-3.92, Propylene-2.5, Propane-0.19, C_4-0.39, C_5-0.38	7.9	6.6

14	Fe/HY	H_2-0.23, Methane-0.06, Ethylene- 0.08, Ethane-0.96, Propylene-1.15, Propane-0.14, C_4-4.48, C_5-0.57	7.7	6.53
15	Fe/Al_2O_3	H_2-0.2, Methane-0.1, Ethylene- 0.1, Ethane-2.84, Propylene-0.18, Propane-1.45, C_4-2.81, C_5-0.69	8.4	7.1

List of Publications

1. Mishra R, Rana P, Parikh P. Microwave-assisted pyrolysis of Low-Density Polyethylene (LDPE) to value-added products over HY, HZSM-5, and Hβ Catalyst. Materials Today Communications 2024; 41: 110829. https://doi.org/10.1016/j.mtcomm.2024.110829.
2. Mishra R, Rana P, Parikh P. Influence of catalyst acidity of spent FCC catalyst and TiO_2 on product distribution in microwave assisted LDPE Cracking. Journal of the Indian Chemical Society 2025; 102: 101873. https://doi.org/10.1016/j.jics.2025.101873.
3. Mishra R, Rana P, Parikh P. Hydrogen-rich gas and value-added hydrocarbon production from LDPE via microwave-assisted catalytic pyrolysis using Ni and Zn supported catalysts. Molecular Catalysis 2026; 596: 115918. https://doi.org/10.1016/j.mcat.2026.115918

Paper to be submitted to international peer reviewed journal

4. Influence of Catalyst Support and Metal Loading on Hydrogen Yield during Microwave Pyrolysis of LDPE